CRANFIELD INSTITUTE OF TECHNOLOGY

SCHOOL OF INDUSTRIAL SCIENCE

PhD THESIS

Academic Years 1980 - 1983

PAUL SMITH

Static and Dynamic Fracture of Structural Steel

Supervisors: Professor P Hancock
Dr J Spurrier

NOVEMBER 1983

Abstract

The present study is concerned with the assessment of structural steel fracture toughness, as close to real service loading conditions as practically possible in the laboratory, using small scale specimens. The effects of stored strain energy content is evaluated for slow-static and dynamic COD tests for maximum load and cleavage instability.

The literature reviews elastic-plastic fracture mechanics and goes on to study the effect of stored strain energy, the COD technique and dynamic testing procedures presently available.

Static and dynamic fracture toughness testing using the COD technique is carried out on BS4360 - 50D structural steel in its normalised state. The testing procedures used closely relate to either the BS5762 COD standard or BS5447 plane strain standard. The specimen size tested is 2B = W = 24 mm, with a fatigue notch size of approximately a/W between 0.48 and 0.57.

Photographic-macros and SEM fractography were carried out after the specimens were tested to assess the micromechanism processes operative during a fracture test.

It is believed the present work is of special significance to determinate structural design using structural steel, for example with liquefied gas pressure vessels. The resulting test data available from this thesis is envisaged to be the closest approach to real service "true limit severity", and consequently is beneficial to fracture prevention technology.

Acknowledgements

I am grateful to Professor P Hancock and Dr J Spurrier for their guidance and advice.

Financial support from the Science and Engineering Research Council is gratefully acknowledged.

The co-operation of the members of technical staff in the laboratories and in the departmental workshop has been of great importance in this work, and is thankfully remembered.

Thanks must also go to my wife for her patience and understanding, and to Sarah who typed this thesis.

Contents

List of Tables

1. *Introduction to Thesis Work*

The traditional design philosophy of structures is based on evaluating the applied loads and converting these to operating stress levels, as long as the operating stress does not exceed the design stress of the material used. The structural component members were believed to be free from failure and safe. The safety factor was assessed from the ratio of yield or ultimate stress to the design stress, the choice of safety factors generally being instituted by the design engineer's personal experience and intuition.

Only in the last forty years has the science of fracture mechanics been developed adequately to overcome the faults inherent in the traditional design stress approach. Many structures have fractured at stresses lower than the design stress of the material, the failures normally occurring near defective welds, or when cracks are present in the structure, for which the traditional design stress approach could not account. Examples include T-2 tankers, liberty ships, the De Havilland comet aircraft crashes, and other structures including bridges, pressure vessels, storage tanks, buildings, guns and cranes, [1,2,3,4].

The earliest theoretical and experimental work related to unstable fracture of brittle-solid glass was carried out by Griffith in 1921.[5]. He assessed the significance of crack-like defects in the material to the fracture properties, and his theoretical approach was the basis of Linear Elastic Fracture Mechanics used today for high strength, low toughness materials.

The LEFM approach can directly relate the size of a defect and applied stress required to produce brittle fracture, but the concept can only be applied if the plastic deformation zone is small, compared with the size of the crack.

With the advent of tougher structural steels, plastic deformation can be predominant prior to fracture, thus invalidating the use of a LEFM analysis for design purposes, and LEFM is now only used for very high strength materials exhibiting low toughness behaviour.

Fracture control when plasticity is present in a material is possible by various elastic-plastic fracture parameters. For initiation prevention these include COD and J-integral approaches, as well as R-curve analysis for even tougher fracture studies. But the COD and J-integral techniques assume plastic deformation occurs at a crack tip, while the maximum load deformation at which fracture instability and fast crack run or plastic collapse occurs is assessed and used as fracture toughness data.

From the laboratory test data obtained from COD and J-integral fracture testing, it is possible to correlate maximum allowable defect sizes in structures using empirical design curves, the most used of which is the COD design curve as proposed by the Welding Institute, England, [17, 22].

The COD design curve is, however, only able to conservatively predict the maximum allowable defect size in a structure, and not a critical size possible with the LEFM approach. Industrial users have complained of consequent over-design against fracture initiation, due to the COD design curves present inability to assess a critical defect size, for a given design loading, [22].

Interest has been shown recently in the occurrence of ductile slow stable tearing during COD and J-integral laboratory testing. The stable tearing can take place at a pre-existing crack tip or stress concentration during loading at slow-static strain rates, while a point of stable growth is reached when the driving force exceeds the crack resistance and instability can result with a transformation from ductile tearing to fast cleavage propagation. It has been proposed by Glucklich [27] and Paris [28] that the point of tearing instability in a structural steel can be affected by the compliance of the loading system, higher compliance or load determinacy inducing a shorter slow stable crack length and earlier instability point.

The compliance dependent instablity of stable tearing during elastic-plastic fracture testing in the laboratory is important for industrial users in relation to determinate-type structural designs, especially gas pressure vessels, gas storage tanks and other determinate structures involving high levels of stored strain energy.

If stable tearing of cracks is present in these structures, then as proposed by De Leiris [64] in 1949, and shown by Almar-Naess [29], Glucklich [27] and Paris [28] with laboratory tests, the ductile to brittle transition temperature of a steel may be raised in temperature simply due to the compliant loading configuration causing an earlier tearing instability in terms of COD and J-integral toughness values.

Data from laboratory COD testing, at service thickness, using stiff or displacement controlled loading systems to evaluate a steels ductile to brittle transition temperature, may therefore be dangerously inaccurate if the steel is to be used in a determinate type, high stored strain energy configuration. In addition, the maximum allowable flaw sizes evaluated using the COD design curve may be too large, causing catastrophic fracture in a supposedly tough steel, simply due to the compliance of the determinate structure inducing an earlier tearing instability point, and a higher ductile to brittle transition temperature.

The inherent empirical conservatism of the COD design curve may therefore be a false sense of security in certain structural situations, especially with determinate structures such as pressure vessels containing low temperature liquefied gas.

Another major area of interest in this thesis is the fracture testing philosophy to prevent instability and catastrophic fracture during high strain rate impactive loading.

One of the principal workers in this field who developed the Drop Weight Tear Test (D.W.T.T.) and the Drop Tear (D.T.) methods was Pellini [118, 119] and co-workers [121, 122, 123]. These test techniques were instituted to replace the Charpy-V test, and establish critical flaw sizes in structures using tough steels, by empirical correlations.

The D.W.T.T. and D.T. techniques were believed to be the worst possible laboratory test conditions which closely compared to the "limit severity", [118, 119], of a real structure with a sharp crack and high strain rate loading, producing the lowest toughness attainable from a given steel structure. The defect analysis procedure was then achieved by the Ratio Analysis Diagram (R.A.D.), which correlated Drop Tear impact energy with Charpy impact energy and the LEFM parameter for stress intensity factor, K_{IC}.

The present author suggests that the Pellini approach did not relate a true "limit severity", since by inspection, when impact loading occurs the structural members are already loaded to a given operating stress dependent on the structures own weight and the load capacity requirements. If the configuration is of a determinate type with high stored strain energy content, then when the transient impact loading occurs, the compliant stored energy will immediately be available if a dynamic instability produces a cleavage crack run condition. The stored energy may then completely sever the component by the catastrophic fast fracture introduced.

The principal drawback of the D.W.T.T. and D.T. tests in relation to determinate structures is that they depend solely on a high momentum impact situation, with no practical use of a compliant static preload on the test specimens equal to the operating stress during the impact stage.

The R.A.D. technique was also generally limited since LEFM K_{IC} was used, with no correlation to elastic plastic parameters such as COD or J-integral, see section 2.2 and 5.

It is hoped that combined impact and statically compliant loading on COD fracture toughness specimens developed in this thesis will indicate the dynamic instability conditions present in BS4360, 50D structural steel, thus improving on the work carried out by Pellini and getting closer to a true "limit severity" fracture testing approach.

The thesis test programme therefore concentrates on slow-static instability COD assessments, then on impactively loaded results, and it is the aim of this thesis to improve the present understanding of elastic-plastic instability conditions, so increasing the confidence of critical COD and limit severity COD fracture testing techniques for structural design criteria.

2. *Review of Elastic Plastic Fracture Mechanics*

To introduce the present day concepts involved in fracture mechanics, a brief resume will now be made of the Linear Elastic and Elastic-Plastic Fracture Mechanics theory. The main emphasis will be in terms of continuum mechanics, and only the primary information relevant to this thesis will be covered.

2.1 *The Linear Elastic Fracture Mechanics Approach*

With certain materials such as high strength maraging steels and non-ferrous alloys, the resistance to fracture is low, or simply they have a low fracture toughness. Only small crack-like defects are required to cause fracture below the yield stress, very little plastic deformation being involved. The initial micro-mechanism of separation may however be based on ductile fracture coalescing into a brittle cleavage fracture, [25].

Fracture prevention with low fracture toughness materials is possible by using the Linear Elastic Fracture Mechanics (LEFM) philosophy which is based on the developments of Griffith [5], in 1921, who studied the fracture behaviour of glass assuming the presence of crack-like defects. The work is applicable to materials exhibiting an elastic or quasi-elastic behaviour only, [5, 6, 7, 8].

Griffith, [5], originally considered an infinite cracked plate of unit thickness with a central transverse crack length of 2a, with fixed ends and an applied stress σ, see Figure 1. Griffith stated that crack propagation will occur if the energy released upon crack growth is sufficient to provide all the energy that is required for the crack growth itself. If the energy is inadequate for crack growth then the stress must be raised.

The condition for crack growth is:-

$$\frac{dU}{da} = \frac{dW}{da} \qquad (1)$$

where U is the elastic energy and W the energy required for crack growth.

The strain energy, U, calculated using Inglis [8] results for the stress distribution around an elliptical hole, in a uniformly stressed plate, under plane stress is:-

$$U = \frac{\pi \sigma^2 a^2}{E} \qquad (2)$$

with E and ν being Youngs modulus and Poissons ratio respectively, thus:-

$$\frac{dU}{da} = \frac{2 \pi \sigma^2 a}{E} \qquad (3)$$

and is usually replaced by:-

$$G = \frac{\pi \sigma^2 a}{E} \qquad (4)$$

which is called the "elastic energy release rate" per crack tip.

In addition, G is called the crack driving force, its dimensions of energy per unit plate thickness and per unit crack extension are also the dimensions of force per unit crack extension.

The energy consumed in crack propagation is denoted by $R = \frac{dW}{da}$ which is called the crack resistance, and may be assumed to be a constant for a perfectly elastic material requiring only surface energy to form two new crack surfaces.

Since R can be assumed a constant in an elastic material, then G must exceed a certain critical value to be greater than R, before crack propagation can occur. This critical value is known as G_{IC}, the subscripts representing opening mode I and critical conditions. (See Figure 2 for mode descriptions).

Hence crack growth will occur when:-

$$\frac{\pi \sigma_c^2 a}{E} = G_{IC} \qquad (5)$$

or

$$\sigma_c = \frac{E G_{IC}}{\pi a} \qquad (6)$$

In ductile materials such as metals, plastic deformation occurs at the crack tip, and much work is required in producing a new plastic zone as well as the cracks surface energy. In metals, R is predominantly a plastic energy term, while the surface energy is so small it may be neglected, [6, 7]. The value of R per crack growth will therefore not necessarily be a constant, dependent on the plastic zone process.

In addition to the energy criteria to be satisfied before crack growth occurs, the material at the crack tip must be ready to fail and unable to undergo further strain. This condition may be sufficiently described by the crack tip stress fields in terms of the "stress intensity factor" K_I, where again the subscript stands for opening mode I, see Figure 2.

The value of K_I may be generalised in terms of the functions of an element dxdy at a distance r from a crack tip in a plate, and an angle θ with respect to the crack plane, see Figure 3.

Thus:-

$$\sigma_{ij} = \frac{K_I \ f_{ij}(\theta)}{\sqrt{2 \pi r}} \qquad (7)$$

where $K_I = \sigma \sqrt{\pi a}$ (8)

From complex stress function solutions the basic relations for mode I opening are:-

$$\sigma_x = \frac{K_I}{\sqrt{2\pi r}} \cos\frac{\theta}{2}\left(1 - \sin\frac{\theta}{2}\sin\frac{3\theta}{2}\right)$$

$$\sigma_y = \frac{K_I}{\sqrt{2\pi r}} \cos\frac{\theta}{2}\left(1 + \sin\frac{\theta}{2}\sin\frac{3\theta}{2}\right) \qquad (9)$$

$$\tau_{xy} = \frac{K_I}{\sqrt{2\pi r}} \cos\frac{\theta}{2}\left(\sin\frac{\theta}{2}\cos\frac{3\theta}{2}\right)$$

with $\sigma_z = 0$ for plane stress or $\sigma_z = \nu(\sigma_x + \sigma_y)$ for plane strain.

As can be judged from inspection of equations (5) and (7), the stress intensity factor at the crack tip is equivalent to the energy criterion, and combining these approaches allows the relation:-

$$\frac{K^2}{E} = G \qquad (10)$$

This further leads to the equation:-

$$G_C = \frac{K_C^2}{E} \quad \text{for plane stress} \qquad (11)$$

and

$$G_{IC} = \frac{K_{IC}^2(1-\upsilon^2)}{E} \quad \text{for plane strain} \qquad (12)$$

Since it is possible to predict failure by brittle initiation and crack growth in an elastic material by the stress intensity at a crack tip, from equations (5), (7), (8) and (10), the LEFM approach can directly relate the size of a defect or crack and applied stress to cause the failure.

Simply:-

$$K_C = \sigma_c \sqrt{\pi a_c} \qquad (13)$$

However, it must be remembered that such a concept is only applicable if the material is linearly elastic in character, but most metals including structural steel exhibit a yield stress, above which they plastically deform in a non-linear manner around the crack tip where plasticity is present. The elastic relations quoted previously for stress singularity around a crack tip, culminating in the use of the stress intensity factor, are thus only a simplified theoretical concept.

Irwin [6] tried to overcome this problem by assuming the plastic zone at the crack tip simply makes the crack act with an effective longer crack size, in relation to the size of the plastic zone itself. However, if the plastic zone becomes larger than the crack, then the stress intensity factor approach is not applicable and another crack tip measurement must be used to assess fracture toughness, for example COD or J-integral which account for plasticity.

The applicability of the LEFM approach using K_{IC} is therefore an important consideration, especially with respect to the state of stress in the crack region. Larger thicknesses of plate material have increasing plane strain stress character within which plastic deformation is restricted and plastic zone sizes are small due to the triaxial stress state. The plane stress regime being a biaxial stress state which will easily allow plastic flow.

The change from plane stress to plane strain by thickness increase is a gradual process, see Figure 4, a recognised condition when plane strain is dominant and the stress intensity approaches may be used, being:-

$$\text{thickness } B \geq 2.5 \left\{ \frac{K_{IC}}{\sigma_{ys}} \right\}^2 \qquad (14)$$

where σ_{ys} is the materials yield stress value, and K_{IC} as defined in Appendix A.

Investigating (14) in terms of BS4360 - 50D structural steel, the thickness B necessary for plane strain behaviour and use of LEFM would be 13 inches. Present usage of 50D steel is usually only in the range of 1 to 3 inches thick. The use of LEFM relations is therefore not recommended, since the steel is used in a plane stress condition.

Because the plastic zones in BS4360 - 50D are large compared to the crack size, this inherent plasticity increases the materials fracture toughness tolerance to defects.

Only at very low temperatures is the LEFM approach applicable to a structural steel, when the yield stress has risen above the fracture stress, culminating in a brittle cleavage initiation process. The steel therefore exhibits a ductile to brittle transition temperature, as shown in Figure 5, (for BS4360 - 50D steels tested at Cranfield).

The ductile to brittle transition range is of great interest in this thesis to ascertain the toughness of 50D steel at a given temperature, but because elastic cleavage initiation behaviour is only present at very low temperatures below normal industrial service, an alternative toughness approach will be followed, namely the COD or Crack Opening Displacement technique developed by Wells, [9, 10].

2.2 *The Yielding Elastic-Plastic Fracture Mechanics Approach*

Structural steels such as BS4360 - 50D may be assessed for its tolerance to defects by the Elastic-Plastic Fracture Mechanics approach, however no exact methodology to treat crack initiation problems in high toughness materials is available as in the LEFM concept.

Wells [9, 10] introduced an elastic-plastic toughness parameter to ascertain the maximum permissible plastic strain before failure at a crack tip. This is now known as Crack Opening Displacement (COD), measured in terms of δ m.m. opening at the crack tip.

A similar parameter gaining popularity is the J-integral, of most interest in the United States, [73, 92, 102].

Empirical design curve approaches have been used [11, 12] to connect laboratory tests of COD and J-integral values to real design criteria for structural applications, and are attaining greater confidence with use. Finite-element design analysis has also been suggested using the J-integral, [13, 104].

To concentrate on COD, from which testing is proceeded within this thesis work, the COD design curve concept allows a fracture mechanics relationship between the defect size, applied strain or stress conditions, and the material properties, [14, 15, 16]. The predictions of defect size obtained are intended to conservatively size the defect, which can be allowed to remain in a structure. It does not specify the criticality condition, [17] as possible in the LEFM relation given in equation (13).

The conservatism of the COD design curve is intentional to ensure safe life working of a structure, involving a wide scope of uses, from pressure vessels to oil platform columns and nodes, [14, 17]. However, further developments are required since the exact safety factor for a given service structure is as yet indefinable, [14, 17, 22, 24], and the complicated behaviour of a structural steel involving plastic flow, work hardening, plastic collapse, ductile tearing instability and cleavage crack growth introduce a continuous interplay of factors, [25, 26].

Occasionally, it is difficult to precisely model microstructural inhomogeneities, inbuilt residual stresses and constraint effective in full scale structures, discrepancies then occurring between the laboratory scale COD test and real structural response [22, 23].

Some investigators, [24, 27, 28, 29, 30] have suggested that stored strain energy in a structure can attenuate the ductile tearing instability to cleavage in the elastic-plastic regime, as measured by COD and J-integral. Assessment of the validity of such a phenomenon in BS4360 - 50D steel is the first objective of this thesis.

Until more direct methodologies are developed in the elastic-plastic regime, questions must still be carefully answered as to whether certain sizes, types, configurations and locations of crack-like defects are significant to fracture prevention. The use of COD in this thesis to investigate the effects of stored strain energy on fracture toughness may help the knowledge required for defect assessment technology, and it is hoped this thesis will improve the confidence of the COD approach.

The next section of this thesis will deal with the service demands of structures, while a complete section on the COD approach will be followed in section 5.

3. *Review of Structural Service Conditions with Significance to Elastic-Plastic Fracture Behaviour*

A review will now be made of real service conditions of most interest in this thesis with respect to the elastic-plastic fracture behaviour of structural steels. It is intended to be of direct use to industrial designers and constructors, so that improved testing for elastic-plastic instability analysis may be developed.

3.1 *The Significance of Determinate and Indeterminate Design of Structures to Fracture Prevention*

The state of the fracture problem to be studied must be defined, whether initiation, propagation or crack arrest, before a laboratory scale test can be developed. Once the decision is made to either prevent initiation or assume initiation is achieved and resist propagation, the type and methodology of fracture mechanics testing to be used for design criteria evaluation can be instituted. Examples being the COD approach for initiation toughness characterisation, [10, 17], wide plate testing for propagation and crack arrest after cleavage instability has occurred, [43], the Robertson crack arrest test, [51], the similar ESSO propagation arrest test, [52], and the Drop Weight Tear Test for dynamic initiation and propagation resistance measurement, [53, 54].

It would be foolhardy to assume that laboratory scale testing, even though highly developed, can precisely evaluate the fracture behaviour of materials in service. As mentioned in the introduction, sections 2.2 and 5 there are too many variables interplaying at one time for complete confidence, especially in the elastic-plastic regime.

The closest approximation that can be made is to test laboratory specimens with a simple model, studying parameters and modifying service factors consecutively, for example to measure for COD initiation toughness for a given temperature and thickness.

Accurate modelling of real service loading behaviour in the laboratory is achieved if the type of structure to be assessed is investigated, the two basic categories of structural load response being determinate and indeterminate.

This is especially important if the COD maximum toughness value is to be evaluated in the transition temperature range of a structural steel, 24, 27, 28, 29, 80, 81.

The indeterminate system can be defined as a design within which load redundancy is operative, reflecting an ability for additive load paths to keep a structure intact even though one of the load paths has been severed by fracture. In terms of loading at a crack tip in the unstable member, the initial high load will reduce to zero quickly and be carried by the "redundant" members in the structure once failure is achieved. The structures' overall load-job capacity may be reduced, but will still be effective for service.

Comparing an indeterminate system in service to a laboratory slow-static test is possible by a stiff or low compliance loading machine. For example, the British Standard COD static toughness test [75] is carried out using displacement controlled mechanical-worm drive or hydraulic machines, which are effectively stiff systems.

In the case of determinate structures, only one load path is operative, and if fracture instability occurs, operable crack tip load will remain high before, during and after the failure. As mentioned in the literature survey in Section 4, if slow stable tearing is present in a ductile structural steel member of determinate nature, the point of crack growth instability at which catastrophic cleavage fracture occurs, may be earlier than for an indeterminate stiff case. Situations of this type are detailed in references by Paris [28], Glucklich [27] and Almar-Naess [29].

The equivalent loading configuration in the laboratory to a determinate type structure is a compliant or spring-like loading system. Since the load decay at instability in a determinate structure is effectively nil, the closest approach in terms of load history would be a load controlled hydraulic machine. However, from experience gained at Cranfield Institute of Technology in the Industrial Science Centre, using computer controlled hydraulic machines, they are prone to spurious and extremely complicated load surges when instability occurs with fast crack growth in a test specimen.

Until such a time as the electronics-hydraulics interface and monitoring system is improved with this in mind, a mechanical spring system of loading seems the most effective and economic.

Obviously, a mechanical spring cannot have infinite compliance and zero stiffness, but in terms of the specimen under test, as long as the testing machine's compliance is much greater than the specimen, a noticeable change in the point of instability during slow stable tearing should be present. This effect may be especially pronounced in the ductile to brittle transition toughness region of the steel, see Section 4.

Further inferences may be introduced in relation to determinate structures with respect to stored fluids in containment, examples being gas pressure vessels and pipelines. Due to the compressible nature of gases, the gas is a source of an enormous amount of stored energy which can be recovered to do work on the surroundings if decompression occurs. Consequently, in addition to the pressure vessel's determinate type design in terms of load distribution, even if a small leak occurs due to slow crack growth of some kind, the loading history at the crack tip will remain at a high magnitude giving rise to a high compliance loading behaviour. If further crack growth with instability were to occur, the decompression energy would be supplied to the fast running crack.

The significance of this approach to laboratory testing by the present author is extremely important in defect assessment of rate sensitive structural steels, as with BS4360 - 50D. More accurate critical flaw size correlations may be possible by evaluating laboratory slow-static COD and impact COD instabilities, by applying the equivalent compliant stored strain energy and dynamic strain rate levels operative with the real structure and service conditions.

A pre-design analysis could be instituted to evaluate the determinacy of the structural configuration, the maximum static loading levels and the probable dynamic impact loading rates over the life of the structure, to model the "true limit severity" toughness testing conditions in the laboratory.

A logical step in this work is now to look at the information referencing work related to stored strain energy effects on fracture behaviour.

3.2 *Modelling Elastic-Plastic Fracture Behaviour with Determinate Slow-Static Loading*

The prevention of initiation in pressure vessels is well advanced with "leak-before-break" theories originating from nuclear encasement integrity studies, which assumes that a part-through elliptical crack in a thin-walled pressure vessel may grow by fatigue or stress corrosion until it reaches the outer wall, [25]. The vessel will then be leaking, and there is a good chance that detection of the leak will follow before the crack attains its critical size for instability, as defined by LEFM correlations taking account of yielding and work hardening processes, [25]. However, if it is assumed further that slow stable tearing characterises the gradual growth mechanism at a given time, the resident high stored strain energy and compliant loading history behaviour could decrease the allowable stable growth, due to an early instability point. Cleavage crack propagation would therefore occur at the instability point culminating in catastrophic fracture of the pressure vessel. This state of affairs was postulated by De Leiris in 1949, [64], in connection with large compressed fluid-gas storage tanks. See Section 4.1 and 4.4.1.

Parallel defect assessment technology gaining popularity to examine pressurised containment situations is the J-integral R-curve "Tearing Modulus" approach, first developed by Paris, [28], see Section 4.4.3, which analyses the crack tearing resistance and driving force balance in flawed structures. In 1981, the Electric Power Research Institute of America (EPRI), [104], commented a favour for the Tearing Modulus approach with slow crack growth and variable compliance loading situations to ascertain expected instability. Unfortunately, the developments so far have only concentrated on highly ductile steels at elevated temperatures away from the ductile to brittle toughness transition, see Section 4.4.4.

At present, the construction industry has a requirement to ascertain reliable data which can indicate the critical instability and defect size allowance in structural design, using the COD and COD design curve approach. This is particularly important in the transition toughness range at lower temperatures for structural steel. For example, from Section 4.4. it can be postulated that the transition from ductile to brittle behaviour moves up in temperature as the stiffness of a loading machine is decreased, or conversely the compliance is increased, simply because the instability point after ductile tearing is affected by the loading compliance. The machine loading compliance is also equivalent to the degree of determinacy in a real structure, so a test programme to evaluate the differences between stiff and compliant loaded COD transition toughness values will be of great importance to fracture-safe design.

Developments of this type would have special significance to the offshore, pressure vessel and general low temperature technology industries, as put forward by Cotton in 1979, [80, 81], and Hancock and Spurrier in 1983, [24].

The requirement of this thesis to identify a possible compliance effect upon slow stable tearing crack growth causing an early instability compared to a stiff test result becomes evident.

It is envisaged that only a test for COD fracture toughness using a testing machine whose compliance is equal to, or greater than the structures equivalent compliance would be safe for structural design criteria in high stored strain energy situations.

To validate this postulate of a compliance effect on "stable" ductile growth in the COD toughness test, it is intended to obtain COD values from standard, [75], notch-bend specimens in a stiff and compliant loading system, varying the temperature to obtain a scatter of the ductile to brittle transition values. The resulting data will have repercussions for the standards used in COD testing, the COD design curve ideology, "leak-before-break" analysis and general determinate fracture-safe design concepts in the transition toughness temperature range.

3.3 *Modelling Elastic-Plastic Fracture Behaviour of Real Structures Prone to Impact Loading*

Thus the knowledge gained so far from the reference literature would suggest that an ability to simulate the real service loading conditions of a structural steel in the laboratory, close to its transition toughness temperature, is very important if the structure is determinate in nature. Static and dynamic fracture toughness testing using a compliant loading system seems the logical development area to assess the "true limit severity", toughness values, see Section 8.

Obviously, it is economically disastrous to become over-safe with respect to low probability of overload or wear damage, but at present there seems to be no way of quantifying the significance of a given impact load on a preloaded compliant structural steel configuration.

It was realised by the author that no test technique had been developed to study in practice the impact loading of structures already stressed to the design loading, (normally ½ to ¾ of the yield strength). Test methods either studied slow-static loading or impact loading toughness separately. Whether by non-cooperation between research bodies, inadequacy of testing rig design engineering, low financial investment or poor inventiveness, a combined compliant static and impact loading testing method was not devised.

Early examples of real structural failure situations when combined impact and static loading was present, were the Liberty Ship failures, [3]. This prompted the author's need for a test technique utilising simultaneously applied impact and static loads to be developed, remembering that many structures today are subjected to similar life-loading histories.

This is made clearer when reports of accidental impact damage occurs when North Sea supply barges and tugs hit the sides of oil rig columns in heavy weather, fluid-shock inducing fast pressure surges in loaded pipelines, and general accidental construction or maintenance damage.

The Liberty Ship failure reports, [3], state clearly the sea condition, temperature, weather, cargo weights etc. A general description is also made of the fracture events themselves by the ships' captain or official. By extracting a number of reports it was discovered that the mode of loading was described when the fracture instabilities occurred. For example:-

Example (a) - Dry Cargo Vessel; Sea condition: very heavy seas; Weather: heavy.

"The vessel came down on a very high sea and split in four places. The cracks did not occur along the welds, but were clear breaks in the plating, which opened and closed with the working of the ship".

Example (b) - Dry Cargo Vessel; Sea condition: heavy; Weather: very heavy.

"The vessel was pounding and pitching when she came down heavily with her fore foot causing a fracture in the girder and deck plating".

Example (c) - In contrast to (a) and (b), the report of the Schenectady, [34], described a failure of the ship splitting in two in harbour, with a small swell and calm weather.

The basic faults of the ship's failures described was the poor welding procedures, faulty design and inherent low toughness of the ship's plate steel used in manufacture, due to a high carbon content. However, the descriptions of the service conditions at failure are of concern here.

In the Schenectady failure, it is clear that loading was slow-static in nature. Due to determinate type - large size structure used, high stored strain and forcing energy was available at crack instability and the following crack propagation stages.

If the failure (c) were to be modelled in the laboratory, then the basic loading would be slow-static with high stored strain energy availability by a compliant loading system or high volumetric strain energy of the specimens size. The wide plate testing technique outlined in Section 4.2 would be the closest approximation in terms of a large specimen size, and slow-static loading rates, however it is debatable if the equivalent crack tip compliance could be achieved.

This limitation occurs because the loading machine used to force the plate edges will have a restricted capacity of load and crosshead movement.

A compliant-spring type loading machine to test a small scale specimen in an equivalent manner to example (c) would therefore have certain advantages, including adequate load capacity dependent on machine and specimen design, ample crosshead movement, large stored energy available external to the specimen in the recoverable spring energy and easier access to the specimen for environmental and temperature simulation. (These advantages are manifested in the thesis testing methods outlined in Section 7 of this thesis).

The other two reports, (a) and (b) detail heavy seas, with the ship's hull falling down from a large wave and then fracturing. This is radically different from (c), a static loading mode. Impact loading is operative in these cases, combined with high levels of stored energy available from the dead weight and cargo. Early development of toughness assessments at high strain rates by impact was largely due to Pellini and co-workers, involving the explosion bulge, drop weight and drop tear techniques described in Sections 6.2.2 and 6.2.3, and assumed that the dynamic impact loading procedure provided a "limit severity" situation, simulating the worst conditions in service of a real structure, [121, 122, 123].

The factors contributing to this theory was that the high strain rate was applied to a sharp, highly constrained crack, possibly with a welded heat cycle and weld seam incorporated in the test specimen, similar to the fabrication of the real structure, [121, 122, 123].

From the evidence of Fearnehough [63], in section 4.1., the accuracy of the dynamic drop weight test to show "limit severity" toughness of the material must now be questioned. If Pellini's "limit severity" approach by impact-only drop weight testing is correct, then the impact-only fracture toughness values would be the lowest possible, while the ductile to brittle transition temperature of these results would be the highest attainable at the specific loading strain rate.

The work by Fearnehough, [63], contradicts this assumption, showing that if a static tensile stress is present during the dynamic impact, then the toughness value is reduced in the transition zone, and the ductile to brittle transition temperature is increased compared to the impact-only test result.

The present author believes that "true limit severity" is only achieved when dynamic impact is combined with a coincident compliant static stress, both applied at the crack tip and in the remaining ligament.

The combination of impact and superposed compliant static stress in the laboratory is logically the closest approximation of loading in a real determinate structure under impactive loading. For example, as shown in Figure 7, if the stress magnitudes of dynamic and static load histories at the crack tip are plotted against time, when impact occurs at time "t_i", then decays rapidly, the compliant static stress level remains relatively constant.

If we assume the dynamic impact load in a rate sensitive structural steel causes an instability at the crack tip, whether by cleavage initiation or a transfer from ductile tearing to cleavage, the superposed static compliant driving force is immediately available to continue the cleavage growth allowing catastrophic brittle fracture. Consequently, a "true limit severity" dynamic toughness test will only be possible if compliant stored strain energy is also present in the specimen during the impact cycle.

4. *Stored Energy Effects Upon Fracture Toughness*

4.1 *Review of Stored Strain Energy and Size Effects Upon Fracture Toughness*

In this section the literature available related to size effects in metals, with emphasis on the effect of stored strain energy will be studied.

The specimen size can influence the fracture toughness of metals in several ways, [25, 27]:-

(i) By flaw statistics

(ii) From technological inaccuracies

(iii) By stress multiaxiality

(iv) By stored strain energy

The first case (i) simply assumes that for a larger size in volume and surface area, the statistical probability that a defect can initiate a crack is greater, as described by Weibull in 1939, [56]. After initiation, such a concept has no validity.

Case (ii) introduces the possibility that variation in material properties from processing and manufacture upon size variation can cause modified behaviour. In most cases specimens are manufactured from the same stock to induce uniformity, however with welded plates the specimen size and heat input gives rise to attenuated microstructural effects, [57].

Case (iii) describes the stress system operative, whether biaxial or triaxial in nature, see Section 2.1 and Figure 4. Larger sizes of material will be increasingly influenced by through-thickness stress, as opposed to biaxial states, when the thickness stress magnitude is insignificant. As the triaxiality increases, plastic deformation is prevented, so decreasing the ductility and overall strength of the component, [25].

The effect of stored strain energy upon fracture behaviour with Case (iv), is of most interest in this thesis. Various references are available studying the effect of size upon fracture toughness, however prior to the late 1950's, certain fracture concepts had not been developed adequately to assess results.adequately.

The brittle theory of Griffith, [5], stated an energy dependence for fracture initiation and propagation, but ductile fracture instability approaches were not introduced until the early 1960's, [9, 10, 21]. For these reasons many references studying the effect of size upon fracture behaviour before 1960 were based upon the flaw statistics principle, [56], material inhomogeneity factors, and stress multiaxiality inducing constraint, Cases (i), (ii) and (iii). Examples of such studies were Lubahn, 1947, [60], Davidenkov, 1947, [61], Lusbahn and Yakawa, 1958, [62], when increased size of components demonstrated losses in strength and ductility, but the prime reasons for this loss did not take account of Case (iv).

Lubahn and Yakawa, [62], made an investigation into the failure of two large generator rotors manufactured of nickel-molybdenum-vanadium steel, the laboratory size tests for this material indicating a ductile character. Lubahn and Yakawa, [62], performed tests on notch-bend specimens of various sizes and notch radii. With increasing size the fracture toughness was reduced, this effect increasing with the sharpness of the notch, reaching the level of one fifth of the strength of small specimens for the worst combination of size and notch sharpness. The ductility also decreased markedly with increasing specimen size.

The authors, [62], concluded that the size effect was caused by flaw statistics, but this assessment is inadequate since the specimens were notched determining the failure cross section, and slow stable crack propagation was present.

From their results, it was noted that bars above a certain size broke suddenly, without warning, in the manner of crack propagation; in smaller specimens, short, discontinuous cracks could be observed prior to fracture.

It is suggested that with the loss of toughness and ductility as size increased, once a stable growing crack existed, the size of the specimen became a factor in determining the availability of strain energy. The instability from stable to unstable fracture would then be affected by the stored strain energy available, the stable crack length prior to instability becoming shorter for increasing size of bars.

Similar results were reported as early as 1932, [58], when Docherty tested geometrically similar slow-static notch-bend steel specimens. This criterion was the absorbed energy as determined from the area under the load-defelction curve to failure. The experiments showed a strong size effect, with absorbed unit energy decreasing with increasing size. The decrease of energy extended over the full range of cross sections, still decreasing over the transition size of plane stress to plane strain.

In terms of analysis by flaw statistics, the crack region was again highly defined by the notch configuration as for Lubahn and Yakawa, [62]. The load-deflection curves indicated the development of a stable tear ahead of the notch root, which would allow the stored strain energy to affect the point of instability similar to Lubahn and Yakawa, [62].

One of the most convincing pieces of work to show the existence of a strain energy size effect was performed by Fearnehough in 1963, [63], by employing the drop-weight test on V-notched beams of mild steel to determine their brittle-ductile transition temperature. To make the tests temperature independent of specimen size, he used a normalisation procedure whereby the beams were allowed to bend to varying angles so that the notch strain was the same for each specimen size. Despite this precaution, the results indicated a strong dependence of transition temperature upon specimen size, large specimens having a higher transition temperature than small specimens.

To support his idea that the results were due to a strain energy effect, Fearnehough, [63], superposed a longitudinal tensile stress on one of the small beams (7 x 0.5 x 0.5 in) while performing the drop-weight test. The transition temperature for this sample was increased, and was found to be equal to that of a larger sample (14 x 2 x 1 in).

Without the superposed stress by tension, the difference between the transition temperatures of these two specimens sizes was about 30°C, see Figure 8.

The tests by Fearnehough, [63], are quite important since increasing the strain energy content by additional tensile stress during the drop-weight test increases the transition temperature, reducing the fracture toughness, while having a constant distribution of flaws and uniform metallurgical constitution of the material. This clearly shows a strain size effect was predominant.

It is of interest to this thesis to further note that the strain energy size effect was present on impact-type drop weight testing in combination with a statically loaded superposed tensile stress.

No mention is made of the compliance of the superposing tensile load, but it is assumed to be relatively stiff.

The specimens used by Fearnehough, [63], were not fatigue-notched, as with present day COD and D.T. testing techniques (see Sections 5 and 6), but used a machined V. This implies the machined notch configuration will be relatively blunt, exhibiting a lower constraint value compared to a sharper fatigued crack tip.

The severity of the machined V notch used by Fearnehough, [63], is therefore considerably less than a fatigued notch in terms of the fracture behaviour, and a fatigued notch should show a lower material toughness. The transition curves shown in Figure 8 are therefore representative of a blunt crack, present on impact type drop-weight testing in combination with a statically loading tensile stress.

Service experience of the possible effects of stored strain energy with increasing structural size and compressible containers were put forward as early as 1949 by De Leiris, [64].

He commented that small laboratory scale testing of materials to observe service fracture properties was inadequate, the size of the structure and potential energy stored being larger in magnitude than the small scale specimens. The effect this would have was suggested, [64], to cause a likelihood of a change from ductile initiation and tearing to a brittle-catastrophic fracture.

4.2 The Wide Plate Test and its Use in Fracture Control

So far the text has looked at tests of varying specimen size to evaluate a possible size effect upon fracture behaviour. A test which has gained considerable popularity over the last twenty six years is the "Wide Plate" test technique, using a large specimen size and a very high capacity loading rig.

It is used primarily as a test for welded structural integrity, assessing weldability, propagation, arrest, parent plate-weld strength and stress relief fracture studies, and is now recognised as the closest laboratory scale test to a real-size structure with welded fabrication.

The basic idea of the Wide Plate test answers part of De Leiris', [64], requirements for a larger size of testing specimen and loading machine, however it must be made clear that the test is simply an assessment of fracture instability and does not use a compliant loading system.

The test method is now principally a practical guide to generate added confidence to defect assessment from COD elastic-plastic testing in welded structures, and has been used to verify the "conservatism" of the COD approach, [22], the justification being that the Wide Plate test is the closest approximation to a real structure as welded, and the confidence of using COD and the COD design curve philosophy for initiation prevention can be evaluated by this comparison, [22, 31, 32].

The reasons for the tests importance is four-fold, allowing constraint, stored strain energy, residual stress distribution and full plate microstructural effects upon welding heat input, [31].

Post-weld heat treatment effectiveness with respect to fracture toughness is therefore an obvious use, [32]. The Wide Plates' inherent high stored strain energy content also allows crack propagation and arrest behaviour, of special interest with continuous welded structures, [33].

The history of the test dates back to just after the war, when engineers were concerned with the occurrence of brittle fracture in welded structures. Thorough investigations were carried out into the brittle fractures of the Liberty Ship tankers Schenectady, [34], and Ponagansett, [35], and oil storage tank failures at Fawley, [36, 37]. These failures were emphasised since the loading conditions were static and at a stress level below the yield stress of the welded plate. While the origin of the failures was associated with faults in the welds laid parallel to the direction of principal tensile stress.

A primary line of thought was the contribution to failure by residual welding stresses, since during the welding of engineering structures fractures occurred which could only be explained in this way, [38]. For this reason, since 1946, low-temperature stress relieving, [39], was applied to all structures which could not be put into a furnace, including T.2 tankers, penstocks, large field-cracked tanks, [40] and pressure vessels, [41].

The process consisted of progressively heating bands on each side of a weld at about 175^{o}C by advancing oxyacetylene gas torches, followed by air-water cooling. In the vicinity of the weld after this treatment, residual stresses were reduced in relation to the as-welded stresses.

Investigations began to concentrate on the effect of residual stresses on fracture behaviour, and in a supplement of the Welding Journal of May 1949, T W Greene, [42], introduced a test procedure designed to evaluate the effect of residual stresses upon the mechanical properties of welded plates. He believed that previous investigations had not been fruitful in correlating laboratory results with known field and service conditions. This he suggested was due to the small size of specimens used for testing in the laboratory, normally of 4 to 6 inches, not allowing sufficient residual stress to be present in the specimen and that many tests were carried out above the yield point, so eliminating the effect of residual stresses anyway.

Greene's tests, [42], were carried out on semi-killed structural steel plate of 0.2%C and 0.51% Mn, in the welded state at temperatures below the Charpy V-notch brittle transition temperature. The size of specimen was 36 inch square, and he comments [42],

"In order that the welding conditions and the resultant stresses might be nearly comparable to field conditions, relatively wide weldments were used, 36 inch x ¾ inch. During welding, reproducible defects, such as notches and triaxial stress raisers, were introduced in the welds".

From service experience Greene introduced jewellers saw-cuts in the bottom half of the bevelled edge of a longitudinal butt weld in the wide plate, hopefully to simululate real service stress raisers. In later work by Wells, [43], such saw cuts proved to be "powerful initiations" of cracking, more effective than notches cut after completion of welding.

With Greene's work in all twenty six tests were made, and comparisons of as-welded and stress relieved specimens showed that as-welded plates developed fractures at bending stresses well below the yield of the material, while stress relieved plates sustained loads well above. It is interesting to note that one as-welded specimen fractured at - 32^{o}C during set up, before loading, implying failure occurred due to residual stresses in the plate only. With such evidence available from Greene's work, [42], it seemed large welded plates were the only practical laboratory correlation to yield conditions.

A report of the British Welding Research Association, published in 1956, [43], by Wells, described a 600 ton capacity loading machine which would accomodate 1 inch thick welded steel plate, of up to 36 inch width, see Figure 9.

The machine employed hydraulic capsules which produced extension of the plate resulting in a tensile stress longitudinal to the weld. Brittle fracture propagation was induced from the butt welds with transverse flaws in the form of saw cuts, which gave rise to crack propagation transversely into the plate.

Previous work by Greenspan, [44], and Irwin and Kies, [45], prompted Wells to use as large a plate size as practically possible, within the limitations of the loading capsules, [43]. The large plate size allowing a high storage capacity of stored strain energy to be available for crack propagation upon initiation or instability.

Wells, [43], decided to fix the size of the wide plate to 36 inches square, probably partly due to the experience of Greene, [42], and partly his own evaluation of the total amount of stored strain energy being available for crack growth. Wells, [43], estimated such a plate size would have three quarters that of an infinite cracked plate.

The use of Wells wide plate machine concept after 1961 includes studies at B.W.R.A. of crack arrest in varying grades of steel, effect of stress relieving on fracture strength, and the evaluation of sub-zero temperature fracture strengths in pressure vessel steel.

An additional machine was reported in 1961, [47], basically the same design as the 600 ton machine, but with a higher capacity of 2000 ton loading. This new tensile machine was primarily developed to test thicker sections, of the order of 3 inch thicknesses. Consequently, gas-cooled nuclear reactor steel could be tested by wide plate techniques also. Woodley, Burdekin and Wells, [48], in an assessment of steel at sub-zero temperatures, published in 1964 a B.W.R.A. report commenting,

"One of the most significant factors has been the development of the B.W.R.A. notched and welded wide-plate tensile test. It simulates actual structural loading and allows the effect of plate thickness, welding and stress relieving treatments to be investigated".

More recent studies involving wide plate testing have been the evaluation of design criteria for flaws in weld metal that is too tough for K_{IC} tests, [49], and an assessment of weldability with COD tests included, [50],.

In 1978, the Welding Institute published a research report examining the validity of the COD design curve approach for specifying defect acceptance levels in welded structures, [22].

A statistical comparison was made between the allowable flaw size predicted from small scale COD tests and the critical size at fracture in wide plate tests. The schematic procedure of calculation is given in Figure 10.

The report, [22], concluded that the COD design curve analysis is 97% confident of producing maximum allowable crack lengths greater than or equal to the critical crack lengths at instability of the wide plate test. This assessment was based on a sample of 80 wide plate and COD minimum test results on various materials at different temperatures, and therefore can only be considered as a limited guide with no consideration of whether COD is measured at fracture (with or without tearing), initiation of crack extension, or attainment of COD maximum load.

Kamath, [22], comments in recommendations for further study that resistance curve studies to confirm and clarify the extent of conservatism is necessary in relation to the definition of a critical COD value.

The prime assumption of the W.I. report, [22], is that the wide plate test is the closest approximation to criticality of a real structure. Unfortunately, one of the main drawbacks of the wide plate test technique is that no set standard of plate and notch configuration has been developed, numerous designs having been used in the W.I. analysis, [22]. Kamath, [22], adds to this general observation by assuming that wide variations in the safety factors evaluated between COD and wide plate crack lengths may be due to sampling of dissimilar regions in the bend and wide plate tests, as exhibited in heat affected zones.

Until further studies are made of standardised wide plate and COD resistance slow stable tearing instability comparisons, critical crack length analysis will not be possible using the COD design curve.

A general relationship of wide plate transition temperature to COD stiff transition toughness results is shown in Figures 11 and 12. This is taken from a Sumitomo steel research paper on steel plates for low temperature service, [105], characterised by a thermo-mechanical treatment in order to refine the grain size after reheating at the same temperature as for normalising.

The steel plates were of chemical composition shown in Table 1, with the wide plate test consisting of a cross-welded configuration to induce residual stress, with a submerged arc welding input of one pass at 45 KJ/cm on 20 mm plate thickness. The COD specimen heat input was similarly 45 KJ/cm and with 20 mm plate and a 0.1 mm radius mechanical notch.

It must be made clear that this reference, [105], is only a guide to relate the COD transition to the wide plate. Information of this type is limited because wide plate transition temperature analysis is extremely expensive and time consuming to do. Very few organisations are equipped to do wide plate testing, while the COD testing procedure is less costly and more applicable to industry via the COD design curve.

As shown in Figure 12 depicting the COD transition, two curves are displayed, obtained from Japanese and British Welding Institute data. The Japanese curve was evolved using a mechanical notch of 0.1 mm radius, while the W.I. curve utilised a standardised fatigue notch. The difference between the two curves is displaced by a temperature of about $25^{o}C$, the fatigue notch curve being lower in temperature than the mechanical notch. This temperature difference is attributed to increased constraint in the material by the sharper fatigue notch, the mechanical notch being effectively blunt.

The COD and wide plate notch is assumed to be in the weld metal-heat zone region, however the exact notch positions and configuration of weld-base metal interface is not known. Diagrams of notch positions are given in Figure 13.

The wide plate transition in terms of stress values in Figure 11 is manifested by a sharp rise at - $115^{o}C$ from low to yield stress failure instabilities. The low stress failures below - $115^{o}C$ are probably due to cleavage initiation and crack propagation caused by an inherent low toughness as the yield stress rises above the cleavage fracture stress. Above - $115^{o}C$ the failure points in terms of stress coincide with the yield strength, plastic yielding occurring in the plate section before fracture instability. Slow stable tearing crack growth prior to cleavage instability is therefore possible above - $115^{o}C$.

The temperature at which only plastic collapse occurs is unknown, but is envisaged by inspection to be above - 10°C. It is unfortunate that the wide plate failure strain versus load records are not specified, slow stable tearing or plastic collapse may then have been recognised in the tests, and these behaviour boundaries could have then been compared to the COD transition processes.

The residual stress distribution in the wide plate due to the cross welding will have a modifying effect on the fracture toughness and transition behaviour, the precise attentuation being dependent on the tensile and compressive residual stress distribution around the notch and in the plate section. The COD specimens will have similar residual stress systems, but will be attenuated due to smaller section size and controlled fatigue notching.

The steel tested in Figures 11 and 12, is not equivalent to BS4360 - 50D steel, but it is feasible to assume that the wide plate and COD transitions in 50D will be comparable. This situation may prove significant in the discussions to follow in thesis work related to compliant and stiff slow COD temperature transitions and the wide plate test, see Section 8.3.

In conclusion, even though the wide plate concept dates back to 1949, [42], it would seem to be the best compromise for fracture toughness "go-no-go" assessments at the present time in the YFM regime. The ability to simulate welded weld metal, heat affected zone, base metal and interface toughness characterisations together with residual stress distrihutions, as in real structures, is especially beneficial to the welding fabrication industry.

It is unfortunate that a set British Standard incorporating weld configuration, size. loading parameters and notch character has not been introduced. This is especially surprising with standards available for COD in BS 5762 DD19, [75], and comparisons made by the Welding Institute, England with respect to wide plate testing. The Welding Institute report, [22], depends solely on the wide plate critical notch size being equivalent to a crack length parameter, $\bar{a}_{crit}$, comparable to the COD design curve maximum allowable crack size, $\bar{a}_{max}$.

This correlation was drafted in British Standard draft reference WEE 37, "acceptance levels for welded plates" published for public comment in February 1976, and shown in Figure 14 of that draft, [106]. The final British Standard following WEE 37 was the present PD6493, 1980, [107], in which the same correlation is given in Figure 12. Even though this correlation has been accepted, because there are no standards directly controlling notch character for the samples of wide plate assessed by the Welding Institute report, [22], it is unlikely that the notches inserted in the plate have exactly the same constraint and local residual stress fields, apart from inaccuracies of notch tip location between the wide plate and COD specimens in the weld and base metal, as mentioned by Kamath, [22].

4.3 *The Witt Equivalent Energy Concept*

The wide plate test, see Section 4.2 previously, was developed to assess the toughness of welded structural steel plate, the large plate section size of 3 ft square being required to allow residual stress distributions and stored strain energy levels, similar to real service structures. A prime drawback of this technique in terms of design criteria is that the plate size is fixed and no direct relations of fracture toughness parameters such as J, COD, or K are presently practiceable.

A possible improvement in fracture toughness characterisation of real structures by laboratory specimens may be possible from work carried out by Witt, culminating in a research paper published in 1981, [68].

Basically, Witt detailed a method of predicting fracture for proportionally sized specimens by comparing volumetric energy, or energy per unit volume of specimen, to fracture in the LEFM regime. He proposed a simple relationship be established, between volumetric energy to fracture and specimen size, with which fracture behaviour for larger structures could be determined from small model fracture toughness tests, [69, 70]. For example, LEFM toughness values of K_{IC} could be evaluated using small specimens, such as instrumented Charpy, see Section 6.1 , whereas a much larger specimen size would be needed for a direct K_{IC} value valid to ASTM requirements, see equation (14) in Section 2.1, [68, 69].

For the Witt, [68], concept using volumetric energy in the LEFM regime, dependent factors are assumed to be only thickness and temperature, with little or no dependence of flaw size, loading or geometry.

The Witt methodology described is known as the "Equivalent Energy" approach to fracture, and is simply an empirical procedure for relating fracture in a structure to fracture in geometrically similar models.

The experimental evidence from Witt, [68], demonstrated the equivalent energy method to be applicable for brittle LEFM behaviour, with possible further expansion into the elastic-plastic yielding regime. However, in the yielding regime, certain phenomena questions the validity of the equivalent energy concept in its present form, for example, failure is operationally defined as the point of maximum load, but whether slow crack growth occurs in a stable ductile tearing manner before the point is ignored, [69]. In addition, because the concept is empirical in origin, its range of applicability in terms of ductile toughness assessment is not formulated yet, [69], and in the EP yielding regime with plasticity formation and stable tearing crack growth, the geometry, flaw size and loading machine/structural stiffness may affect the volumetric energy ratio to fracture or maximum load considerably.

4.4 *Effects of Externally Stored Energy in Fracture Testing by Compliant Loading Systems*

The effects of stored strain energy with variation of specimen size has been concentrated on in Sections 4.1, 4.2 and 4.3, and can be recognised as internally stored energy of the specimen. Another technique to supply increased stored energy to a crack tip in fracture testing apart from size increase is to decrease the stiffness of the loading system applying the load. If a spring is placed in series with the prime mover or cross head of a loading machine and the specimen, the equivalent compliance and stored energy available to the specimen crack tip is very high.

This technique of testing is gaining greater popularity in crack resistance studies, see Section 4.4.3. While specimens remain of constant size, variation of the effective stored energy available is possible by variation of spring compliance.

The loading system compliance could also be made similar to the service structures value, as propounded by Cotton, [65], and Hancock, [24]. Consequently, accurate assessment of ductile to cleavage instability fracture toughness testing with full service thickness plate could be possible in the E-P yielding regime, [27, 28, 29, 30]. This type of fracture testing approach could prove beneficial to develop critical flaw size relations using the COD Design Curve approach.

4.4.1. *The Work of Almar-Naess*

The first work carried out to test notch bend specimens using a variable compliance technique was by Almar-Naess in 1957, [29]. Internal and external energy was added to the specimen configuration by three methods:-

(1) The specimen arms were prevented from bending by sleeves, allowing only energy to be stored close to the notch in a small volume, internal energy of the specimen consequently being low; see Figure 14.

(2) The specimen arms were extended and allowed to deflect, so increasing the internal energy of the specimen; see Figure 15.

(3) A series spring was put with a short specimen, so introducing a high external energy, but small internal energy; see Figure 16.

Almar-Naess, [29], considered that if the total energy of the system was of a higher order than that of a shortened specimen length, this energy would be available for the fracture process, partly or fully.

The loading arrangements used showed a definite influence on the mode of fracture, the spring system and increased length of specimen arms moving the transition temperature curve up in temperature. For a given temperature in the transition range, it was found that the deflection before fracture instability was less with the spring in series, see Figure 17. Since deflection of a notch bend specimen is roughly proportional to the crack tip COD, decreased deflection corresponding to higher stored energy content would infer lower maximum COD values.

This reference therefore has important implications in this thesis.

The principal conclusions in the Almar-Naess, [29], paper were:-

(a) The maintaining force (or driving force) of a crack propagation condition can be supplied by internal specimen energy.

(b) The transition temperature of a metal is influenced by the response of the testing machine, a soft or high compliance machine giving a higher transition temperature than a stiff one.

(c) Whether a service fracture is likely to go brittle is not only dependent on the static stress distribution around the fracture, but equally on the stiffness of the entire structure.

If a ductile crack develops in a stressed member, it often stops because the change in geometry due to plastic deformation makes other stress members take over part of the stress. When there is a high strain energy release in the structure, it may, however, be suggested that the ductile initiation is more likely to change to a brittle and catastrophic fracture.

The work of Almar-Naess, [29], is significant to the present thesis because he studied the effect of internal and external stored energy on a structural steel in the transition temperature range. The decrease in allowable specimen deflection at a given temperature for increased external stored energy from a spring, can be assimilated to lower COD values.

This information gives considerable weight to the conviction that differences occur between COD transition temperature values using stiff and compliant loading systems.

In addition, the conclusions of Almar-Naess, [29], in category (c) as described previously, are directly in accordance with the postulates of De Leiris, [64], related to compressible fluid containment by large pressure vessels and the materials ductile to cleavage instability point - high amounts of stored energy content inducing a higher probability of cleavage instability in a ductile steel.

It is interesting to note that the De Leiris and Almar-Naess references were published as early as 1949 and 1957 respectively, however the significance of their work is only just beginning to be realised in relation to structural steel behaviour and elastic-plastic COD testing techniques.

Their work may be an important step towards evaluating critical crack lengths in the yielding regime by the COD design curve approach, instead of a "conservative" maximum allowable crack size as presently predicted.

4.4.2. The Glucklich Approach

In 1959, Glucklich, [66], studied the effect of sustained loads by a high compliance/high stored energy supply loading system, using a spring in series with the loading crosshead. He showed a decrease in the "strength" and ductility of concrete for increasing compliance, simply meaning a reduction of the fracture toughness, and postulated that the effect could be present in a ductile steel.

A further paper by Glucklich and Cohen, [67], in 1967 mentioned further evidence of the effect of high stored energy reducing toughness in plaster of paris and concrete.

In the 1967 paper, a hypothesis was put forward, [67], examining the driving force for stable fracture working against the crack growth resistance, it will be explained here because of its directness and simplicity of approach.

If we look at the condition of a stable growing crack in a real material with reference to the driving force for crack growth and the crack tip resistance or restraining force, we find that the "R-curve" presentation of the forces displays kinks and breaks, due to inhomogeneities, Figure 18.

If the crack encounters a grain if a dispersed phase harder than the matrix, the energy demand curve should show a bulge, since the cutting through the grain, or by passing it, energy absorption per unit effective propagation distance is achieved.

Once clear of the obstacle, the curve resumes its previous course.

When a void is encountered, the energy demand curve should show a trough. Most important in this context are satellite voids or cracks in the line of advance of the major crack. The diagram in Figure 19 demonstrates these effects in terms of energy demand and driving force.

As shown in Figure 20, if the system compromising the specimen is so rigid as to contain limited or no stored strain energy, the restraining force is always greater then, or equal to, the driving force. Equilibrium is maintained by this balance, and when the resistance to propagation is reduced suddenly, the driving force will similarly decrease. When the loading system is flexible, however, and considerable stored strain energy is available, a sudden drop in resistance is not followed by a corresponding decrease in the driving force. In fact, the unlimited energy content ensures the driving force never drops below the level, once reached by it. Also, whenever a lapse in resistance is encountered, the energy release rate exceeds that of energy demand, equilibrium breaks down and acceleration takes place.

In 1970, a detailed technical report by Glucklich, [27], was published by NASA describing the strain energy size effect for various materials, including glass, concrete and steel. Basically, the report was a summary of references which re-appraised experimental research data related to size effects.

With respect to ductile steels, it was postulated that slow stable tearing is a process of unstable equilibrium, so that instability and consequent fast cleavage fracture can be easily induced by momentary overloads at the crack tip, in high stored strain energy systems.

Glucklich, [27], summarised the following conclusions with respect to a size effect on fracture toughness:-

(1) The size effect is observed in a great number of metals from the viewpoint of fracture toughness.

(2) In brittle materials it is easily observable, but in ductile metals a condition must first be fulfilled to convert the ductile failure to one of crack propagation, e.g. a notch with triaxial stress, high strain rate or low temperature.

(3) The three dimensions of the specimen contribute to the effect, but the relative importance of these has not yet been determined.

(4) The thickness giving rise to multi-axiality of stress is only operative as a size effect within the limited range of the plane stress to plane strain transition.

Glucklich, [27], also gave emphasis to consideration of the effects of stored strain energy alone affecting fracture toughness:-

(5) The change from stable to unstable crack growth on a fracture surface is clearly visible, with evidence of stable crack tearing existing in smaller specimens, while being absent in larger specimens.

(6) Fracture instability in large specimens is explosive and relatively unannounced, in smaller specimens fracture is accompanied by an initial low intensity tearing sound.

(7) The size effect is dependent on the coarseness and heterogeneity of the material.

(8) Superposed tensile stress affects the transition temperature of V-notched impact bend specimens, (after Fearnehough, [63]).

Glucklich, [27], postulated the level at which size ceases to affect fracture toughness varies for different materials, increasing with the ductility, but interfering factors such as triaxial stress from notches, temperature and strain rate may obscure this tendency.

The conclusions of Glucklich, [27], added to the work of Almar-Naess, [29], are relevant to the present thesis work since the presence of a stored strain energy effect upon fracture toughness, during slow stable crack growth in steel, would suggest that BS4360 - 50D structural steel is prone to this phenomenon, (as will other types of structural steel).

4.4.3. *The Paris Tearing Modulus Theory*

Paris et al, [28], in 1979 published important work outlining the effect of stored strain energy upon fracture behaviour in the elastic-plastic regime, investigating the instability point of the slow stable tearing mode.

The analysis utilised a J-integral R-curve diagram, Figure 21, with which J is plotted against stable crack growth by tearing, Δa. The J-integral itself simply describes the rate of potential energy per unit thickness absorbed during crack growth, and is similar in concept to G, as explained in Section 2.1. The R-curve shown in Figure 21 is an approximate construction using mean straight lines, initially showing crack blunting from a fatigue notch, then gradual stretching until void coalescence gives way to a stable ductile tearing crack growth. This type of behaviour is present for ductile steels above its ductile to brittle transition temperature, [25, 28], below the transition temperature cleavage initiation proceeds tearing.

Paris, [28], gave attention to the stable tearing portion of the R-curve, and examined the balance between the stored strain energy of a specimen to its increase in J per crack extension.

The analysis assumed instability to cleavage from ductile tearing would occur when the magnitude of the specimens elastic shortening was greater than the corresponding lengthening. Thus:-

$$\text{Instability occurs if } d(\Delta L \text{ ELASTIC}) \geq (\Delta L \text{ PLASTIC}) \qquad (15)$$

and for a centre-cracked strip plate in tension,

$$\text{where } d(\Delta L \text{ ELASTIC}) = \frac{-2.\sigma_o . da . L}{WE} \qquad (16)$$

$$\text{and } d(\Delta L \text{ PLASTIC}) = \frac{dJ}{\sigma_o} \qquad (17)$$

$$\text{then} \quad -\frac{2.\sigma_o.da.L}{WE} \geq \frac{dJ}{\sigma o} \qquad (18)$$

and rearranging,

$$\frac{dJ}{da} \cdot \frac{E}{\sigma_o^2} \leq \frac{2L}{W} \qquad (19)$$

where σ_o = Flow stress $\approx \left\{\frac{(\sigma_{yield} + \sigma_{ultimate})}{2}\right\}$

da = Increment of crack growth

L = Specimen length

W = Width

E = Youngs' Modulus

The L.H.S. of equation (19) depends on material properties dJ/da, which is determined from the tearing slope of the J-integral R-curve and is named the "Tearing Modulus", after Paris, [28].

An equivalent equation may be developed by using COD, δ, instead of J-integral, and the present author has evaluated the tearing modulus instability relation for a 3-point notch bending situation in Appendix A of this thesis.

The tearing modulus instability approach by Paris, [28], is the first attempt to quantify and eventually predict tearing instability for a given elastic stored strain energy or compliance content, during slow-static loading.

Experimental evidence, [73], supported the tearing modulus concept, and three main conclusions were developed:-

(a) Tearing instability in notch bend tests was slower to occur under fully plastic plane strain conditions.

(b) Tests varying the compliance of the loading system showed a transition from stable to unstable behaviour for increasing compliance.

The experiments carried out by Paris, [73], used a compliant spring loading configuration as shown in Figure 22. In essence, the work was an updated version of Almar-Naess's work, [29], utilising the elastic-plastic fracture parameter J, and tried to quantify the point of tearing instability by a semi-empirical approach by assuming the tearing modulus, T, was a material property.

A low tearing modulus value would indicate a high probability of tearing instability, but this would be dependent on the mode of testing, for example whether 3-point bend or double cantilever beam.

The tearing instability relation in equation (19) does not contain the crack size dimension a. This is in contrast to the LEFM initiation criteria of equation (13). The absence of the crack size in the tearing modulus equation (19) occurs since it is an investigation of the balance between the elastic energy driving force remaining after a given amount of ductile crack extension, and the plastic relaxation. If the elastic energy remaining is high per extension, then the stable dynamic equilibrium at the crack tip is lost and cleavage instability may occur.

In the LEFM approach, equation (13) shows the crack length determines the stress intensity factor of the crack tip stress fields, which in turn will allow the Griffith, [5], energy criterion to be satisfied, and unstable cleavage will occur.

The tearing modulus theory by Paris, [28], is therefore of enormous significance recognising that instability from ductile to cleavage crack growth is a function of the materials' tearing modulus (or tearing resistance energy with respect to a given crack extension) and the loading system or specimen compliance and stored strain energy content.

4.4.4 *The Practical Use of the Tearing Modulus Approach*

In a recent paper, 1981, sponsored by the Electric Power Research Institute (EPRI) of America, [104], viable parameters to characterise crack initiation and continued extension were investigated. The work was related to effects of flaws and the safety margins of pressure boundary components of light-cooled type nuclear steam supply systems.

The work exploited the consequences of the Paris, [28], approach to material resistance with stable growth and eventual instability, investigating the J-controlled crack growth and driving forces as determined by elaborate deformation plasticity analysis via a finite element model.

The general conclusion was that an engineering approach to treat crack growth and onset of instability in flawed structures, using the J-integral R-curve and driving force approach, was simple and readily employable in design applications and margin of safety analysis. It must be realised however, that this analysis was designed for crack growth and instability at higher temperatures elevated from the ductile to brittle low temperature transition, where this thesis will concentrate. In addition, the EPRI paper, [104], mentions that a tearing modulus based on COD could be an attractive alternative to J-integral testing, (see Appendix A), using,

$$T_\delta = \frac{E}{\sigma_0} \frac{d\delta}{da} \qquad (20)$$

It is envisaged that this type of approach will gain greater popularity in the next few years.

Until further development is preceeded with, in relation to the Tearing Modulus approach, either by J-integral or COD, especially in the ductile to brittle transition temperature range of a structural steel, information and data to build a critical flaw size approach in the ductile tearing regime will remain limited. A likely method of analysis could involve the Tearing Modulus in terms of COD and the COD design curve, thus enabling laboratory fracture toughness testing with variable compliance loading machines allowing instability COD assessment, and translating this data to a critical flaw size value via the COD design curve at a given temperature.

5. *Introduction to the COD Approach Used in This Thesis*

The COD test and design curve approach provides a link between the applied conditions of stress or strain, the material and the defect just as K_{IC} does for LEFM, see Section 2.1. The technique is important for evaluating toughness and assessing the significance of defects in low and medium strength engineering metals in the elastic-plastic regime.

Before the COD development is derived and studied in detail, the main considerations for the use of the approach in this thesis will be explained. It must be remembered that an elastic-plastic toughness parameter is only required to ascertain if decreased in toughness occur when high amounts of stored strain energy or compliance are present in a loading system. From the literature in Section 4, this would seem logical, but direct tests are required on structural steel BS4360 - 50D.

The prime considerations in using the COD approach for fracture assessment in this thesis is as follows:-

1) The COD value reflects the concentration of strain at the crack tip, such a criteria is most suited to describe ductile fracture.

2) COD would appear from 1) to be relevant in describing ductile stable crack growth if present.

3) The COD approach is popular in England, especially for welded constructions, and is becoming increasingly used world-wide, with British and American standards.

4) Slow and impact loading COD procedures are similar, with a British Standard to be drafted for impact testing, [74].

5) In terms of equipment and testing, the techniques developed for this thesis are simple, but adequately comprehensive for analysis.

6) The results from this thesis can be compared directly with COD results of previous works.

7) There are certain disadvantages with the COD technique, but no present E-P parameter is perfect, and a large amount of experience has been gained since COD's inception in 1961-1963 period, [14, 17].

8) It is generally accepted that COD is used and understood more in the structural industry than any other parameter, except for K in LEFM for high strength alloys, [14].

5.1.1. *The Derivation of COD*

It is not the intention of this thesis to argue the pros and cons of the COD method, but to use the testing technique in the results package to follow in Section 8. A short derivation of COD will be made here, outlining the important details to the concept.

The COD approach to yield fracture mechanics was proposed by Wells in 1961, [9]. In 1963 Wells published a more detailed appraisal of the theory, [10], based simply on the analysis of superposing the effect of a plastic zone at the crack tip in relation to the yield stress of the material, with the equatio .s of stress, strain and displacement developed by Westergaard in 1939, [87].

The most widely known and used analytical model for simulating the effects of plastic deformation ahead of a crack is the strip yield model, [88, 89], from which COD can be derived. This approach is often recognised as the "Dugdale Strip Yield Model", [88].

By combining the crack stress intensity factor to the opening displacement equations developed from Westergaard-type stress fractions, [88], the COD at the crack tip is given by,

$$COD = \left(\frac{8 . \sigma_{ys} . a}{\pi E} \right) \log \sec \left(\frac{\pi \sigma}{2 . \sigma_{ys.}} \right) \qquad (21)$$

A series expansion of log sec yields,

$$COD = \frac{8.\sigma_{ys}.a}{\pi E}\left\{\frac{1}{2}\left(\frac{\pi\sigma}{2.\sigma_{ys}}\right)^2 + \left(\frac{1}{12}\right)\left(\frac{\pi\sigma}{2\sigma_{ys}}\right)^4 + \right. \tag{22}$$

As long as σ is small compared to .

$$COD = \delta = \frac{\pi\sigma^2 a}{E.\sigma_{ys}} = \frac{G}{\sigma_{ys}} \tag{23}$$

which is the same as developed by Wells in 1963, [10], apart from a factor $4/\pi$, which was shown to depend upon the choice of the plastic zone correction.

In general then,

$$COD = \delta = \frac{G}{\lambda.\sigma_{ys}} = \frac{K_1^2(1-\nu^2)}{E\lambda.\sigma_{ys}} \tag{24}$$

where the factor $(1 - \nu^2)$ can be deleted for plane stress situations.

The value of λ depends on the exact place where the COD is determined, or in other words, which place is considered as the crack tip. Values of λ vary, but reference is given to Robinson and Tetelman who found λ to be unity, careful measurements being made by silicone rubber infiltration, [90]. Other values of λ vary from 1.27 to 2.14, [91, 92, 93].

5.1.2. *The Practical Measurement of the COD Value*

The COD testing method is specified in the British Standard BS5762 DD19, [75], and has been used to characterise fracture toughness in the linear-elastic and elastic-plastic regimes. The basic technique involves evaluation of the crack opening displacement at the original crack tip, [76], usually by clip gauge measurements of surface displacements at the crack edges, then converting these displacements to values at the crack tip using a geometric ratio formula, [75].

Other methods have been used including photography, [77], and rubber compound infiltration into the crack tip, by permitting it to set while the specimen is maintained under load, [78]. Additionally, some success has been shown in making measurements in the scanning electron microscope of the stretch zone at the crack tip, [79], but this technique is limited.

The COD test investigates fracture initiation, as are those for K_C and J_C, and has been widely used in the offshore industry.

The main application of COD is in the field of welded structures, pressure vessels and other structural components, of how to medium strength. Such materials exhibit a ductile to brittle transition range of temperature, which can be of extreme significance in structures for offshore, liquid gas and arctic conditions, [80, 81], see Figure 23.

For relatively brittle materials on the lower shelf and for structures subjected to essentially elastic stresses, LEFM is applicable and toughness is measured in terms of K_{IC}. In the transition regime, yielding fracture mechanics based on COD and J is applicable. On the upper shelf, failure in structural steels is generally controlled by plastic collapse and it will be sufficient to ensure that the net stress does not exceed the flow stress, however in this regime assessment of the resistance to ductile crack extension by void coalescence using R-curve concepts may be necessary, [14].

The early tests for COD used testpieces being notched, but not fatigue cracked, the notches being prepared by a fine jeweller's saw, as used for wide plate testing, see Section 4.2. It was soon appreciated that the use of a fatigue crack was essential, so that the notch acuity would match that of an actual crack in a structure, and to maintain continuity with the K_{IC} test.

The experimental formula used to calculate the COD at the crack tip, using the crack mouth opening measurement, assumed that the specimen rotates about a fixed point one third of the distance down the remaining ligament ahead of the crack tip. The COD is then calculated by a simple geometric relationship of similar triangles, see Figure 24.

Experience showed that this manipulation was simplified, [82], the point of station moving initially from close to the crack tip, to a point half way through the ligament as maximum load and collapse was approached.

The present BS5762 formula, as developed by Dawes, [83], recognises the movement of the station point to a certain degree, and comprises an elastic component which stems from the connection between COD and the crack driving force G.

COD is given by,

$$\delta = \delta e + \delta p = \frac{K^2(1-\nu^2)}{2.\sigma ys.E} + \frac{0.4\ (W - a)\ Vp}{0.4\ W + 0.6a + Z} \qquad (25)$$

Also,

$$G = m\,\sigma ys\,\delta = \frac{K^2}{E} \qquad (26)$$

Dawes, [83], assumes m = 2 with regard to the elastic component.

The distance to the hinge point from the crack may be expressed by r (W - a), r approaching r_p at collapse, which is the plastic component of the rotational factor, r = 1/12. Various values of r_p have been reported within the range 0.45 by Wells, [84], 0.4 by Dawes, [85], and Kanazawa et al of 0.33 → 0.42, [86]. British Standard at present specifies Dawes value of r = 0.4.

5.1.3. *Definition of the Type of COD Measured*

The COD value thus developed is a measure of toughness, the higher the COD value, the greater the toughness. Unfortunately, such a clear proposal is misleading, laboratory scale COD tests may not exactly relate the "toughness" of a real structure. Difficulties of interpretation of the COD test load-displacement record causes ambiguity in assessing the significance if a given COD value, [14].

This occurs with the behaviour of the structural steel in the transition temperature range, changing from brittle-elastic at lower shelf to tough-plastic at upper shelf and plastic collapse temperatures.

The BS5762 COD standard recognises a member of definable COD values, which may or may not be significant for a given service condition and structure. These include δc, δi, δu and δm, explaining CODs for initiation of cleavage, initiation of ductile stable tearing, initiation of cleavage fracture after stable crack growth and maximum load plateau respectively.

The value of δc is without question, since it simply originates from an elastic cleavage instability of the steel.

Initiation of stable ductile tearing at δi relates the measureable value of COD δ at which a ductile crack is formed by void formation and coalescence ahead of the crack tip. The behaviour of propagating tears are at present under considerable study, [94, 95, 96], and there is a general view that events at the tearing tip after initiation are affected by geometry, [14].

From reference to works by Docherty, [58], Almar-Naess, [29], Glucklich, [27], and Paris, [28], the balance of the driving force to absorbed energy during slow stable crack growth is highly critical, and if instability were to occur when the driving force momentarily exceeded the crack resistance, then cleavage crack run could occur. The micro-mechanism growth process at the stably growing crack tip must also be beneficial to the transfer from ductile tearing to fast cleavage fracture, [25, 26].

In terms of a defined COD value, this point of cleavage instability transfering from a slow stable ductile tear is equivalent to δu. The point of tearing instability has also been shown to be dependent upon the initial crack size, [25], or by analogy, the ligament remaining in a notch bend situation, [28].

In some cases instability of the ductile tear transforming to a cleavage run may take place, but the length of the run distance or "pop-in" is small due to a deficiency of stored energy to run the crack. If the "pop-in" is below a certain magnitude, then the clip gauge transducer may not detect the coincident displacement at the specimen surface. For this reason the exact value of δu can be open to question, dependent on the specimen size, geometry, loading system compliance and displacement transducer sensitivity ratio.

The importance of the above concept is extremely significant to a stable tear condition in a real full size structure, with which high levels of stored strain energy and compliance may be present in a determinate structure, [28].

The laboratory scale test for COD on a stiff machine may show a displacement record up to maximum load plateau δm, however in the real structure the true value of instability and fracture may be closer to δu, considerably before δm.

The Welding Institute, England, at present state that use of maximum load COD values from standard specimens and loading configurations (stiff systems using displacement control), may be used with confidence to give conservative predictions of structural steel behaviour, [14, 22]. They suggest the use of δi is unnecessarily over-conservative and invariably δu or δm may be used without loss of safety, [14, 22]. Towers and Garwood, [96], further justify the use of maximum load COD values for design criteria of real structures from their observations that the deeply notched bend specimen has a low tearing resistance R-curve with a steep and dominant driving force. Garwood, [97], later speculated that it may be necessary to impose specific specimen size limits on the maximum load validity, ensuring sufficient constraint is present in the specimen cross section.

Until further analysis effectively models the relationships of δc, δi, δu and δm with unstable fracture in real structures, a controversy will still exist on the particular value of COD that should be used to define a critical condition.

5.1.4. *Effects of Strain Rate and Thickness on COD*

In addition to the effect of temperature on the maximum COD value, strain rate and plate thickness may attenuate the toughness measurement of a material as measured by the COD technique.

The influence of loading strain rate depemds on the plastic deformation properties of a material, and strain rate sensitive materials such as structural steels show effects of this in terms of the ductile to brittle transition temperature, Figure 25. An upward shift in temperature due to increased strain rate can be as large as 30^{o} to $80^{o}C$, [14, 25], dependent on the material.

The increase in temperature of the toughness transition due to the higher strain rate is caused by the rate-sensitive metal having less ability to yield, in steels this is manifested by reduced plasticity from an increase in the relative yield stress, [25]. In addition, for a dynamic propagation condition, a rate-dependent material may show a decaying R-curve, [25], implying the absorbed energy for propagation is less at higher deformation rates.

Recently, proposals for dynamic toughness measurement have been published by the UK Briefing Group on Dynamic Testing for the I.I.W., [74], which includes consideration of dynamic COD testing. However, the report comments that the significance of existing impact and other high strain rate test techniques is not fully clear yet, with respect to industrial use and applicability. Until a full British Standard is accepted, then impactive COD testing developments are still required.

The thickness of plate can influence the state of stress in the plate section, the plastic zone size being affected by the allowance for yielding. If yielding is prevented in the thickness direction, the plastic zone size is small and in a state of plane strain or triaxial stress. With increasing constraint in a section of material, the effective COD value will decrease, reducing the relative toughness of the plate section.

Generally, cleavage resistance is decreased by constraint and plane strain, however resistance to the initiation of ductile tearing is relatively unaffected by such cleavages. This is to be expected in the case of ductile tearing, due to its dependence on local strain for microvoid coalescence and growth, McClintoch, [99], as opposed to the cleavage stress-dependence. Consequently, in terms of COD definable values, δc is dependent on thickness, while δi is believed at present to be independent.

The industrial use of the COD concept relies on ensuring that the constraint in the testpiece is as great or greater than that in the real structure. BS5762 requires COD tests to be carried out on full section thickness of interest, thus ensuring the constraint is sufficient for reliable test data. In addition, a high level of constraint is achieved with the deeply notched preferred geometry testpiece which is used extensively in construction type applications.

5.1.5. *COD Scatter and Sampling Considerations*

As with all elastic-plastic test procedures investigating toughness, a major problem in applying the COD method is the Variability in data. This reflects the variation in notch-material-specimen behaviour.

The conventional technique to obtain a useable COD value is to test three specimens at a given temperature, thickness, crack length and strain rate. The minimum value of the three is then used as a basis for accepting a material on welding procedure, or for assessing the significance of defects.

There is a growing opinion that three tests are inadequate in terms of statistical studies made by Johnston, [100] and Kamath, [22]. Kamath, [22], recommends the sample size for COD testing be increased from three to six or even nine specimens, so increasing the confidence of the COD design criteria to be used in a structural situation.

Obviously, COD testing becomes more expensive for a larger sample size, while Harrison, [14], states it will seldom be possible to perform enough tests in any particular case to establish the true statistical nature of data.

Johnston, [101], indicates that the scatter of COD results is particularly pronounced in the ductile to brittle transition zone. Consequently, the sample size will have a much lower confidence level if the design temperature for testing coincides or is close to this transition. To overcome this possibility, it would be required to test a limited number of specimens over a temperature range encompassing the minimum design temperature, in this way the user would have some idea of the closeness of the transition to the minimum design temperature. Sample sizes may then be more accurately decided upon to ensure a high confidence of the data and a cost-effective study.

5.2. *The COD Design Curve and Industrial Usage*

Having obtained a COD maximum load value from a B.S. testpiece, the next problem facing engineers is to convert the laboratory test data into a criteria for design of a structure, ensuring failure by fracture is reduced to a very small probability. A relationship is required encompassing the defect size, applied loading conditions, and the material properties.

Finite element or numerical methods are possibilities of assessment for the future, however at present such techniques are usually too costly, very complicated and prone to unacceptable variations in accuracy, [102]. The most popular application of COD to design criteria is achieved by the "COD Design Curve", which is basically an empirical relation involving considerable conservatism in the analysis to ensure safe design, see Figure 26.

Recently, criticisms from industry has stemmed from the possible over-design incurring excessive costs for construction, [22]. Until improvements in the selection of relevant COD data from laboratory tests to real structures is achieved, controversy will remain with the use of the "conservatism" inbuilt in the COD design curve.

A prime limitation of the design curve's conservatism is that it predicts a maximum allowable flaw size, and not a critical one with the actual margin of safety not strictly defined. As more development of elastic-plastic behaviour is introduced in relation to real structures, a critical value may be possible.

The concept of the design curve utilises the maximum load COD value from laboratory tests to be non-dimensionalised and related to the strain levels to be operative in the full size structure, and within the requirements of the strip yield model, an estimation for the tolerable flaw size in a yielding situation is evolved. This procedure was introduced by Burdekin and Stone, [103], in non-dimensional form,

$$\frac{\delta}{2 \pi e_{ys} a} \qquad (27)$$

and relating non-dimensional COD, ϕ, to overall strain e / e_{ys} from the present COD design curve specification,

$$= \frac{e_1}{e_{ys}}^2 \quad \text{for} \quad \frac{e_1}{e_{ys}} \leq 0.5 \qquad (28)$$

and

$$= \frac{e_1}{e_{ys}} - 0.25 \quad \text{for} \quad \frac{e_1}{e_{ys}} > 0.5 \qquad (29)$$

where e_1 represents effective strain, including residual stress and concentration effects; and $\bar{a}$ is the half crack length.

The Welding Institute report that the design curve encompasses a safety allowance of 2 to 2.5 for the allowable flaw size predicted, [14]. A recent survey by the Welding Institute, [22], which examined the relation between the allowable crack size predicted from small scale COD tests and the critical crack size at fracture in wide plate tests, showed an average safety ratio of 3, with a 96.7% probability of the allowable size predicted being less than or equal to the critical crack size in the wide plate. This statistical information was based on a sample size of three, while using the lowest COD value of the sample. If the mean COD value was used for the same sample size, a reduction in the safety ratio occurred to 2.3 and the probability of the correct flaw size went down to 91.6%. From this information a mean COD approach was not recommended.

The study also demonstrated that an acceptable margin of safety was obtained using the maximum load plateau COD values, δm, as opposed to the stable tearing initiation COD, δi, giving extra weight to the suggestion that δ_{max} values need only be used to generate design criteria.

In essence, the COD design curve is a quick and unified design approach which can be safely used in a variety of structural applications, unfortunately this produces the major drawback of the technique in terms of safe design criteria. In some circumstances of construction the COD design curve procedure may be over-conservative, evolving over-spending for no measurable increase in safety, on the other hand there may be other applications where much stricter control is necessary. For example, as postulated by De Leiris, [64], Cotton, [65], and Glucklich, [27], with allied experimental evidence from Almar Naess, [29], and Paris, [28], the point of tearing instability after δi may be affected by stored strain energy availability, so pushing the ductile to brittle transition temperature up, and increasing the discrepancies possible between laboratory COD data and a real high stored strain energy structure.

Gas pressure vessels and pipelines are prime examples of this problem. An indeterminate structural design utilising redundant safe bearing members may additionally transform through damage or simply service conditions into a determinate high energy system. "Wear and tear" of this type has been reported officially and uniformally in the North Sea oil platform domain, certain circumstances reported by Cotton, [65], and by verbal course discussion.

6. *Review of Dynamic Toughness Testing Concepts Applied to Structural Steels*

The following section deals with fracture toughness assessment using dynamic impactive loads to initiate crack propagation in steels. Emphasis is on the practical use of the testing techniques, and its applicability to structural steels.

Since a low to medium toughness structural steel has a definite strain rate sensitivity on the material yield stress, increasing for higher strain rates by approximately 1.0 to 2.2 times the static value, below yield fractures can be produced which are effectively linear-elastic in character. This situation is made use of for K_{id} dynamic fracture toughness evaluation, even though some approximations must be made and some liberties taken with the fracture mechanics analysis.

It is usual to find the value of K_{id} obtained at Charpy impact strain rates of $200^{s\ -1}$, to be lower in stress intensity factor than the static K_{IC} value up to about + $20^{o}C$, dependent on type of steel. This condition can be viewed as an advantage in terms of conservatism of the toughness evaluated. However, a principal drawback is knowing how much of the elevated static toughness, K_{IC}, above the dynamic, K_{id}, is due to a genuine material increase in plane strain toughness with temperature, and to what extent the departure from an effective plane strain condition is due to yield stress drop with increasing temperature and decreasing strain rate. This situation is of special significance with respect to defect assessment.

The use of COD and J-integral techniques for defect assessment, even though using empirical relations for application to real structures, are more defined in terms of increasing material toughness.

The use of larger scale drop weight testing has similar inherent disadvantages from using the rate sensitivity effect of structural steels. A main assumption of this type of testing is that "limit severity" conditions are applied to the steel, and that the data obtained is for the worst conditions possible at a sharp crack tip in a rate-sensitive steel, namely high strain rate and (if possible) full thickness of service and metallurgical conditions after welding.

6.1. *The Charpy Impact Test by Standard V-Notch and Fatigued Crack Kid Evaluation*

One of the oldest material testing techniques used for relative toughness assessment is the Charpy impact test. The method dates back to 1905, Charpy Keyhole and Charpy Vee being the two main variants, of which the Keyhole test was judged to be totally inadequate as a generator of toughness values due to its excessively blunt notch.

The Charpy Vee technique is now also recognised to be unacceptable as a definitive view of the fracture behaviour that would be present in structure containing sharp flaws, and does not accurately define the shelf level toughness and the transition temperature range. Furthermore, there is no way to determine the fracture load and hence the dynamic fracture toughness parameter K_{Id} from a conventional Charpy test.

The Charpy method is however popular because of its cost-effectiveness to evaluate relative toughness by absorbed energy measurement for production quality checking, alloy development, neutron irradiation studies, general weld toughness assessments etc.

Fearnehough and Hoy, [108], used gauges on the pendulum and analysed their results in terms of time to fracture and the effective load, see Figure 27. However this method was still limited since the test did not produce below yield fractures, except at very low temperatures, and such information was therefore not readily applicable to service behaviour, nor could it be linked to other brittle fracture test methods.

Fearnehough and Nichols, [109], were able to show that derivation of the dynamic equivalent of K_{IC} stress intesnity factor could only be calculated at temperatures where fracture occurs at or below general yield.

This information prompted the development of modified Charpy specimens utilising pre-fatigue cracking and in the case of Radon and Turner, [110], added 0.02 inch deep side grooves. The temperature at which fracture starts to occur at general yield was markedly increased; for mild steel tested by conventional Charpy V specimens gave above yield cleavage from - 40°C upwards, whereas the fatigue cracked-side grooved specimen gave above yield cleavages

up to + 20°C, [110].

In effect, the below dynamic yield fracture where LEFM could be applicable was brought to a temperature of direct everyday engineering interest for steels.

The value of dynamic stress intensity factor K_{id} using the pre-fatigued Charpy specimen could be evaluated by assessing the fracture load by an instrumented tip or strain gauged specimen, [109, 110, 111, 112, 113], and used the fracture mechanics formula for three-point bending, [114],

$$K_{id} = \frac{6\ Y\ M}{B\ W^2}\ a^{\frac{1}{2}} \qquad (30)$$

where:-

M = The applied moment at fracture pop-in, when fracture occurs before general yield.

W = Width

B = Thickness

a = Total crack depth

using the Y correction factor of:-

$$Y = 1.93 - 3.07\left(\frac{a}{W}\right) + 14.53\left(\frac{a}{W}\right)^2 - 25.11\left(\frac{a}{W}\right)^3 + 25.8\left(\frac{a}{W}\right)^4 \qquad (31)$$

The technique has however certain disadvantages, a prime consideration being that the dynamic response of the notch bend specimen in 3-point mode is prone to loading inertia resistance and added vibrations which may confuse the accurate assessment of the load and moment at fracture pop-in.

In addition, contact between the pendulum and specimen may be lost due to flexure, inducing bounce effects, the stiffness of the striker also affecting the magnitude and time to reach first peak loading on the specimen, [115].

Basically, the Charpy-type K_{id} method utilises a steel's strain-rate sensitivity which induces a condition which closely staisfies the linear-elastic mathematical model, but the small size of the Charpy specimen does not usually meet the ASTM criterion for minimum size to assess plane strain fracture toughness of low to medium strength steels, see Equation (14) in Section 2.1. This situation can cause fundamental problems in the assessment of whether changes in effective toughness evaluated from the dynamic stress intensity factor K_{id} are genuine increases in the plane strain toughness, for example it is difficult to establish the extent of departure from plane strain conditions as yield stress drops with increase in temperature and decrease in strain rate, [25, 115].

A given toughness value of K_{id} is relative to the specific impactive strain rate used in the test, and would be apparently applicable to structures which are susceptible to similar loading rates. Simplified estimates of loading rates in tension is given in Table 2, from proposals by the UK Briefing Group of the I.I.W. on Dynamic Testing, [74].

The variation of K_{id} for steel in relation to the strain rate is greatest at high and low strain rates, Radon and Turner, [110], also suggest that by coincidence, the straining rate of a Charpy-type test of approximately $200s^{-1}$ or K of 2×10^6 Ksi$\sqrt{in}/S$ (2×10^6 MN/m$^{3/2}/S$) achieves the minimum or lower trough of the toughness versus strain rate response, Figure 28.

In certain circumstances, as for example with tests on A-533B pressure vessel steel, [116], K_{id} toughness using Charpy pre-fatigued specimens was found to be lower than slow-static K_{IC} toughness values representing valid ASTM plane strain fracture criterion in equation (14), see Figure 29. This situation may not apply with all steels exactly, but a rough guide to K_{id} values of low strength structural steels is 30 Ksi$\sqrt{in}$ (33 MN/m$^{3/2}$) at - 60^{o}C rising to 55 to 60 Ksi $\sqrt{in}$ (60 to 66 MN/m$^{3/2}$) at 0^{o}C, [25, 115, 116], see Figure 30.

At present, no recognised standard is used for K_{id} evaluation in ASTM or B.S. standards, the definition of K_{id} must therefore be interpreted as the dynamic equivalent of the ASTM and B.S. categorisation of K_{IC}, as given in Appendix A which states "the critical value of K_I at which the first significant extension of the crack occurs".

During a K_{id} dynamic test, due to uncertainties of initial load analysis from vibration noted earlier, the precise load and displacement of the specimen when "significant extension" occurs may be inaccurate and effectively vary for different testing machinery. However, improved procedures have been recently developed for the EPRI Fracture Toughness Programme in the United States, making the K_{id} test method more controlled and restricted so that improved reliability of the dynamic fracture toughness measurements is achieved, [113].

The K_{id} test does not seem to have gained interest for evaluation of BS4360 - 50D steel, but the basic concepts involved will be of interest with respect to the dynamic COD testing procedures followed in this thesis work, see Section 8.3.

6.2.1. *The Pellini Explosion Bulge Test*

The American view of the 1950 era was directed to fracture studies involving natural cracks. A basic postulate was that clevage instability in a welded structure is first developed in embrittled metal adjacent to the weld, such as the heat affected zone (HAZ). Once the cleavage instability is developed within relatively few grains in the embrittled HAZ region, the base metal grains in line are then subjected to the dynamic extension of an ultrasharp crack. As a consequence, the mechanical behaviour of the structure as a whole was believed to be equivalent to a dynamic loaded test, [118]. If laboratory tests involving cracks of an ultimate sharpness are applied with a dynamic load, it was suggested that the highest temperature range for initiation of clevage fracture would be achieved in this way, thus inducing the worst case of cleavage failure, [119].

High triaxial constraint would be operative at the crack tips and the dynamic loading rate would suppress yielding due to the higher yield stress value, [118].

By enforcing these adverse laboratory conditions the test specimen size could be theoretically reduced, while maintaining an assumed match to the highest temperatures of possible service failure, [119]. From such basic ideas the "Explosion Crack Starter Test" was developed, utilising a brittle weld bend in a 1 in x 14 in x 14 in plate placed over a circular die and loaded by an explosive change detonated in the die, [118].

Dynamic conditions at the initiation phase and a maintaining soft loading on the plate were achieved by the offset explosion, the fracture propagating from the centre to the edges of the plate. By testing plates over a range of temperatures, the ductile to brittle transition at high loading rates could be judged by plastic overload bulge, changing to an elastic cleavage flat fracture mode. The critical point in descending temperature when the fracture mode changed to flat break with no ductility was defined as the NDT or Nil Ductility Transition, and is still seen today in slightly modified forms, but still explains the same critical point.

Further definitions were evolved, the Fracture Transition Elastic (FTE) and the Fracture Transition Plastic (FTP). The FTE simply related the highest possible temperature for unstable fracture propagation, for the explosion bulge test continuous propagation is obtained through the plastically loaded centre regions. Ultimately, a higher temperature is reached at which only ductile tearing is possible, and is defined as the FTP point, [119].

6.2.2.1. *The Drop Weight Test (DWT) Procedure*

The failure of the Charpy-V test to provide an invariant method for characterising the temperature transition of steels, emphasised the need for a natural crack test technique, and from experience of the explosion test, a new procedure was developed in 1953, known as the Drop Weight Test or DWT, [118, 119].

The DWT specimen featured a brittle weld seam of the explosion test, with a saw cut across the weld localising the fracture of the weld bead to a single crack at the centre of the specimen. A dropping weight provided dynamic loading of the specimen in a simple edge-supported beam configuration, with a stop placed under the centre position, restricting the deformation to a small amount; thus the deformation was kept constant for steels of different yield strengths.

The DWT was designed specifically to determine the NDT temperature for steels which exhibit high upper shelf ductility levels, i.e. the low and intermediate strength steels.

6.2.2.2. *The Fracture Analysis Diagram (FAD) from DWT Data*

In 1960 the first attempt to couple flaw size considerations with transition temperature concepts was made. At this time the engineering significance of fracture mechanics definitions of stress intesnity factors was beginning to be appreciated, but no experimental data of fracture mechanics parameters required for calculating flaw sizes at the NDT temperature, or for establishing the temperature dependence of the stress level above the NDT were available.

Extensive studies of service failures were conducted and carefully catalogued with respect to the fracture initiation flaw size, the NDT, the service failure temperature and the stress level which had been applied to the flaw region of the structure, [118, 119]. Eventually, a NDT indexed Fracture Analysis Diagram (FAD) was evolved from the service experience, and is shown in Figure 31.

The FAD was able to provide a generalised definition of the flaw size, relative stress and temperature relationships with reference to the NDT temperature. The simplicity of the approach entailed conducting DWT tests to determine the NDT temperature from which the location of the generalised FAD would be pivoted. The FAD analysis gathered considerable faith in its use internationally, but was improved upon with the advent of the RAD diagram in 1968.

6.2.3.1. *The Drop Weight Tear Test (DWTT)*

By 1962 it became apparent that a test on similar lines to the DWTT was required for steels of low toughness and low upper shelf ductility, [119]. These steels were the high and ultra high strength level variety, in addition to intermediate strength steels which exhibited weakness in certain directions as found in rolled steels.

The new test method was first defined as the Drop Weight Tear Test or DWTT, and the first version featured a notched brittle bar welded to the test specimen. The purpose of the brittle bar was to develop a sharp natural crack.

In 1964 the DWTT was redesigned to eliminate the brittle crack starter bar and be replaced by a deep sharp crack introduced by Fe.- Ti alloy embrittled electron beam weld. This test was redefined as the Dynamic Tear or DT test. The narrow embrittled weld was fractured easily in loading and thus provided a reproducible sharp crack. After further work it was established that equivalent results may be obtained by using a deep sharp crack produced by fatigueing.

The need for the DT test was faced by the rapid increase in the engineering utilisation of high strength steels, titanium and aluminium alloys. The method was notably evolved during the period 1967 - 1969, and it was shown to be an expensive technique to determine the full behaviour of transition temperature range from NDT to FTP, additionally showing the magnitude of rise to upper shelf levels, [118, 119].

The basic philosophy of the DT test specimen design and loading procedure was similar to the early explosion bulge and DWT test, to provide a "limit severity" situation simulating the worst conditions in service of a real structure, i.e. high strain rate and a sharp, highly constrained crack, [118, 119, 120].

A further development of the DT test method came when a materials tolerance to flaws was evaluated by relating the fracture mechanics stress intensity factor K_{IC} to the DT energy. This was made possible by assuming all measurements of fracture resistance are manifestations of the size of the plastic zone

associated with the crack, [120], see Figure 32. For elastic-plastic flaw size, analysis extrapolated data of estimated Kc values were used, [121, 122, 123].

The DT testing equipment used for the flaw size correlation included instrumented strain gauge sensing devices in the drop weight tup, specimens and anvils, dependent on the conditions of test, [124]. Peak strain records were then correlated to equivalent DT energy values, [124, 125].

A detailed analysis was also insituted to determine the hammer (tup) forces and specimen bending moments in the dynamic response of the system, so that dynamic stress intensity factors could be computed directly, [125]. Unfortunately, this study was found to be very complicated and restrictive, especially during stages of gross yielding of specimens, [125]. The main emphasis of the NRL DT test consequently depended on the correlation of DT energy with the stress intensity factor K_{IC} obtained by separate testing procedures, [118, 119, 125].

6.2.3.2. *The Ratio Analysis Diagram*

The method described in Section 6.2.3.1 relating DT energy to the K_{IC} stress intensity value provided information to evolve the Ratio Analysis Diagram, or RAD in 1968, [119]. This method was important to the development of DT usage, because the diagram could now be moved to represent regions which related to specific K_{IC}/σ_{ys} ratios. The final version of the RAD is shown in Figure 33, [119]. The dotted line noted as the infinity (α) ratio represents the best estimate that can be made as of 1971 to unstable plain strain toughness measured by valid K_{IC} tests of large section size, see equation (14).

The practical use of the RAD was designed to evaluate either a Charpy C_V shelf energy value or a DT energy value of a specific steel and extract relevant flaw size data. The critical flaw size information was available from the equivalent K_{IC} value of the DT energy correlation, [120].

The validity of such an approach in the elastic-plastic regime could cause controversy, especially if valid ASTM K_{IC} values are unavailable in a tough material.

Another disadvantage of the RAD system is the continued use of Charpy Cv, when many years previous to RAD, the method was found to be unreliable. A general industrial user could easily assume that flaw data may be specified by a Charpy-Vee test programme, via the RAD, which would prove extremely dangerous in terms of possible failure. The continued force of industrial users' requirements is probably to blame here, since Charpy testing is an easy and low cost technique for which many companies are equipped for.

Apart from these disadvantages, the RAD technique was an improvement over the FAD, which depended on practical service experience only.

Today, both the FAD and RAD techniques seem to have been overshadowed by K_{IC}, K_{id}, COD and J testing techniques for toughness control studies. However, the FAD and RAD methodologies are important in terms of the literature survey of this thesis, discovering the progression of impact-type fracture toughness test procedures and their significance in structural specification.

7. *Development of the Test Programme for Static and Dynamic COD Testing in This Thesis*

This section is basically an introduction to the testing procedures used in this thesis, to experimentally determine the effect of compliance and stored strain energy on the elastic-plastic fracture toughness of RS4360 - 50D structural steel, during static and dynamic transient loading.

The COD technique was used for its simplicity and popularity, see Section 5, while test methods were kept as close to specific standards in use, including the COD standard BS5762, [75], and the K_{IC} plane strain toughness standard BS5447, [127].

Simplifications and approximations are used in certain test procedures, but where possible these are defined and assessed in terms of possible percentage error of results.

Most of the original experimental objectives of the test programme were achieved, except the determination of dynamic load during impact testing, see Section 7.2, but this was not a major drawback since COD was also determined. The equipment used for testing was checked regularly for calibration, and apparatus wear and tear was not found detrimental, even though impact loading was used.

7.1. *Slow-Static COD Toughness Test Procedure Using High and Low Compliance*

Investigation of the effects of compliance and stored strain energy on the elastic-plastic toughness value of COD measurements at maximum load was carried out on a standard structural steel, BS4360 - 50D, machined to W = 2B = 24 mm configuration.

The notch orientation was transverse to the rolling direction, with the specimen length longitudinal, and an overall span of 4W = 96 mm, see Figure 34.

The notch was prefatigued in the three point bend mode using the fatigue load test procedures as outlined in BS5762 (Section 7.1), using an R value of 0.1. Some difficulty originally occurred in obtaining the specified crack length for the authors specifications, due to uneven crack growth, but this was remedied in later stages of the specimen preparations by maintenance of the fatiguing apparatus. The a/W values eventually obtained varied between 0.49 and 0.58, the BS5762 standard specifying a value of 0.45 to 0.55 for application to the COD design curve approach and universal validity. The values of a/W over 0.55 are therefore invalid in relation to the BS5762 requirements, but the variation of resulting a/W values used in the test programme is not detrimental to the main aims of this thesis.

During the slow-static COD tests, the loading machine cross head velocity was restricted to between values of 1.8 and 10 x 10^{-3}mm/s, using a hydraulically driven 50 ton Denison machine in the compression mode, as specified in Section 7.3.1 of BS5762.

The compliance of the loading system (in series B data) was achieved by placing a modified lorry leaf spring in series with the specimen and Denison cross head, see Figure 35 and 36. The average compliance of the spring was 3.78 mm/KN, with a maximum capacity of about 3 tons (30 KN).

The spring system was later packed and bolted in position so that the loading system became stiff and rigid. A second set of COD tests reducing the compliance to zero, and depending upon the Denison displacement control stiffness alone (Series A data).

The COD value was measured by a calibrated double clip gauge transducer, first assessing the opening Vg by graphic recording versus load P, and then applying the standard plastic hinge rotation formula for the crack tip COD as specified in BS5762.

The specimen temperature was controlled by a nitrogen cooled methylated spirit bath placed on top of the spring, the temperature being measured by two thermocouple units, one embedded in an equivalent mass steel specimen to simulate the conductivity of the real test specimen, and the second to check the general temperature of the bath when new additions of liquid nitrogen were required.

It was also decided to produce values of the variation of the point of initiation of slow stable tearing δi with respect to temperature at - 40, -70 and - 100^{o}C. The technique used was to load the COD specimens at temperature to a value between the elastic region and maximum load, then unload, colour by tempering and break open by cooling at liquid nitrogen temperatures. The slow stable average crack lengths were then measured macroscopically and correlated to the COD values attained, basically producing an R-curve depicting δ vs Δa. By back plotting to zero Δa, the value of δi initiation was then obtained, as specified in BS5762, Section 6.6.

7.2. *Impact Plus Superposed Static Preload Test Procedure and Development*

Following the slow static toughness assessment of BS4360 - 50D with high and low compliance loading, further experiments were carried out to ascertain the steel's dynamic fracture toughness at specific values of a superposed static preload. By incorporating the leaf spring configuration discussed in Section 7.1, it was possible to vary the static preload from a stiff to highly compliant response.

Similar specimens were developed to the slow-static COD test geometry recommended in BS5762, [75], with additional shoulders either side of the central tip on the upper face, to enable an impact load to be applied. The basic shape and size of the static specimens of 2B = W = 24 mm being retained, see Figure 37.

The impact shoulders included hardened pins through which a hardened steel ram could be pushed in to open the crack tip to a specific COD value, if required, see Figure 38. The impact ram was pushed through the specimen shoulders by a massive pendulum hammer, with which final velocity and total mass available for momentum could be varied. During this process, the superposed static preload would be operative, and the basic schematic load conditions are shown in Figure 39.

A maximum final velocity of 4.1m/s was possible from the pendulum corresponding to a crack opening rate of 154 mm/s ($\dot{\delta}$) and a strain rate of approximately $17s^{-1}$ ($\dot{\epsilon}$), as evaluated from the recommendations of the IIK Group for IIW on dynamic testing, [74], for a 7^{o} angle taper on the ram, a/W specimen ratio of 0.52 and size 2B = W = 24 mm.

The pendulum mass values attainable were 11.8 kg, 17.93 kg, 23.61 kg and 31.11 kg, corresponding to impact energies at the maximum velocity of 4.1m/s to be 61.9J, 94.1J, 123.9J and 163.3J at a radius of gyration, R = 0.36m.

The preload value, as measured by stress intensity factor from $K = \frac{YP}{BW^{\frac{1}{2}}}$, [75], was preset in two domains, the first being in the linear or quasi-elastic load vs displacement range of the specimen, between about zero and 1.60 $KN/mm^{3/2}$, and the second in the non-linear or non-recoverable plastic range, between about 1.7 $KN/mm^{3/2}$ and 2.0 $KN/mm^{3/2}$ (as measured at - $80^{o}C$), see Figure 40. The stress intensity value about which these two ranges pivoted was the first point of non-linear crack tip behaviour or when the load vs displacement record showed the limit of proportionality for the crack tip configuration, see Figure 68.

The test rig layout is shown in Figure 41, being a front view, and in Figure 42 at the side. The photo of Figure 43 shows a closer scruting of the pendulum arm and weights, together with the static preload anvils protruding from the Denison crosshead, (bottom centre of picture), to the left of the pendulum weights. The impact ram, rested between the specimen shoulders and protruded outwards to the pendulum's lowest transverse point, at which the impact pendulum tip would push the ram into the specimen shoulders, as shown in Figure 38.

The black and yellow striped box on top of the spring, shown clearly in Figures 41 and 43, contained the methylated spirit bath which could be cooled by addition of liquid nitrogen. The temperature control and measurement was proceeded with as described in Section 7.1.

During the stages of initial increase of preload to a preset value, the load and crack opening value was monitored. The amount of crack opening was obtained by a displacement transducer which measured the increase in shoulder opening, as shown in Figure 44. It was hoped this monitor could describe the opening of the crack tip during impact and instability, but bounce effects and shock precluded such a technique.

The final COD after impact was obtained by using the BS5762 COD formula, [75], but modification was made to account for the impact application height above the specimen upper face, into the value for Z abutment height, See Figure 45.

The modifed formula then becomes:-

$$\delta_{impact} = \frac{0.4 \ (W - a_{NB}) \ Vp}{0.4W + 0.6\, a_{NB} + Z_{imp}} \qquad (32)$$

where $Z_{imp} = 12.5$ mm

$W = 24$ mm

and a_{NB} is applicable to the crack length of the notch-bend standard configuration, (see later).

The elastic component of the COD formula in BS5762 is ignored in this case because load P during impact was not recorded, however the value of δ will not be noticeably changed since the elastic component only accounts for about 3% of the maximum COD value.

The accuracy of the formula (32) is mainly dependent on the ratio of Z to the width of the specimen, as explained by Harrison, [14], of which errors of ± 20% are possible for Z/W = 0.3. For the specimens in use here, Z/W = 0.5, so the error would be assumed to be greater than ± 20% for the COD toughness value obtained. However, after static calibration of a dummy specimen, the error in the linear clip gauge was found to be a maximum of ± 3%, and in the non-linear range above 1.6 KN/mm$^{3/2}$ the error varied from ± 5% to ± 15% at 2.6 KN/mm$^{3/2}$.

Since the impact plus superposed preload tests were used to evaluate instability in the dynamic linear range, the errors of COD at instability may be assessed with an error of ± 3%. The maximum possible error of COD instability using the specimen shown in Figure 37 and equation (32) is expected to be - 6%. This represents - 0.06 mm COD discrepancy for instability at 1 mm COD, while for lower instability COD's the errors may be assumed to be negligible. The accuracy of determination will allow comparison to the static COD values with confidence.

Two of the main advantages of the present testing rig over other impact techniques are:-

(1) Coincident application of dynamic impact and superposed compliant static preload is possible.

(2) The load application directions of impact and static loads are perpendicularly operative at the crack tip at the same time.

The specimen configuration and testing rig design were developed with point (2) in mind, from the outset, which was envisaged to overcome the pitfalls encountered with tests like Charpy K_{id}, see Section 6.1 and Drop Weight, see Section 6.2.3.1. With these methods, flexural vibration and bounce were inherent due to the specimen's elastic behaviour. In addition, after preliminary appraisals of testing techniques by the author, a drop-weight technique was not used due to the high cost of modifications necessary to an existing drop weight tower, and the inability to directly compare static COD results.

The combined impact and superposed preload specimen eventually developed, Figure 37, may be assumed equivalent to two "standard" K test configurations which are recognised in BS5447 for plane strain fracture toughness testing, [127]. Obviously, this is an approximation, but if it is assumed the specimen static preload is applied by a notch bend configuration, and the impact load by a double cantilever beam, the stress intensity factors for dynamic loading and static preload may be calculated at instability, Figure 46. Using BS5447 for notch bend, see Figure 47,

$$K = \frac{3\,P_{NB}\,L_{NB}}{B\,W_{NB}^{3/2}} \left\{ 1.93 \left(\frac{a_{NB}}{W_{NB}}\right)^{\frac{1}{2}} - 3.07 \left(\frac{a_{NB}}{W_{NB}}\right)^{3/2} + 14.53 \left(\frac{a_{NB}}{W_{NB}}\right)^{5/2} - 25.11 \left(\frac{a_{NB}}{W_{NB}}\right)^{7/2} + 25.80 \left(\frac{a_{NB}}{W_{NB}}\right)^{9/2} \right\} \quad (33)$$

and for $L_{NB} = 2W_{NB}$,

$$K = \frac{P_{NB}\,Y_1}{B\,W_{NB}^{\frac{1}{2}}} \quad (34)$$

then for DCB configuration, see Figure 48, (35)

$$K = \frac{P_{DCB}}{BW_{DCB}^{\frac{1}{2}}} \left\{ 29.6 \left(\frac{a_{DCB}}{W_{DCB}} \right)^{\frac{1}{2}} - 185.5 \left(\frac{a_{DCB}}{W_{DCB}} \right)^{3/2} + \right.$$

$$\left. 655.7 \left(\frac{a_{DCB}}{W_{DCB}} \right)^{5/2} - 1017 \left(\frac{a_{DCB}}{W_{DCB}} \right)^{7/2} + 638.9 \left(\frac{a_{DCB}}{W_{DCB}} \right)^{9/2} \right\}$$

and

$$K = \frac{P_{DCB}}{BW_{DCB}^{\frac{1}{2}}} \qquad (36)$$

(where Y_1 is f (a/W) for notch bend K, and Y_2 is f (a/W) for DCB K).

Because this analysis is only an approximation, errors will be inherent in the method, especially for DCB equivalent. However, no exact magnitudes of percentage error is available at present.

The technique developed was able to estimate the rate of stress intensity increase at the crack tip during impact, being 3×10^6 $MN/m^{3/2}/S$, at 4.1m/s and $\dot{\delta}$ = 154 mm/S.

Equations (34) and (36) were also found useful to evaluate the equivalent loads for a given COD at the crack tip, thus $P_{NB} = 1.4. P_{DCB}$, and from this the dynamic energy was found to be a factor of 0.71 less than the notch bend stored strain energy for a given COD at the crack tip.

Since the notch bend and double cantilever beam geometry is recognised in BS5447 as valid for the testing, [127], the impact plus preload specimen, Figure 37, was partly envisaged to enable analysis of fracture toughness K and COD δ, using the K relations in BS5447, [127], and the COD relation in equation (32). In addition, it was hoped a K dynamic and K preload instability analysis could have been made, for which load P determination would be necessary for dynamic and static loading. Unfortunately, dynamic transient load analysis was extremely limited due to oscillations of the impact ram, the test technique was therefore restricted to impact energy determined by momentum equations in this thesis. As will become clear in the discussion to follow, such a technique would be extremely useful for "true limit severity" evaluation and defect assessment.

The same pre-fatigue techniques described in Section 7.1 were used to prepare the impact specimens, and the test procedure in terms of temperature control and static preload loading rate was also equivalent.

In addition to the instability cleavage results described later, it was possible to evaluate a value of δi dynamic at - 30°C, - 42°C and - 50°C by impacting an oversize ram at progressively higher impact energies. The dynamic technique used was kept as close to that recommended to evaluate δi slow in BS5762, [75].

7.3. *Review of Test Results Available for Analysis and Discussion*

All of the COD tests in this test programme use a notch transverse to the rolling direction in a L - T configuration, using a 20 mm plate of Japanese manufacture, specific to BS4360 - 50D.

From micrographic and SEM fractography, the steel used for testing was found to be relatively clean and homogeneous in its (as-received) normalised parent-plate state, with inclusions essentially comprised of segregated clusters of oxides of aluminium and silicon, and occasional flat or elongated stringers of manganese sulphide, see Figure 92.

The chemical composition of the steel is given in Table 3, with the carbon equivalent values.

Previous to this thesis, tension tests were carried out at Cranfield on 50D steel, evaluating the yield stress values over a range of temperature plotted in Figure 49.

The analysis is applicable to tension tests longitudinal to the rolling direction, in direct similarity to the notch bend COD test orientations. These values of yield stress from Figure 49 have been used in the calculations relevant to this thesis, for example with static COD maximum load values, via BS5762.

Pre-fatiguing was carried out in a similar manner for all specimens, and it was intended to keep a/W close to the requirement.of BS5762 for a/W between 0.45 and 0.55. The final a/W was found to vary between 0.49 to 0.57, due to some problems with the fatigue machines, see Section 7.1.

The test results carried out may be summarised into the following categories:-

A Static COD maximum load - stiff

B Static COD maximum load - compliant

C Dynamic impact cleavage instability

D Dynamic impact plus superposed static/stiff preload cleavage instability

E Dynamic impact plus superposed static/compliant preload (< 1.6 $KN/mm^{3/2}$) cleavage instability

F Dynamic impact plus superposed static/compliant preload (> 1.7 $KN/mm^{3/2}$) cleavage instability

G Static Loading tests for evaluation of δi slow

H Dynamic loading tests for evaluation of δi dynamic

The following tabulations relate to categories A to H, with relevant Figures in brackets:-

A Table 4 (50, 52, 53, 54, 55, 56, 59)

B Table 5 (51, 52, 53, 54, 55, 56, 59)

C Table 8 (62a, 62b, 65, 66)

D Table 12 (see Series C and text)

E Table 9 (63a, 63b, 65, 66, 68)

F Table 10 (64a, 64b, 65, 66, 68)

G Table 5a (57, 67b)

H Table 5b (65, 67a, 67b, 69b)

(In addition, all results are used for construction of Figures 70a/b and 71).

The tabulations quote the COD at maximum load or instability dependent upon test category, temperature of test, a/W ratio, loading conditions, relevant macro or SEM photographs, and nature of crack opening: whether tear-blunting, tear to cleavage instability or cleavage initiation and growth etc.

The series of slow-static COD tests of series A and B were carried out at the temperature specified, by loading gradually to BS5762 requirements, and the maximum load was recorded by P vs clip gauge instrumentation. The maximum load opening displacement was then converted to a crack tip COD, δ. (See Section 5.1.3. for definition of types of COD measured).

Series A results are shown in Figure 50, Series B in Figure 51, while the mean transition lines for A and B are given in Figure 52.

In Figure 53 it is possible to locate a sample of these tests in terms of temperature at - 40, - 80, - 90, - 95, - 105 and - 120/- 125^{o}C, and compare a series A test result with a series B. The specimens chosen were felt to be a good representation of the fracture behaviour with and without a spring loading system to apply the load, and are within standard of BS5762 for crack length of $0.45 < a/W < 0.55$.

The relevant macro-photos and SEM photos of specimens of interest is then obtained by inspection of Figure 53.

By using the maximum load COD toughness values obtained in series A and B data, it is possible to calculate the maximum allowable half length a flaw size from the COD design curve analysis. By assuming the design working stress ratio of $\sigma_1/\sigma_{ys} \geq 0.5$, a values relative to temperature from the mean transition lines of Figure 52, and plotted in Figure 56.

Series G slow loading tests to ascertain δi slow were carried out using the "back-plotting" technique in BS5762. The values for δi at - 40, - 70 and - 100^{o}C are given in Table 5 and plotted relative to temperature in Figures 57 and 67b.

Test results categorised in series C, D, E and F are dynamic tests, loading rate of 3×10^{6} MN/m$^{3/2}$/S and a COD displacement rate at the crack tip of 154 mm/S. A preload was effective in D, E and F data, of which D was stiff in character, while E and F were compliantly loaded by the spring system described in 7.2.

The dynamic tests entailed opening of the crack tip by a set size ram, for a new specimen, ram size was increased until a condition of cleavage instability was achieved. The data points of crack blunt or run are shown in Figures 62a, 63a, 64a and the boundary between cleavage instability or blunting is represented by mean instability transition lines in Figures 62b, 63b, and 64b (on transparencies).

The dynamic instability lines may therefore be defined as "the lowest COD at which cleavage instability will occur at a given temperature, for a given dynamic strain rate at the crack tip, and a specific stored strain energy content at the instant of instability".

Series D results, using a stiff preload, were found to be only equivalent to series C impact-only results. This is not surprising since the stiff preload will quickly decay to zero at the instant of dynamic impact and consequent specimen displacement.

Series H data investigated the estimated value of δi dynamic, as opposed to δi slow. A loading rate of $\dot{\delta}$ = 154 mm/S, was used as in series C, D, E and F results. However, an oversize ram was used and a progressively higher mass pushed the ram in further, which produced a larger COD each time. Dynamic tearing occurred for a given COD, and the results for - 30, 42 and - 50°C were used to find δi dynamic, by following as closely as possible the back-plot technique used for δi slow. The results of series H data are represented in Figures 65, 67a/b and 69b.

The following figures relate to test data described and discussed in section 8, using macro-photography and SEM fractographic records, and refer to specific points of interest.

(a) The stretch zone, see Table 7, Figures 92, 93, 95, 106 and 109.

(b) Slow-static tearing morphology, Figures 73 to 87 and 90, 97, 98, 99, 100, 101, 102, 103, 104, 105, 119 and 120.

(c) Dynamic tearing morphology, Figures 106, 107, 108, 109 and 110.

(d) Dynamic impact plus superposed preload, Figures 88, 89, 94, 96, 111, 112, 113, 114, 115, 116, 117 and 118.

8. *Description of Fracture Toughness Behaviour and Discussion of Results*

This section deals with the fracture toughness behaviour obtained from the experimental programme of this thesis, described in Section 7.

At first, the resulting data will be described in detail, and secondly, the results will be discussed with reference to the fracture processes and micro-mechanisms operative.

8.1.1 Description of Static COD Test Results (Series A and B Data)

From the COD maximum load fracture toughness tests of series A and B data, a marked increase occurs in the ductile to brittle transition temperature for the high compliance test results of series B, using a spring in series with the load machine crosshead of 3.78 mm/KN, see Section 7.1, Figure 52. (Refer to Tables 4 and 5, with COD vs T. plots in Figures 50 and 51, for results of A and B tests respectively).

For the purposes of discussion only, it will be assumed the lower shelf toes of the data occur at 0.1 mm COD, and the upper shelf toes at 1.1 mm COD, see Figure 54, this only being an aid to description.

The mean transition curves at 0.1 mm COD occur at - 121^{o}C for series A and a higher temperature of - 100^{o}C for series B. Representing a temperature difference of 21^{o}C, see Figure 54. In addition, the value of COD at - 130^{o}C is 0.08 mm for series A and 0.025 mm for series B.

Fracture surfaces for specimens B15, B14 and A10 are shown for comparison in Figures 87, 86 and 78 respectively, which are relatively similar in morphology and show no crack tip blunting or tearing, except for specimen A10 which did achieve the non-linear load behaviour as shown in Figure 78 and exhibited a very small sketch region by inspection with the SEM.

The fracture toughness of series A results start to increase rapidly into the transition toughness range at - 121^{o}C, and at - 100^{o}C the mean transition indicates an improvement in COD to 0.85 mm, close to the upper shelf toe.

However, at - 100°C the series B results indicate only the lower shelf toe of 0.1 mm COD has been attained.

These differing toughness values indicate that tests carried out with the high compliance are less tough in terms of COD value than the stiffly loaded specimens, and that the ductile to brittle transition temperature is displaced from - 105°C for series A results to - 91°C of B at 0.6 mm COD, representing a middle transition shift of 14°C, see Figure 54.

The COD specimen fracture surfaces of series A and B results were investigated after testing by macro-photography and the SEM.

As shown in Figure 59 depicting percentage surface of tearing, the series B ductile tearing region is considerably reduced from the series A values.

Macro-photographs shown in Figures 73 to 78 and Figures 79, 81, 84, 85, 86 and 87 with corollary load vs clip displacement records show a marked decrease in the stable tearing lengths and maximum COD values for series B data, being compliantly loaded, see Figure 53.

However, comparison was not made between series A and B crack extension, Δa, from stable tearing, because the tearing in series B was found to be highly irregular, see later. The % tear areas in Figure 59 and fracture surface macro-photos are adequate to differentiate between series A and B toughness behaviour.

By inspection of Figures 81, 82, 83 and 84, depicting compliantly loaded COD tests of B5, B6, B8 and B10 at - 75°C, - 80°C, - 86°C and - 90°C respectively, the ductile tearing regions are inherently irregular compared to stiffly loaded tests as shown in Figures 74, 75 and 76 at - 80°C, - 90°C and - 95°C respectively.

By comparing the morphology of tearing in Figure 90, between B10, A4 and A6 specimens at - 90°C, - 95°C and - 105°C, the surface of B10 is clearly pitted, and at a higher magnification in Figures 99 and 105 for A4 and B10 specimen surfaces, the mode of tearing seems radically different at a magnification of x 725.

For Figure 99, A4 stiffly loaded, at x 725, the normal type of ductile tearing morphology is present for Mode I, crack opening. Between the larger ductile dimples are dispersed small microvoids, see also Figure 100 of specimen A4.

However, the same magnification of x 725 on Figure 105 shows a mixed mode stress system across the diagonal of the photo. To the left, Mode I failure morphology as seen in Figure 99 is present, to the right, a dominant Mode III plane tear occurs close to the edge of one of the large pits seen in Figures 81, 82, 83, 84 and 103.

Between the Mode I and Mode III plane plastic flow, a clear interface is shown, where the two modes become mixed.

In addition, the Mode I morphology to the left of Figure 105 shows the usual microvoid presence of specimen A4, Figure 99, but to the right in the Mode III plane system the microvoids seem absent on the surface, and plastic flow seems more pronounced.

The general impression is that the tearing for stiffly loaded COD tests seems to be Mode I zig-zag type process with a random distribution of ductile dimples and microvoids, as depicted in Figure 58a.

The compliantly loaded COD tests show tearing surfaces to be dominantly Mode I opening, but with Mode III plane tearing, distinguished as pitting. The Mode I tearing surface also shows "tram-lines" of growth down from the original crack tip, on a flatter surface than that of the stiff load zig-zag tear, see Figure 103.

The tearing shape is depicted in Figure 58b, and represents a preference for the tear to grow in a straighter line than Figure 58a.

Only at - 72^{o}C does the mean transitions of A and B data coincide, but the exact upper shelf temperature when series A and B behaviour is identical is believed to be considerably higher at about - 20^{o}C, (see later). For the imaginary toe of 1.1 mm COD, series A and B transitions are still displaced at - 90^{o}C and - 83^{o}C respectively.

The upper shelf region of both series A and B results is attributed to greatly increased toughness and ability for plastic flow, the specimen ligament then acts as a simple plastic hinge and is in the plastic collapse domain, of which the highest COD value obtained is 1.38 for test number B1, see Figure 51.

The mean transition curves shown in Figures 52 and 54 are only scaled averages, and were not evaluated in terms of a statistical distribution because of insufficient data, but they are suggested to be good representatives of the COD values relative to temperature.

The minimum scatter of results occurs for both A and B data in the lower shelf toughness range, however increases considerably above about 0.2 to 0.3 mm COD. The transition results of series A data between 0.35 and 0.9 mm COD are scattered evenly about the mean transition line on Figure 52, thereafter above the upper shelf toe (1.1 mm COD) the scatter again decreases at upper shelf values between 1.1 mm and 1.17 mm COD, from - 90^{o}C to - 40^{o}C. This type of behaviour is representative of other COD transitions carried out before on structural steel to BS5762.

The distribution of the compliantly loaded results, series B, in terms of scatter was found to be significantly different. It was initially decided that a sample of ten or eleven specimens could indicate a transition temperature trend, as used for series A tests, but the scatter of results in series B was found to be "unfamiliar", and eventually fifteen specimens were tested. A sharper transition slope was expected at a higher temperature from the literature, but what originally "threw" the investigation was specimens B13, B11 and B4, as well as B5 and B3 to B4.

Scatter was shown to be small below - 95^{o}C, but increased between the beginning of toughness recovery at - 90^{o}C and the low COD value of 0.4 mm of specimen number B4 at - 70^{o}C. Within this band the stability of tearing is very poor, and it would seem from specimens B3, B2 and B1 that the COD toughness is still "recovering" from the poor tearing stability even at upper shelf temperatures, in the temperature range where series A results seem fully recovered.

Further evidence that the "upper shelf" tests of series B data are not exactly equivalent to the series A upper shelf specimens is given in Figure 59, which shows percentage area of tearing and shear lip zones on the fracture surface. The resultant graph shows reduced % area of shear lips of the series B specimens even at - 40°C, suggesting that the shear lip plasticity in series A upper shelf specimens is easier than in series B. This may be due to the driving force energy during the static loading being preferentially absorbed per crack growth by the ductile tearing.

However, as shown in the mean transition curves of Figure 52, 53 and 54, the upper shelf data of series A and B above - 70°C were averaged together to form a mean upper shelf COD of both samples of data. Until further evidence is obtained with larger sample sizes for stiff and compliant static COD testing above - 70°C, the present upper mean shelf is assumed sufficient for this thesis work.

A plot of δi, the COD value at which ductile tearing initiates, is given in Figure 57, and also shows the transition to cleavage initiation, δc, for series B compliant data. This curve is also shown in Figure 54, 55 and 69, and will facilitate certain parts of the discussion to follow.

8.1.2.1. Introduction to Discussion of Static COD Results

Having looked generally at the slow-static results of series A and B tests, the data will now be analysed in terms of fracture processes and micromechanisms at the crack tip in relation to the loading systems' compliance and stored strain energy.

First the lower shelf, low temperature range of the COD results will be discussed, then processes above a COD of 0.2 mm, in the transition toughness range, and finally the upper shelf toughness processes will be investigated.

8.1.2.2. *Discussion of Static Lower Shelf Results*

It is generally recognised that cleavage fracture depends on two compnents: the initiation and propagation of microcracks, [128, 129].

At the lower shelf temperatures, microcracks are initiated by slip dislocations piling up against a barrier, for example, a grain boundary carbide, while the fracture criterion necessitates sufficient load tensile stress to propagate the microcracks through the ferrite grains.

The reduced COD value of series B tests at lower shelf temperatures, being 0.025 mm at - 130°C, while series A is higher at 0.08 mm, is attributed to increased loading compliance and external stored strain energy available at the vicinity of the crack tip.

If crack nucleation is achieved in carbide platelets, or similar brittle microstructural phases which can act as dislocation barriers, when the brittle phase breaks a dynamic strain rate is produced in the adjacent ferrite matrix. Since steel is rate-sensitive, the matrix is subject to decreased toughness, and if there is sufficient energy in the matrix, then the breaking brittle phase will trigger a cleavage crack.

The cleavage crack produced may run for a number of grain diameters, but if the supply of strain energy is poor, then the cleavage crack will arrest.

A high compliance load applied at the crack tip will however allow the running cleavage crack to continue further into the matrix, and cause complete fracture of the remaining ligament.

The decreased COD of series B data at lower shelf does not therefore indicate the matrix needs less stress for cleavage initiation, but that the high compliant stored strain energy allows an earlier cleavage initiation micromechanism at the crack tip to have "measurable" effect due to continued crack growth.

It is clear from this discussion, that the low temperature - lower shelf COD δi value will depend on the distribution of hard microstructural phases and the loading compliance operative at the crack tip, as well as the steels rate-sensitivity.

It is interesting to note that the degree of scatter in the lower shelf below 0.2 mm COD is small. This would indicate that the cleavage initiation - propagation process is very similar below - 115°C for series A, and - 95°C for series B, and that the microstructural hard-particle distribution is regular.

8.1.2.3. *Discussion of Static Transition Range and Upper Shelf Results*

The value of measurable cleavage initiation, δc, is dependent on the compliant energy available in the matrix, as mentioned in section 8.1.2.1. However, the point of initiation by ductile rupture, δi, is principally a strain controlled process, when voids form around inclusions ahead of the crack tip, and the value of δi is dependent on the inclusion spacing and distribution.

A transition occurs from δc cleavage initiation at low temperature to δi rupture initiation at a higher temperature, and for series A results using a stiff loading system, this occurs at - 122°C to - 105°C, while for series B the transition is higher in temperature at - 95°C due to increased stored strain energy content increasing the cleavage initiation temperature range, see Figure 57.

This micromechanism change is indicative of decreased yield stress and an increasing material toughness from plasticity, when the steel exhibits less afinity to initiate by cleavage, simply because the yield stress drops below the fracture stress.

Due to the work hardening capacity of the steel and the plastic flow at the crack tip, a void will be formed around the nearest second phase particle in the plastic zone to the crack tip, at temperatures above the δc to δi initiation transition.

The measurable point at which stable tearing begins, or the ductile rupture initiation COD δi, is shown to occur at 0.2 mm COD between - 100°C and - 65°C, evaluated by static-stiff COD tests. This is in fairly close proximity to δi reported for A-533B pressure vessel steel at 0.175 mm, [129], while the value of COD equivalent to K_{IC} of 175 $MN/m^{3/2}$ for BS4360 - 50D steel is 0.19 mm, and would suggest that the "significant extension of the crack" in the K_{IC} test is in fact δi evaluated in this work at -25°C, see Fig.70.

At temperatures above - 65°C, the value of δi increases to 0.63 mm at - 40°C, which is indicative of increased toughness at the crack tip and much easier plastic flow before voids will form. In addition, geometry effects of the specimen may also modify the effective value of δi measured by the back-plot technique in BS5762, [75].

The first initial crack tip blunting, due to plasticity, is usually known as the "stretch zone" and is quoted to be approximately equal to δi/ 2 in width, at the point when the first void cusp is formed, [129]. This is in agreement with estimated stretch zone COD values of 150 μm in the - 90° to - 70°C temperature range where δi = 0.2 mm, using the SEM to measure the crack tip opening, see Table 7 and Figures 111, 116 and 118.

After crack stretching has occurred, it is probable that the void coalescence process will occur at a Manganese Sulphide (Mn S) inclusion, of which a good example of a MnS stringer is shown in the stretch zone from SEM analysis in Figures 92a and 92b.

Expansion of the forming voids will occur in the region of maximum triaxial stress at a distance of about > 1.9δ ahead of the crack tip, from which coalescence will eventually occur with the crack tip to form the first stages of a ductile tear, [128].

Ductile crack growth is finally introduced by smaller intermediate particles which are sub micron size, and for the steel tested such particles were found to be aluminium and silicon compounds, from SEM energy dispersive analysis.

The interface between the particles and the matrix looses coherence when extensive plastic flow takes place, tiny voids then being formed by slip. The voids gradually neck down to form the characteristic small dimples interspaced by larger voids caused by large second phase inclusions of MnS. Classic examples of this type of behaviour is shown in Figures 99, 100, 101, 111 and 112, with ductile dimples, inclusions and microvoids formations clearly seen.

The growth of stable tearing after ductile initiation, δi, is therefore essentially a mechanism of nucleation, growth and coalescence of voids around large and intermediate size inclusions, see Figure 58a, and is a strain controlled process. Toughness assessment using the COD approach is therefore suitable when stable tearing is present, see Section 4.4.4.

The decreased stable crack lengths of series B results, using a compliant loading system, suggests that the spring stored strain energy is causing an earlier tearing instability to cleavage propagation and failure. The overall effect, as shown in Figures 52, 53, 54 and 55 is to increase the effective ductile to brittle transition temperature for a higher compliance and stored strain energy content.

The mechanism of instability from ductile tearing to cleavage crack growth is envisaged to be due to void coalescence at the growing crack tip, which causes a dynamic strain rate ahead of the coalescence and triggers cleavage in the rate-sensitive matrix. If the stored strain energy is sufficient, then the crack will continue to run and sever the remaining ligament. This process is similar to the low temperature cleavage initiation and propagation process, but in this case the cleavage crack growth is triggered by the ductile tearing crack growth.

For stability during slow ductile tearing,

$$G = R$$

but assuming cleavage is produced ahead of the growing crack tip during a void coalescence process, and,

$$G > R$$

then cleavage instability will be continued with a cleavage crack run condition.

The compliance of the driving force is also important, since as shown in Figure 60, a stiff load driving force will follow the crack resistance decrease if a ductile void jump occurs. However, if the driving force compliance is high, then G continues as its previous value and the condition for instability occurs when G > R.

Consequently, for a given tearing void coalescence at the crack tip, there is more probability that instability will occur with a compliant loading system.

This explains the reduced COD maximum load values of series B results compared to series A in the transition temperature range, which effectively increases the ductile to brittle transition temperature, for series B data by $14^{o}C$ at 0.6 mm COD, (comparing mean transitions).

The distribution of maximum COD values in Figure 51 for the compliant tests, shows a very steep rise in toughness at - $90^{o}C$ from low transition COD's of B11 and B12, to a group of values at the upper shelf toe comprising B5, B6, B7, B8, B9 and B10.

The results of B11 and B12 are attributed to the high compliance of the driving force causing an earlier instability than the stiff COD transition data, as shown in Figures 50, 51 and 54.

These results are in agreement with the work by Almar-Naess, [29], who found a reduced displacement of steel notch-bend specimens for increased compliance of loading in the transition temperature range, see Section 4.4.1.

From inspection of the ductile tearing morphology described in Section 8.1, it is also apparent that the micromechanism and mode of tearing growth is changed if a compliant loading system is used instead of a stiff system for slow-static COD notch-bend tests. This situation will also apply whenever

an opening Mode I elastic-plastic fracture test is carried out, but possibly to varying degrees dependent whether 3-point, 4-point or DCB specimen geometry is used.

The tearing surfaces of series B results are considerably different from series A in the range of - 90°C to - 75°C, even though the COD maximum load values would alone indicate upper-shelf plastic collapse behaviour is dominant, see Figures 50, 51 and 52. Examples of the difference between series A and B results is shown in Figures 119 and 120 by schematic diagram, while photographs of relevance are also shown in Figures 74, 75, 81 and 84. (A full description is also given in Section 8.1).

In the upper shelf range of series A results above - 90°C, plastic collapse takes precedent due to the increased toughness and ability to form plastic shear lip zones at the specimen surface where biaxial stress is present.

The maximum load COD at upper shelf of series A is dependent upon the size and work hardening ability during the plastic collapse process, ductile tearing instability present in the temperature range of - 121°C to - 90°C is absent in tests A1 and A2 corresponding to macro-photos in Figures 73 and 74 respectively.

Series B fracture surfaces appear less tough than series A results in the temperature range - 75°C to - 90°C, as shown in comparison Figures 119 and 120. The series A results are more ductile and of a plastic collapse nature, compared to series B, of which specimens B5 and B10 shown in Figures 81 and 84 respectively, have small shear lip zones at the surface edge of the crack tip, while the tearing zone is interspaced with pits elongated in the direction of growth, see Figures 102, 103 and Section 8.1.

The tearing surfaces of specimens B5, B6, B8 and B10 is not a "zig-zag" type tearing growth as for series A results, see Figures 98 and 99, but a much straighter growth pattern, with "tram-line" type void coalescence in the direction of growth, see Figure 103 and Section 8.1. The type of tearing present in series B results discussed is shown in Figure 58b.

The pitting of specimens B5, B6, B8 and B10 is probably due to void coalescence from large inclusions being transformed into an opening mode transverse to Mode I, by triaxial stress at the crack tip. The transverse opening rupture, described as Mode III in the description section 8.1, is clearly shown for specimen B10 in Figure 105 using the SEM.

The pits themselves vary between 0.3 x 1.2 mm long and the smallest being egg shaped of 0.1 mm.

The high triaxial stress required to form the pits, is assumed to be present because of the limited shear lip size and restricted stress relaxation at the crack tip as the tear grows for specimens B5, B6, B8 and B10.

The final maximum load COD dictated by failure instability is by plastic collapse for series A specimens in the upper shelf above - 90°C, see specimens A1, A2 and A3 in Figures 73, 74 and 75, but usually tearing instability for series B between - 90°C and - 70°C for specimens B4, B5, B6 and B10 in Figures 80, 81, 82 and 84. (Please note, B7 and B9 are also applicable to this discussion, but photos are not available). Above - 70°C, the series B results for specimens B3, B2 and B1 become predominantly plastic collapse , but still have fracture surfaces different to series A upper shelf results, see description, Section 8.1.

It is suggested that due to a modified mechanism of tearing growth during high compliance static loading, as shown in Figure 58b, the strain required for stable crack growth is increased.

This explains the reduced % shear lip area in the results of series B data compared to series A, Figure 59, since the driving force has to firstly overcome the high absorption energy effective during slow stable crack growth before shear lip zones may be formed at the specimen surface. In addition, the progressively increasing COD toughness of specimens B3, B2 and B1 give weight to this theory, since the fracture surfaces still have smaller % area of shear lip than the equivalent series A results, and yet the COD toughness rises above the series A upper shelf.

The energy required for crack growth may be expressed by R, containing components of the work for formation of a new plastic zone at the tip of the stable advancing crack, plus the work required for initiation, growth and coalescence of microvoids.

Above - 90°C for series B data, the increasing toughness of the material precludes a low COD tearing to cleavage instability as exhibited by specimens B11 and B12 discussed previously, simply because a void coalescence discontinuity does not trigger a significant cleavage event ahead of the growing crack tip. The tearing crack tip therefore continues to grow, but because more work is required at the growing crack tip due to the modified growth process for compliant loading, less energy is available for shear lip formation.

At first, this may be judged as an advantage in terms of crack stability during tearing, because R for tearing increases, but the driving force will principally be used to drive the crack forward, and the shear lip formation which is responsible for the relaxation of stress in the series A results is prevented.

As the stable crack grows, triaxial stress will become quite high from the opening mode of the crack tip, since the shear lip formation is restricted and the triaxial component of stress is not relaxed, the pitting formations shown in Figures 81, 82, 83 and 84 of specimens B5, B6, B8 and B10, will be formed in the tearing region.

It is postulated that this tearing model during compliant static loading explains the difference in fracture instability surfaces in Figures 119 and 120.

Even though the normalised plate material used in tests for this thesis is tough enough to prevent void coalescence discontinuities that trigger cleavage, the stability of series B results above - 90°C is highly dependent upon the homogenuity of the tearing process. Microstructural inhomogeneities such as large inclusions, porosity, lamellar tearing, weld defects etc, could easily mis-balance the G = R tearing stability, simply because shear lip relaxation is prevented.

These contributing factors have probably caused a low COD value of specimen B4 at only 0.4 mm COD, see Figure 51 and Figure 80, instability possibly due to a large MnS stringer present just ahead of the crack tip in specimen B4.

The significance of this discussion is important with respect to welded structures. Microstructural inhomogenuities are commonplace, and the only "conservative" estimate of maximum load COD for a determinate structure with high stored strain energy content would be a value close to δi initiation, or with reference to BS4360 - 50D in this thesis, the corollary K_{IC} value, see Fig 70.

For the series B results, even above - 65°C, the fracture surfaces exhibit reduced shear lip areas compared to series A results, see Figure 59, indicating the compliance of the spring loading system is still affecting the tearing process.

It is also interesting to note that the highest upper shelf COD value obtained was from B1, at - 25°C and a COD of 1.38 mm, which is higher than the upper shelf value expected from series A data. The scarcity of results at upper shelf limits the conclusions to be made with confidence, but is suspected that series A and B data would coincide with plastic collapse behaviour at - 10°C.

Further information of the micromechanisms during compliantly loaded tearing processes would be possible by TEM analysis of the growing crack tip and plastic zone, but this was not carried out in this thesis.

8.2.1. *Description of Dynamic COD Test Results (Series C, E, F and H Data)*

The dynamic results of series C, E and F data will be described in this section, which are defined and commented on in Section 7.3. Basically, the loading rate is dynamic, the rate of stress intensity increase in the elastic range being,

$$\dot{K} = 3 \times 10^6 \text{ MN/m}^{3/2}/\text{S}$$

and the crack tip is opened at,

$$\dot{\delta} = 154 \text{ mm/S}$$

For the series C results, only impactive loading is operative, series E has a superposed compliant preload of a linear or quasi-elastic nature below 1.6 KN/mm$^{3/2}$, while series F results have a superposed compliant preload of non-linear and generally plastic behaviour at the crack tip above 1.6 KN/mm$^{3/2}$ and below 1.9 KN/mm$^{3/2}$, see Section 7.3.

The value of 1.6 KN/mm$^{3/2}$ represents the mean stress intensity at the crack tip when the P vs clip gauge record becomes plastic, and changes from a linear to non-linear behaviour. An exact plot by linear regression of K_{clip} vs K_{clip} is given in Figure 68, evaluated from static COD data of series A and B results.

The effect of increasing the static preload from zero to a value just above 1.7 KN/mm$^{3/2}$ at the original fatigue crack tip is shown in Figures 110, 94 and 96 from SEM fractography.

If no preload is applied, in other words "impact-only", dynamic instability to cleavage as depicted in Figure 62a will occur ahead of the crack tip, with no initial blunting or tearing being present, Figure 110. For a linear preload value, the fatigue crack is shown to just stretch a small amount, allowing fatigue crack tip striations to be made, just visible by stretching, Figure 94. Finally, at a preload which is just higher than 1.6 KN/mm$^{3/2}$, the crack tip exhibits considerable stretching equivalent to $\delta i/\sqrt{2}$, see Table 7, while the first growth of ductile rupture is being formed, Figure 96.

Microvoids are visible ahead of the stretched crack tip, which are growing prior to the development of a "measurable" tear at δi COD. (Using the back-plot technique described in BS5762, Appendix A).

The stretch zone COD in Figure 96 for specimen F20 (plotted in Figure 64a/b), measures 138 μm with a microvoid tear depth of 0 to 5 μm, this being in good agreement with the estimated stretch zone size of $\delta i/\sqrt{2}$ when δi is 0.2 mm at - 70°C, see also Section 8.1.2.2.

Having described the initial conditions of series C, E and F data before dynamic impact is introduced, detailed descriptions will now be made of the dynamic test results individually.

The impact-only data of series C, represents tests at zero preload with test data results shown in Figure 62a and the mean instability transition line in Figure 62b.

The mean instability line bounds the results between - 81°C and - 53°C, of which cleavage instability with ligament failure is above the transition.

At - 81°C the transition line occurs at a COD of 0.3 mm, and as temperature increases, so does the COD for instability, until at - 53°C the transition COD is 0.48 mm.

An example of the type of failure instability by cleavage is shown in Figure 110 for specimen number C21 at - 60°C.

The maximum energy of impact available from the pendulum mass was not sufficient to cause cleavage instability above - 53°C, so the transition instability is assumed to follow the dotted line in Figure 62 which is representative of the instability data from groups E and F.

The small sample size of the results below - 82°C precludes exact positioning of the instability boundary, but it is assumed to decrease in maximum COD required for cleavage as the temperature decreases.

As shown by Figure 110, the crack tip shows no evidence of stretching or microvoids, inferring that cleavage has been initiated and propagated in the specimen without any plastic flow or tearing processes present. The failed ligament exhibits only cleavage run shear lip plastic zones on the specimen side faces.

The mean instability transition to cleavage for series E data is shown in Figure 63a/b, representing impact plus superposed compliant preload below 1.6 KN/mm$^{3/2}$. The series E transition shows a marked decrease in the critical COD to produce cleavage instability between - 100°C and - 70°C. In fact, it is of interest to mention that even the smallest impact runs available for dynamic crack opening to 0.07 mm COD still caused cleavage crack run, see Table 9.

For a clearer evaluation of the instability COD value of the series E lower shelf, it was decided to look at the crack tip morphology by the SEM.

It is believed the instability COD may be as low as 0.01 mm at - 100°C, while at - 80°C it is slightly higher at 0.02 mm. A low COD instability fracture surface is shown in Figure 94 for - 70°C, and the test result is shown in Figure 63 as ordinate E12.

The lower shelf static test results of series B for - 130°C give 0.025 mm maximum COD, which justifies the estimated dynamic values of 0.02 mm for series E at - 80°C, remembering from Section 5 that critical COD's caused by dynamic loading will be increased in temperature from the static results by 30° to 80°C.

In addition, the lower shelf instability values of about 0.01 to 0.02 mm estimated from SEM measurements of crack tip stretch, is close to the equivalent COD values of K_{id} of a structural steel, see Section 6.1, being 0.015 mm and 0.0034 mm COD (K_{id}) at 0°C (60 ksi$\sqrt{in}$) and - 60°C (30 ksi$\sqrt{in}$).

The critical instability COD for cleavage as temperature is increased quickly rises from 0.03 mm at - 70°C to coincide with the transition exhibited by series F data at - 51°C, see Figure 65. As the temperature is increased to - 40°C the instability COD for cleavage is 0.89 mm.

A representative cleavage failure from series E results at - 42°C is shown in Figure 88, and is specimen E9 in Figure 63. The fatigue crack tip is also shown by the SEM in Figure 113, and shows minimal stretch at the fatigue crack tip.

The third group of tests to be described are series F, using the same dynamic impact conditions of series C and E data, see Section 7.3, but this time a compliant preload stress intensity factor of about 1.7 $KN/mm^{3/2}$ was superposed during impact.

Since this preload was past the K_{clip} turn value see Figure 68, increased crack stretch and blunting is present at the crack tip prior to impact and cleavage instability. Microvoid coalescence is also present, and is shown clearly in SEM photos, Figure 96 at - 70°C, and Figures 111 and 112 at - 40°C for specimens F20 and F12 respectively.

The instability transition to cleavage is shown in Figure 64a/b. The lower shelf of the cleavage instability between - 100 and - 70°C seems to coincide with the value of δi dynamic at 0.18 mm COD, see later. As temperature is increased above - 70°C, the transition begins to rise, coinciding with series E transition at - 51°C, see Figure 65.

An interesting experiment was conducted to see if a value of δi dynamic could be determined by measuring the length of dynamic tearing for a given COD value, and back-plotting to find the point of initiation of dynamic rupture. Since no British Standard is presently available to specify the technique to evaluate a δi dynamic value, it was decided to copy as closely as possible the recommendations in BS5762, [75]. By increasing the pendulum weight from 11.80 kg to 31.11 kg for $\dot{\delta}$ = 154 mm/S, and using an oversize ram to open the crack tip, while always checking the ram was free from the impact specimen shoulders after test, an average value of about 0.18 mm COD is obtained for - 30, - 42 and - 50°C, see Table 5b.

However, because the test method relied on an initially high impact momentum decaying to zero from the resistance of crack opening, the values obtained for δi dynamic are subject to the definition that the original strain rate was high and decayed to zero.

The temperatures of - 30, - 42 and - 50°C were chosen simply because the value of static δi starts to effectively rise in this temperature range, and a full variation of pendulum mass could be used.

Typical dynamic tearing surfaces obtained are shown in Figures 106 and 107 for - 42°C and in Figures 108 and 109 for - 50°C, using the heaviest pendulum mass of 31.11 kg.

The tearing surfaces of both Figure 107 and 108 is indicative of a "zig-zag" growth, Figure 58a, but Figure 108 seems generally less ductile than Figure 107, in which the ductile tearing appears to have an increased microvoid distribution.

The difference of the tearing surfaces in Figure 107 and 108 would probably be of significance in assessment of dynamic tearing resistance relative to temperature, but seems to have had no effect on the estimated measureable value of δi dynamic at the point of initiation of ductile rupture.

8.2.2. Discussion of Dynamic COD Results (Series C, E, F and H Data)

The dynamic ductile initiation COD, δi dynamic, estimated to be constant at 0.18 mm COD over the range - 30, - 42 and - 50°C, see Section 8.2.1, suggests that higher strain rates suppress the increase in δi, even though the steel is becoming tougher and plastic flow is easier as the temperature increases, see Figure 57 and 67. This is clearly shown with δi slow-static being 0.63 mm COD at - 40°C.

The value of δi is believed to be dependent upon the inclusion spacing and distribution, and the extent of work hardening possible in the matrix, as measured by "n", the work hardening exponent, [25, 129].

In addition, it has been reported that an approximate linear relationship occurs between n^2 and δi, [131]. Because the amount of plastic flow is less at higher strain rates, due to an increased dynamic yield stress, the extent of plastic work hardening is reduced, and it is probably this change in the work hardening exponent which has produced a lower δi dynamic value than δi slow-static.

Since the ability for plastic flow decreases at higher strain rates during ductile tearing, the tearing surfaces of specimens H7 and H10 in Figures 107 and 109 appear less ductile than slow-static surfaces of specimen A4 in Figure 99.

The value estimated for δi dynamic of 0.18 mm COD, is very close to the lower slow-static δi slow value of 0.2 mm. In one respect this is reassuring in relation to the formula used to calculate the value of δ during impact tests, but is a little frustrating since it has not been possible to determine if δi slow at 0.2 mm COD coincides exactly with δi dynamic measured as 0.18 mm COD.

The closeness between δi slow (lower shelf) at 0.2 mm and δi dynamic at 0.18 mm may be assumed to be effectively equal, even though the value of δi dynamic may be slightly different due to the constrained effects on plastic flow and yielding when the first tearing process begins.

If it is assumed that the value of δi dynamic at 0.18 mm COD is relatively constant down to - $90^{o}C$, then from this estimated initiation COD it is possible to determine the temperature at which the cleavage instability transition from series E data crosses the δi dynamic value, see Figures 67a/b and 69a/b.

The transition from series E cleavage initiation to the δi dynamic initiation value at - $58^{o}C$ in Figure 69a/b is very significant, for it is now possible to evaluate a dynamic ductile to cleavage initiation transition for the size and geometry of specimens used, as well as a superposed compliant preload stress intensity and strain rate at the crack tip. This situation is similar to the slow-static loading cleavage to ductile initiation of series B data, explained in Section 8.1.2.3.

The ability to evaluate a genuine increase in the toughness of a structural steel during dynamic loading is of great benefit, and is in contrast to the Charpy K_{id} technique detailed in Section 6.1, which is unable to establish if an increase in toughness is actually a departure from plane strain conditions as yield stress drops for a higher temperature. (Please see Section 8.3 for furtherdiscussion of this point).

The cleavage instability COD at lower shelf of series E data, being dynamic tests with a compliant preload less than 1.6 $KN/mm^{3/2}$ and of linear nature, see Section 8.2.1, is lower than the estimated δi dynamic and δislow COD values in the range - $100^{o}C$ to - $55^{o}C$. As mentioned previously, a ductile to cleavage initiation transition occurs at - $58^{o}C$ for δi dynamic of 0.18 mm COD.

The process of cleavage instability for series E results over the range - $100^{o}C$ to - $55^{o}C$ is attributed to the presence of compliant stored strain energy being available at the relatively sharp crack tip (i.e. not blunted), continuing any cleavage which is initiated during dynamic loading because of the rate-sensitivity of the steel matrix.

It is suggested by the author that these conditions at a crack tip in a structural steel, such as BS4360 - 50D, are the worst possible in terms of fracture behaviour, and institute a "true limit severity" assessment of fracture toughness.

Improvements in fracture toughness as the temperature increases is easily recognised, as shown in Figure 63a/b and Figure 65, above - $70^{o}C$, when the critical COD for cleavage instability increases.

If a higher preload is initially introduced at the crack tip by static loading, a point is reached when the crack's plastic zone becomes large and the displacement is non-linear with respect to load. This point for the specimens tested in this thesis is shown in Figure 68, and is approximately 1.6 $KN/mm^{3/2}$ between - 40 and - $100^{o}C$.

Above 1.6 KN/mm$^{3/2}$, as with series F data, the crack tip is blunted and microvoid coalescence is beginning which will eventually form a ductile tear at δi, (see Section 8.2.1 for full descriptive details).

Since plastic stretch and a small rupture cusp is formed at about 1.7 KN/mm$^{3/2}$, cleavage propagation will be produced from a ductile to cleavage instability transformation, and not from rate-sensitive cleavage initiation as with series E lower shelf results.

From previous knowledge, it is logical to assume that δi dynamic at 0.18 mm COD represents the first "measureable" inclusion cusp to be formed during dynamic crack opening, following from Section 8.1.2.3. As void coalescence occurs around the inclusion(s), there will be a relatively large strain discontinuity at this point. The impactive load will open the crack tip through δi dynamic, and this will be the first significant dynamic strain discontinuity which will be present to change the dynamic rupture growth to cleavage, because of the steels rate sensitivity. The high stored strain energy available external to the specimen from the compliant spring will then continue the cleavage instability to a cleavage crack run condition.

The effective critical COD for cleavage instability of specimens having a preload of approximately 1.7 KN/mm$^{3/2}$ as in series F data, is the value of rupture initiation δi dynamic, at which the first significant strain discontinuity will occur.

As for series E results, above about - 70^{o}C the critical COD for cleavage increases, and coincides with series E data at - 51^{o}C.

The test results of series C utilising impact loading only, with no preload, were principally carried out for comparison with the preloaded test data of series E and F results. Cleavage instability was achieved, but at a higher effective COD value than for series E and F instability transitions. Over the temperature range of - 82^{o}C to - 55^{o}C, series C instability transition occurs at 0.27 mm and 0.46 mm respectively, see Figures 62a/b and 65.

During the impact-only tests of series C results, the crack tip is dynamically opened at a rate of 154 mm/S, however no preload is present so the initial stored strain energy content is much less than series E and F tests, being proportional to the instantaneous opening of the crack tip δ. In addition, the energy available from load applied at the specimen's shoulders is two thirds less than for the notch-bend preload geometry, determined from assumption of Figure 46 that the impact mode is basically a DCB system, see Section 7.2.

Consequently, even though the dynamic load may cause cleavage near the crack tip, if the stored strain energy is not sufficient to run the crack, then a measurable cleavage instability does not occur.

The impact only COD tests must therefore attain a high COD value before adequate energy is available in the specimen to run the crack, and this explains the higher COD instability transition of series C data above series E and F, see Figures 65 and 69a.

The difference between resulting transition instabilities of C data to E and F data, is the increased static stored strain energy content in E and F tests with the superposed compliant preload. For E and F tests, the instant a "significant" cleavage discontuity is produced at or near the crack tip, then the high stored strain energy will continue the cleavage propagation and sever the ligament.

This difference of behaviour between impact only and impact plus superposed preload testing echoes the work of Pellini's drop weight impact to Fearnehough's drop weight plus superposed tensile stress, see Sections 3.3 and 4.1.

These results also show that the Pellini approach of "limit severity" as explained in Section 6.2.1 is not the worst possible laboratory test of a structural steel, unless a compliant superposed preload tensile stress is operative at the crack tip, as used in this thesis for series E and F tests and previously by Fearnehough, [63].

The limited momentum capacity of the pendulum precluded continued testing for an impact-only cleavage instability transition above - 50°C, but it is estimated such an instability transition would require a larger crack opening than series E and F transitions, to allow cleavage initiation and continued propagation in the ligament.

Above - 50°C, series E and F results coincide in terms of cleavage instability, and the materials dynamic toughness increases markedly, see Figures 63, 64 and 65. A larger crack opening is required for instability as temperature increases, due to increasing ability for a plastic zone to be formed and grown at the crack tip, thus relaxing triaxial constraint.

The equivalence of series E and F critical COD's for cleavage instability above - 50°C indicates the final micromechanism of failure is similar, and that preloads in the linear and non-linear range have equal effect. Thus the steel is less prone to instability from dynamic loading triggering cleavage, simply because the dynamic yield stress drops below the fracture stress above - 50°C.

A group of tests to verify the importance of available stored strain energy in the specimen to continue a cleavage discontuity triggered by dynamic loading is given in Table 11, applicable for - 42°C.

As shown in Figure 66, specimens E9 and E6 have low dynamic impact energies of 61.9J, while the compliant preload stress intensity factor is approxiamtely 1.KN/mm$^{3/2}$. For a lower stress intensity factor of about 0.5 KN/mm$^{3/2}$, the dynamic energy of impact must be increased to 163.3J to achieve cleavage instability and crack run, as shown by EM2 and represented by Figure 89 showing the fracture surface. The failures described as E9, E6 and EM2 may vary in combined energies for failure by cleavage, but the critical COD remains constant at about 0.85, see Figures 63, 64, 65 and 69.

The critical COD for a given strain rate at the crack tip therefore defines whether a cleavage discontuity will be triggered ahead of the crack tip, and the combined dynamic and superposed compliant preload energy available when the cleavage event occurs, controls whether the stored strain energy content is sufficient to continue the cleavage into a propagation condition.

The microvoid presence at the crack tip with specimens EM1 and EM2, see Table 7, shown in SEM photos, Figures 111 and 112 respectively, is due to the breaking of forming microvoids in the plastic zone after dynamic impact "damage" and separation at the crack tip from the cleavage instability ahead of the crack tip.

At intermediate values of impact and preload energy, cleavage instability still occurs, but as shown from specimens E6, E7, E8 and E9, in Table 7, and in Figure 66, only small amounts of stretching and microvoid presence occurs.

For preloads above 1.6 $KN/mm^{3/2}$, present with specimen F12 in Figures 111 and 112, show static microvoids have formed in the plastic zone, and are severed when cleavage instability failure occurs.

Because of the minimal presence of rupture processes at the crack tip for E6, E7, E8 and E9 tests of Figure 66, the principal micromechanism of failure by dynamic loading, inducing rate-sensitive cleavage ahead of the crack tip is clearly indicated, instead of a change from dynamic tearing to cleavage instability.

The cleavage initiation and propagation behaviour shown in Figure 66 at - $42^{o}C$ is assumed to continue up to about - $24^{o}C$, as obtained from back-plotting the cleavage run length versus temperature and investigating a "crack arrest" temperature, see Figure 72. However, due to the limited impact momentum available with the present testing rig to attain a higher crack opening, see Section 7.2, cleavage instability tests to ascertain impact and preload energy balance required for continued cleavage growth were not possible above - $42^{o}C$.

The condition of energy balance for series E and F lower shelf transitions between - $100^{o}C$ and - $70^{o}C$ would be interesting to study, but conversely the impact pendulum was found to be too heavy for such tests.

8.3. *Discussion of Significance of Static and Dynamic COD Tests to Real Structures*

For slow-static fracture toughness testing of a notch-bend COD specimen, if the loading system compliance is increased, then the ductile to brittle transition temperature increases. This condition occurs from cleavage instability occurring at a lower COD value at lower shelf temperatures, and an earlier stable tearing instability, due to increased compliance and stored strain energy in the transition toughness range. This is shown clearly in Figure 52, where the ductile to brittle transition temperatures exhibit a difference of 21^{o}C at 0.1 mm COD and 14^{o}C at 0.6 mm COD.

The upper shelf COD values above - 90^{o}C for stiff and compliant COD testing are similar in COD value, but the stiff loaded results exhibit a dominance of plastic collapse behaviour, while the compliant results show less tough fracture surfaces and a modified tearing micromechanism process.

The tearing surface shown in Figure 103 for a compliantly loaded tear at - 90^{o}C suggests that stable crack growth takes a straighter path down from the crack tip, as opposed to stiffly loaded specimen tearing surfaces which are of a zig-zag nature, see Sections 8.1.1 and 8.1.2.3. for details.

During slow ductile tearing of the compliantly loaded tests between - 90^{o}C and - 65^{o}C, at the "upper shelf", the maximum allowable COD value is principally dependent on the stability of the growing crack. This condition occurs because the plastic shear lip formation is limited compared to the stiffly loaded tests, and a plastic collapse character is not yet dominant.

Discontinuities during the process of stable tearing between the transition upper shelf toe and roughly + 30^{o}C from this, may become very important to the stability of the tearing.

Microstructural discontinuities such as large inclusions, porosity, weld defects etc could easily upset the balance of stable tearing and induce cleavage instability with brittle failure. (As exhibited by specimen B4 in Figures 51, 80 and 101).

Additionally, accidental low energy impact or loading machine load surges during the tearing process could cause a driving and restraining force misbalance, as well as elastic wave interaction in the specimen causing reflected tension pulse transients at the growing crack tip.

Therefore, the compliant COD results of series B data would suggest that between - 90°C and - 65°C it is advisable to use design criteria based on δi slow-static for conservative estimates of allowable defect sizes in high stored strain energy determinate structures, for example, liquefied gas pressure vessels.

Since the upper shelf toes of the compliant and stiff COD transitions coincide, see Figure 52, safe design of the type described could be related to the upper shelf toe, evaluated from stiff loading COD toughness tests, (using the BS5762 specifications and a displacement controlled stiff loading machine). Defect analysis using the COD design curve would then determine allowable crack sizes using δi slow-static from the upper shelf toe to about + 30°C, and thereafter reverting to the COD value at upper shelf. This is shown in Figure 61 and 70.

It is of interest to note that δi slow-static of 0.2 mm COD evaluated from back-plot COD testing, is equivalent to the value K_{IC} of 175 $MN/m^{3/2}$, which gives a value of δi = 0.19 mm COD, at about -25°C.

Therefore, recommendations outlined for safe design with determinate-compliantly loaded structures where δi slow-static is mentioned, can be replaced by K_{IC} equivalent in COD, measured for a normal engineering range of temperature.

Another interesting field of study is to help understand pop-in during slow-static COD and K_{IC} tests should be relevant for a given structural application.

As of yet, there is no established concept for assessing the relationship between a given pop-in and crack arrest properties of materials for LPG and LNG gas storage tanks. However, it may be possible to ascertain the significance of a pop-in event if a compliant loading system is used for testing as opposed to a stiff system. The stored strain energy at the crack tip will then be available to continue the pop-in discontinuity if it is critical, as would be the case for unavoidable failure of a pressure vessel.

In addition, it has been shown in this thesis that a low initial stress intensity preload at the crack tip keeps the crack form relatively sharp, and for dynamic impact plus superposed quasi-elastic preload between - 100^{o}C and - 70^{o}C, the critical dynamic COD value for cleavage instability is only 0.01 mm and 0.04 mm respectively.

This emphasises the importance of a low load pop-in at a crack tip, when the stress intensity factor is not sufficient to cause a blunted crack and fully formed plastic zone, but reserves of stored strain energy are available to continue a pop-in event and cleavage instability process.

As shown from the present test results in Figures 73 to 87, no pop-in was found on the P vs clip turn traces during COD tests. This is probably due to the small section size and homogeneity of the microstructure, larger thicknesses and non-homogeneous structures like weld regions will exhibit pop-in more regularly. See recommendation number 3 in section 9.2.

The usefulness of the wide plate testing technique to assess propagation and arrest toughness is without question, but from the evidence put forward in this thesis, its use in terms of initiation and instability toughness assessment is debatable.

This is because the wide plate test cannot induce compliant loading character at the crack tip, therefore the delicate "stable" tearing balance present with a non-decaying opening mode load is not achieved. This would suggest, by reference to wide plate tests described in section 4.2, Figures 11 and 12, [105], that the tearing instability of a wide plate crack tip is not so detrimental as a compliantly loaded notch-bend specimen, such as described in series B test data, Figure 51.

The tests to assess dynamic fracture toughness using the dynamically initiated COD technique have achieved what is suggested by the author to be the "true limit severity" toughness behaviour of BS4360 - 50D normalised structural steel.

This has been achieved by combining dynamic impact and superposed tensile preload at a crack tip, with high levels of stored strain energy available externally from a spring loading system, see section 7.2.

One of the most significant discoveries using this technique is that a dynamic cleavage to ductile initiation transition has been detected at - 58^{o}C, see Figures 67, 69,70 and 71, see also section 8.2.2. The testing technique used in this thesis is therefore a great improvement on the Charpy K_{id} test method, which cannot relate true increases in dynamic fracture toughness, see section 6.1.

The ability to ascertain an initiation transition for a given dynamic strain rate, preload value, load complaince and stored strain energy content of a notch-bend specimen with a pre-fatigued crack is very important. If the service loading conditions of a real structure are modelled in the laboratory, as for example in the tests carried out in this thesis, it should be possible to specify at what temperature design of a dynamically loaded steel structure should be based on K_1 or K_{IC}.

The initiation transition obtained at - 58°C, for the specimens in series F tests of this thesis, being the bounding temperature. Lower temperatures should use K_1 , while for higher temperatures above - 58°C, K_{IC} can be used with confidence.

This is shown from investigation of the instability transitions of series E results above - 58°C, the steel toughness increases in terms of critical COD required for cleavage instability and seems to rise in a manner echoing the rise of δi slow-static, see Figure 57.

At a temperature of - 51°C, series E and F transitions coincide, and combine in terms of required critical COD, for example at - 42°C the critical COD is 0.85 mm, see Figure 65 and Figure 66.

Because of the equivalence of series E and F results above - 51°C, it is realised that the initial static preloads above and below 1.6 KN/mm$^{3/2}$, (or the point of P vs Clip displacement non-linearity, see Figure 68), does not affect the critical COD for failure as shown at lower temperatures.

The compliant preload used will only determine the available stored strain energy in the specimens, but will also introduce a plastic zone at the crack tip.

If it is now assumed the plastic zone size is equal to:-

$$r_y = \frac{1}{2\pi} \left(\frac{K_1^2}{\sigma_{ys}^2} \right) \qquad (37)$$

and by assuming the fatigue crack has an effective crack length of:-

$$a_{\text{fatigued}} + r_{y\ \text{plastic zone}}$$

then it is found that at - 42°C $a_{\text{effective}}$ is 15.43 mm.

By replacing a $_{effective}$ into the equation to find the COD at the crack tip, equation (32), using an opening Vp for criticality as 5.41 mm for δ = 0.85 mm, then the effective COD at instability is modified to 0.59 mm. Similarly, at - 30°C, δ_{eff} = 0.72 and at - 50°C, δ_{eff} = 0.32, see Appendix C.

It is now interesting to find that the values of $\delta_{effective}$ at - 30, - 42 and - 50°C are nearly equal to the values of COD for δi slow-static, in Table 6a and mean line in Figure 57.

The increasing COD for critical instability by cleavage propagation in series E and F data is therefore closely related to the rising value of δi slow-static above about - 65°C, from the point where the δi slow-static curve parts from the δi dynamic estimates, see Figure 67.

These relationships introduce a very important supposition, that with a static preload above about 0.5 KN/mm$^{3/2}$, (determined from specimen EM2 at - 42°C, see Figure 66), over the range of temperature - 51°C up to - 24°C (estimated, see section 8.2.2), dynamic cleavage instability is determined by the value of δi slow-static. The dynamic impact loading therefore causes cleavage instability at the head of the crack tip plastic zone, approximately 3 mm ahead of the original crack tip.

Dynamic cleavage instability caused by impact alone, without any initial preloading, may therefore be dependent on the values obtained for δi dynamic, at 0.18 mm COD, see Table 6b and Figure 67. This would explain some "scatter" cleavage instabilities which occurred during the impact tests of series H data for determination of δi dynamic, see Table 6b.

It becomes clear that further work is required in this domain of fracture research, but two clear observations may now be inferred:-

(1) Above about - 65°C, where δi dynamic remains at 0.18 mm COD, if a preload above 0.5 KN/mm$^{3/2}$ is applied at the crack tip, the cleavage instability is dependent on the value of δi slow-static.

(2) For no preloading, impact only, cleavage instability is related to the value and initiation processes of δi dynamic.

There may be an intermediate range between (1) and (2), and this may be significant for larger specimens, where the stored strain energy is higher for a given size of plastic zone or stress intensity factors, for a given size of crack.

The basic ideas so far developed are envisaged to be of considerable industrial importance, for when a crack of a given size in a structure has a "significant" plastic zone present at the crack tip, a dynamic failure condition is produced when cleavage instability occurs from the tip of the plastic zone relative to δi slow-static initiation processes.

For industrial purposes, it may be possible to generate safe design criteria for dynamically impacted structures, using the COD design curve approach, with the added ability to distinguish the initiation or instability process when a structure is or is not already statically loaded. Obvious uses here would be with respect to welded structures exhibiting built-in residual stress systems.

Further, for dynamic fracture toughness below - $60^{o}C$, the discussion in section 8.2.2 of series E and F results at the lower shelves, it is clear that a low preload stress intensity factor < 1.6 $KN/mm^{3/2}$, which is linear in nature, induces a statically compliant stored strain energy in the specimen, but does not influence the effective sharpness of the crack tip.

For a higher preload, just above 1.7 $LN/mm^{3/2}$, crack stretch has occurred with corresponding blunting and the first stages of microvoid rupture have formed at the crack tip.

Over the series E and F lower shelf range of temperature from $\simeq 100^{o}C$ to - $58^{o}C$, as shown in Figures 65 and 69, the point at which non-linear crack tip behaviour occurs on the P vs clip diagram varies from 1.7 $KN/mm^{3/2}$ to 1.6 $KN/mm^{3/2}$ respectively, as shown in Figure 68, this point being related to the decrease in yield stress as temperature increases.

Because the value of K clip turn is effectively constant over the range - 100°C to - 58°C, if the preload is < clip turn then cleavage initiation occurs during dynamic loading at levels of 0.01 mm to 0.04 mm COD, (for the - 100°C to - 70°C range), whereas, if the stress intensity > K clip turn then the critical dynamic COD for instability to cleavage rises to 0.18 mm at δi dynamic, close to the equivalent COD of 0.19 mm for K_{IC} of the material.

This information is extremely important in terms of industrial proof testing of pressure vessels. If a commissioning proof test is carried out at a temperature of + 20°C, the estimated K clip turn from Figure 68 will be 1.45 KN/mm$^{3/2}$, and this stress intensity factor at a crack will blunt the crack tip. A cleavage instability would only occur at δi dynamic or the (COD) K_{IC} equivalent if a dynamic impact were to occur during low temperature service, over the range - 100°C to - 65°C, see Figure 69 and 70.

However, smaller cracks will have a lower stress intensity applied to them for the given proof loading, and since the smaller cracks will remain effectively sharp, then cleavage initiation will be caused by dynamic impact between - 100°C and - 58°C, if a high level of stored strain energy is present from the compliant preload. These laboratory loading conditions are representative of a low temperature gas pressure vessel.

By using equation (13), $K = \sigma\sqrt{\pi a}$, from section 2.1, for a K value of 1.45 KN/mm$^{3/2}$, (from K clip turn at + 20°C, Figure 68), and assuming a yield stress loading at ≈ 350 N/mm^2 which is the value for 50D steel at + 20°C, then crack sizes larger than 5.46 mm will be "blunted" and cleavage instability will only occur at δi dynamic of 0.18 mm COD, between - 100°C and - 65°C. From the assumption that there is a distribution size of cracks, crack sizes smaller than 5.46 mm will allow dynamic cleavage initiation at much lower COD values, which would be for example, 0.01 mm at - 100°C, 0.04 mm at - 70°C and up to the value of δi dynamic at - 58°C. Defect assessment using K_{id} up to - 58°C would therefore be advisable, if the pressure vessel will be prone to impact loading.

The present discussion seems to contradict the fracture mechanics concepts described in section 2.1, that a large crack is more dangerous than a small one, dependent on the plane strain stress intensity factor K_{IC}. But it is interesting to note that the work by Glucklich, [27], and Paris, [28], exclude considerations of the size of a crack present in a structure, but just that if the combined stress and stored strain energy conditions at a crack tip are favourable, cleavage instability and crack propagation can occur. A structural steel like BS4360 - 50D will satisfy the cleavage initiation condition at a sharp crack tip, if a dynamic loading rate is applied, and the rate-sensitivity of the steel induces the dynamic yield stress to rise above the fracture stress. High stored strain energy available in the matrix will then continue the brittle running crack causing catastrophic failure.

The comments made here, are based on the experimental evidence of this thesis, and are relevant to a normalised structural steel like BS4360 - 50D with a plate thickness of 12 mm.

It seems certain that equivalent effects will be present for structural engineering thicknesses of 50D plate in the plane stress domain, the temperatures and COD values of specific events may be attenuated slightly.

The experimental results of static COD testing, using a compliant-spring loading system has shown that further developments are needed in the assessment of fracture toughness relative to determinate structures for safe-life operation.

The dynamic test programme, combining impact and superposed compliant preload at a crack tip, has been able to show "true limit severity" conditions of a normalised structural steel. The testing method used has also been able to assess real dynamic toughness increases and initiation criteria.

Combining the static and dynamic test results in Figures 70 and 71, it is possible to produce a fracture toughness analysis diagram. This enables a determination to be made of the effects of loading compliance, stored strain energy, dynamic impact and crack tip micromechanism on both the static and dynamic toughness behaviour of any given steel.

9. *Conclusions and Proposals for Future Work*

9.1 *Conclusions*

1) The slow-static ductile to brittle transition temperature of a structural steel is increased for a higher compliance loading and increased stored strain energy content.

2) During static COD testing in the notch-bend mode, the tearing process and micromechanism is modified by the compliance of the loading machine.

3) During dynamic impact, a superposed compliant preload increases the available stored strain energy and can continue cleavage discontinuities into a propagation condition, culminating in ligament brittle failure.

4) Dynamic cleavage instability requires a given strain, strain rate and stored strain energy for cleavage discontinuity and propagation.

5) Above the change from a linear to non-linear P or K vs displacement (K clip turn) behaviour at the crack tip, stretch and blunting occurs. Below the K clip turn described, the crack tip is still relatively sharp, (see Figures 93 and 95).

6) Below - 60^{o}C with dynamic impact during superposed preload < K clip turn, cleavage instability occurs at a low COD, 0.01 mm at - 100^{o}C to 0.04 mm at - 70^{o}C.

7) Below - 60^{o}C with dynamic impact during superposed preload > K clip turn, cleavage instability occurs at δi dynamic at 0.18 mm COD.

8) Above - 65^{o}C δi slow-static rises from 0.20 mm COD to 0.63 mm COD at - 40^{o}C. δi dynamic ($\dot{\delta}$ = 154 mm/S) remains low at about 0.18 mm COD up to - 30^{o}C.

9) Above - 65°C a preload above 1/3(K clip turn)will only allow dynamic cleavage instability ahead of the crack tip, at the statically formed plastic zone boundary (size r_y, see section 8.3).

10) Above - 65°C dynamic impact with no initial preload, initiation and possible cleavage instability occurs at δi dynamic at 0.18 mm COD.

11) After a yield value proof test of a pressure vessel, crack sizes which introduce a static stress intensity factor ≥ K clip turn will be prone to dynamic cleavage instability at δi dynamic = 0.18 mm COD. Crack sizes with stress intensity factors < K clip turn will be prone to dynamic cleavage instability between 1/20 and 1/5 of δi dynamic. (See section 8.3 and Figure 68).

9.2 Recommendations

1) Dynamic impact plus superposed compliant preload tests be carried out:

   (a) Above - 50°C using an increased momentum capacity of pendulum.

and (b) Below - 60°C using a lower momentum of pendulum, and using the $K_{dyn} + K_{static}$ analysis suggested in section 7.2.

2) It is recommended to assess the tearing process in terms of micro-mechanism at a growing crack tip during statically stiff and compliant loading, possibly by utilising the SEM and especially TEM analysis techniques.

3) The effect of a dynamic impact load during the stages of slow-static stable tearing loaded by a compliant loading system, in the range - 90°C to - 65°C or upper shelf toe to + 30°C range. This will allow assessment of the "stability" of tearing, and may help evaluation of the importance of pop-in during slow-static loading, see section 8.3., and Figure 61.

List of References

1. ANDERSON, W E - An engineer views brittle fracture history. Boeing Report, (1969).

2. BIGGS, W D - The brittle fracture of steel. McDonald and Evans, (1960).

3. Journal of the American Welding Society, Vol 26, No 7, July 1947.

4. Report of American Bureau of Shipping, special sub-committee to investigate the failure of S S Schenectady, 11 March 1943.

5. GRIFFITH, A A - The phenomena of rupture and flow in solids. Phil Trans Roy Soc of London, A221 (1921), pp 163 - 197.

6. IRWIN, G R - Fracture Dynamics, Fracturing of Metals, pp 147 - 166, ASM, publ (1948).

7. OROWAN, E - Energy criteria of fracture. Welding Journal, 34 (1955), pp 1575 - 1605.

8. INGLIS, C E - Stresses in a plate due to the presence of cracks and sharp corners. Trans Inst Naval Architects, 55 (1913), pp 219 - 241.

9. WELLS, A A - Unstable crack propagation in metals, cleavage and fast fracture. The Crack Propagation Symposium, pp 210 - 230, Cranfield, (1961).

10. WELLS, A A - Application of fracture mechanics at and beyond general yielding. British Welding Research Ass, Report M13, (1963).

11. BURDEKIN, F M and STONE, D E W - The crack opening displacement approach to fracture mechanics in yielding. J Strain Analysis, 1 (1966), pp 145 - 153.

12. BEGLEY, J A and I ANDES, J D - The J-integral as a fracture criterion. ASTM STP 514, (1972), pp 1 - 20.

13. LEVY, N, et al - Small scale yielding near a crack in plane strain: a finite element analysis. Int J Frac Mech, 7, (1971), pp 143 - 156.

14. BURDEKIN, F M and DAWES, M G - Paper C5 - 71, I Mech E, Conf on Pract App of Fracture Mechanics to p.v.tech, London, May 1971.

15. HARRISON, J D, et al - Elastic-plastic fracture. ASTM-STP-668, ASTM, 1979, 606 - 631.

16. BURDEKIN, F M - Assessment of defects: the COD approach. Conf F.M. in design and service, Living with defects. The Royal Society, London, Dec 1979.

17. HARRISON, J D, et al - The COD approach and its application to welded structures, Elastic-Plastic F.M.

18. WILLOUGHBY, AA; PRATT, P L; TURNER, C E - Inst J of Fract, Vol 17, No 5, October 1981, pp 449 - 466.

19. BERGKVIST, H and ANDERSON, H - Int J of Fract Mech, Vol 8, No 2, June 1972.

20. McCLINTOCK, F A - J of App Mech, Trans ASME, June 1968, pp 363 - 371.

21. SRAWLEY, J E and BROWN, W F - ASTM STP 381, (1965), pp 133 - 195.

22. KAMATH, M S - The COD design curve: an assessment of validity using wide plate tests. W I Research Report, September 1978, 17/1978/E.

23. PUTTICK, K E - J Phys D: Appl Phys, Vol 12, 1979.

24. HANCOCK, P - Stored strain energy effects upon fracture toughness. Proc Int Conf, Fracture toughness testing and methods, interpretation and application, London, 9 - 10 June 1982.

25. BROEK, D - Elementary engineering fracture mechanics. Sijthoff and Noordhoff, 1978.

26. CHELL, G G - Fracture mechanics in the elastic-plastic regime. Proc Int Nat Conf on fracture, Johannesburg, S.A., 7 - 9 November 1979.

27. GLUCKLICH, J - Strain energy size effect. NASA Tech Report, 32 - 1438, August 15, 1970.

28. PARIS, P C, et al - The tearing instability approach, ASTM STP 668, p 5.

29. ALMAR-NAESS, A - Influence of external energy on brittleness in bend tests. Brit Weld J, February 1957.

30. SPURRIER, J et al - Eng Fract Mech, Vol 13, pp 829 - 840, 1980.

31. WELLS, A A - The brittle fracture strengths of welded steel plates, Spring Meeting. Inst of Nav Arch, March 22 1956.

32. WELLS, A A - Brit Weld J, Vol 8, August 1961.

33. WELLS, A A - Brit Weld J, Vol 8, May 1961.

34. GRAF, S H - American Bureau of Shipping, Report on metallurgical aspects of tanker S.S. Schenectady failure, 27 February 1943.

35. WILLIAMS, M L and ELLINGER, G A - Weld Res Supp, Vol 18, No 10, October 1953, p 498 - 500.

36. WILLIAMS, M L and ELLINGER, C A - Brit Weld J, Vol 2, No 6, June 1955, p 254.

37. SHANK, M E - Weld Res Council Bull, No 17, January 1954.

38. BROWN, D P - Weld Journal, Vol 31, No 9, September 1952, p 765.

39. GREENE, T W and HOLZBAUR, A A - Weld Res Supp, Vol 11, No 3, March 1946, p 129 - s.

40. SHANK, M E - Control of steel construction to avoid brittle fracture, N.Y. Weld Res Council, 1957.

41. SINGER, E - Eng Fract Mech, 1 (196º), pp 507 - 517.

42. GREENE, T W - Weld Res Supp, Vol 14, No 5, May 1949, p 193 - s.

43. WELLS, A A - Brit Weld J, Vol 3, January 1956, p 25.

44. GREENSPAN, M - J Res Nat Bur Stand, 1943, Vol 31, p 305.

45. IRWIN, G R and KIES, J A - Weld J, 1952, Vol 41, p 95 - s.

46. IRWIN, G R - J App Mech, 1957, Vol 24, p 361.

47. WELLS, A A - Brit Weld J, 1961, Vol 8, p 259.

48. WOODLEY, C C, et al - BWRA Report, Brit Weld J, March 1964, p 123.

49. BAKER, R G, et al - 2nd Int Conf on Pr Vess Tech, San Antonio, 1 - 4, October 1973.

50. MARIGUE, C and BRAGARD, A - Metal Const, 11, (6), 1979.

51. ROBERTSON, T S - Engineering, 172 (4471), 445, 5th October 1951.

52. COTTON, H - Proc I Mech E, 1979, Vol 193, No 26.

53. PELLINI, W S and LOSS, F J - NRL Report 6913, April 1969.

54. FEARNEHOUGH, G D - Int J of PV and piping, 2 (4), 257 - 282, October 1974.

55. FEARNEHOUGH, G D et al - Proc. Conf. on Pract. App. of F.M. to P.V. technology. p. 156. IMech.E.

56. WEIBULL, A - Proc Roy Swed Inst Eng Res, No 151, 1939.

57. WELLS, A A - Weld Res Supp, May 1952, p 266 - s.

58. DOCHERTY, J G - Engineering, Vol 133, p 645, 1932.

59. DOCHERTY, J G - Engineering, Vol 139, p 211, 1935.

60. LUBAHN, J D, et al - Weld J, Vol 26, p 554 - s, 1947.

61. DAVIDENKOV, N, et al - J App Mech, Vol 14, p 63, 1947.

62. LUBAHN, J D and YAKAWA, S - Proc ASTM, Vol 58, p 661, 1958.

63. FEARNEHOUGH, G D - Brit Weld J, Vol 10, p 607, 1963.

64. DE LEIRIS, H - Sur les conditions de production des dechirures semi-fragiles. Ass Tech Maritime et Aero, 1949.

65. COTTON, H - Materials for Offshore Engineering, Proc I Mech E, 1979, Vol 193, No 26.

66. GLUCKLICH, J - Rilem Bull, No 5, Eng, December 1959.

67. GLUCKLICH, J and COHEN, L J - Int J of Fract Mech, Vols 3 -4, 1967 - 68, p 278.

68. WITT, F J - Eng Fract Mech, Vol 14, pp 171 - 187, 1981.

69. BEGLEY, J A and LANDES, J D - ASTM STP 536, pp 246 - 263, 1973.

70. WITT, F J - The equivalent energy method for calculating elastic-plastic fractures. 4th Nat Symp, Fract Mech, Pittsburg, Pennsylvania, 1970.

71. WITT, F J - Fracture toughness parameters obtained from single small specimen tests. WCAP - 9397, Westinghouse E Corp, 1978.

72. WITT, F J - The equivalent energy method. WCAP - 9521, Westinghouse E Corp, 1979.

73. PARIS, P C, et al - Initial experimental investigation of tearing instability theory, ASTM STP 668, p 251.

74. IIW Commission X, UK Briefing Group, Dynamic Testing - proposed specifications, Metal Construction, September 1975, p 473.

75. BS 5762: 1979, BSI.

76. DAWES, M G - E-P fracture, ASTM-STP-668, 1979, pp 307 - 333.

77. HOLSTEIN, T and BLANEL, J G, Berg Huttenmann Montatsh, 5, 77.

78. ROBINSON, J N and TETELMAN, A S - ASTM STP-559, pp 139 - 158, 1974.

79. ERHARDT, K - Mater Techn (Switz), 1974, 1, 10.

80. COTTON, H C and MACAULAY, I M - Using steel in arctic constructions. Conf on Matls Eng in the Arctic, September 27 - October 1, 1976, Ouebec, Canada.

81. COTTON, H C - Tube and.pipe production. The I and SI, ISI P135, 1976.

82. INGHAM, T, et al - The effect of geometry on the interpretation of COD test data. Paper C54/72, I Mech E, Conf on p.v tech, May 1971.

83. DAWES, M G - ASTM STP-668, 1979, pp 307 - 333.

84. WELLS, A A - The status of COD in fracture mechanics. Canadian Congress of App Mech, Calgary, 1971.

85. DAWES, M G - PhD Thesis, CNAA, December 1976.

86. KANAZAWA, T, et al - IIW Doc X - 702 - 73.

87. WESTERGAARD, H M - J App Mech, 61 (1939), pp A49 - A53.

88. DUGDALE, D S - J Mech Phys Sol, 8, 100, 1960.

89. BILBY, B A, et al - Proc Roy Soc, A272, 304, 1963.

90. ROBINSON, J N and TETELMAN, A S - Un Cal Los Angeles. Rep Eng. 7360 (1973).

91. LEVY, N, et al - Int J Fract Mech, 7 (1971) pp 143 - 156.

92. RICE, J R - J App Mech, 35 (1968) pp 379 - 386.

93. RICE, J R and JOHNSON, M A - In elastic behaviour of solids. Kanninen Ed, pp 641 - 672, McGraw-Hill, (1970).

94. TOWERS, O J and GARWOOD, S J - Weld Inst Res Bull, 1979, 20 (10), 292 - 299.

95. GARWOOD, S J - W I Report, 114/1980.

96. TANAKA, K and HARRISON, J D - Int J PV and piping, 1978, 6 (3 May), 177 - 201.

97. KAMATH, M S and HARRISON, J D - Weld Inst Report, No 36/1977/E.

98. HARRISON, J D, et al - Eng App of Fract Analysis, 1st Nat Conf on Fract, Johannesburg, S.A., 7 - 9 November, 1979, pp 249 1 267.

99. McCLINTOCK, F A - J of App Mech, June 1968, pp 363 - 371.

100. JOHNSTON, G O - Weld Inst Report, 106/1979.

101. JOHNSTON, G O - Weld Inst Report, 110/1980.

102. CHELL, G G - Fracture mechanics in the E-P regime, (as ref 98).

103. BURDEKIN, F M and STONE, D E W - J Strain A, 1, (2), 1966, 145 - 153.

104. SHIH, C F, et al - Int J Pres Ves and Piping 9, (1981), pp 159 - 196.

105. Sumitomo Steel Research Report, No 19, May 1978.

106. BS draft WEE/37, 75/77081 DC, February 1976.

107. BS PD6493, BSI.

108. FEARNEHOUGH, G D and HOY, C J - J I and Steel Inst, Vol 202, 1964, p 912.

109. FEARNEHOUGH, G D and NICHOLS, R W - Int J Fract Mech, 1968, p 4, 245.

110. RADON, J C and TURNER, C E - J I and S I 204, 842 (1966).

111. AUGLAND, B - Brit Weld J, 9, 7, 434, (1962).

112. COTTERELL, B - Brit Weld J, 9, 2, 690, (1962).

113. SERVER, W L, et al - ASTM STP 631, 1977, pp 446 - 461.

114. SRAWLEY, J and BROWN, W - ASTM STP 410, (1966).

115. TURNER, C E - ASTM STP 466, (1970), pp 93 - 114.

116. SERVER, W L and TETELMAN, A S - Eng Fract Mech, 1972, Vol 4, pp 367 - 375.

117. SHOEMAKER, A K and ROLFE, S T - Eng Fract Mech, 1971, Vol 2, pp 319 - 339.

118. PELLINI, W S - WRC Bulletin, 130/May 1968.

119. PELLINI, W S - WRC Bulletin, 1971, Adams Lecture, Weld Res Supp, March 1971, p 91s.

120. LAUGE, E A and LOSS, F J - ASTM STP 466, 1970, pp 241 - 258.

121. PELLINI, W S, et al - NRL Report 5920, 15 March 1963.

122. GOODE, R J, et al - NRL Report 6779, 5 December 1968.

123. JUDY, R W, et al - NRL Report 6879, February 1969.

124. VENZI, S, et al - ASTM STP 446, 165 (1970).

125. NASH, G E - NRL Tech Report 6864, January 1969.

126. EIBER, R J - Fracture Propagation, AGA 4th Symp Cat No L30075, 1969.

127. BS5447, K_{IC} plane strain standard, BSI.

128. KNOTT, J F - Proc ICF4, Waterloo, ed DMR Taplin, Pergamon/Waterloo Press, Vol 1, 61 - 92.

129. KNOTT, J F - The fracture toughness of metals, I Mech E Pub 22 August 1975.

130. BROEK, D - Eng Fract Mech, 5 (1973) pp 55 - 66.

131. GARNETT, G E, PhD Thesis, Cambridge.

132. GREEN, A.P. and HUNDY, B.B., Journal of the Mech. and Phys. of Solids. Vol 4, 1956, pp. 128 - 144.

TABLE 1. SUMITOMO SHT STEEL.

CHEMICAL COMPOSITION.%						YIELD STRENGH (kg/mm^2)
C.	Si.	M.	P.	S.	Ceq.	
0.07	0.21	1.34	0.021	0.004	0.29	Longi. 37.5 Trans. 38.8

TABLE 2. SERVICE AND TESTING LOADING RATES, REFERENCE 74.

Estimates of $\dot{\varepsilon}$, $\dot{\Delta}$, and also $\dot{K}$ for flat plate structural elements in tension

Parent structure	$\dot{\varepsilon}$, sec^{-1}	$\dot{\Delta}$, $mm\ sec^{-1}$	$\dot{K}$, $Nmm^{-3/2}sec^{-1}$
Storage tanks	$<10^{-6}$	-	<10
Hydro tests on pressure vessels and pipelines	$<10^{-5}$	-	$<10^{2}$
Buildings during erection, bridges, and cranes	$<10^{-3}$	-	$<10^{4}$
Aircraft undercarriages	-	10^{4}	$<10^{5}$
Earthmoving and mechanical handling equipment	-	10^{3}	$<10^{6}$
Drop forging press	-	10^{4}	$<10^{7}$
Ships in collision	-	10^{4}	$<10^{7}$
Road and rail transport	-	10^{5}	$<10^{7}$
Military equipment subject to explosive or projectile attack	-	10^{7}	$<10^{12}$

$\dot{K}$ for standard three-point SENB K_{IC} steel test specimens

Load point displacement rate, $\dot{\Delta}$, $mm\ sec^{-1}$	Stress intensity rate, $\dot{K}$, $Nmm^{-3/2}sec^{-1}$		
	Thickness, B, mm		
	10	B	150
Static tests 10^{-3}	9.1		2.3
Static tests 10^{-2}	9.1×10^{1}		2.3×10^{1}
10^{n}	$9.1 \times 10^{3+n}$	$\frac{2.87 \times 10^{4+n}}{B^{1/2}}$	$2.3 \times 10^{3+n}$
Pendulum and falling weight impact tests 10^{3}	9.1×10^{6}		2.3×10^{6}
Pendulum and falling weight impact tests 10^{4}	9.1×10^{7}		2.3×10^{7}

TABLE 3. BS4360-50D CHEMICAL COMPOSITION.

CHEMICAL COMPOSITION.%							
C	Mn	S	P	Si	Nb	AL	Ti
0·110	1·360	<0·005	0·012	0·470	0·028	0·020	<0·010

V	Ni	Cr	Mo	Cu	Fe
<0·010	0·060	0·50	0·010	0·070	balance.

TABLE 4. SERIES A STATIC COD MAX. LOAD - STIFF.

SPECIMEN NUMBER.	T °C.	g/W.	MAX. LOAD δ mm.	FIGURE NUMBER. PvsVp.	SEM FIGURE NUMBER.	VALID BS5762? >0·45>0·55
				See Fig 53.		
A1	-40	0·562	1·169	73		× just.
A2	-80	0·537	1·159	74		✓
A3	-90	0·557	1·099	75		× just.
A4	-95	0·566	0·819	76	90,97,98 99,100.	×
A5	-99	0·541	0·516			✓
A6	-105	0·560	0·843	77	90	× just.
A7	-105	0·527	0·709			✓
A8	-110	0·541	0·848			✓
A9	-110	0·528	0·349			✓
A10	-125	0·542	0·081	78		✓
A11	-135	0·548	0·080			✓
A12	-196	0·548	7.4×10^{-3}	-	-	✓

TABLE. 5. SERIES B STATIC COD MAX. LOAD - COMPUANT.

SPECIMEN NUMBER.	T°C.	o/w.	MAX LOAD.	FIGURE NUMBER.	SEM FIGURE NUMBER.	VALID BS5762? 70·457055
			δmm.	PvsVp.		
				See Fig. 53.		
B1	-25	0·488	1·381			✓
B2	-38	0·535	1·266	79		✓
B3	-60	0·570	1·105			x
B4	-70	0·498	0·397	80	101	✓
B5	-75	0·535	1·110			✓
B6	-80	0·534	1·213	82		✓
B7	-80	0·530	0·888			✓
B8	-86	0·535	1·194			✓
B9	-85	0·589	0·930			x
B10	-90	0·533	1·033	84	90, 102, 103, 104, 105	✓
B11	-91	0·535	0·459			✓
B12	-95	0·581	0·317	85		x
B13	-95	0·556	0·161			x just
B14	-105	0·578	0·052	86		x
815	-120	0·508	0·026	87		✓

TABLE 6. EVALUATION OF δi SLOW + DYNAMIC.

	SPECIMEN NUMBER	T °C.	δ m.m.	Δa m.m. S.S.T.	* Some specimens failed unexpectedly - see section 8.3.	δi by Linear regression	Estimate of δi mm. transition
SLOW-STATIC δi. FIG 57.	G1	-100	0.746	0.433	at -100°C	0.23	≃0.2
	G2	-100	0.495	0.239			
	G3	-100	0.391	0.070			
	G4	-100	0.268	0			
	G5	-70	0.896	0.718	at -70°C	0.20	≃0.2
	G7	-70	0.574	0.379			
	G6	-70	0.823	0.628			
	G8	-40	1.006	1.029	at -40°C	0.64	±0.64
	G9	-40	0.785	0.407			
DYNAMIC δi. FIG 57.	H1	-30	0.334	0.1521	at -30°C	0.186	±0.18
	H2	-30	0.388	0.398			
	H3	-30	0.625	0.450			
	H4	-30	0.794	0.625			
			*		* ONE SPECIMEN FAILED BY CLEAVAGE AT ABOUT δ = 0.50mm, SEE FIG 62a|b		
	H5	-42	0.341	0.184			
	C2	-42	0.436	0.241	at -42°C	0.202	±0.18
	H6	-42	0.580	0.359			
	H7	-42	0.787	0.642			
			*		* ONE SPECIMEN FAILED BY CLEAVAGE AT ABOUT δ = 0.67mm, SEE FIG 62a|b		
	H8	-50	0.247	0.062			
		-50	0.396	0.222	at -50°C	0.174	≃0.18
	H10	-50	0.709	0.503			

TABLE .7. CRACK TIP STRETCH AND TEAR SIZES FROM SEM.

SPECIMEN NUMBER.	STRETCH COD. μm.	TEAR DEPTH. μm.	T°C.	SEE TABLE.
E9	22·6	0-5	-42	11
E6	110	0-62	-42	11
EM2	152	62-123	-42	11
EM1	152	77	-42	11
F12	152	46-108	-42	11
E8	46	0-62	-42	11
E7	46	0-77	-42	11
E4	318	40-55	-42	11
E20	138	0-5	-70	9
E12	22	0	-70	9
E5 SEE FIG 93*	17	0	-60	9
F8 SEE FIG 95*	190	0-15	-68	9

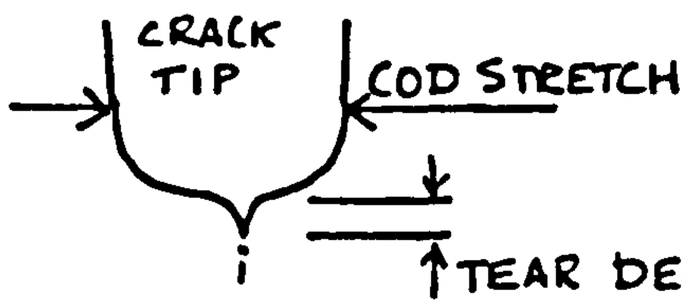

TABLE 8. Dynamic impact only, no preload, go-no-go instability.

SPECIMEN NUMBER.	T°C.	IMPACT ENERGY J.	g/w.	INCREASE IN CRACK LENGTH.	δ DYNAMIC COD.
C1	-30	94·1	0·534	BT	0·388
C2X	-42	94·1	0·553	0·1T	0·436
C3	-47	94·1	0·540	0·1T	0·349
C4	-50	94·1	0·534	0·5T	0·396
C5X	-60	94·1	0·544	0·2T	0·383
C6	-60	94·1	0·530	0·15T	0·370
C7	-67	94·1	0·525	0·6T	0·372
C8X	-48	94·1	0·566	2·5R	0·747
C9X	-55	94·1	0·544	1·8R	0·525
C10	-55	94·1	0·548	1·8R	0·512
C11	-60	94·1	0·534	1·5R	0·549
C12	-60	94·1	0·538	2·2R	0·539
C13	-60	94·1	0·538	3·5R	0·899
C14	-85	94·1	0·540	4·5R	0·376
C15*	-100	94·1	0·530	2·5R m.m.	0·196 m.m.

B - BLUNT, T - TEAR, R - CLEAVAGE INSTABILITY RUN.

Table applies to Fig. 62a1b and Fig. 65.

TABLE 9. Dynamic impact plus superposed compliant preload $< 1{\cdot}6 kN/mm^{3/2}$, go-no-go instability.

SPECIMEN NUMBER.	T°C.	IMPACT ENERGY. J.	ø/w.	INCREASE IN CRACK LENGTH.	& DYNAMIC COD.	PRELOAD K VALUE. $kN/mm^{3/2}$
E1	-33	94·1	0·554	BT	0·760	1·40
E2	-40	94·1	0·576	BT	0·748	1·59
E3	-42	94·1	0·550	BT	0·583	1·06
E4	-42	94·1	0·546	BT	0·422	0·52
E5	-60	94·1	0·553	BT	0·106	0·86
E6	-42	61·9	0·539	4·6 R	0·986	1·02
E7	-42	94·1	0·546	4·9 R	0·953	1·05
E8	-42	94·1	0·547	4·8 R	0·937	0·73
E9	-42	61·9	0·552	4·0 R	0·906	0·86
E10	-60	94·1	0·532	3·9 R	0·389	0·80
E11	-60	94·1	0·543	5·4 R	0·361	1·14
E12	-70	94·1	0·594	7·0 R	0·075	1·00
E13	-77	94·1	0·544	9·4 R	0·109	0·83
E14	-88	94·1	0·598	7·8 R	0·072	1·27
E15	-100	94·1	0·518	9·0 R	0·177	1·05
EM2	-42	163·3	0·537	4·0 R	0·940	0·51
EM1	-42	163·3	0·531	4·1 R	0·912	0·99
				m.m.	m.m.	

B - BLUNT , T - TEAR , R - CLEAVAGE INSTABILITY RUN.

Table applies to Fig. 63a1b and Fig. 65.

TABLE 10. Dynamic impact plus superposed compliant preload > 1·6kN/mm$^{3/2}$ or > Kclio tum (see Fig. 6B.

SPECIMEN NUMBER.	T°C.	IMPACT ENERGY. J.	a/W.	INCREASE IN CRACK LENGTH. m.m.		δ DYNAMIC COD. m.m.	PRELOAD K VALUE. kN/mm$^{3/2}$
F1	-21	94·1	0·533	BT		0·583	1·52
F2	-32	94·1	0·539	BT		0·798	1·64
F3	-41	94·1	0·575	BT		0·800	1·65
F4	-47	94·1	0·536	BT		0·606	1·64
F5	-50	94·1	0·549	BT		0·446	1·72
F6	-50	94·1	0·536	BT		0·405	1·58
F7	-60	94·1	0·534	BT		0·200	1·61
F8	-68	94·1	0·531	BT		0·162	1·55
F9	-85	94·1	0·528	BT		0·005	1·38
F10	-88	94·1	0·554	BT		0·142	1·90
F11	-100	94·1	0·538	BT		0·086	1·74
F12	-40	94·1	0·518	4·8	R	0·989	1·53
F13	-39	94·1	0·528	4·6	R	0·964	1·68
F14	-48	94·1	0·579	4·5	R	0·771	1·68
F15	-50	94·1	0·553	7·0	R	0·451	1·55
F16	-50	94·1	0·546	7·0	R	0·434	1·70

PTO.

B - BLUNT , T - TEAR , R - CLEAVAGE INTABILITY RUN.

Table applies to Fig. 64a1b and Fig. 65.

* table continued overleaf.

TABLE .10. (CONTINUED).

SPECIMEN NUMBER.	T°C.	IMPACT ENERGY. J.	a/W.	INCREASE IN CRACK LENGTH.	δ DYNAMIC COD	PRELOAD K VALUE. KN/MM$^{3/2}$
F17	-58	94·1	0·541	8·0	R 0·539	1·71
F18	-60	94·1	0·539	8·5	R 0·428	1·92
F19	-60	94·1	0·541	5·9	R 0·368	1·49
F20	-70	94·1	0·549	8·0	R 0·212	1·80
F21	-70	94·1	0·551	7·4	R 0·218	1·71
F22	-70	94·1	0·548	8·5	R 0·425	1·97
F23	-70	94·1	0·531	9·0	R 0·554	1·77
F24	-80	94·1	0·556	9·5	R 0·412	1·76
F25	-100	94·1	0·537	9·0	R 0·171	1·59
F26	-100	94·1	0·531	3·8 m.m.	R 0·171 m.m.	1·69

TABLE 11. CLEAVAGE INSTABILITY ENERGY REQUIREMENTS DURING DYNAMIC IMPACT AND SUPERPOSED PRELOAD.

$\delta = 0{\cdot}85$ m.m. (SEE FIG. 65).

SPECIMEN NUMBER.	TEMP. °C.	PRELOAD K. kN/mm$^{3/2}$.	IMPACT ENERGY J.	IMPACT PENDULUM MASS kg.	CLEAVAGE RUN OR BLUNT.
EM1	-39	1·00	163·3	31·11	RUN
EM2	-40	0·51	163·3	31·11	RUN
EM3	-42	0·41	163·3	31·11	BLUNT
H7	-42	0	163·3	31·11	BLUNT
H6	-42	0	123·9	23·61	BLUNT
F13	-42	1·68	94·1	17·93	RUN
F12	-42	1·53	94·1	17·93	RUN
E7	-42	1·05	94·1	17·93	RUN
E8	-42	0·74	94·1	17·93	RUN
E4	-42	0·53	94·1	17·93	BLUNT
C2	-42	0	94·1	17·93	BLUNT
E6	-42	1·03	61·9	11·80	RUN
E9	-42	0·86	61·9	11·80	RUN
E11	-42	0·85	61·9	11·80	BLUNT
H5	-42	0	61·9	11·80	BLUNT.

Data applies to Fig. 66.

TABLE 12. Dynamic impact plus superposed stiff preloads. As described section 7.3., equivalent to series C impact only.

SPECIMEN NUMBER.	T°C.	IMPACT ENERGY. J.	a/W.	INCREASE IN CRACK LENGTH.	δ DYNAMIC COD.	PRELOAD K VALUE $KN/mm^{3/2}$
				m.m.	m.m.	
D1	-42	94·1	0·540	0·3T.	0·522	1·03
D2	-42	94·1	0·532	0·2T.	0·557	1·53
D3	-42	94·1	0·587	0·1T	0·635	1·22
D4	-60	94·1	0·537	1·0T	0·905	1·02
D5	-70	123·9	0·610	1·5 T+R	0·451	1·33

B - BLUNT , T - TEAR , R - CLEAVAGE INSTABILITY RUN.

TABLE 13.

THE FOLLOWING LIST SHOWS THE AUTHORS' ABBREVIATIONS FOR VARIOUS DESIGNATORY DATA IN THIS THESIS.

ABBREVIATION.	DESCRIPTION.
δ	CRACK OPENING DISPLACEMENT RELATIVE TO ORIGINAC CRACK TIP.
$\dot{\delta}$	COD OPENING RATE.
$\dot{\epsilon}$	STRAIN RATE AT CRACK TIP.
δi dynamic	Impact STABLE TEARING INITIATION.
δi slow-static.	Static STABLE TEARING INITIATION.
Kclip turn.	PRELOAD AT WHICH STATIC LOADING NON-LINEARITY OCCURS IN $KN/mm^{3/2}$.
$Z_{imp.}$	"ABUTMENT" HEIGHT FOR RAM IMPACT, SEE EQ.(32).
$a_{NB.}$	CRACK LENGTH RELATIVE TO NOTCH-BEND, SECTION 7.2.
$a_{DCB.}$	CRACK LENGTH RELATIVE TO DCB, SECTION 7.2.
$\sigma_{ys.}$	YIELD STRESS IN TENSION.

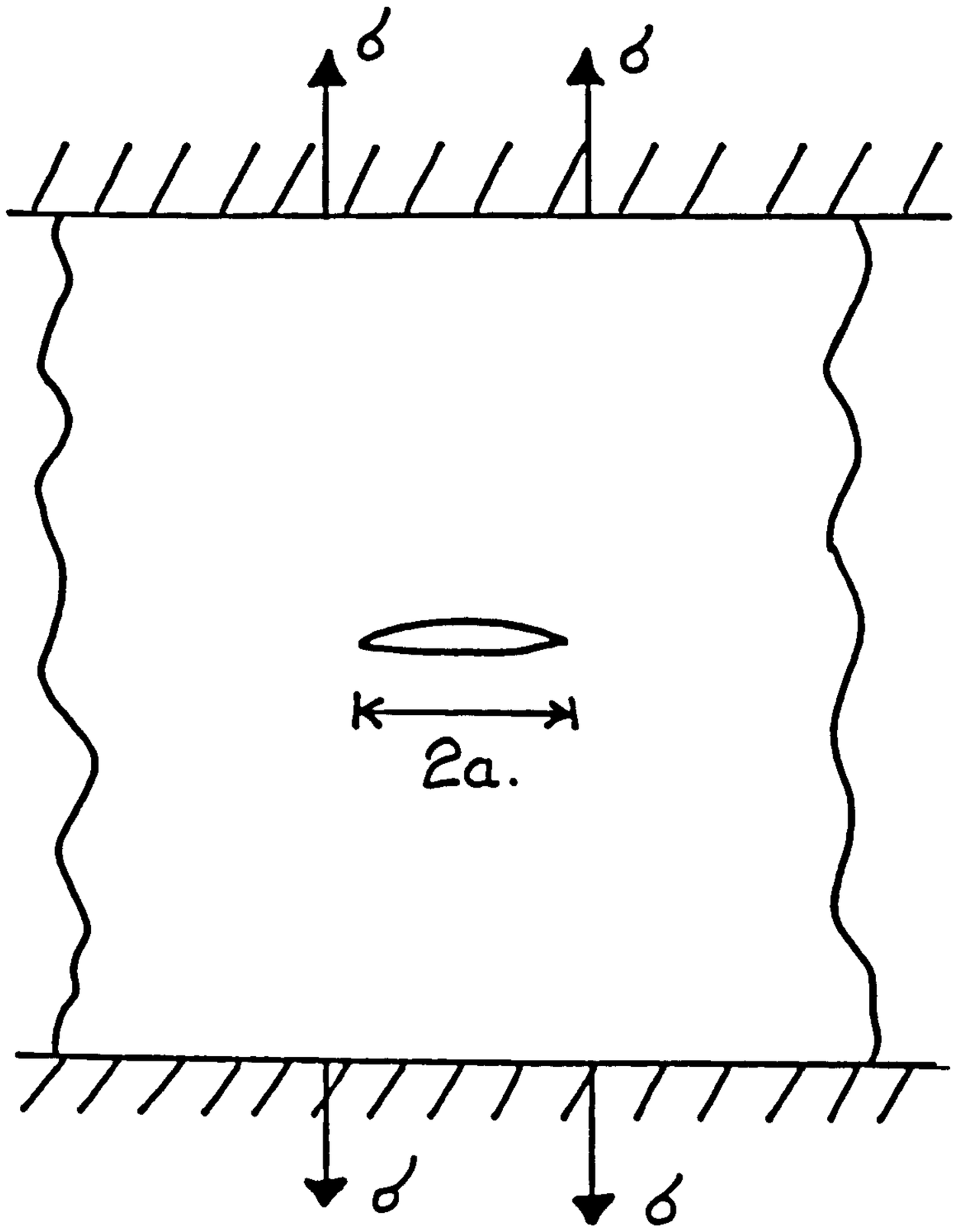

Fig 1. Griffith cracked plate with fixed ends.

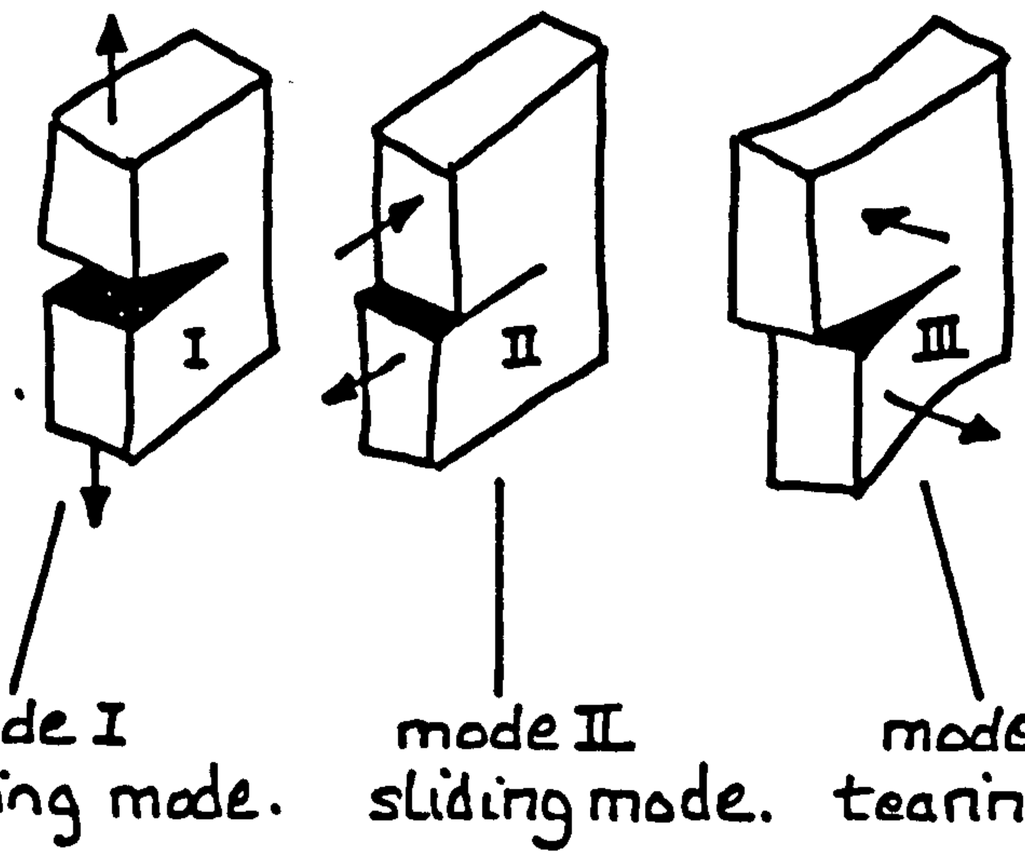

Fig 2. The three modes of cracking.

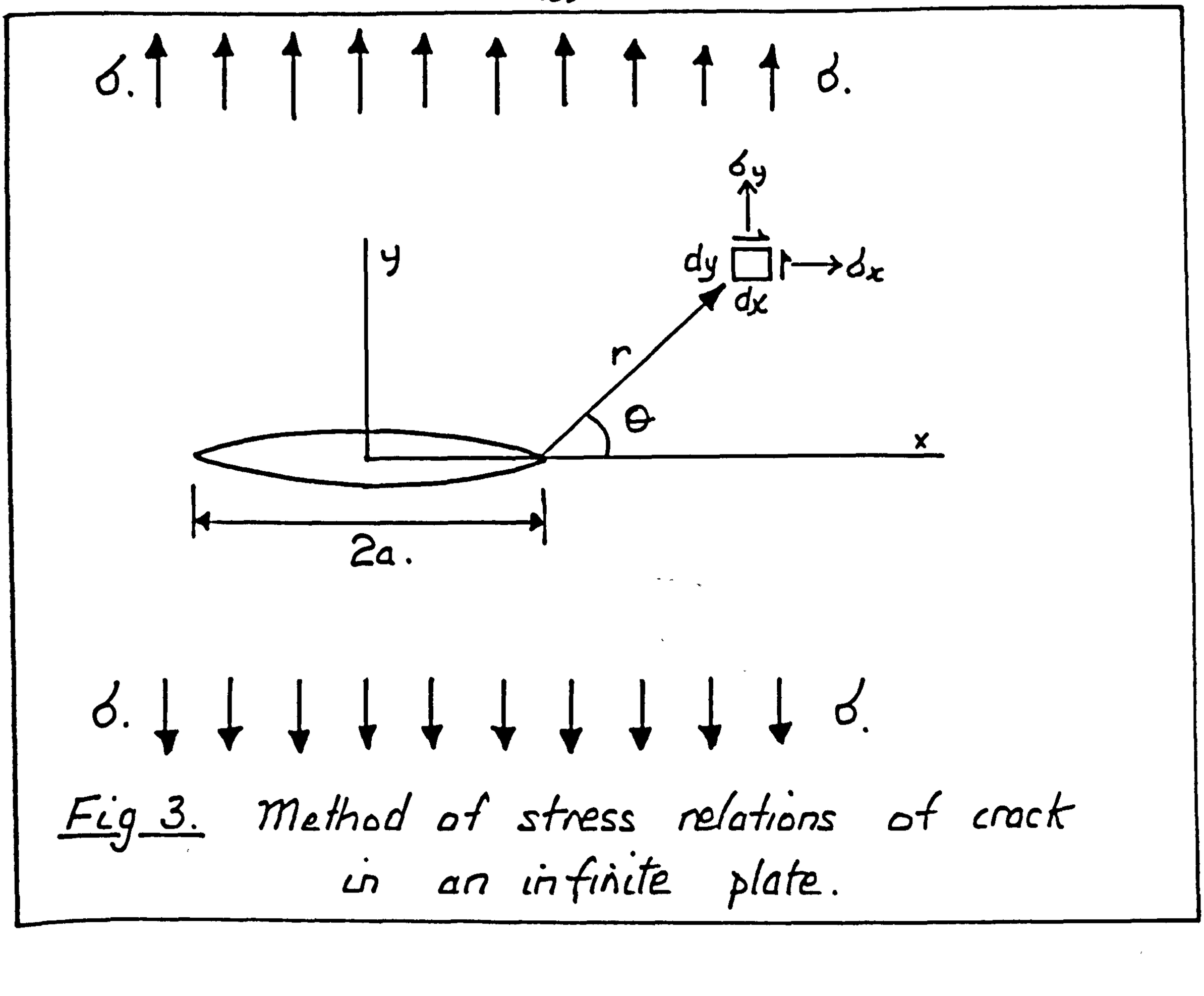

Fig 3. Method of stress relations of crack in an infinite plate.

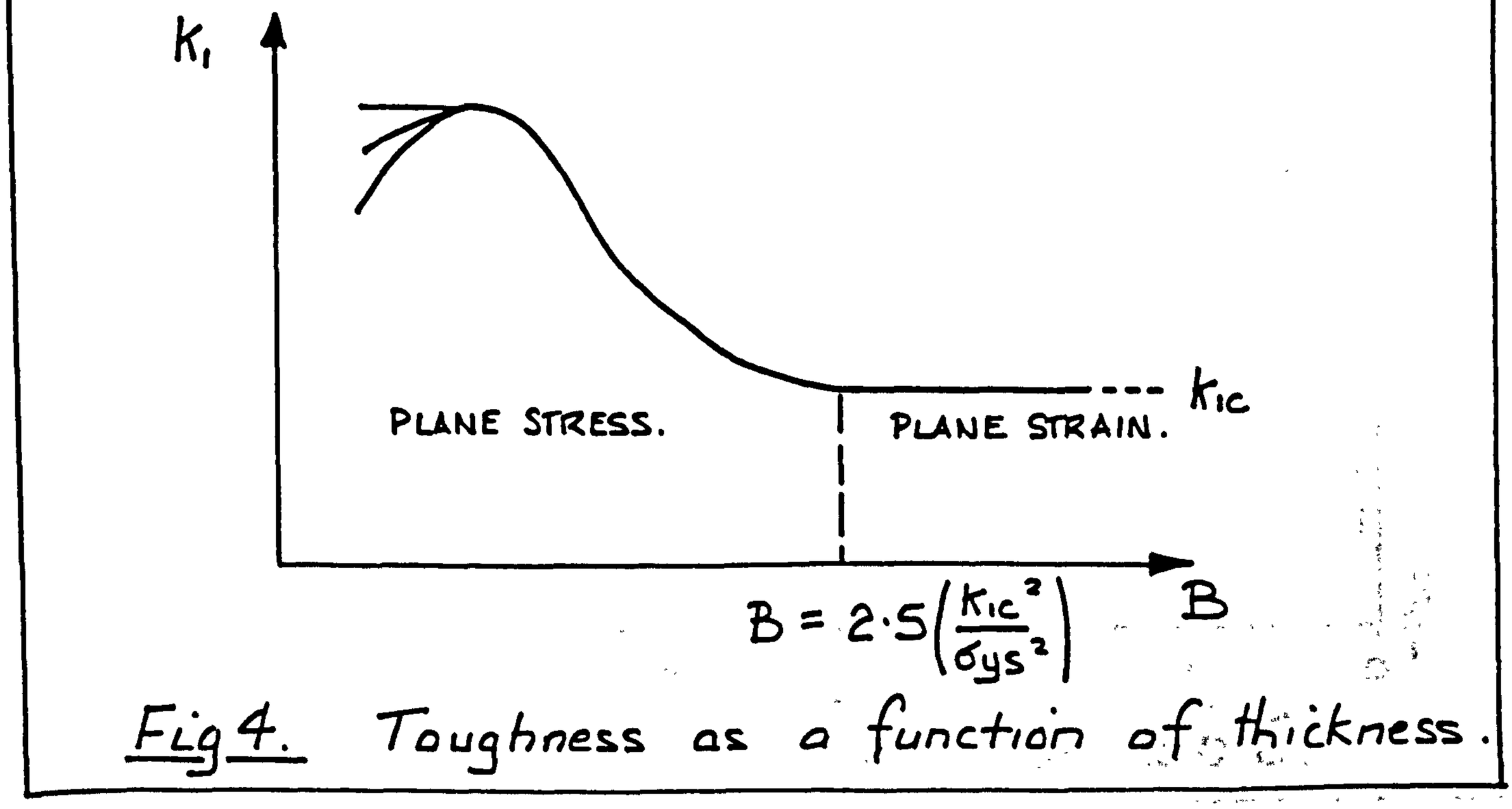

Fig 4. Toughness as a function of thickness.

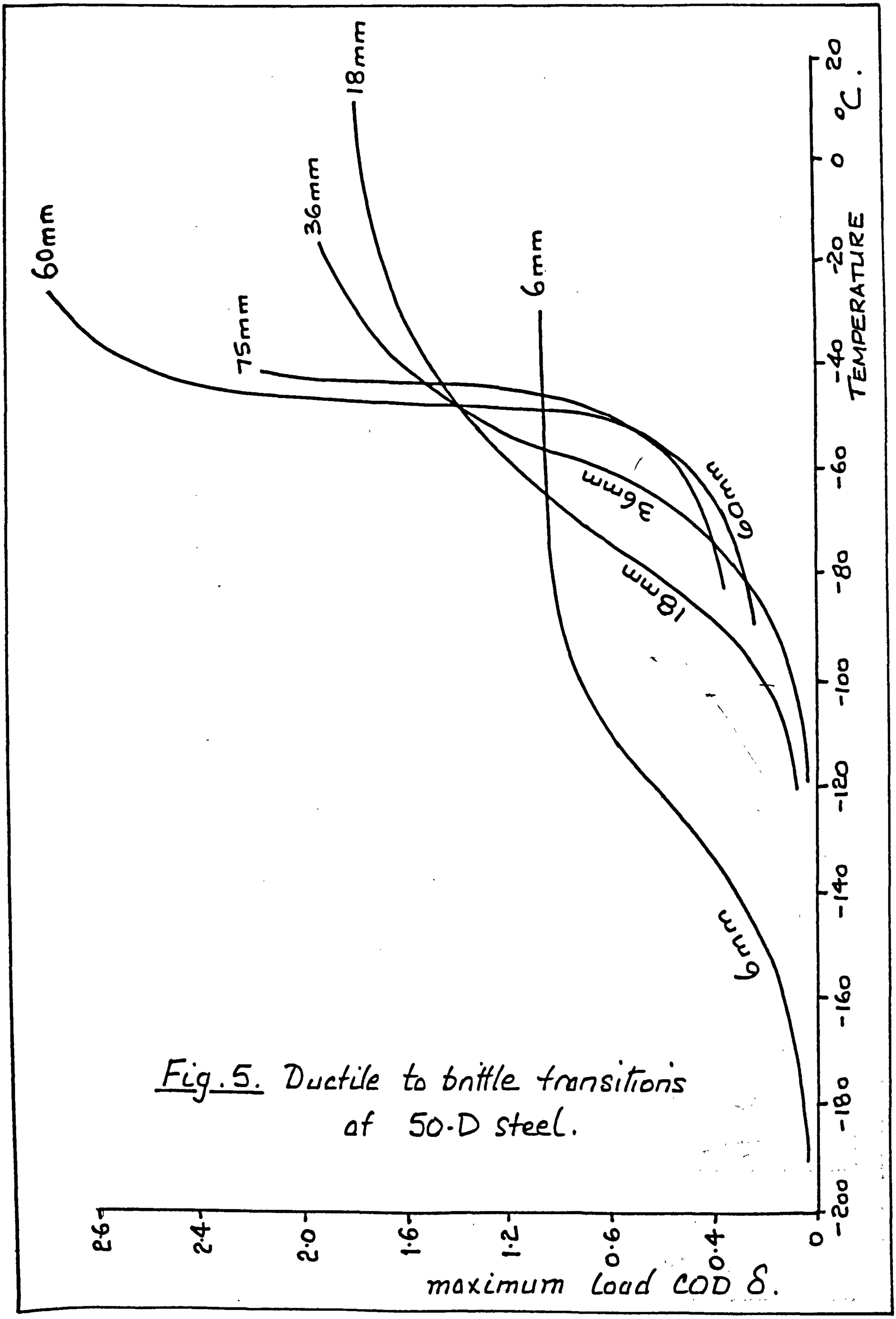

Fig. 5. Ductile to brittle transitions of 50-D steel.

INDETERMINATE STRUCTURE

LOAD REDUNDANCY.

LOAD DECAYS QUICKLY, TAKEN BY OTHER MEMBERS.

but!

DUE TO DAMAGE DURING SERVICE MAY TRANSFORM PART OR ALL OF STRUCTURE TO A SEMI-DETERMINATE TYPE, e.g. ACCIDENTAL DAMAGE, FATIGUE, CORROSION ETC..

LABORATORY EQUIVALENT, DISPLACEMENT CONTROL, STIFF.

DETERMINATE STRUCTURE

SINGLE LOAD MEMBER - NO LOAD REDUNDANCY.

HIGH STORED STRAIN ENERGY AVAILABLE IF FRACTURE INSTABILITY OCCURS.

for example.

LIQUIFED GAS PRESSURE VESSELS.

LABORATORY EQUIVALENT, LOAD CONTROL, COMPLIANT.

Fig.6. General considerations of industrial structures and laboratory testing.

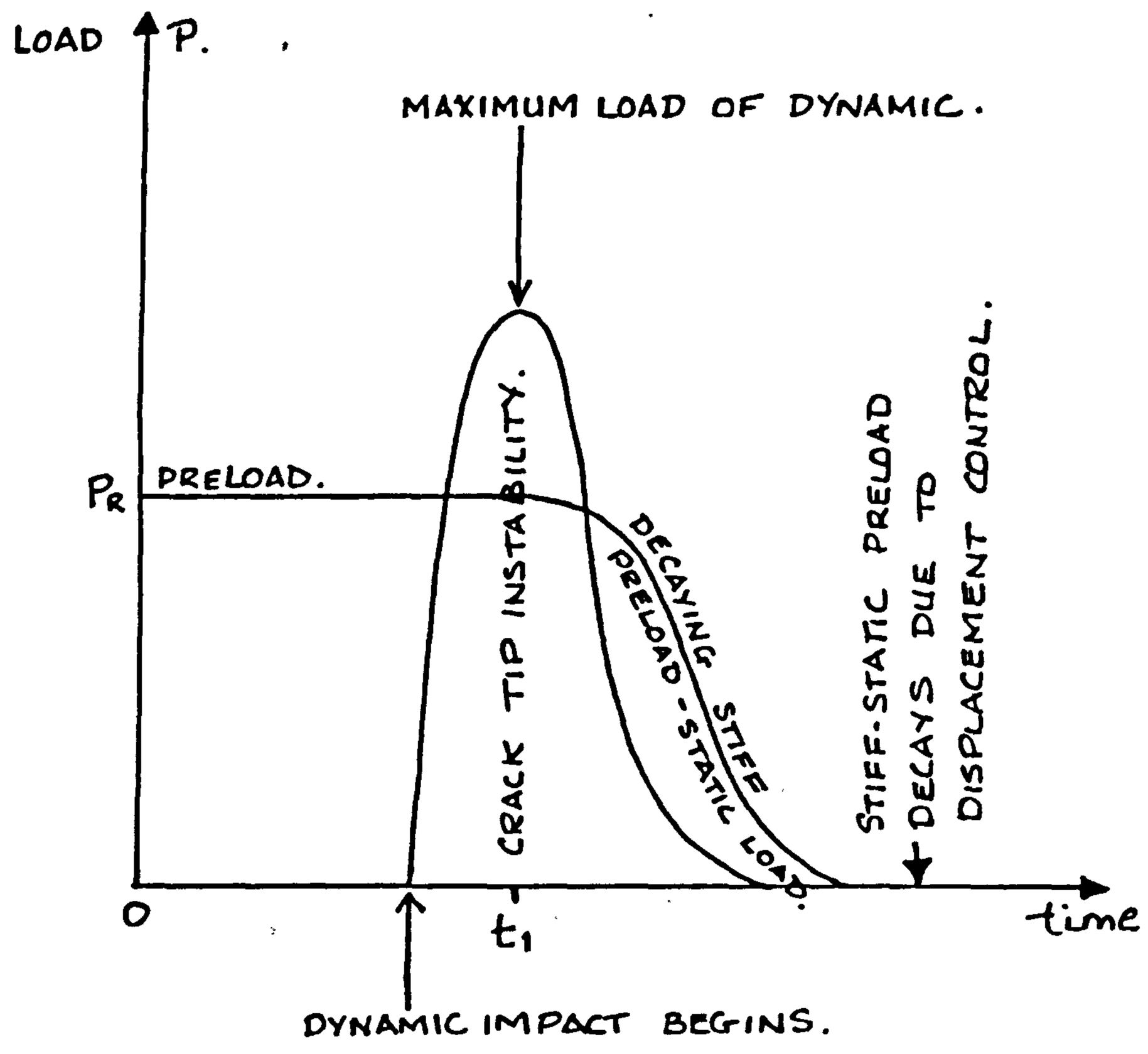

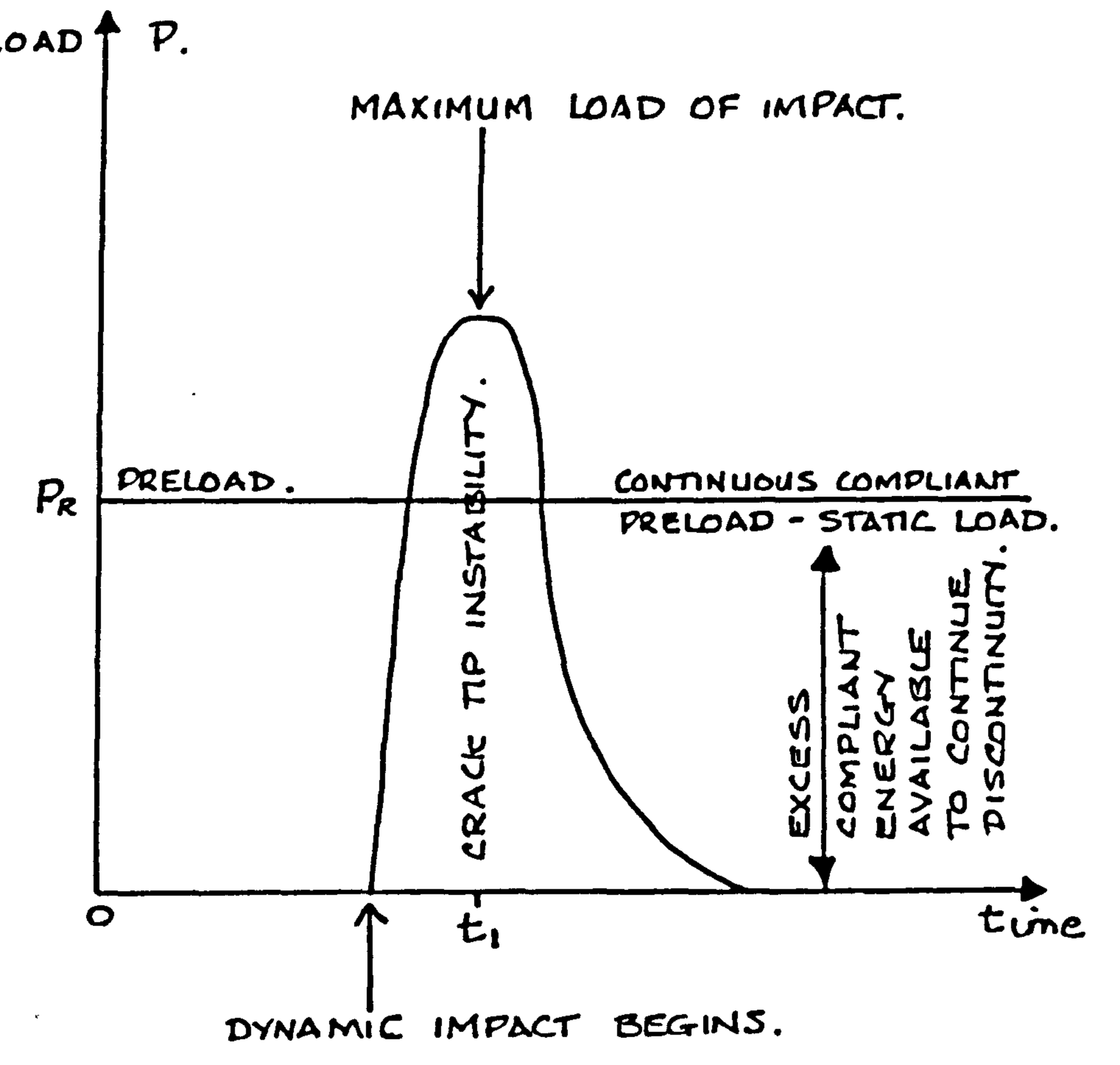

Fig. 7. Load behaviour during impact instability at a crack tip during stiff and compliant preload, P_R.

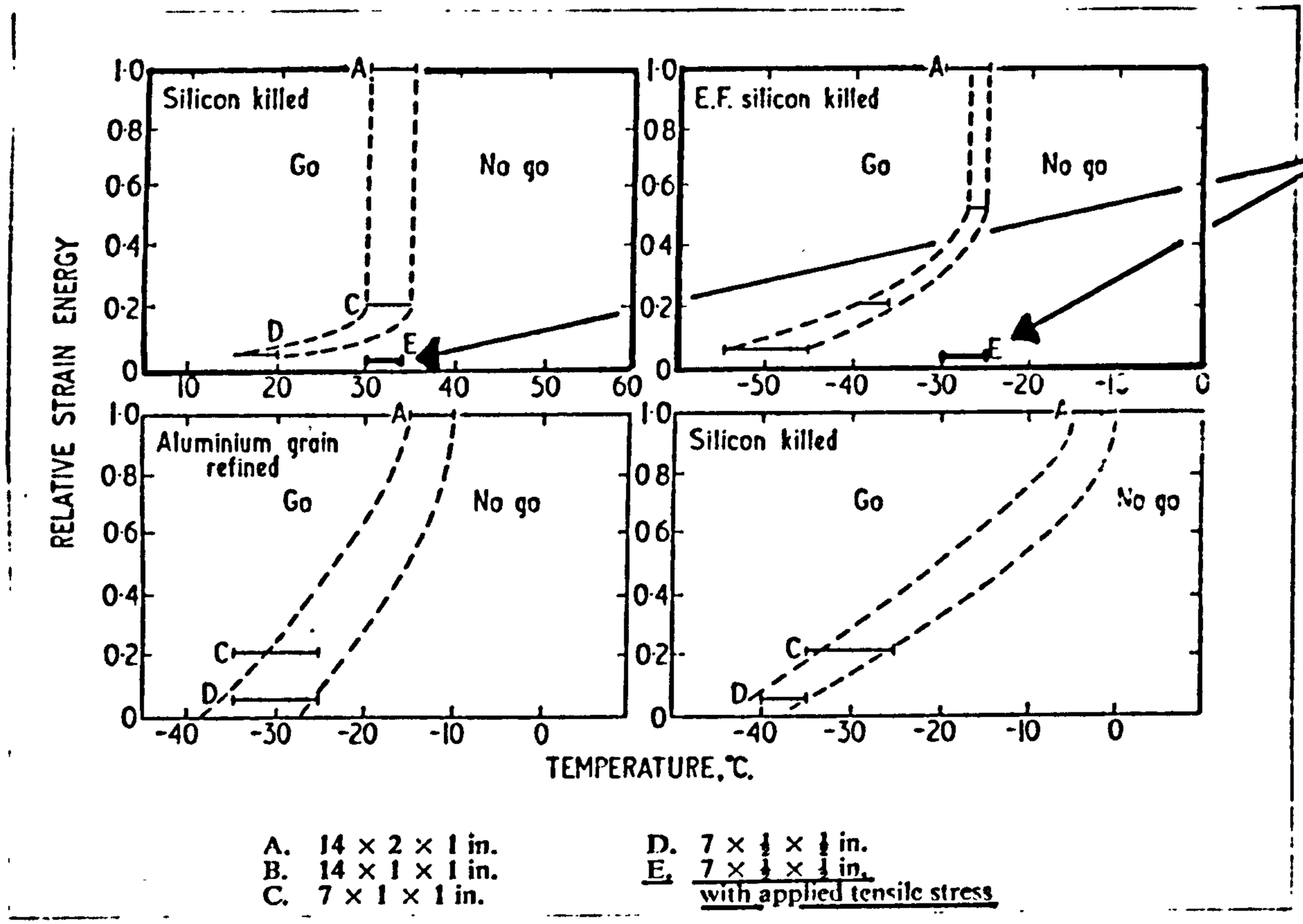

Fig.8. Increase in 'go-no-go' transition temperature from increased stored strain energy. Superposed tensile stress shown with tests E, from Feamehough Ref. 63.

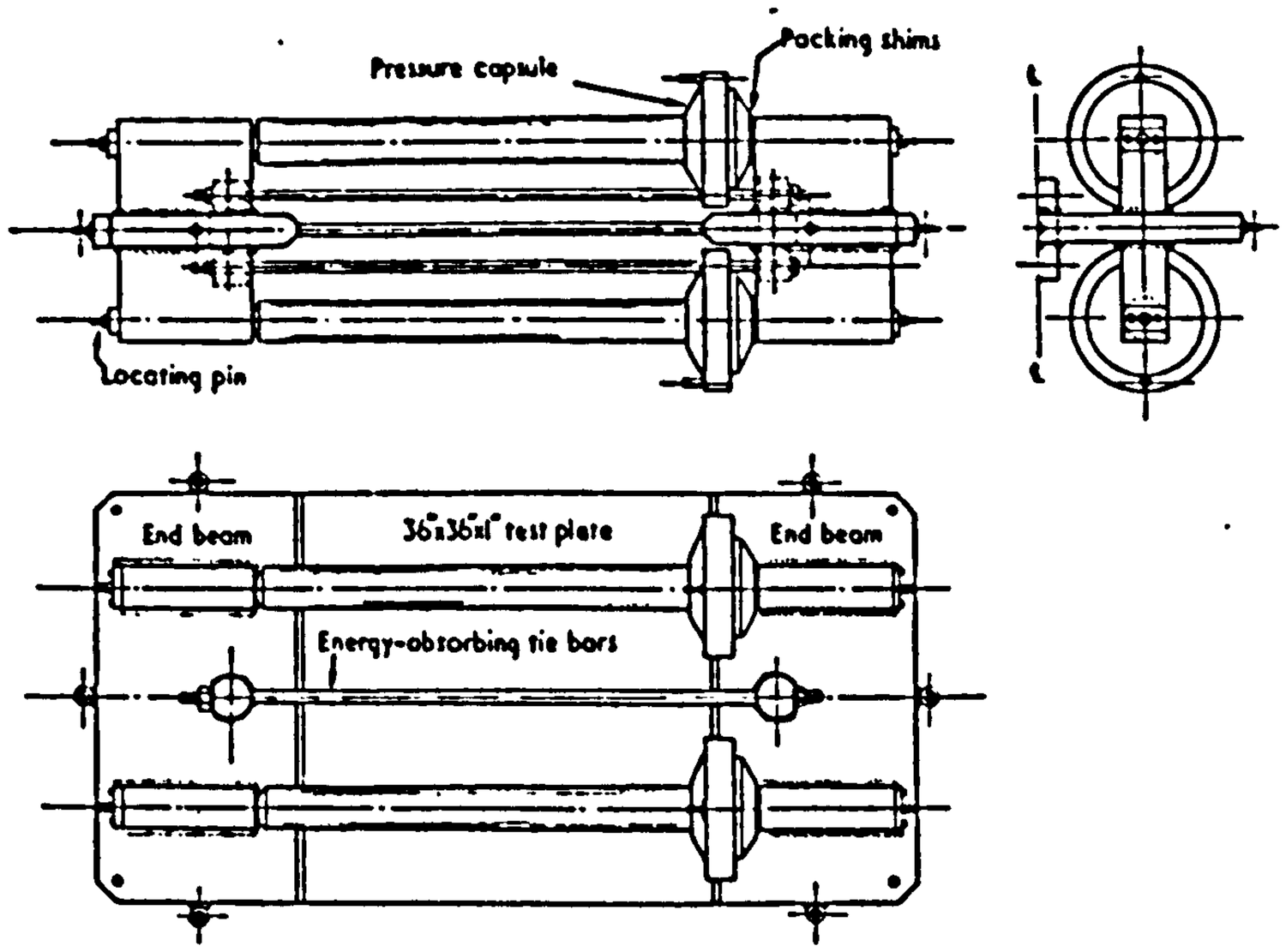

Weights: Test plate 360 lb.
End beams (each 1075 lb.) 2150 lb.
Thrust units (each 280 lb.) 1120 lb.
Total 3630 lb.

Fig. 9a. 600 ton wide plate testing rig.

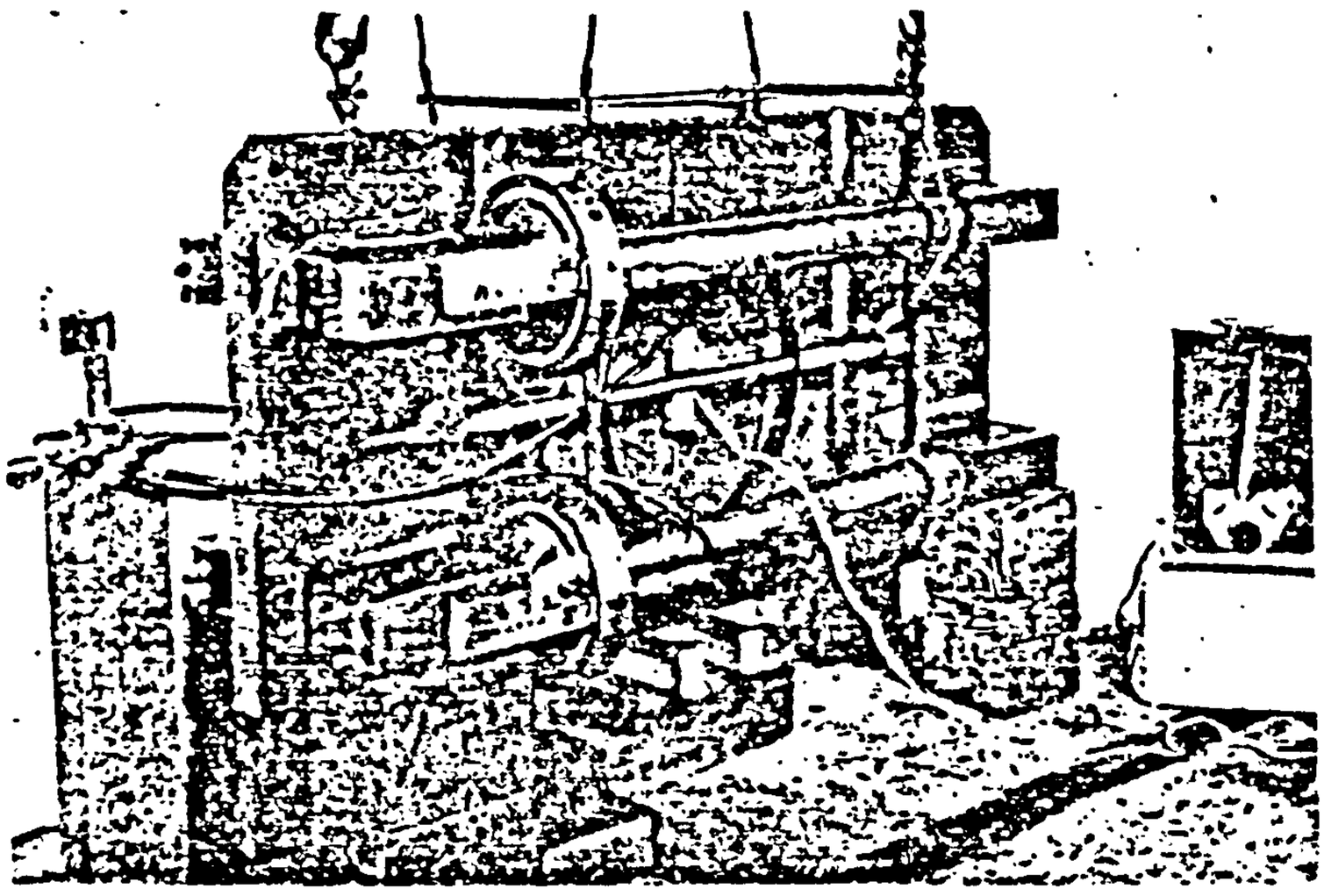

Fig. 9b Photograph of 600 ton rig, both 9a and 9b from Ref. 43.

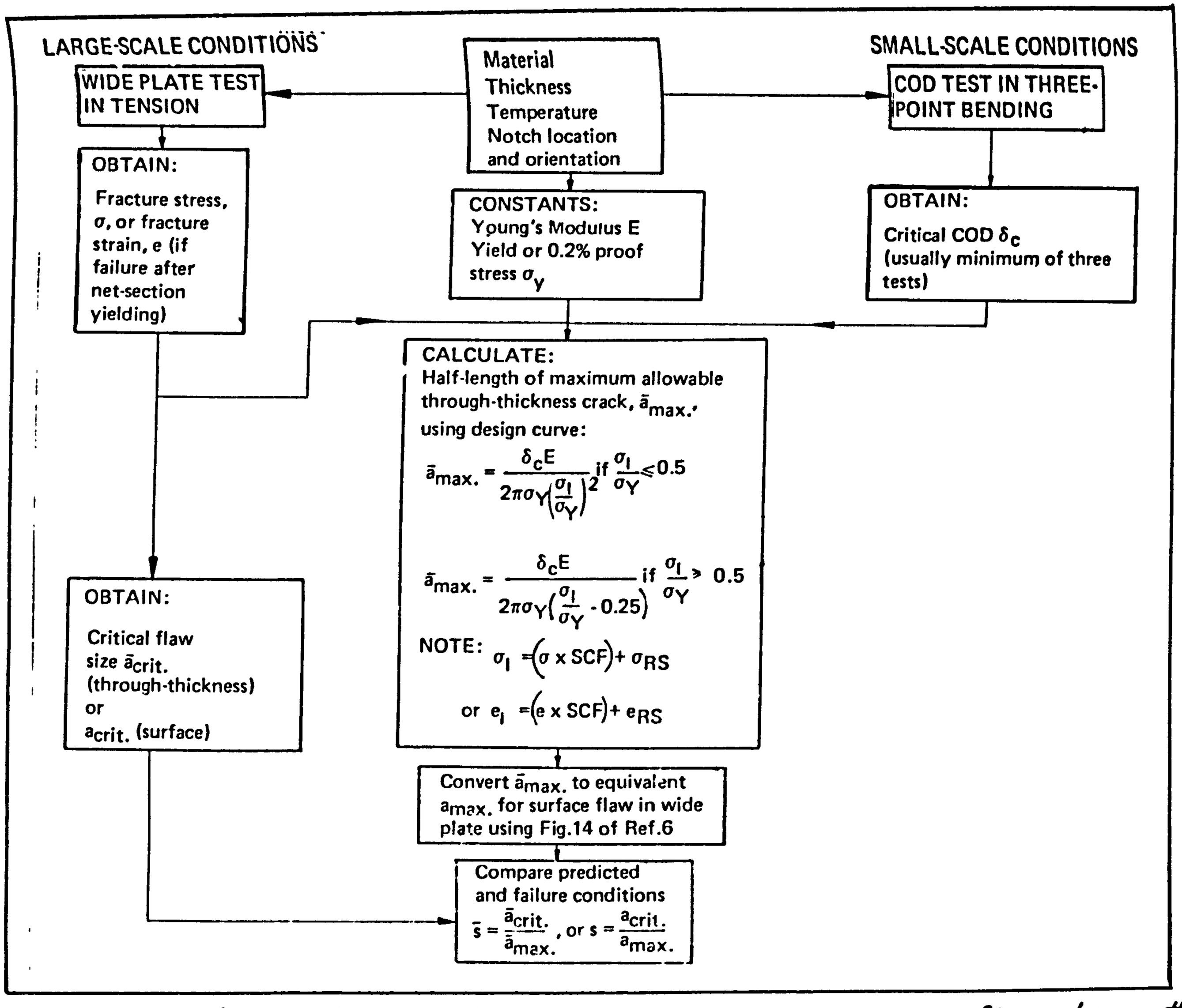

Fig.10. Comparison of wideplate $\bar{\sigma}_{crit}$ to COD $\bar{\sigma}_{max}$ after Kamath, Ref22.

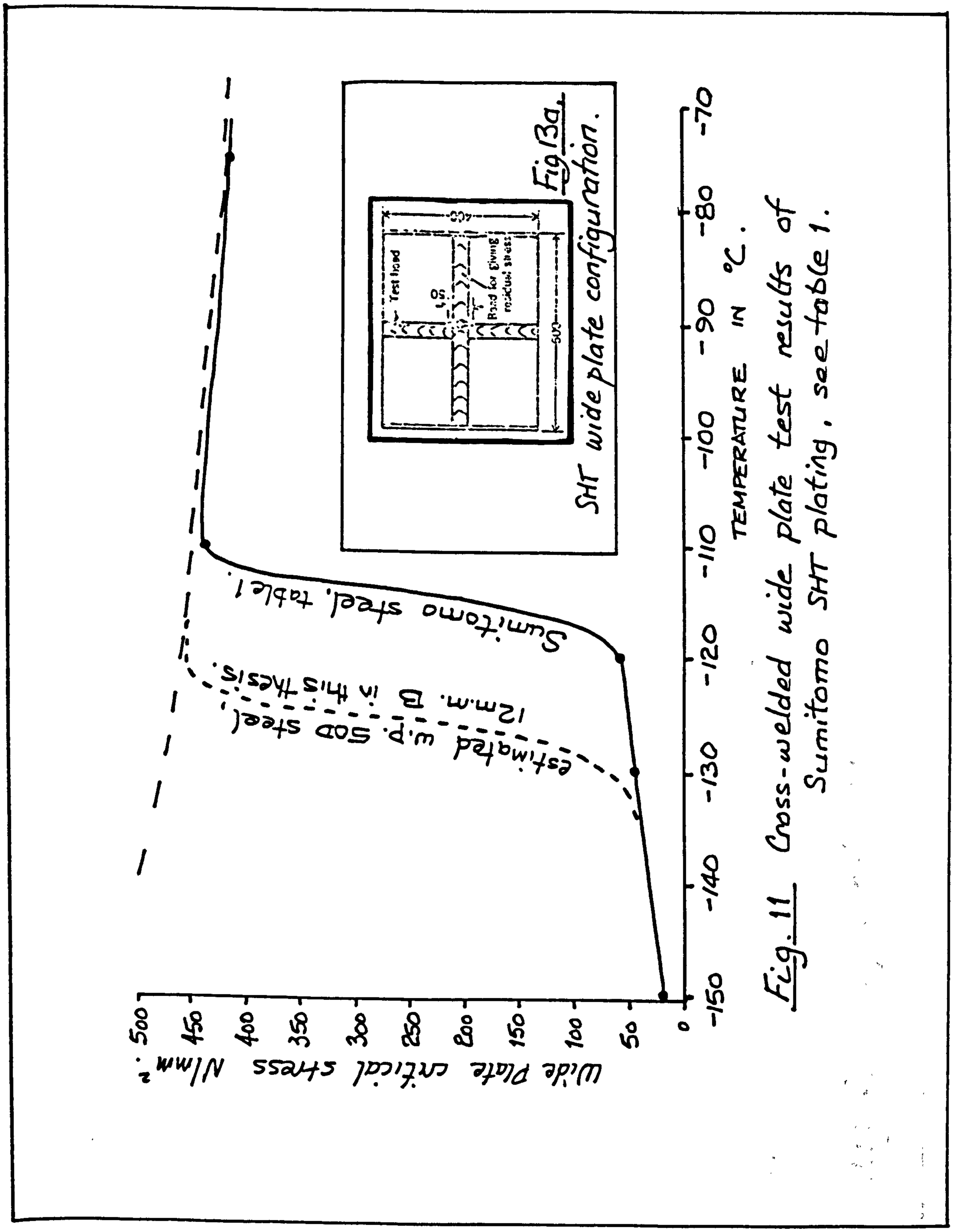

Fig. 11 Cross-welded wide plate test results of Sumitomo SHT plating, see table 1.

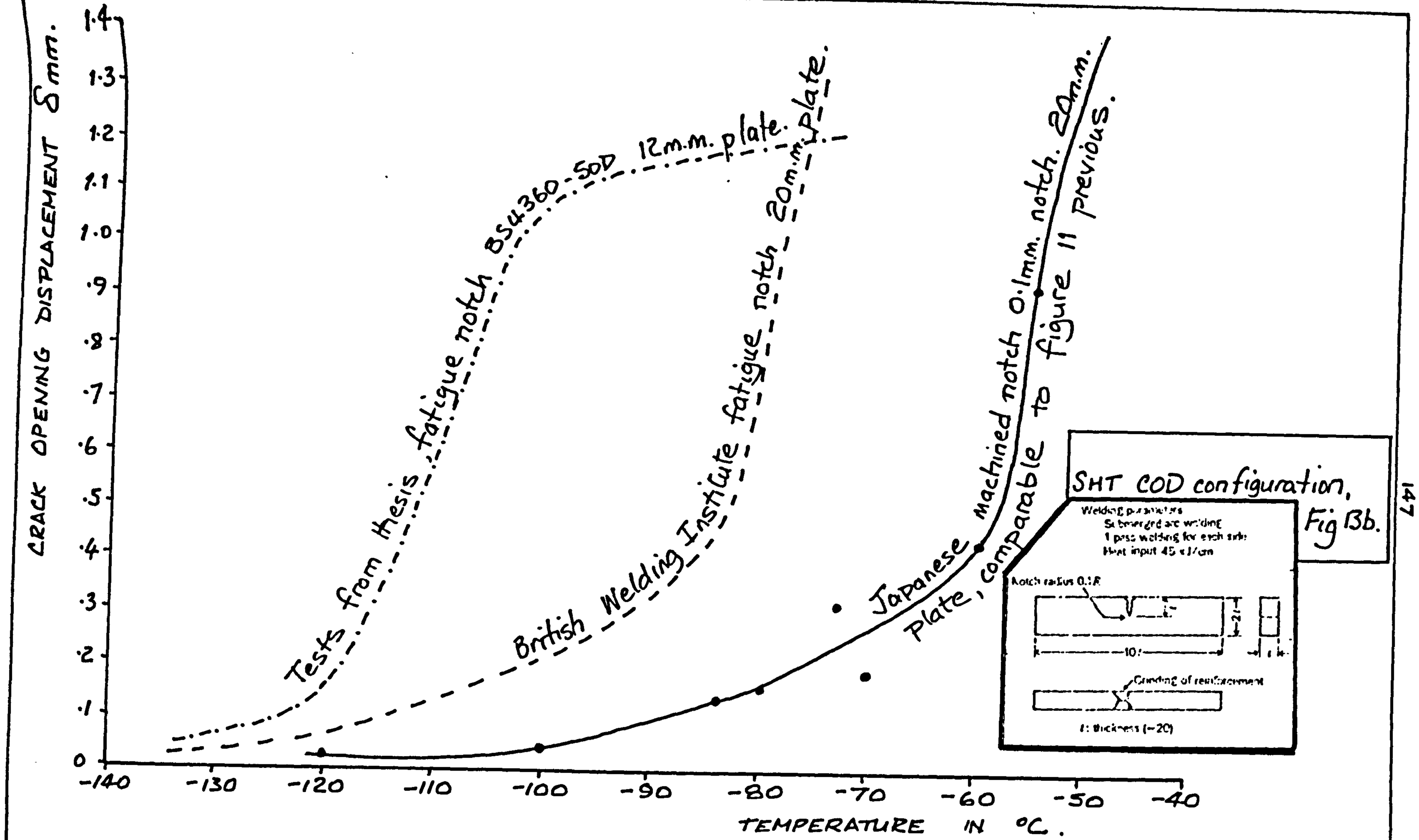

Fig 12. Equivalent COD evaluations relative to figure 11.

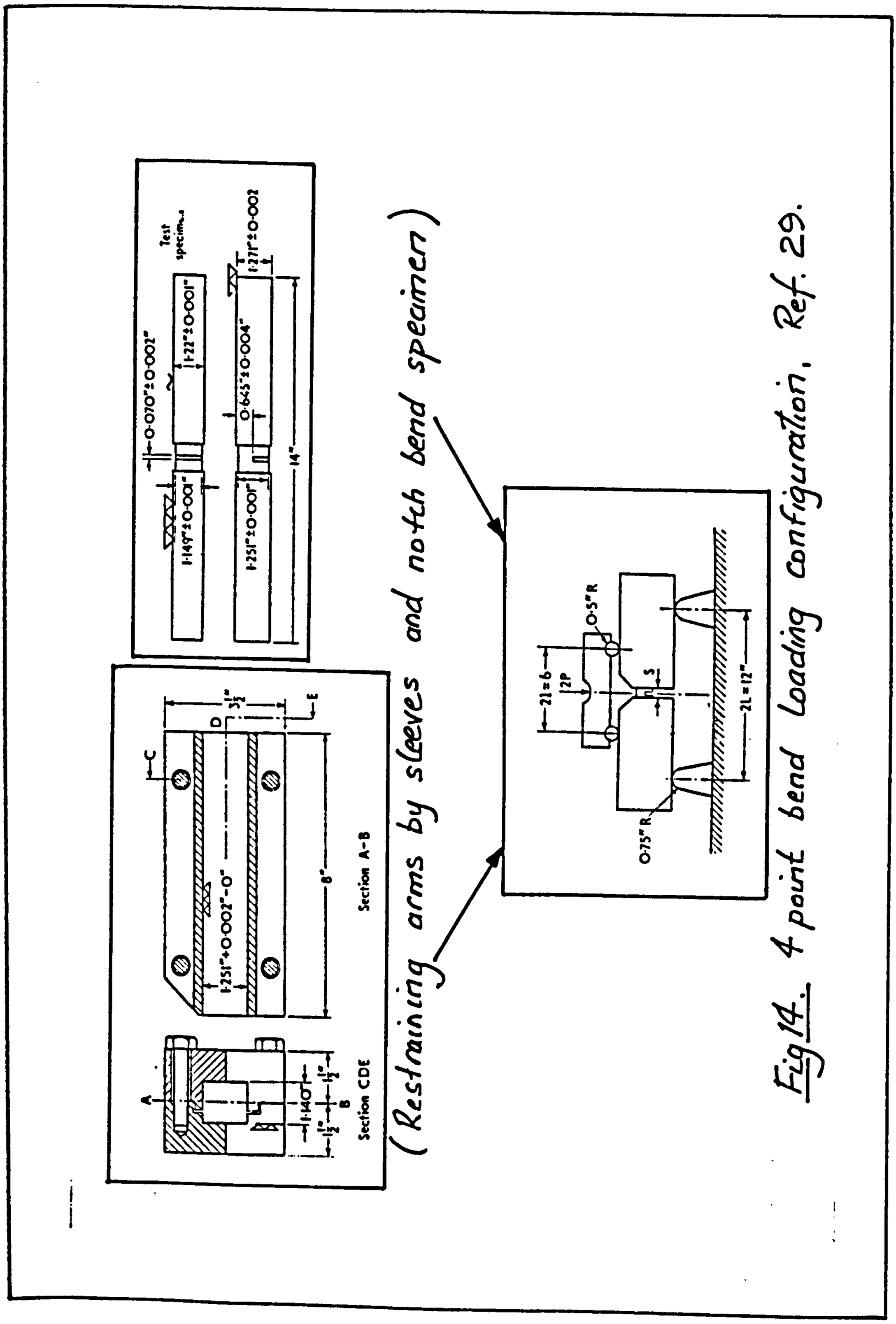

Fig 14. 4 point bend Loading configuration, Ref. 29.

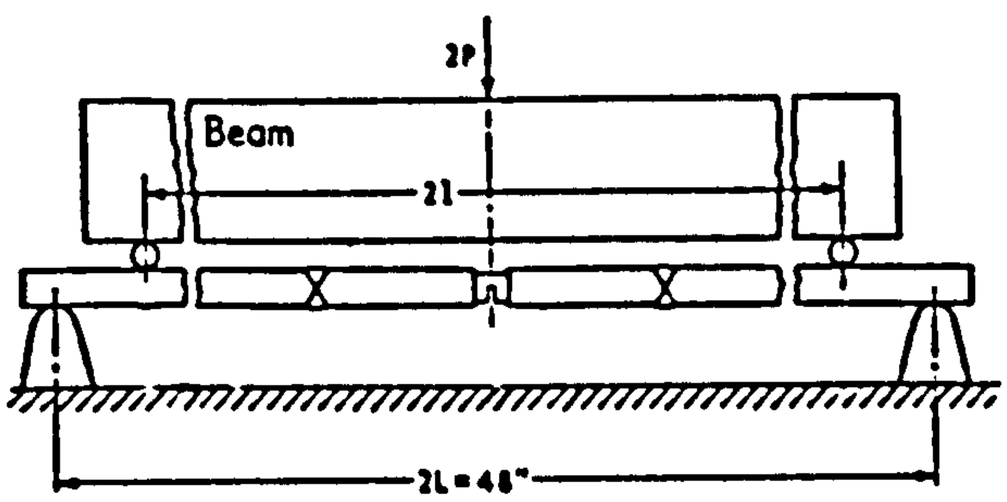

Fig.15. Extended arms to the 4point specimen, Ref. 29.

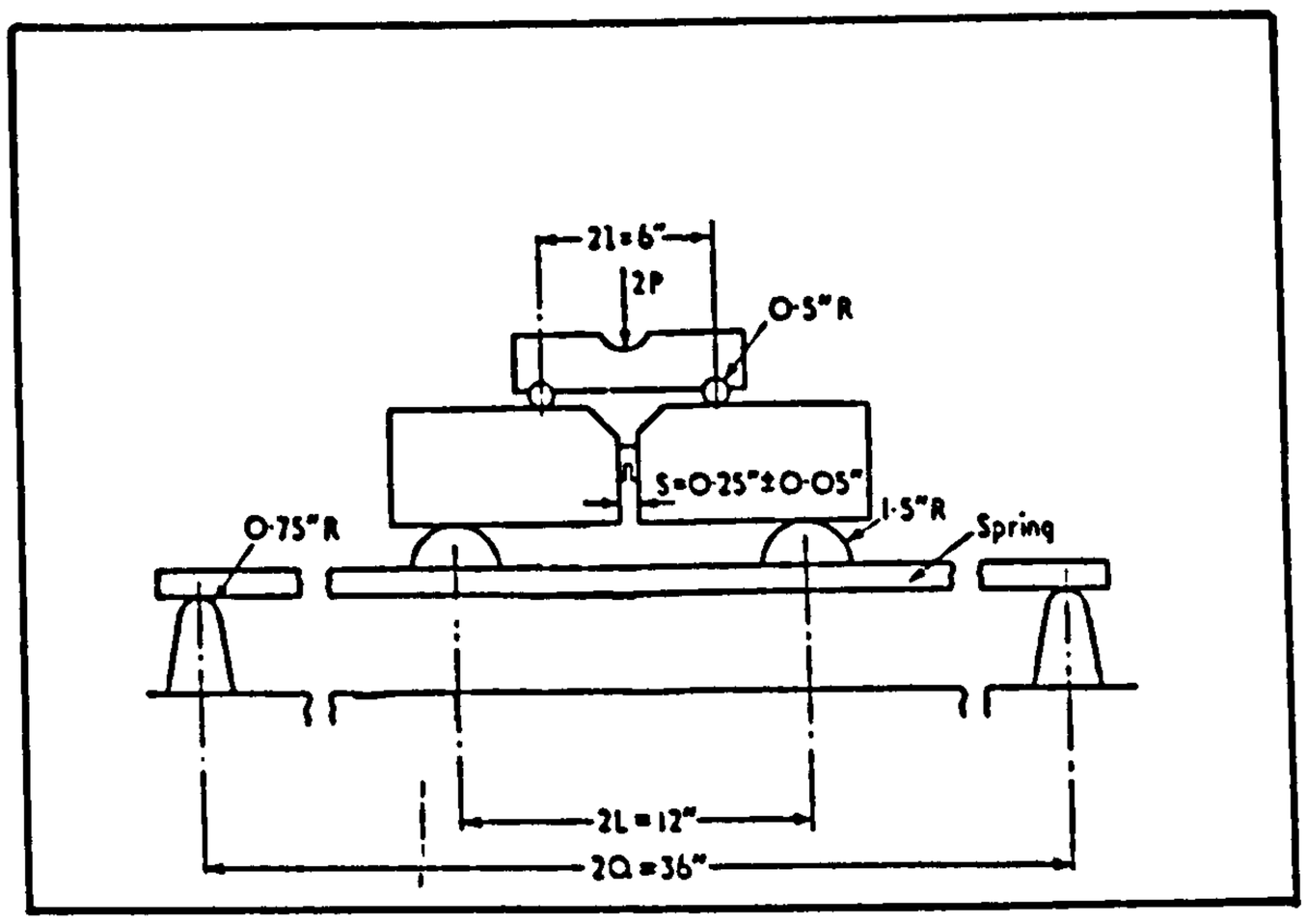

Fig.16. Spring loading system in series with 4point bend specimen, Ref. 29.

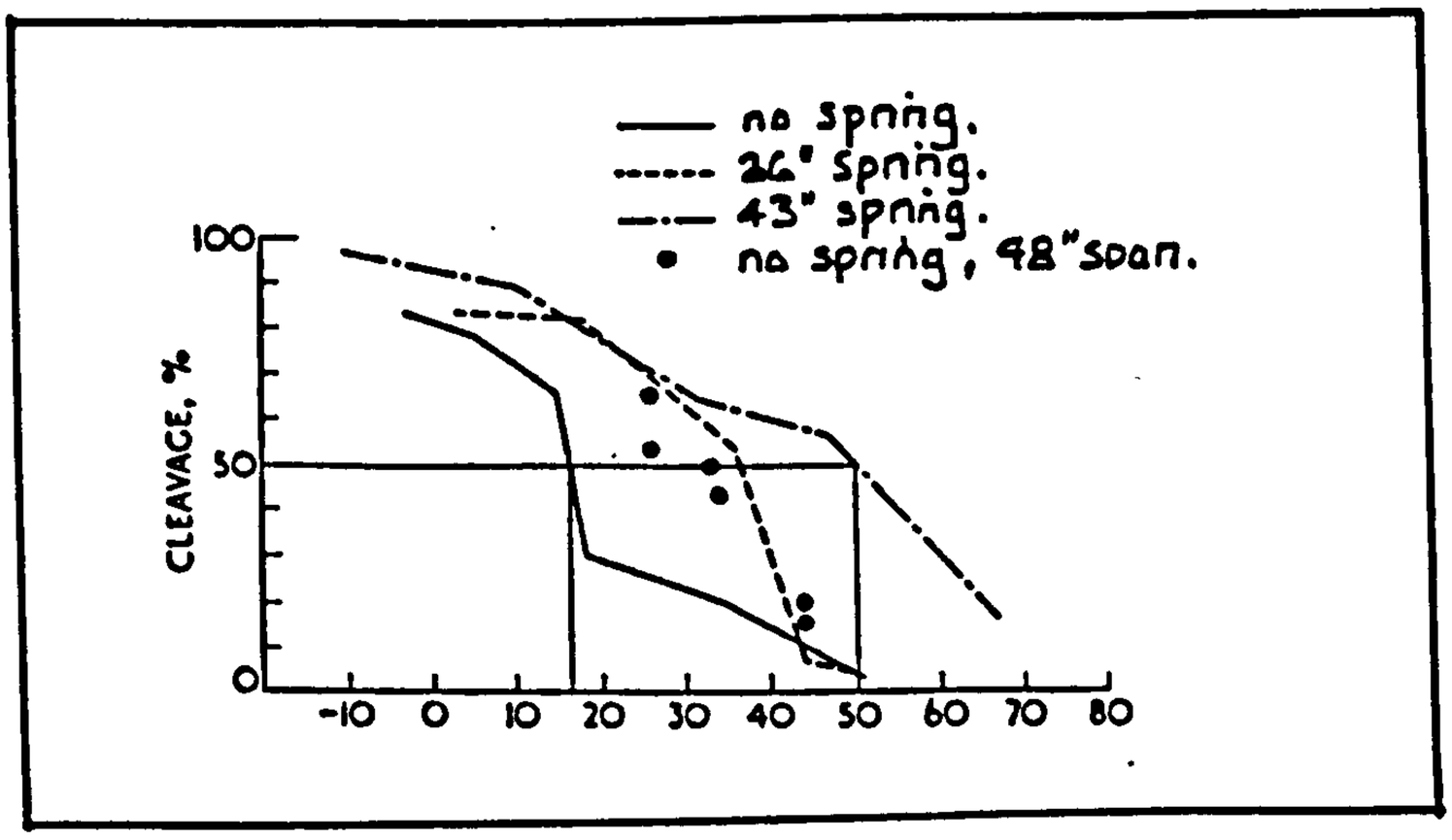

Fig. 17. Transition temperature shift to higher due to increased stored strain energy content available.

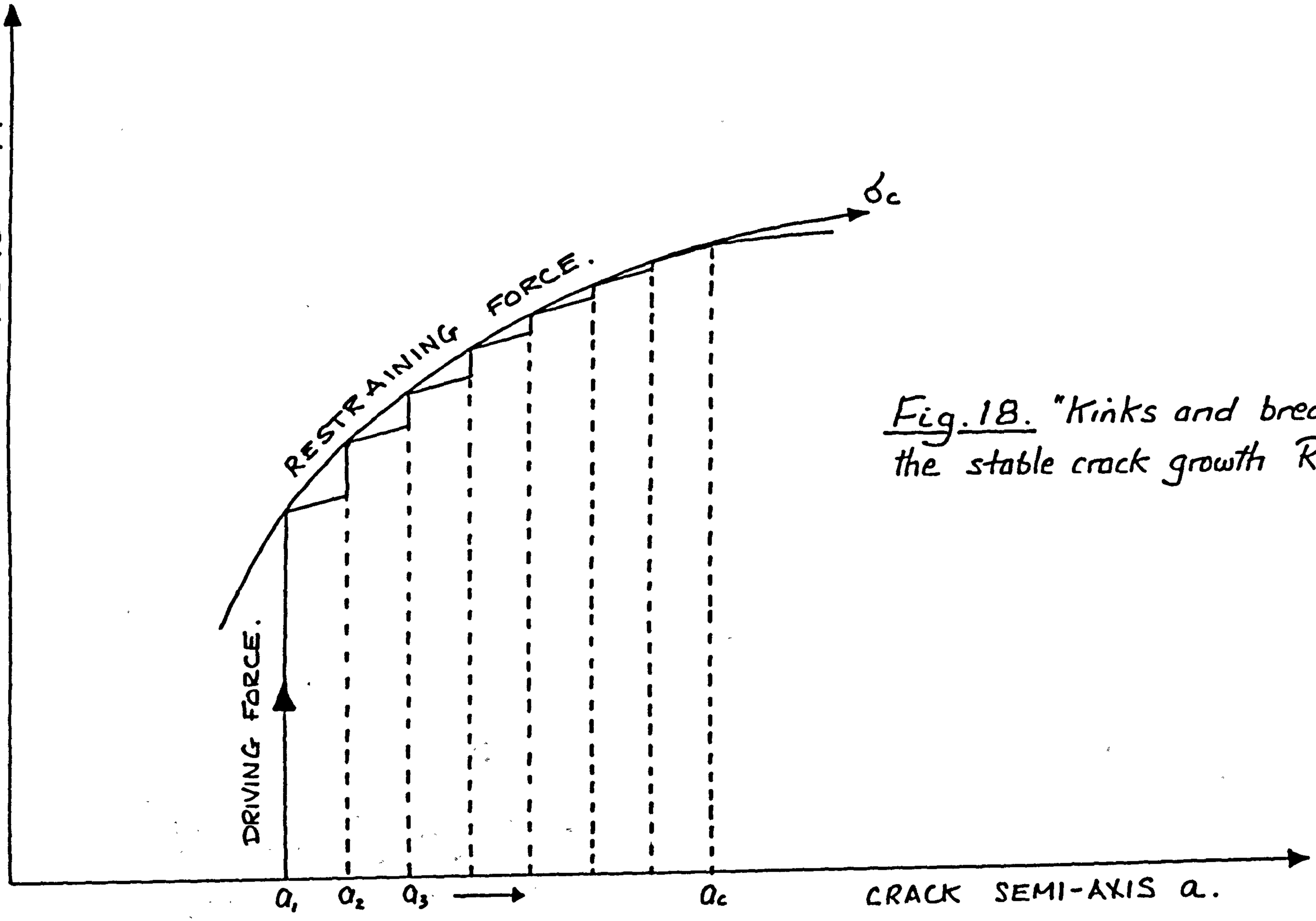

Fig. 18. "Kinks and breaks" in the stable crack growth R-curve.

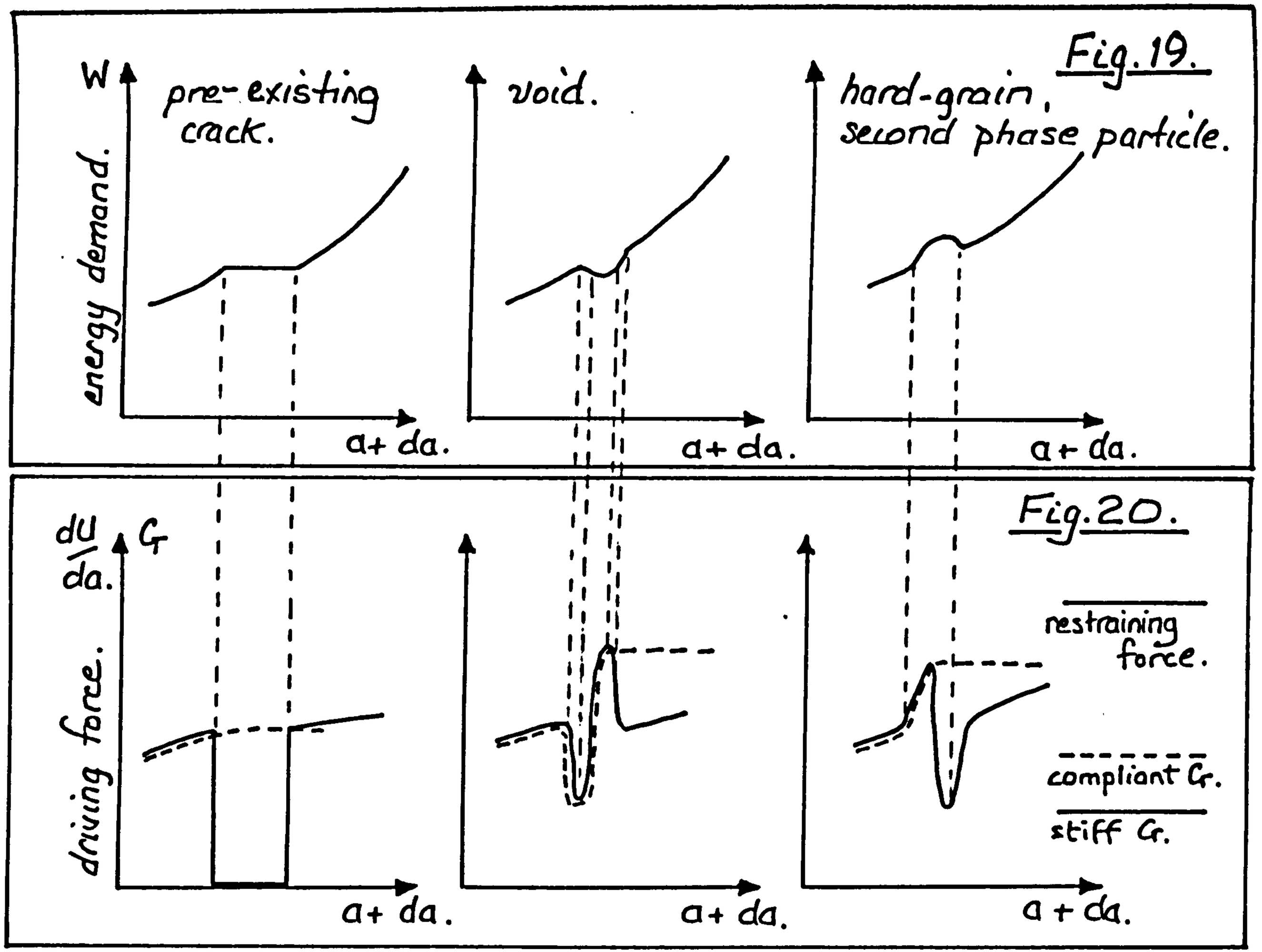

Fig.19. Energy demand of various microstructural inhomogeneities.

Fig.20. Driving force behaviour of rigid-stiff and compliant loading systems.

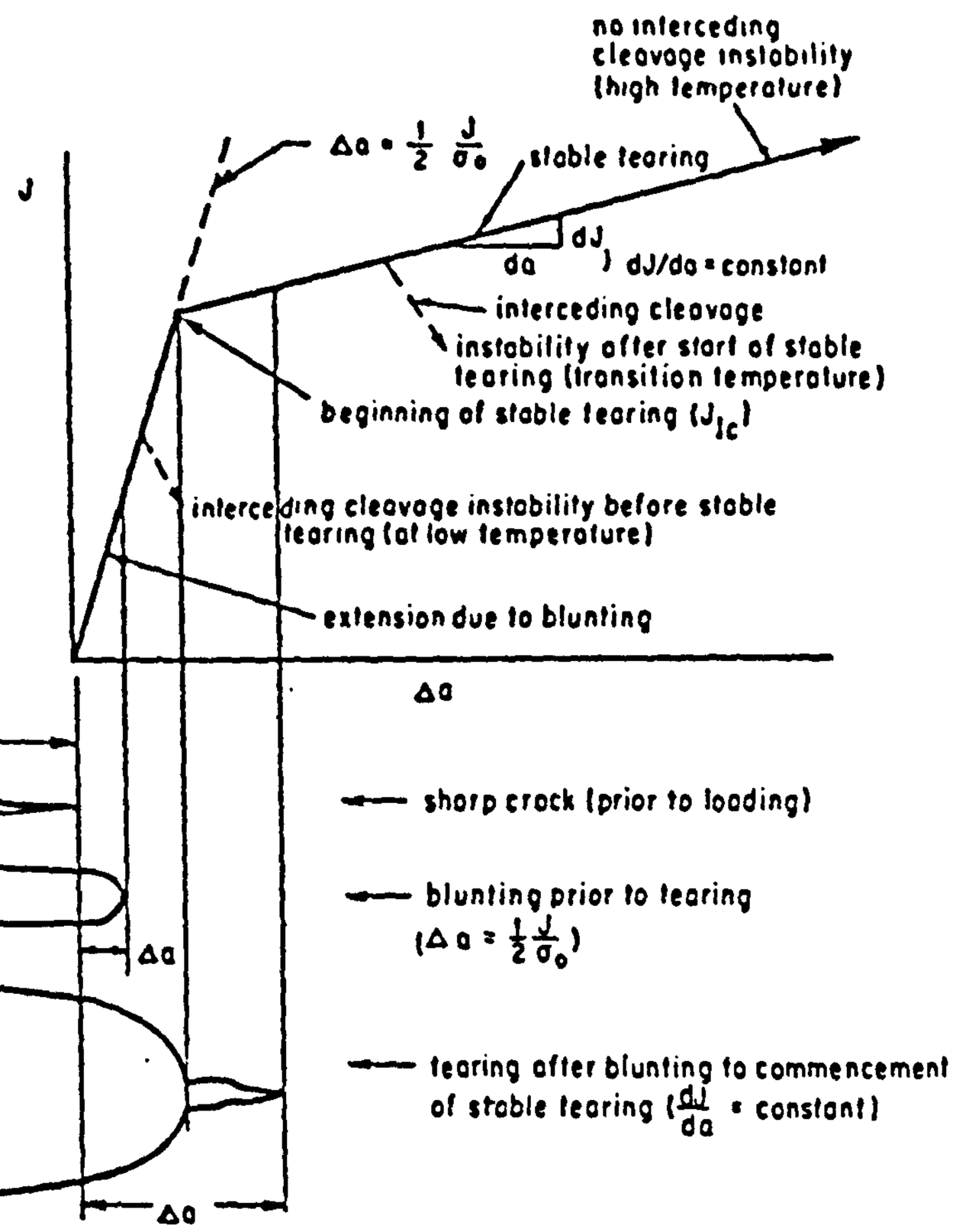

Fig. 21. J-integral R-curve showing blunt stretch and tearing.

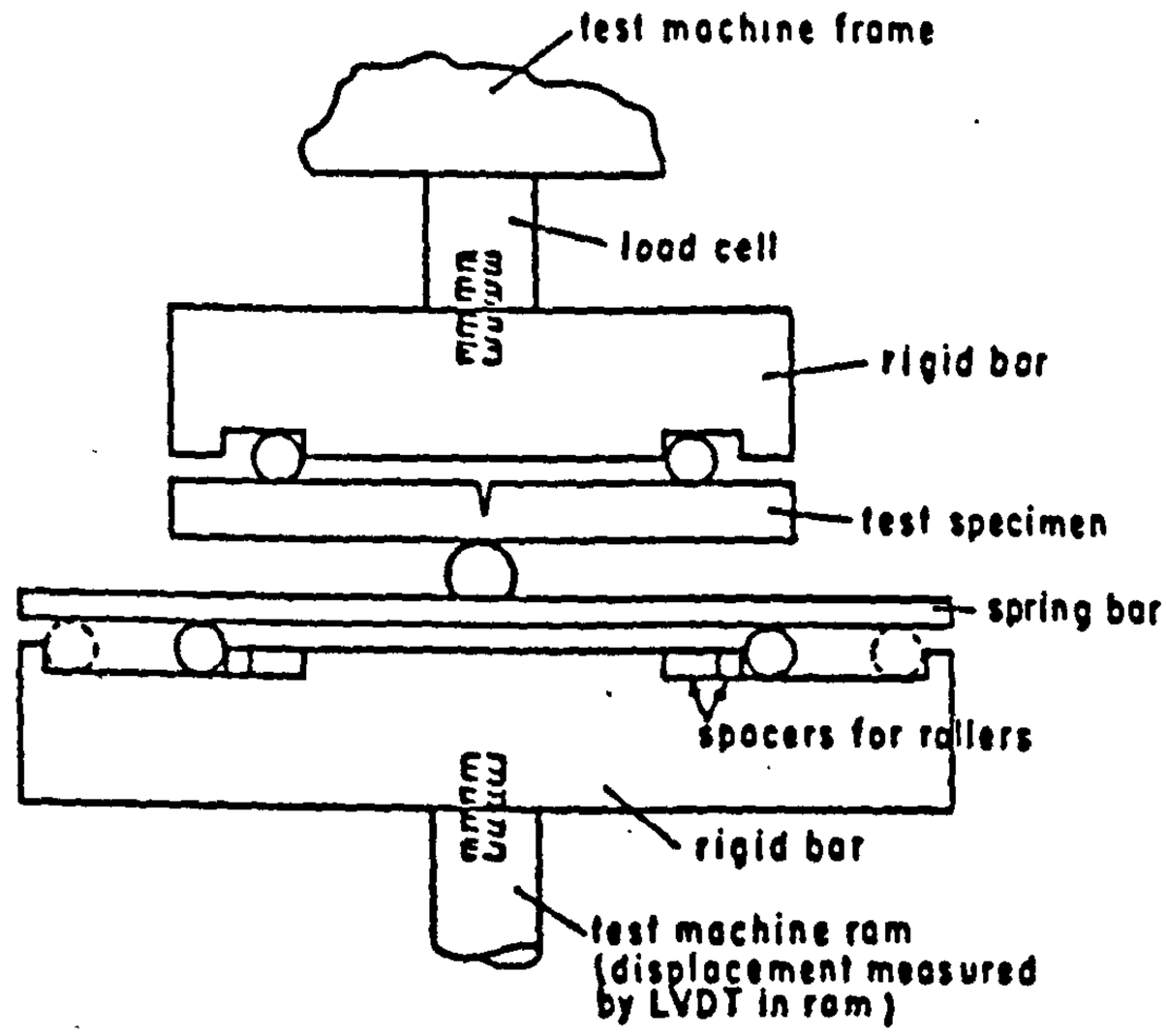

Fig 22. "Paris-beam" used to check validity of Tearing Modulus concept.

Fig. 21 and 22 from Ref. 28.

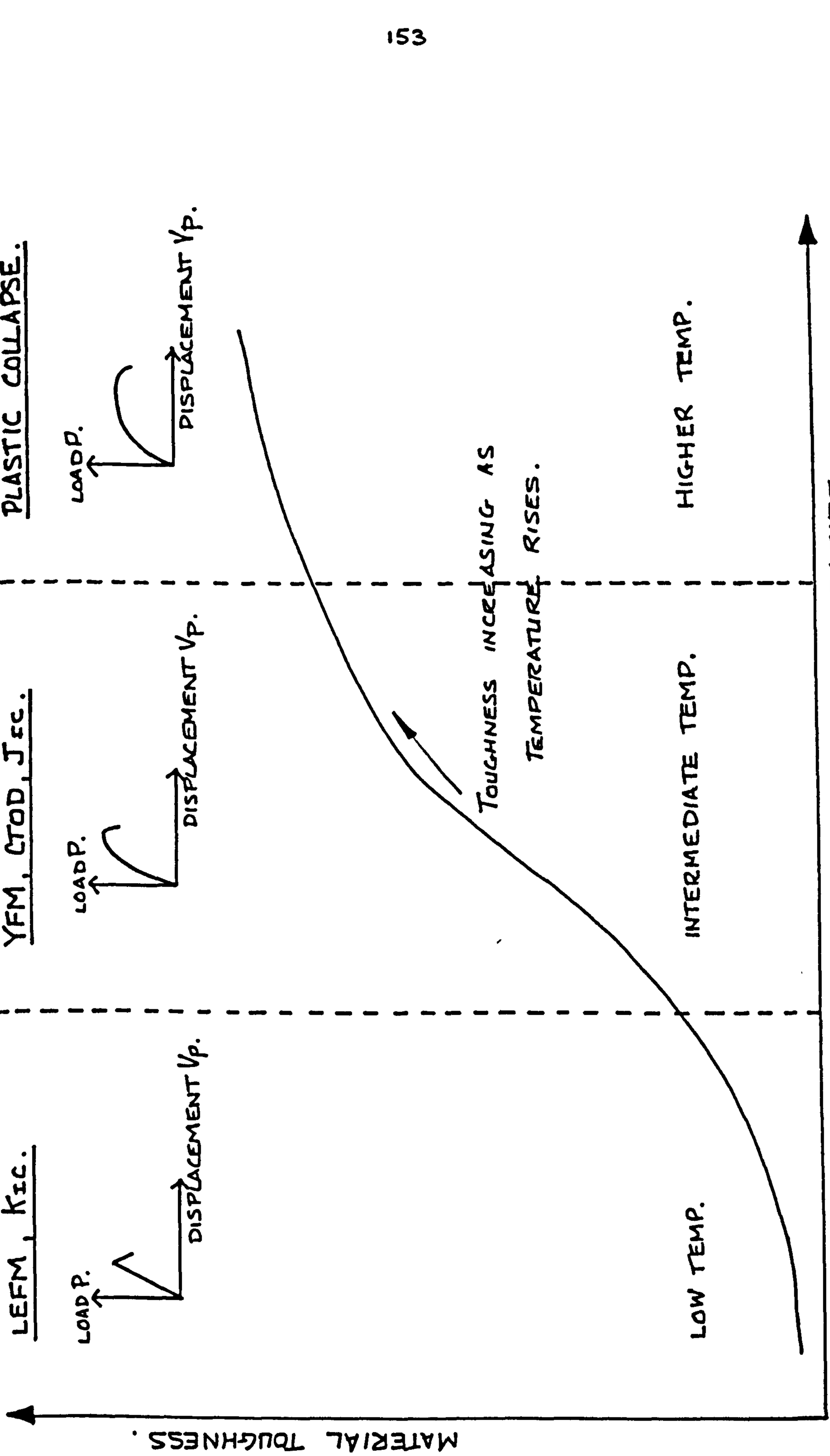

Fig. 23. Toughness increase per temperature rise and toughness characterisation parameters.

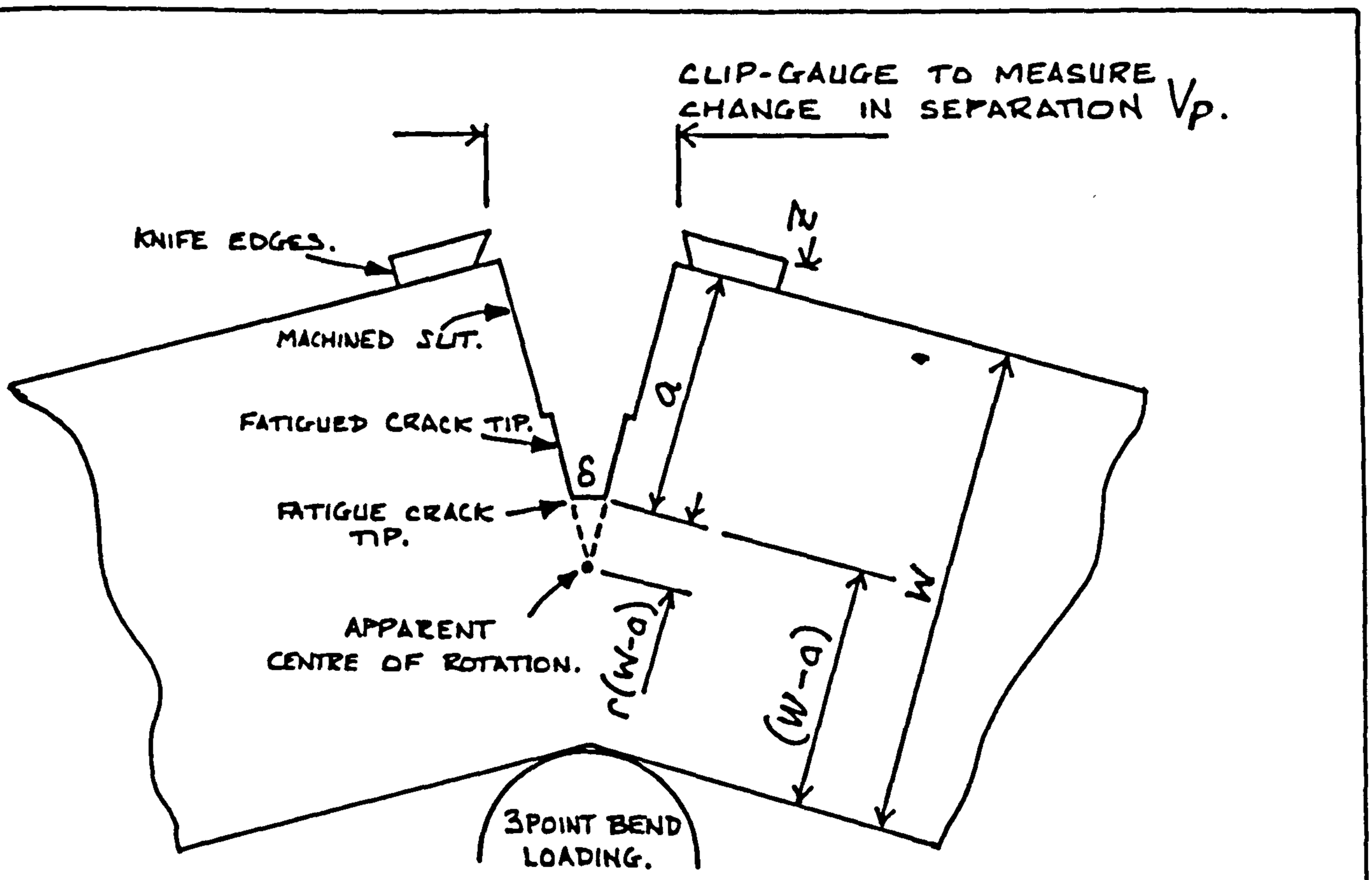

Fig. 24. Simplified COD evaluation assuming proportion by similar triangles,

$$\frac{\delta.}{V_p.} = \frac{r(W-a).}{r(W-a)+a+z.}$$

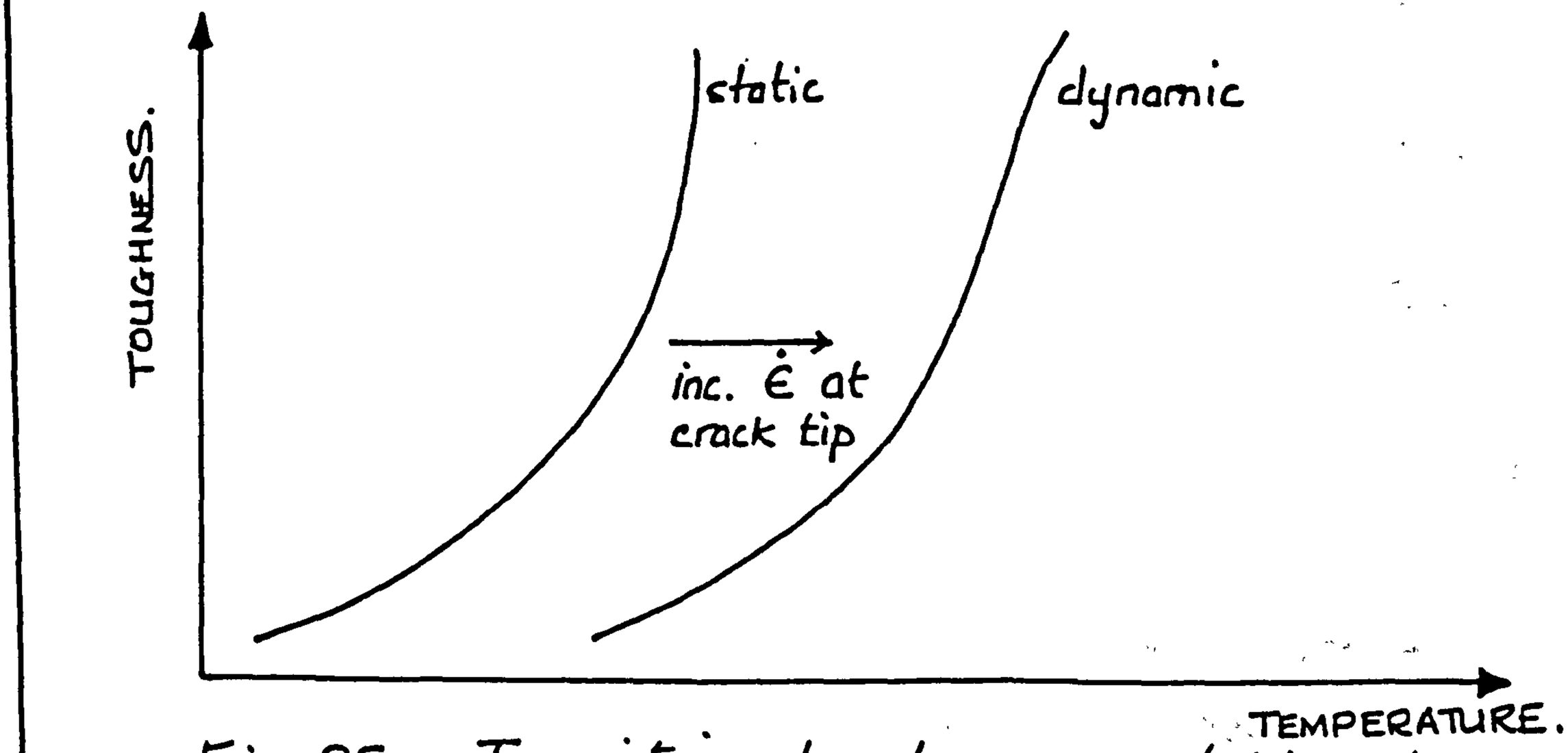

Fig. 25. Transition toughness relative to strain rate $\dot{\epsilon}$ at crack tip

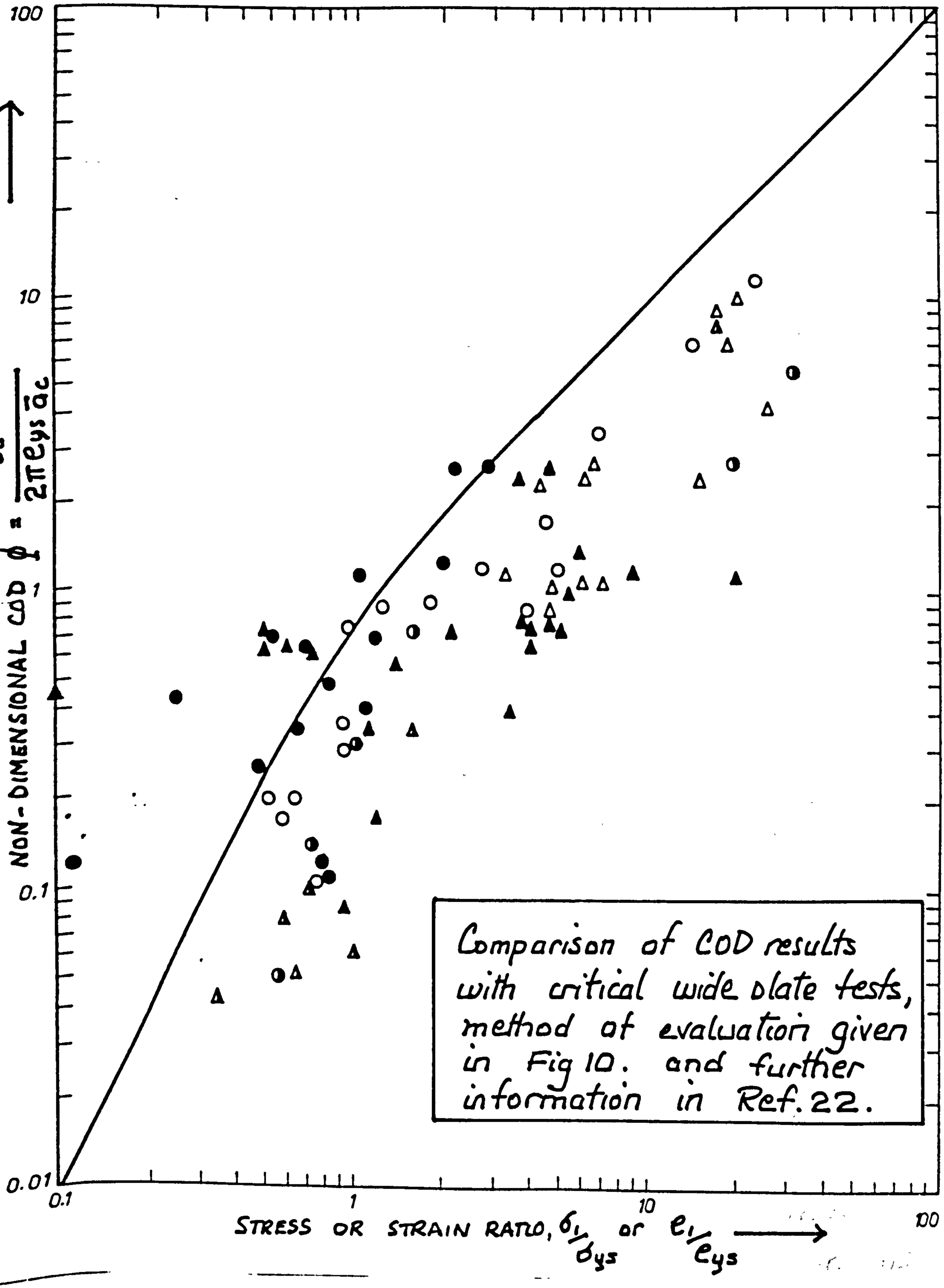

Fig. 26. Design Curve relationship between non-dimensional COD and applied strain or stress, after Kamath, Ref. 22.

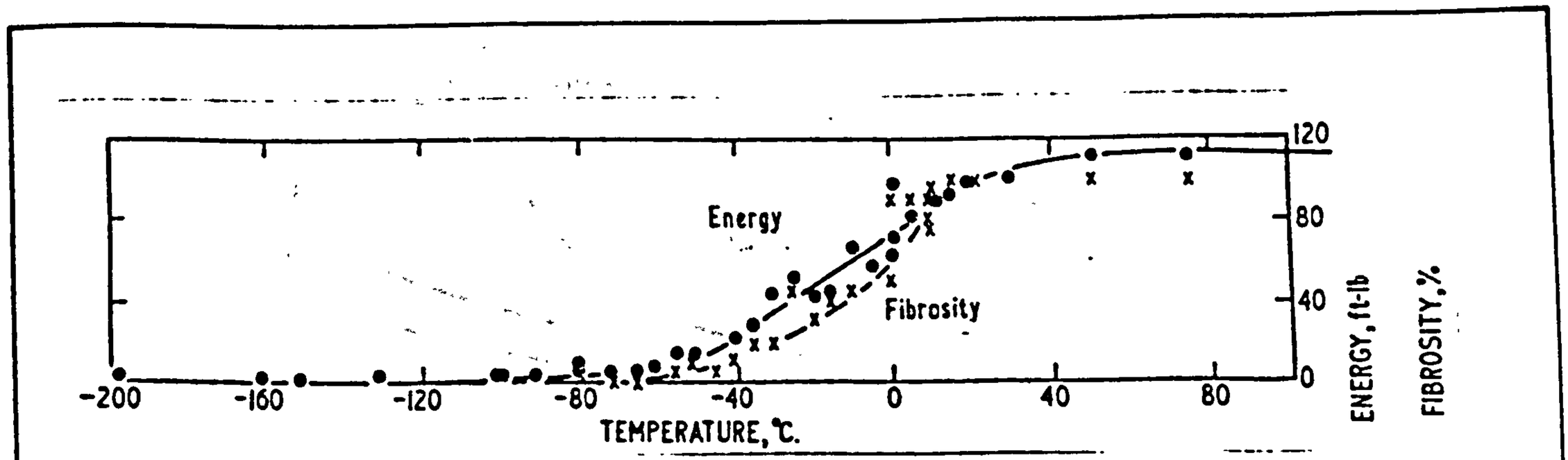

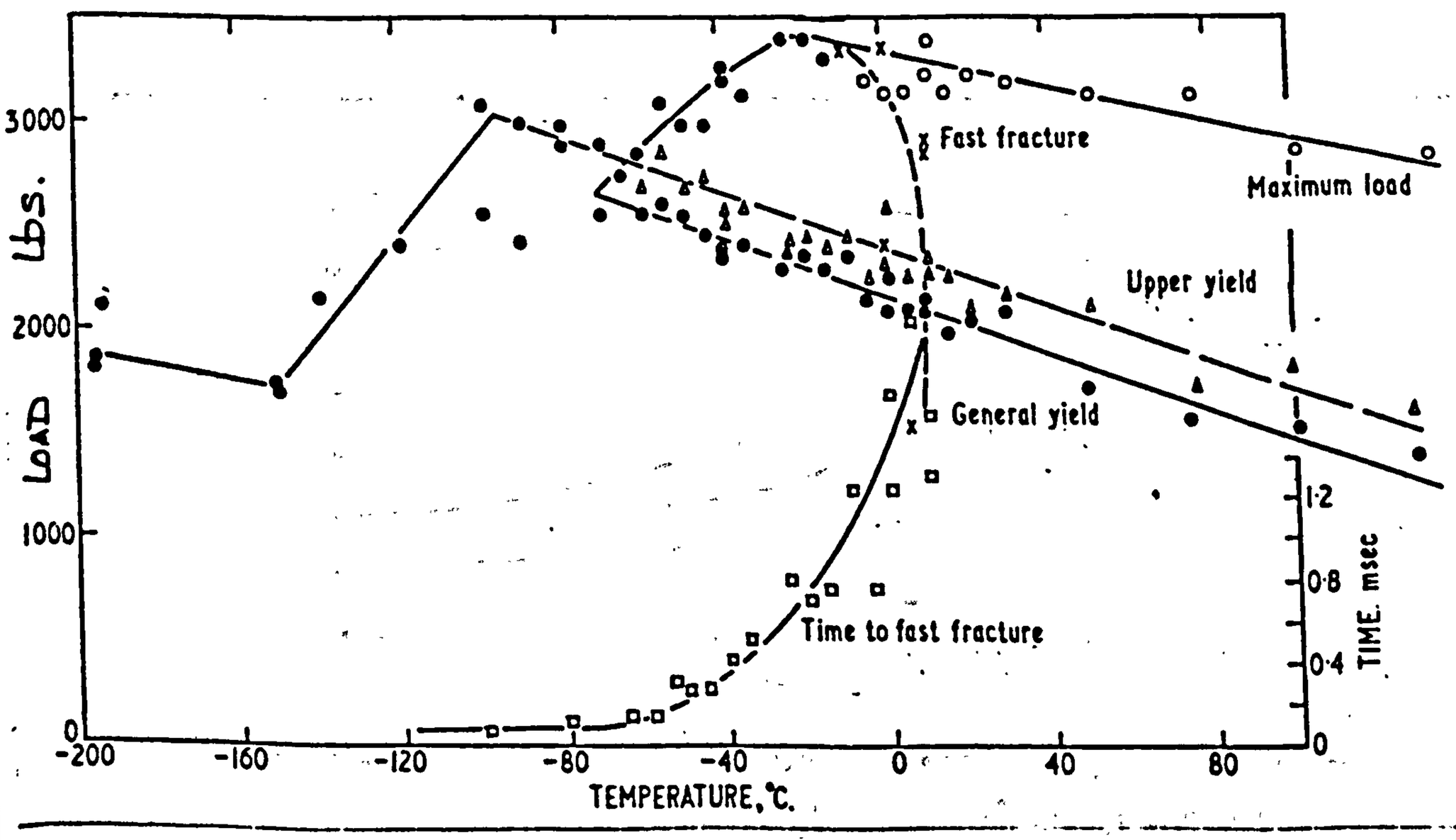

Fig. 27. Charpy impact information available using machined notch, Ref. 108, and instrumented tup.

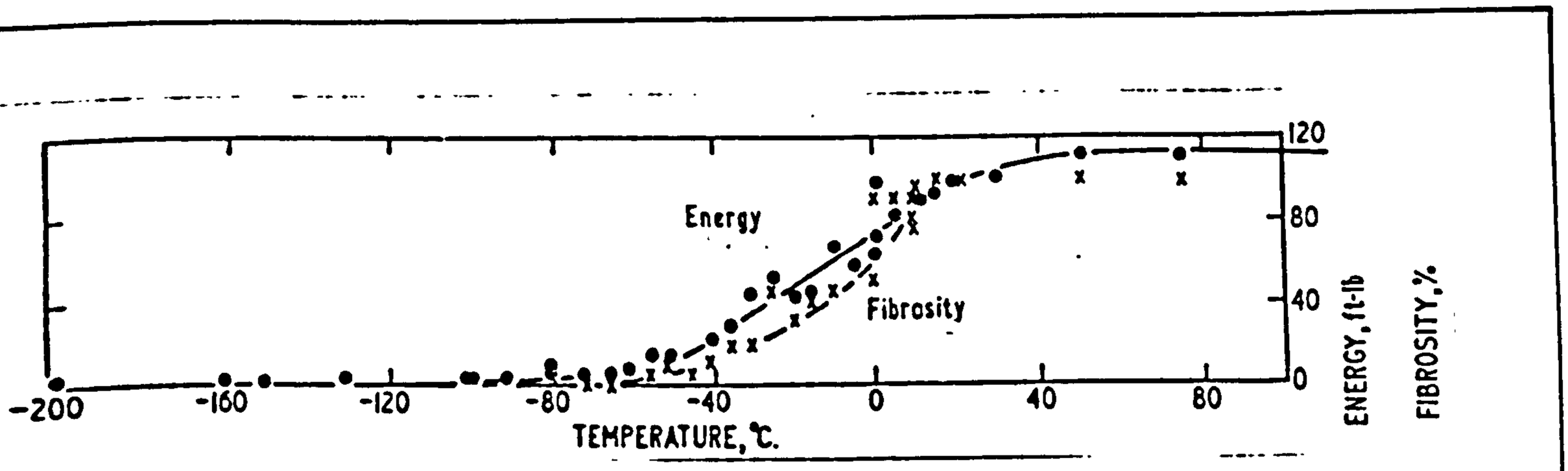

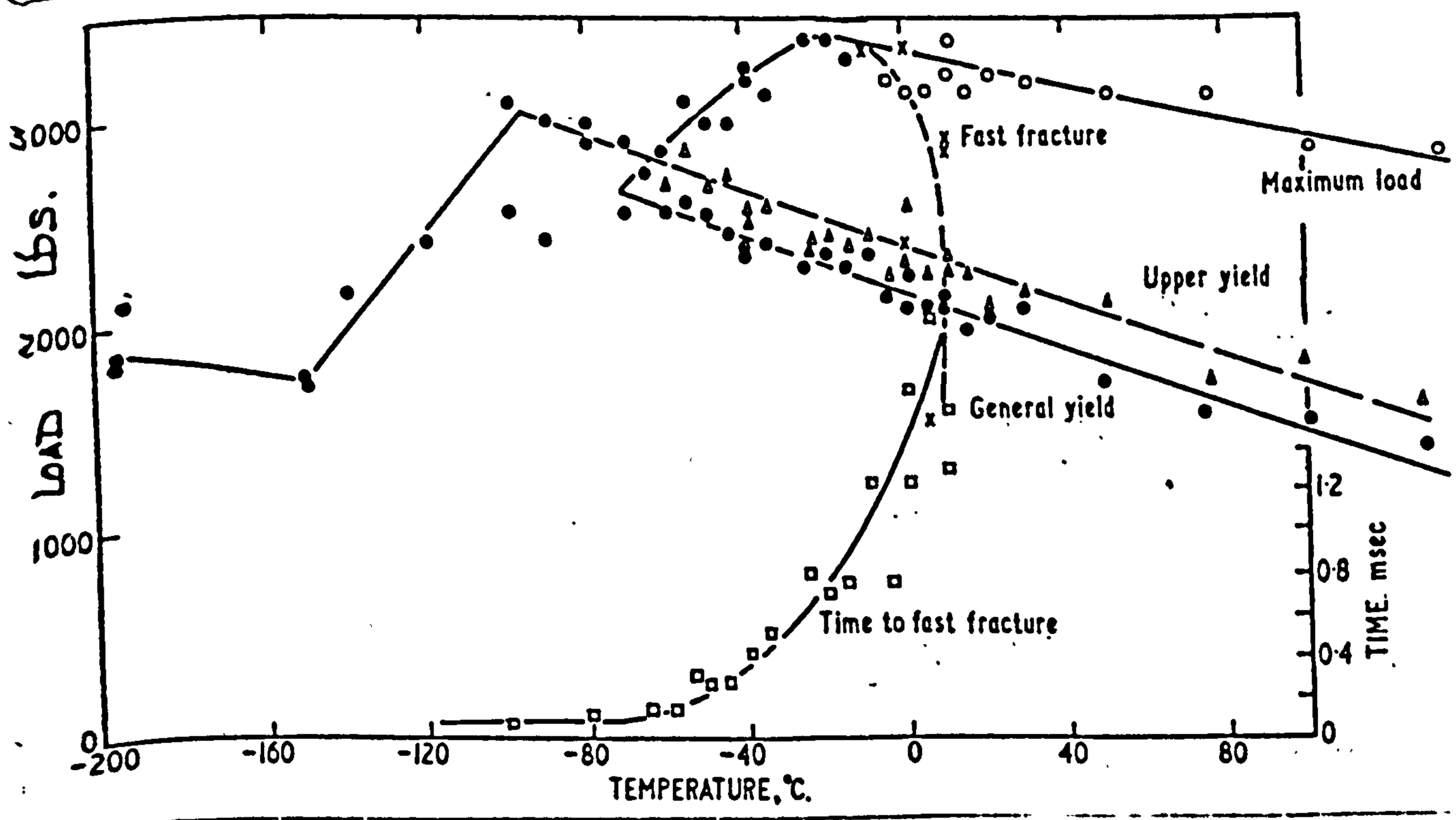

Fig. 27. Charpy impact information available using machined notch, Ref. 108, and instrumented tup.

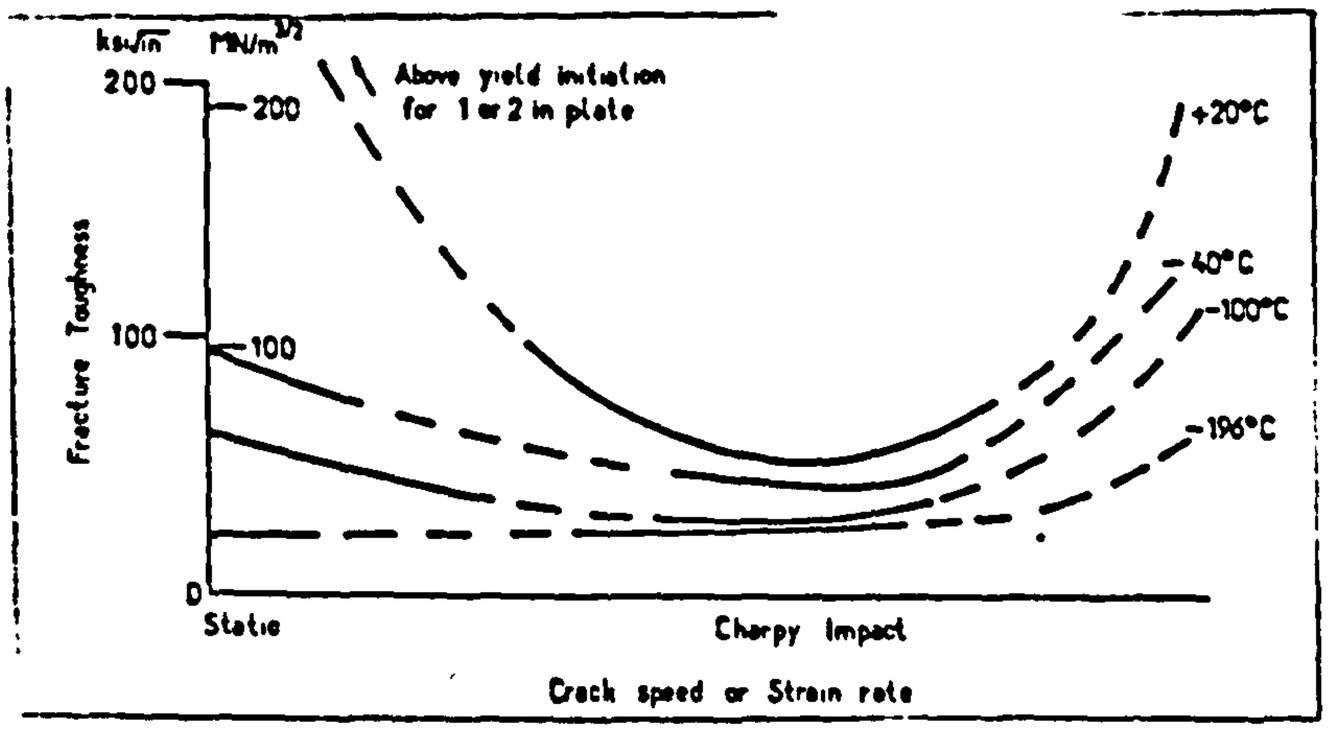

Fig. 28. Effect of strain rate on fracture toughness, Charpy impact corresponds to $\dot{\varepsilon} \simeq 200/s$, and $\dot{K} \simeq 2 \times 10^6$ ksi$\sqrt{in}$/s, Ref 115.

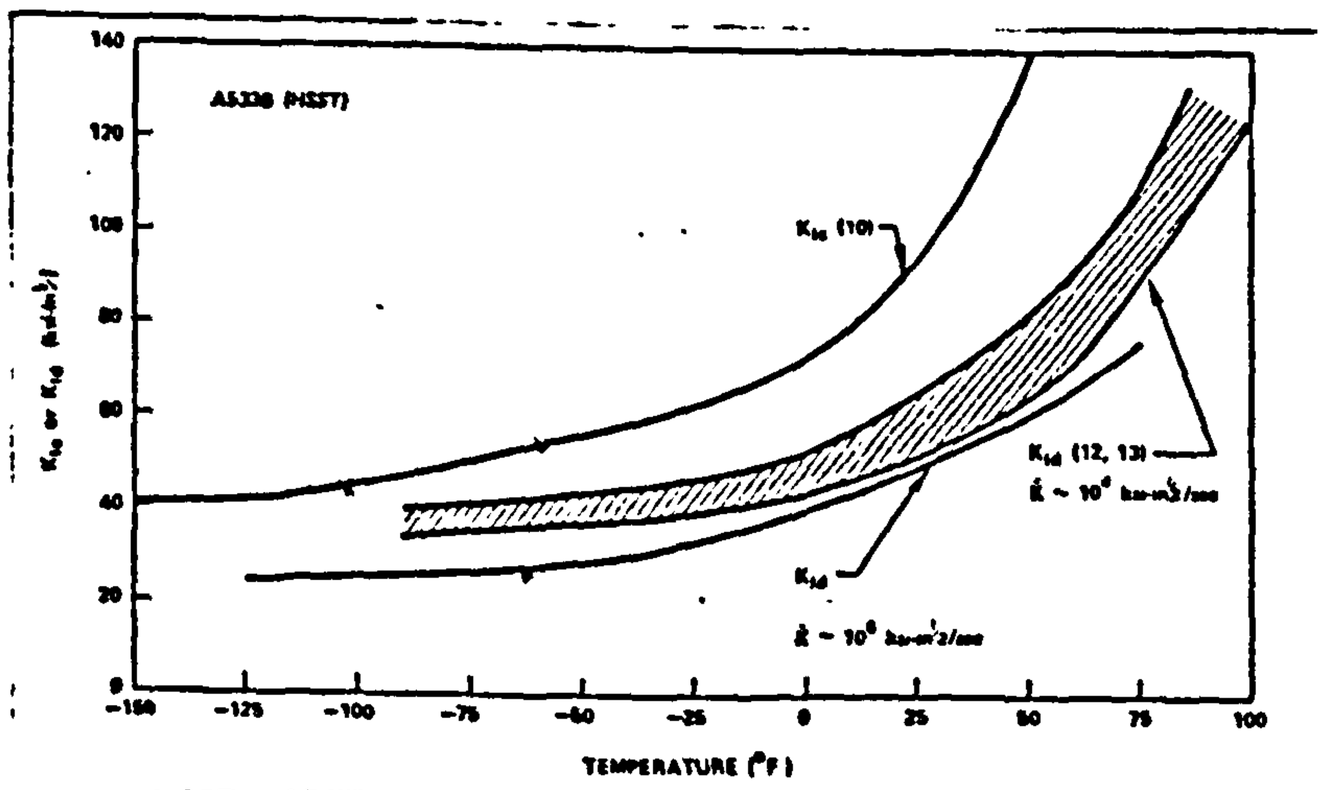

Fig 29. Relationship between K_{Ic} and K_{Id} fracture toughness for A-533B steel, after Ref. 116.

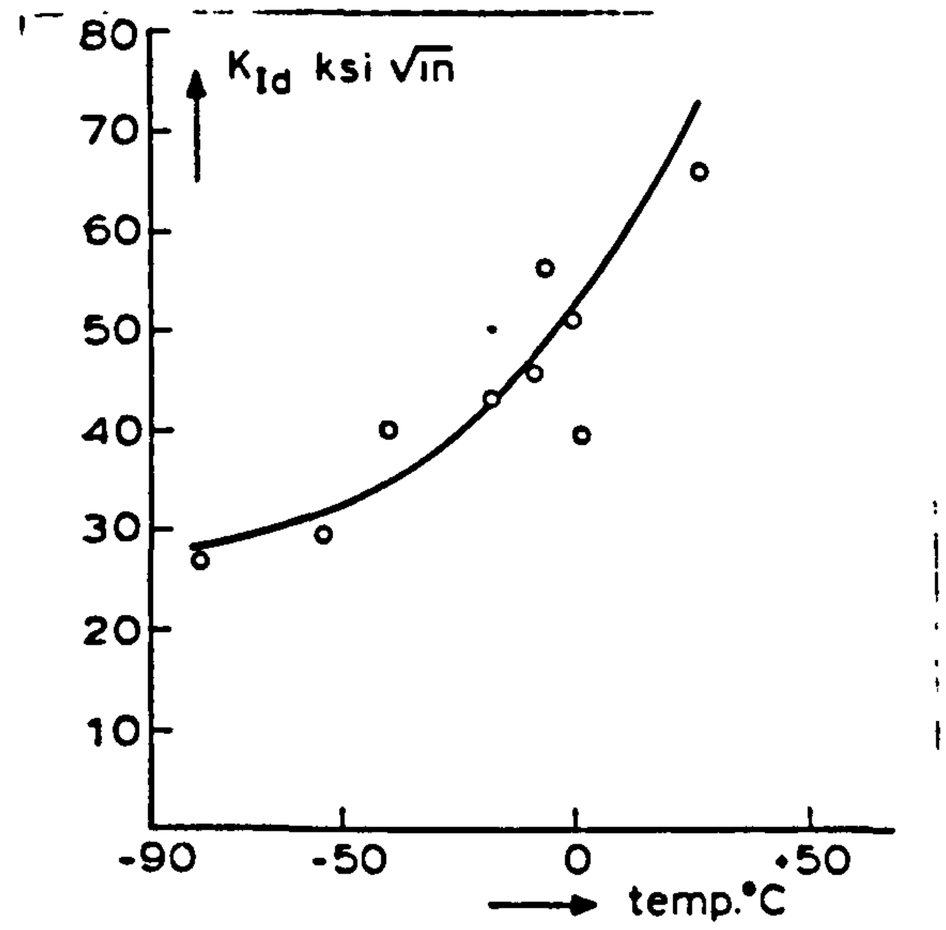

Fig.30. Variation of K_{Id} for a structural steel, Ref. 25.

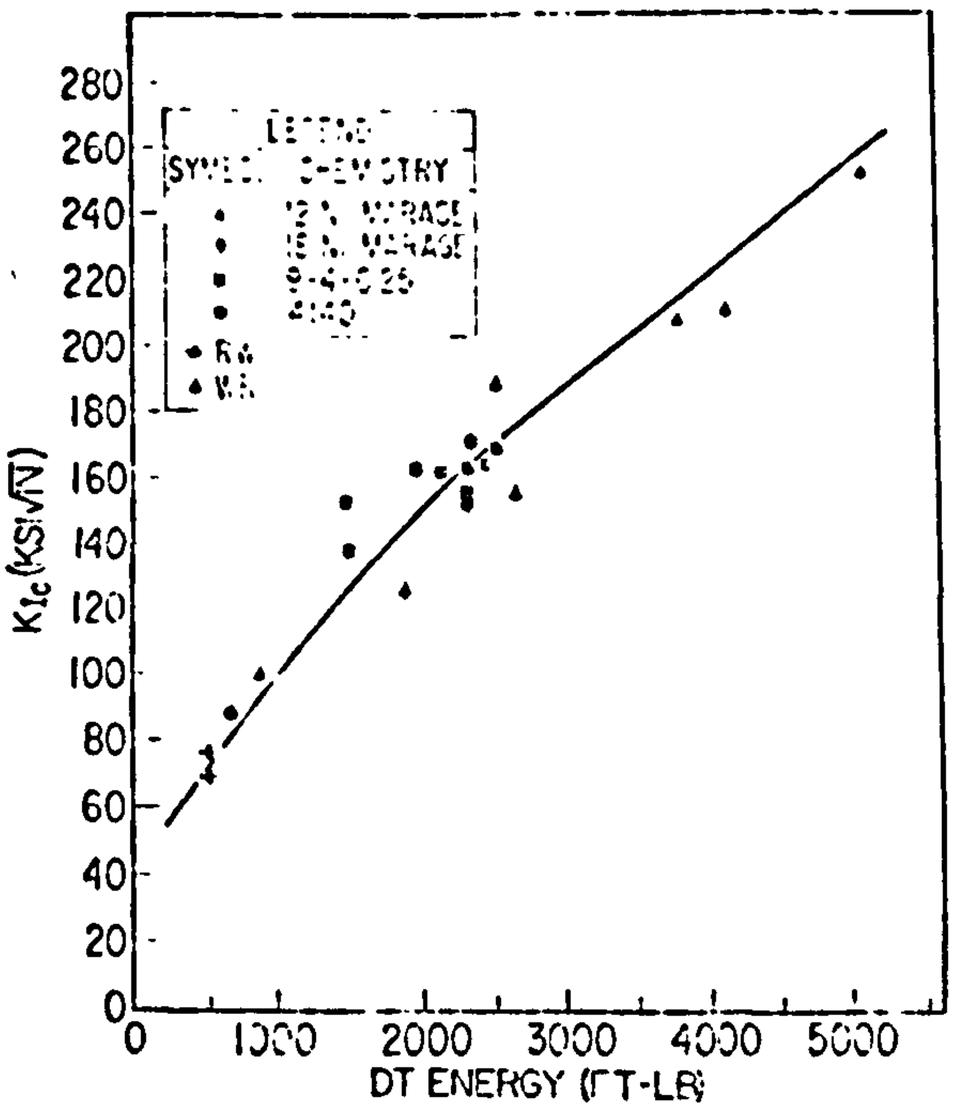

Fig.32. Relationship between 1-in dynamic tear energy and K_{Ic} values of various high-strength steels, Ref 120.

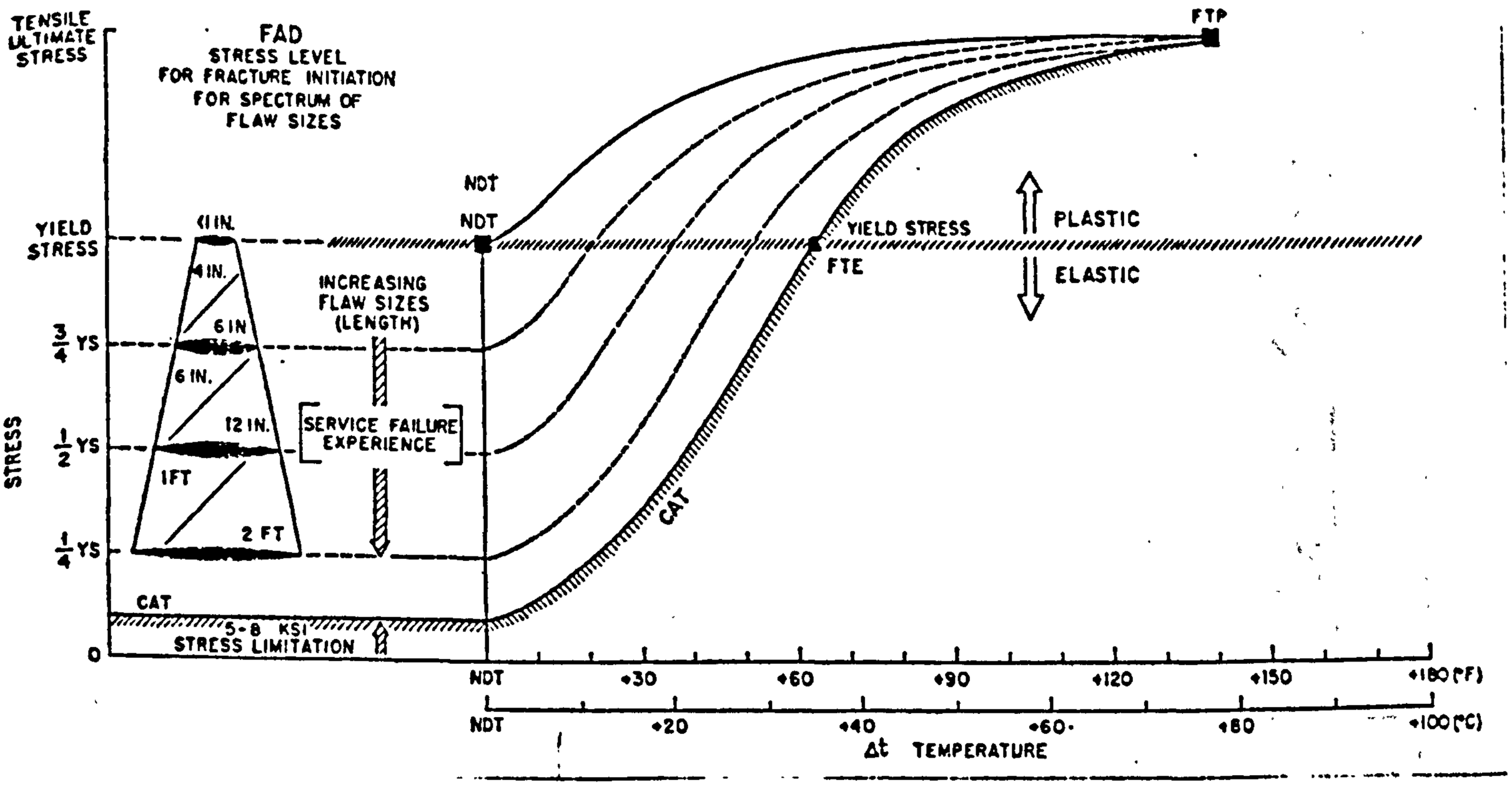

Fig. 31. Generalised Fracture Analysis Diagram, after Pellini, Ref. 118.

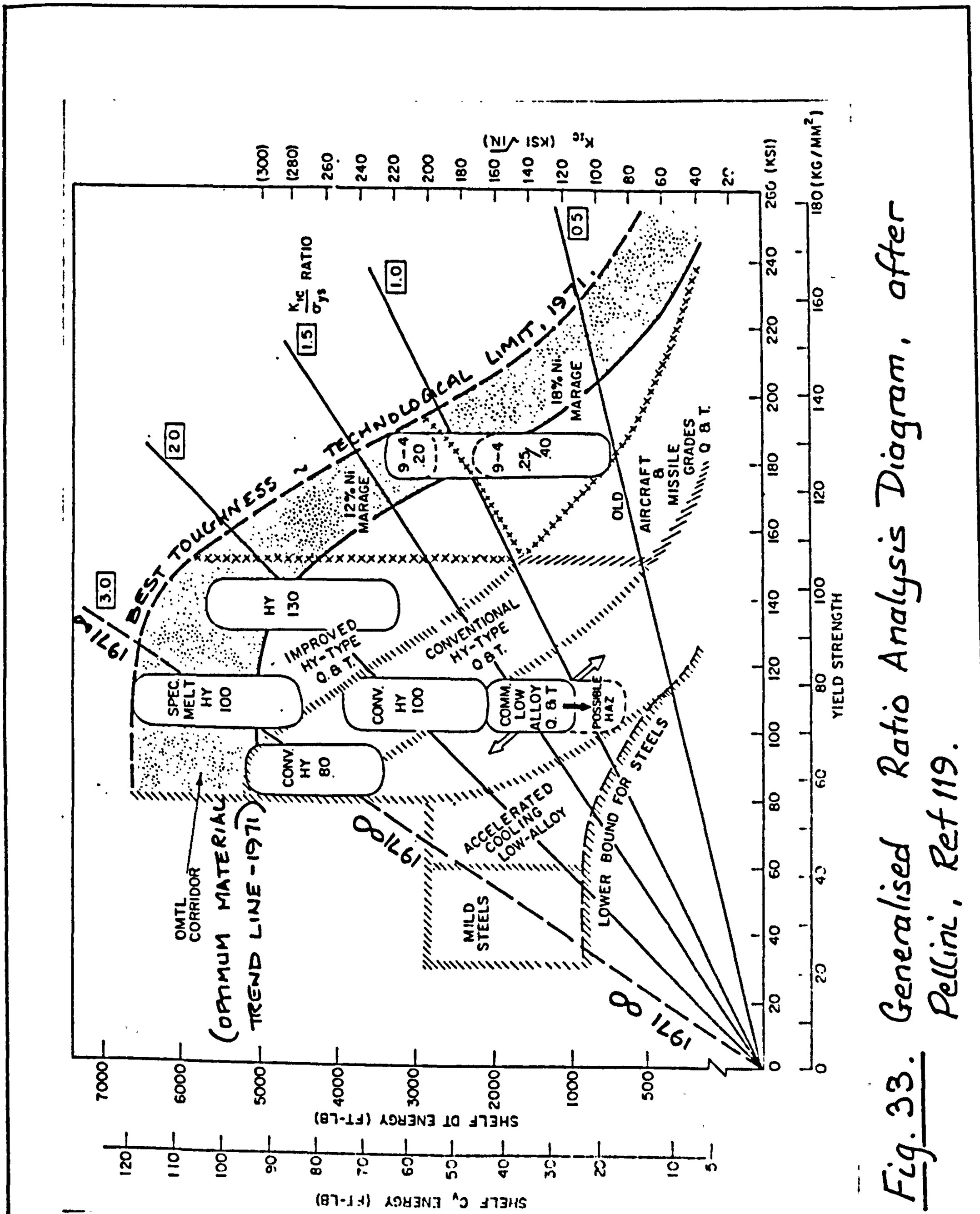

Fig. 33. Generalised Rat[illegible] Analysis Diagram, after Pellini, Ref 119.

Fig. 34. COD specimen to BS5762 2B=W=24m.m.

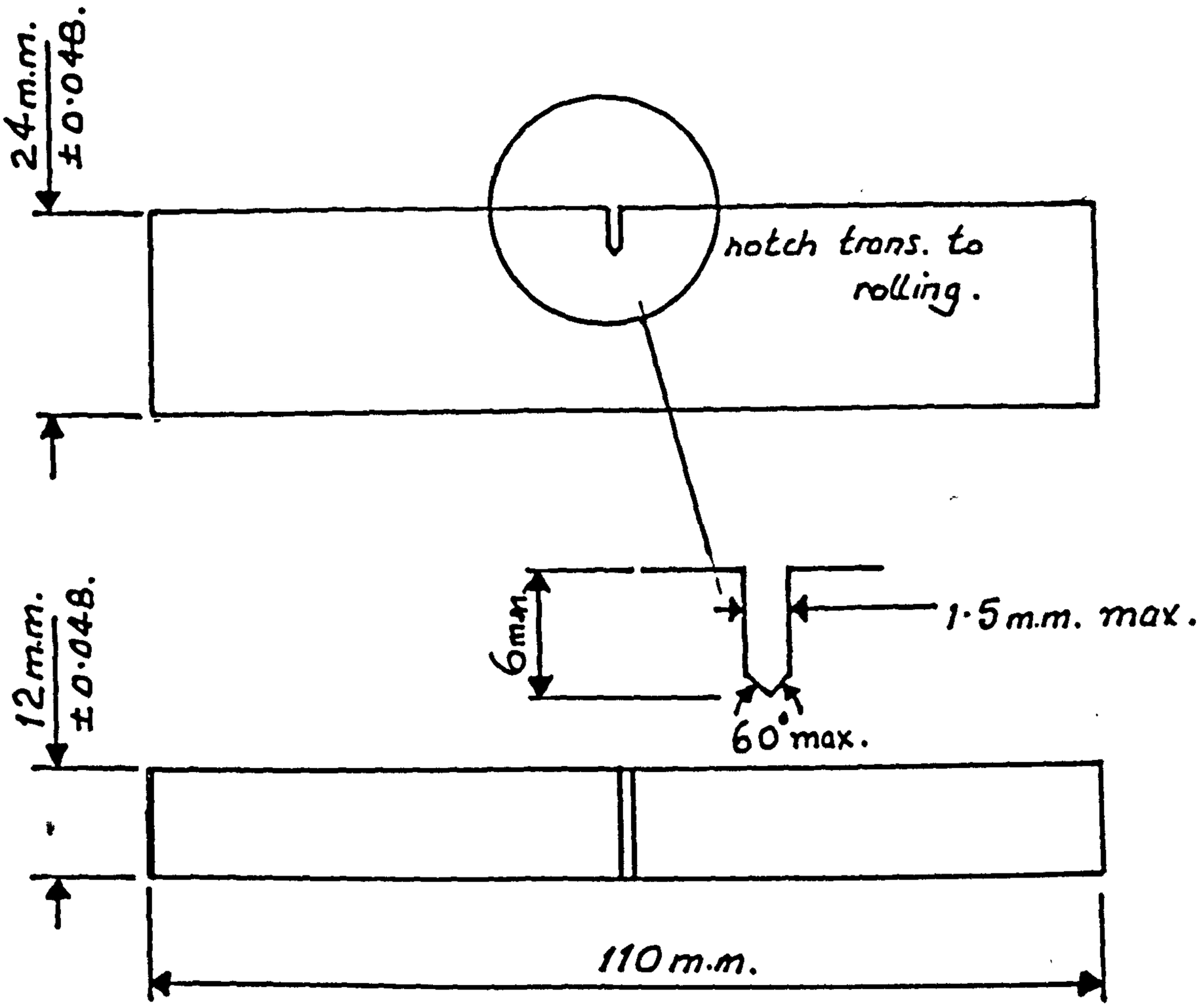

Fig. 35. COD SLOW-STATIC SPRING LOADING SYSTEM.

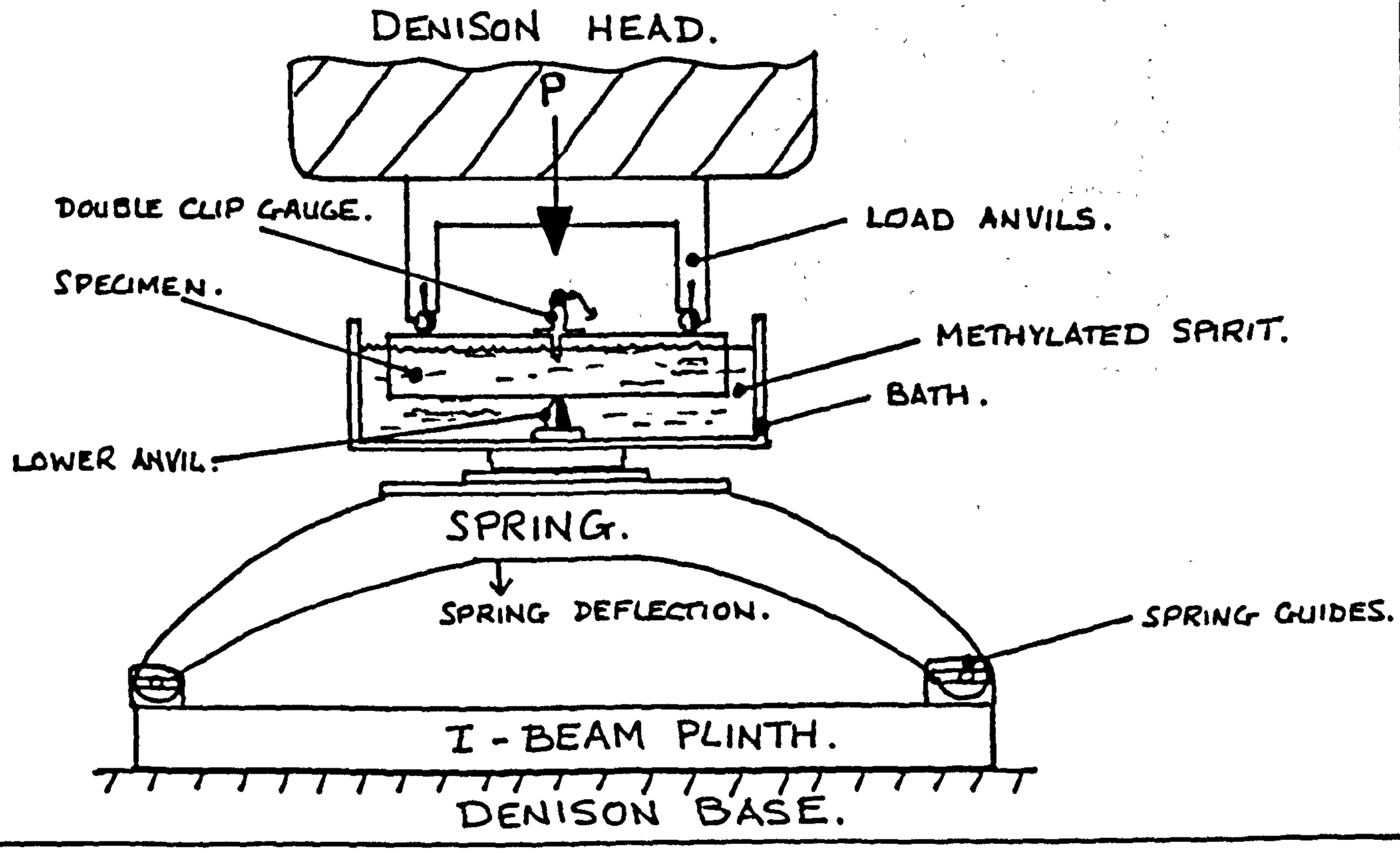

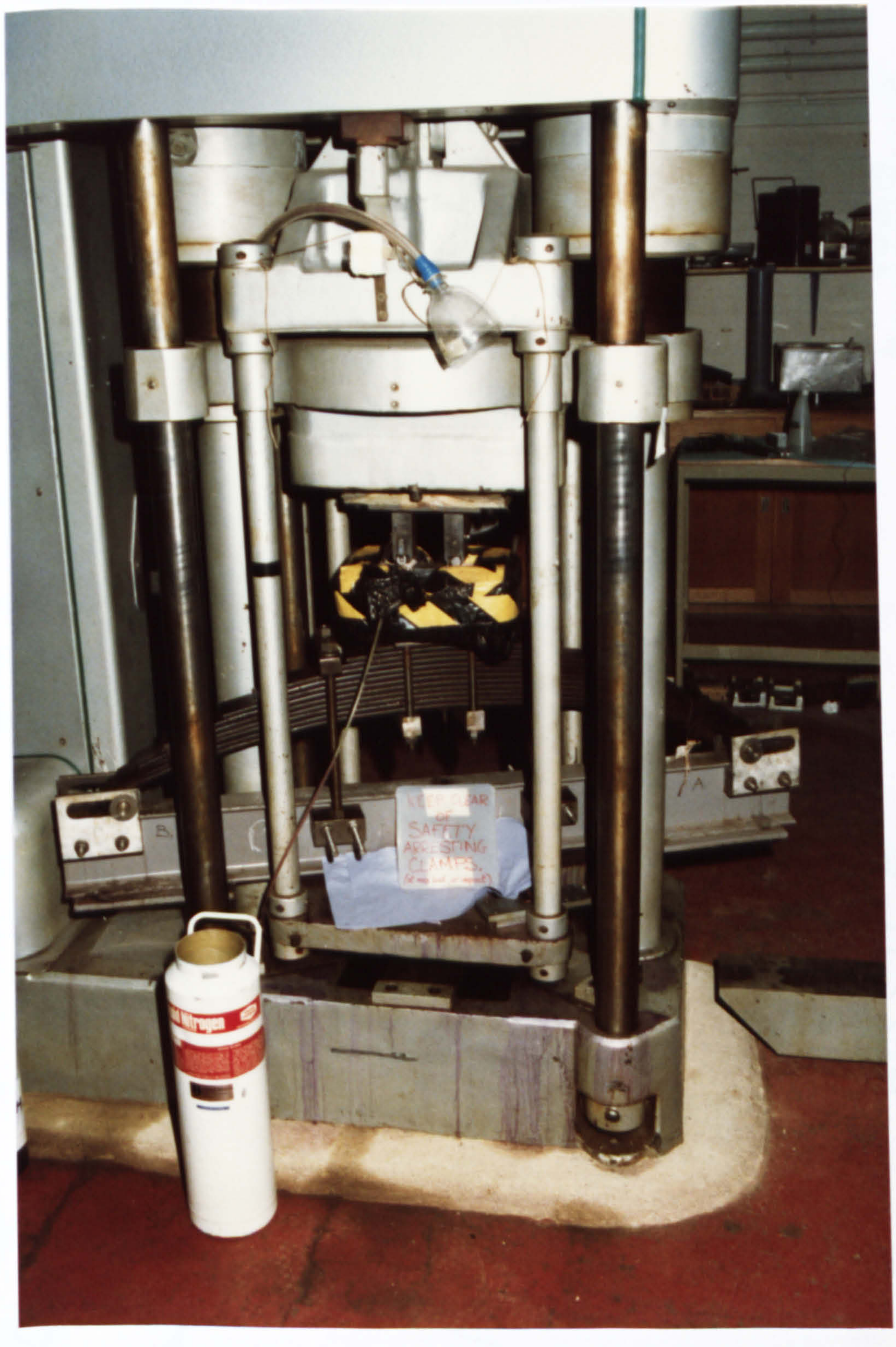

Fig. 36. PHOTOGRAPH OF SLOW-STATIC SPRING LOADING SYSTEM. SEE FIG 35.

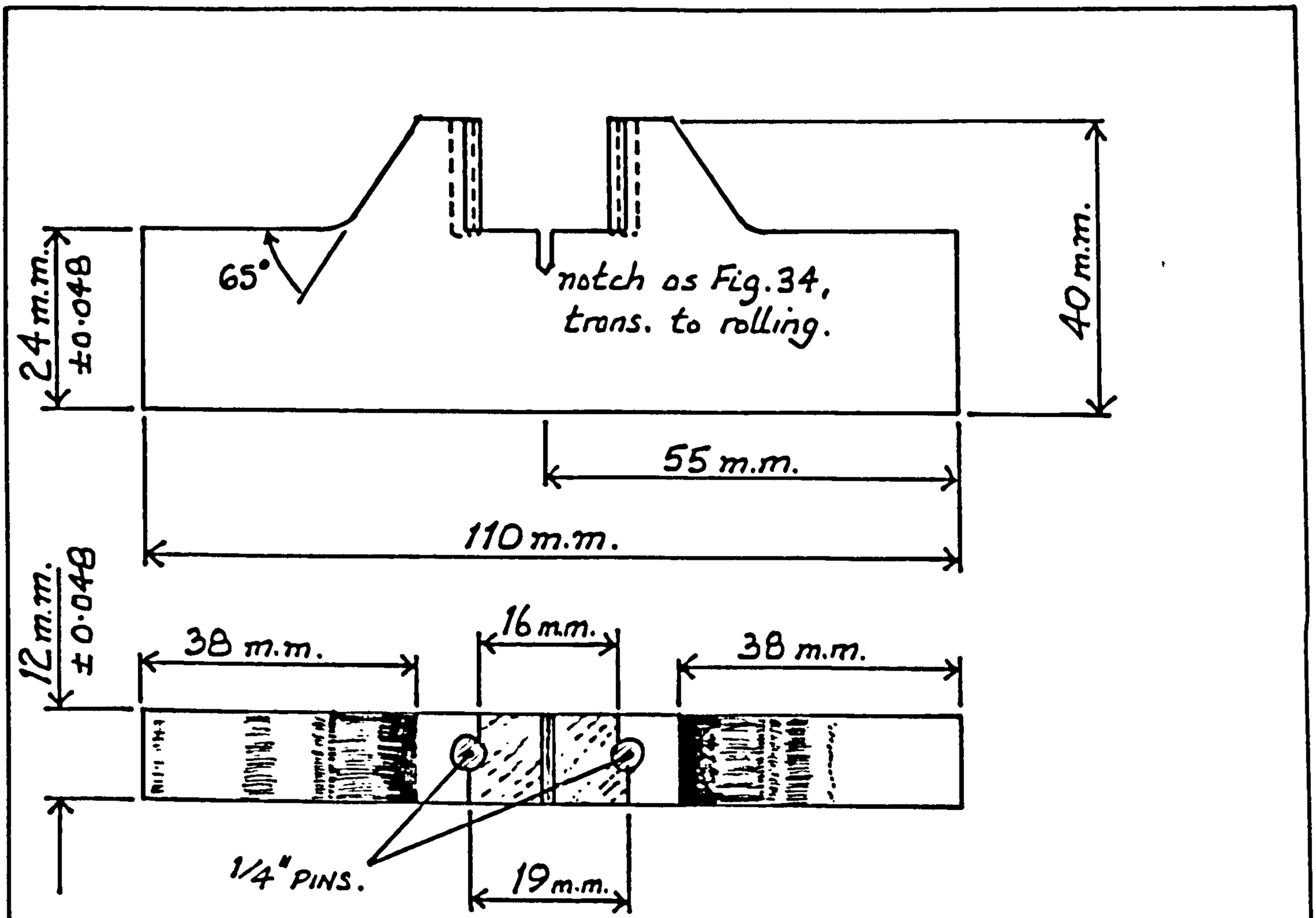

Fig.37. Impact and superposing preload COD specimen.

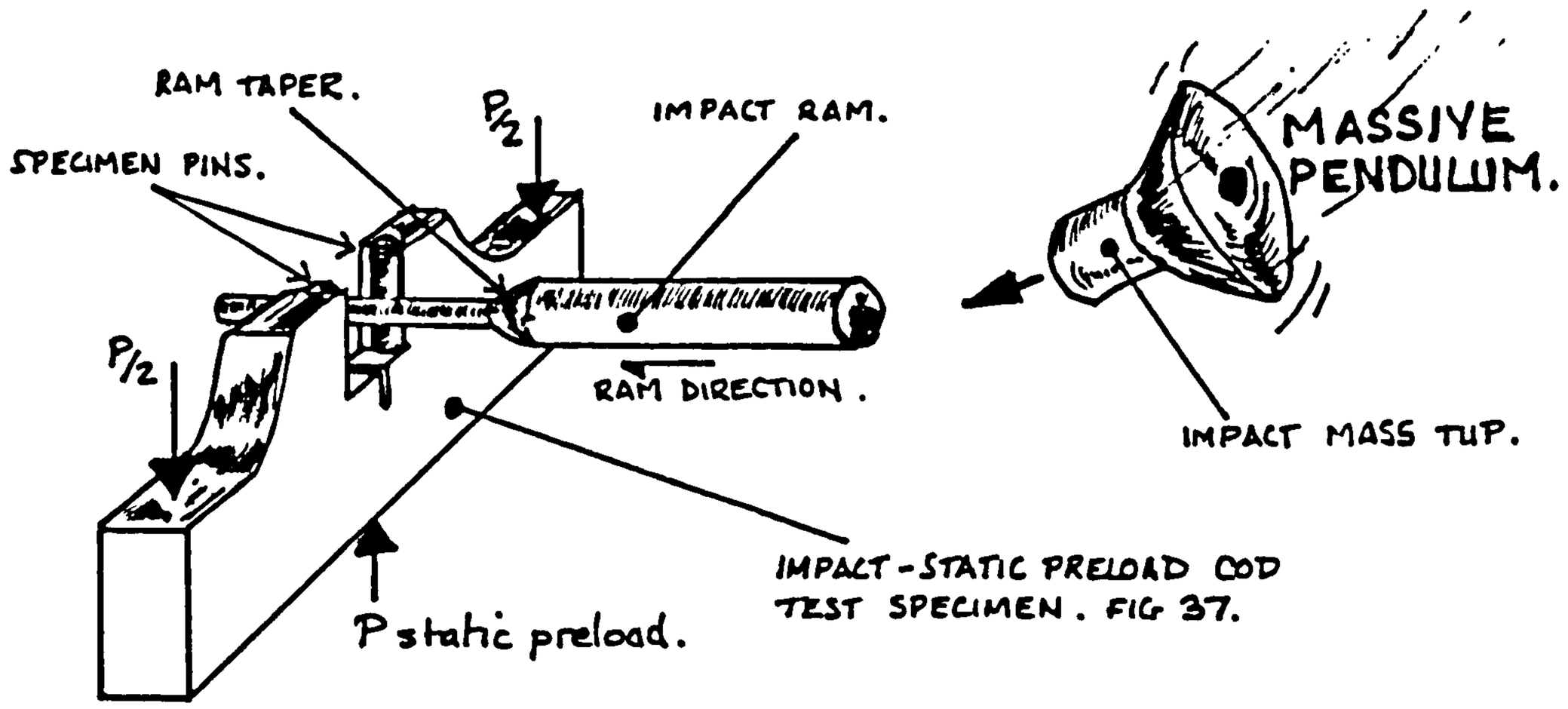

Fig. 38. Impact and superposing preload specimen impact method.

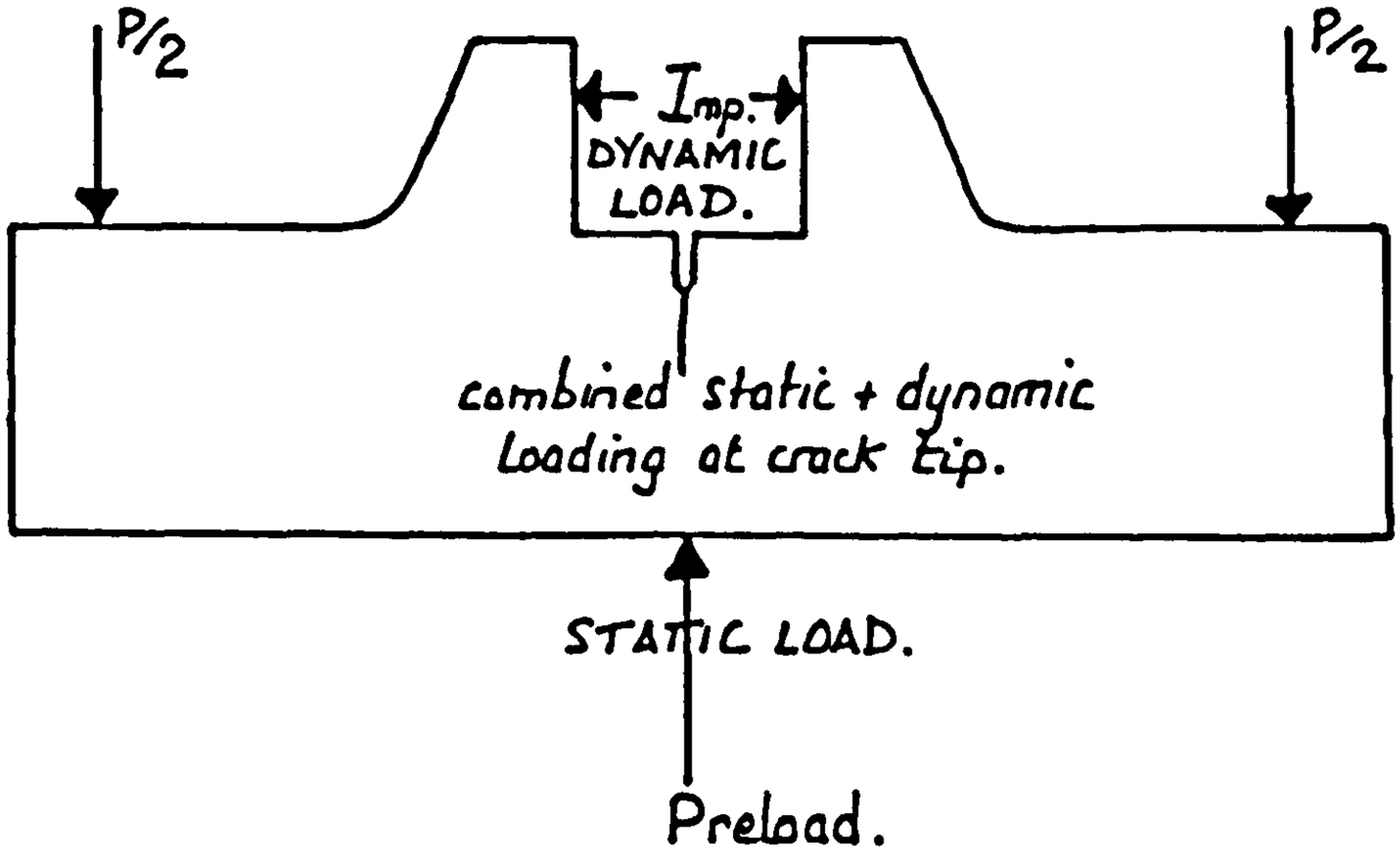

Fig. 39. Loading configuration of impact plus superposed preload specimen of Fig 37.

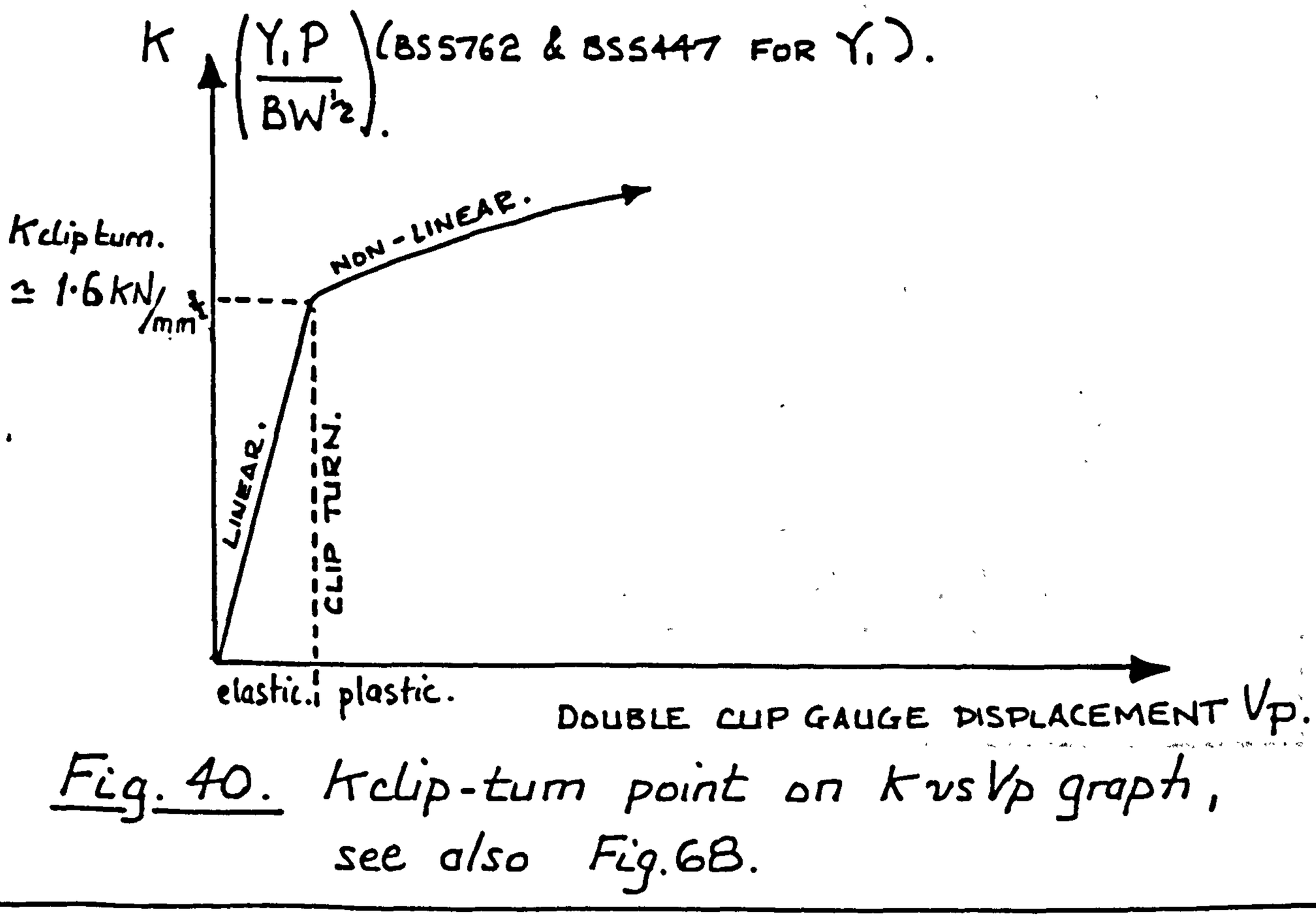

Fig. 40. Kclip-tum point on K vs Vp graph, see also Fig. 68.

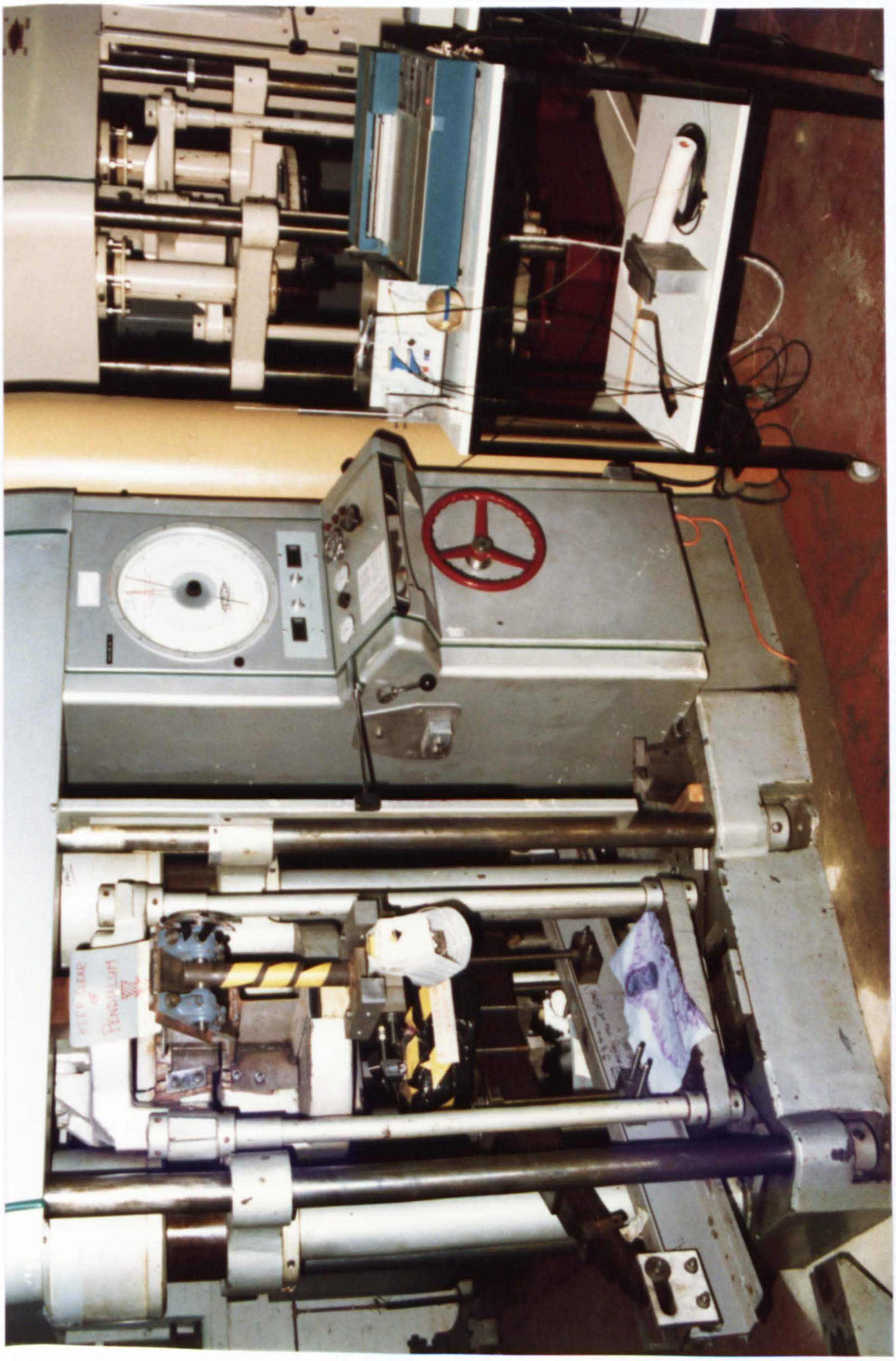

Fig. 41 Full view of test equipment, in impact mode with compliant spring loading system.

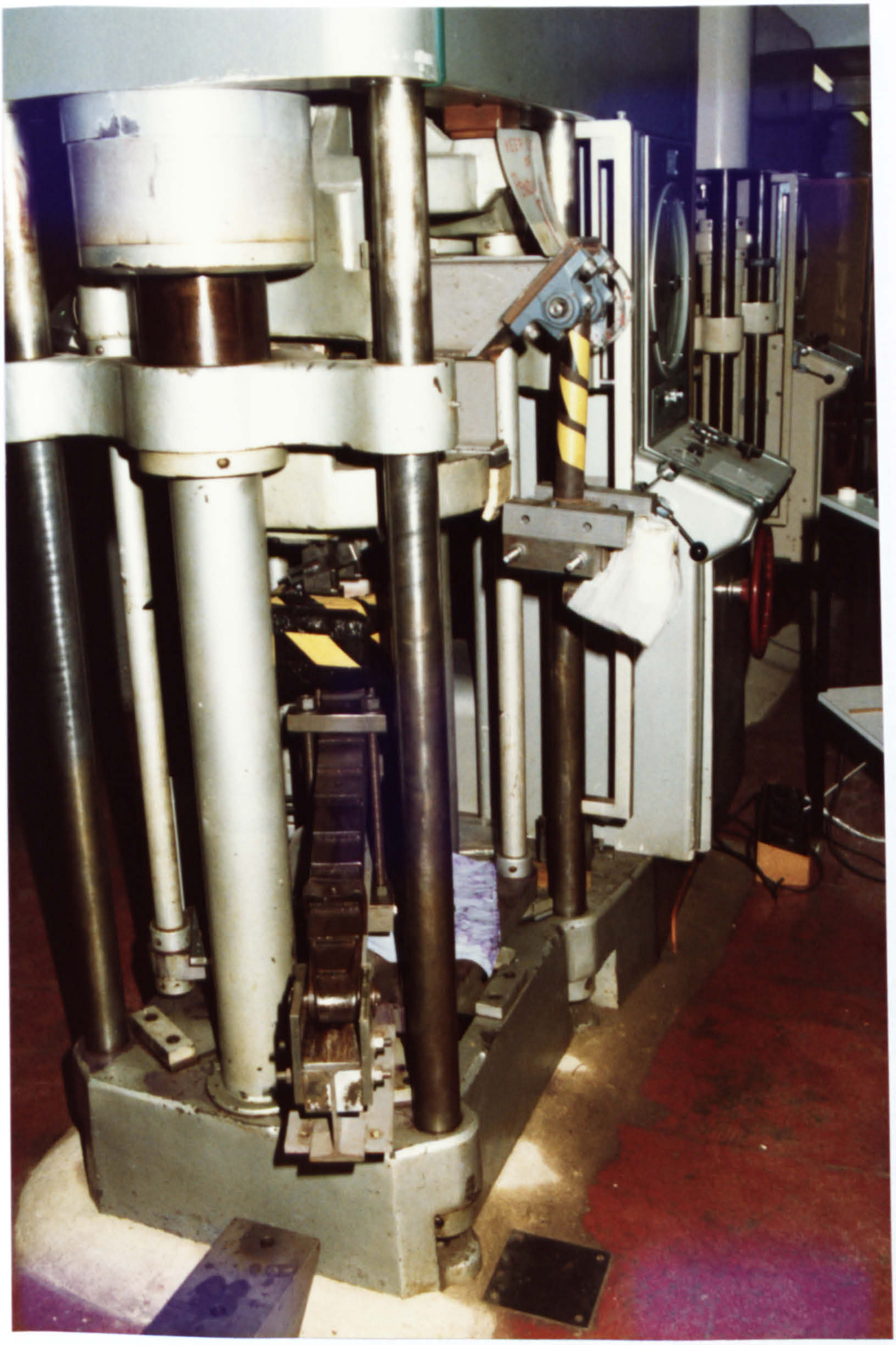

Fig. 42. Side view of impact tup and mass with side of spring.

Fig. 43. Closer view of impact pendulum and mass, with preload anvils just visible above spirit bath.

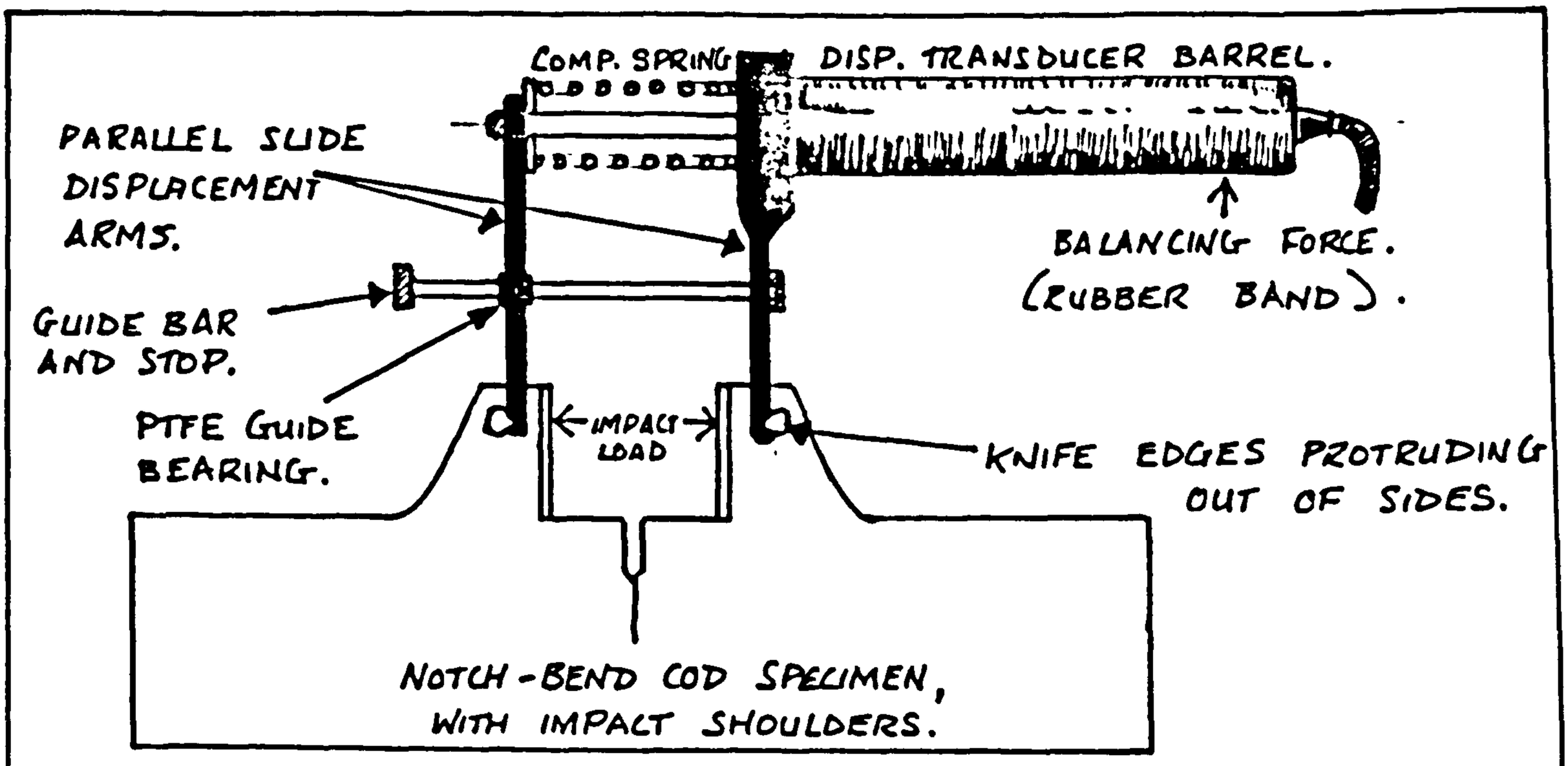

Fig.44. Displacement transducer gauge to monitor preload displacement at the shoulders.

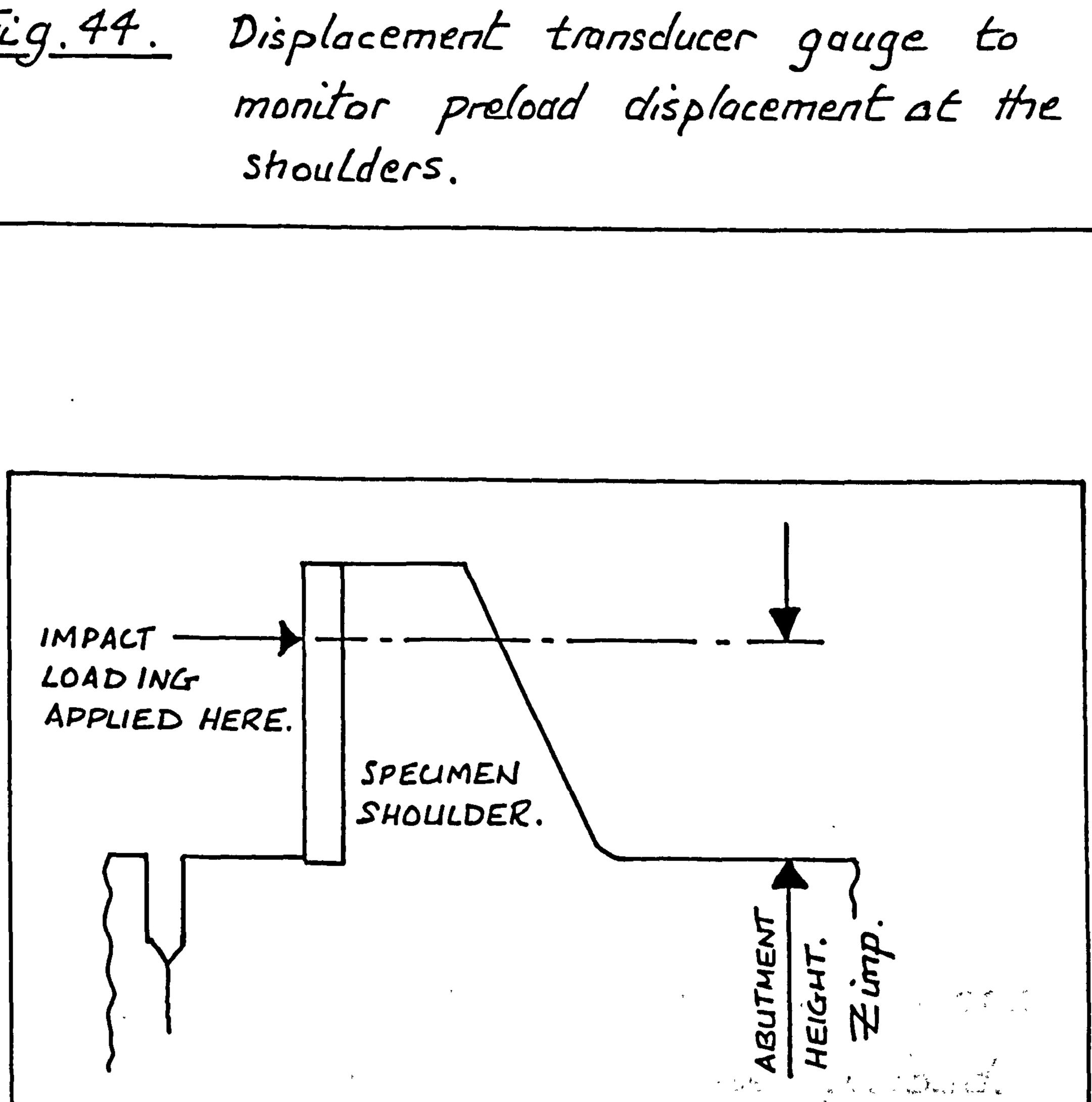

Fig.45. Impact abutment height Zimp for COD equation (32) in section 7.2.

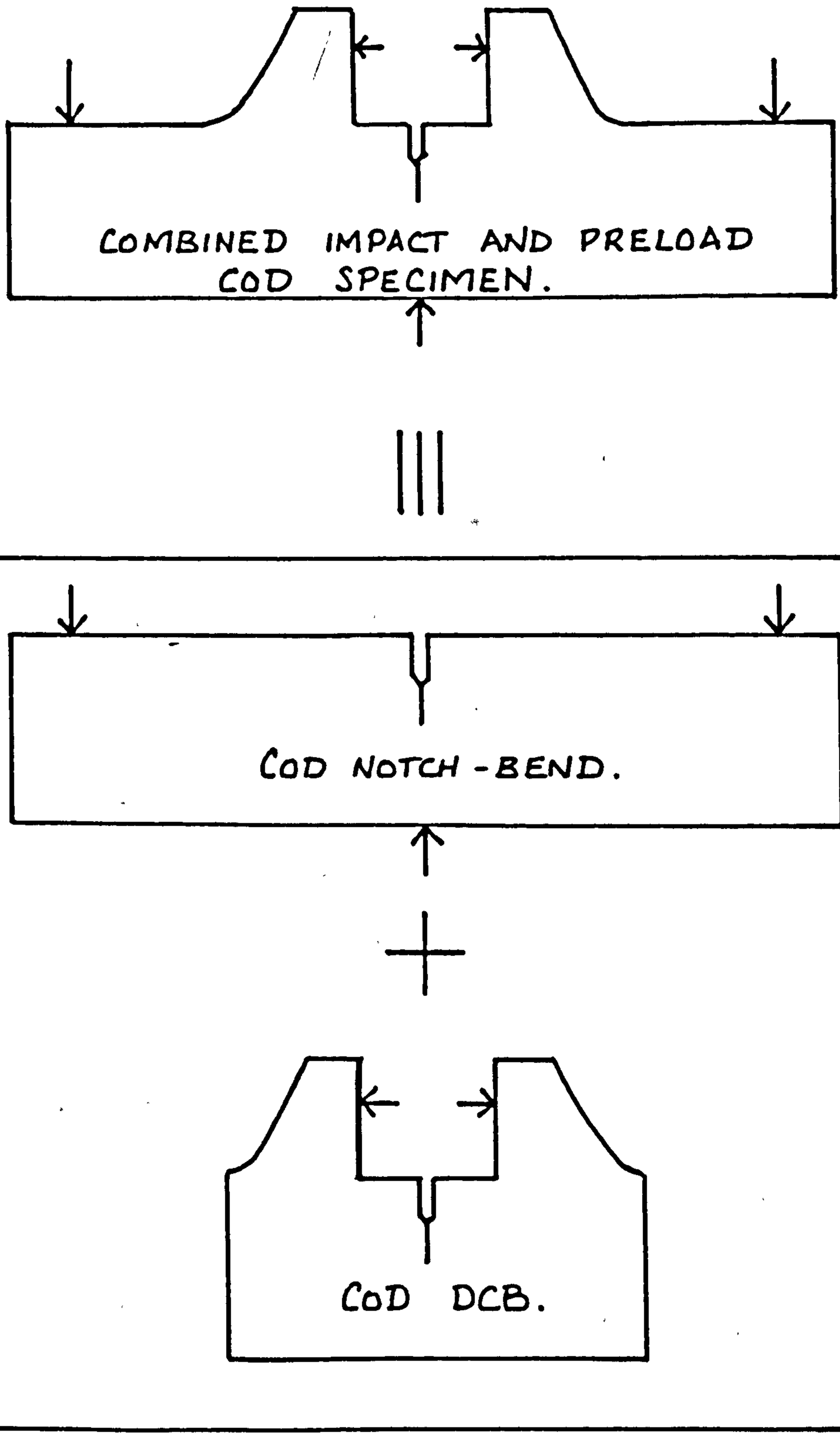

Fig. 46. Equivalent loading arrangements of impact and superposed preload.

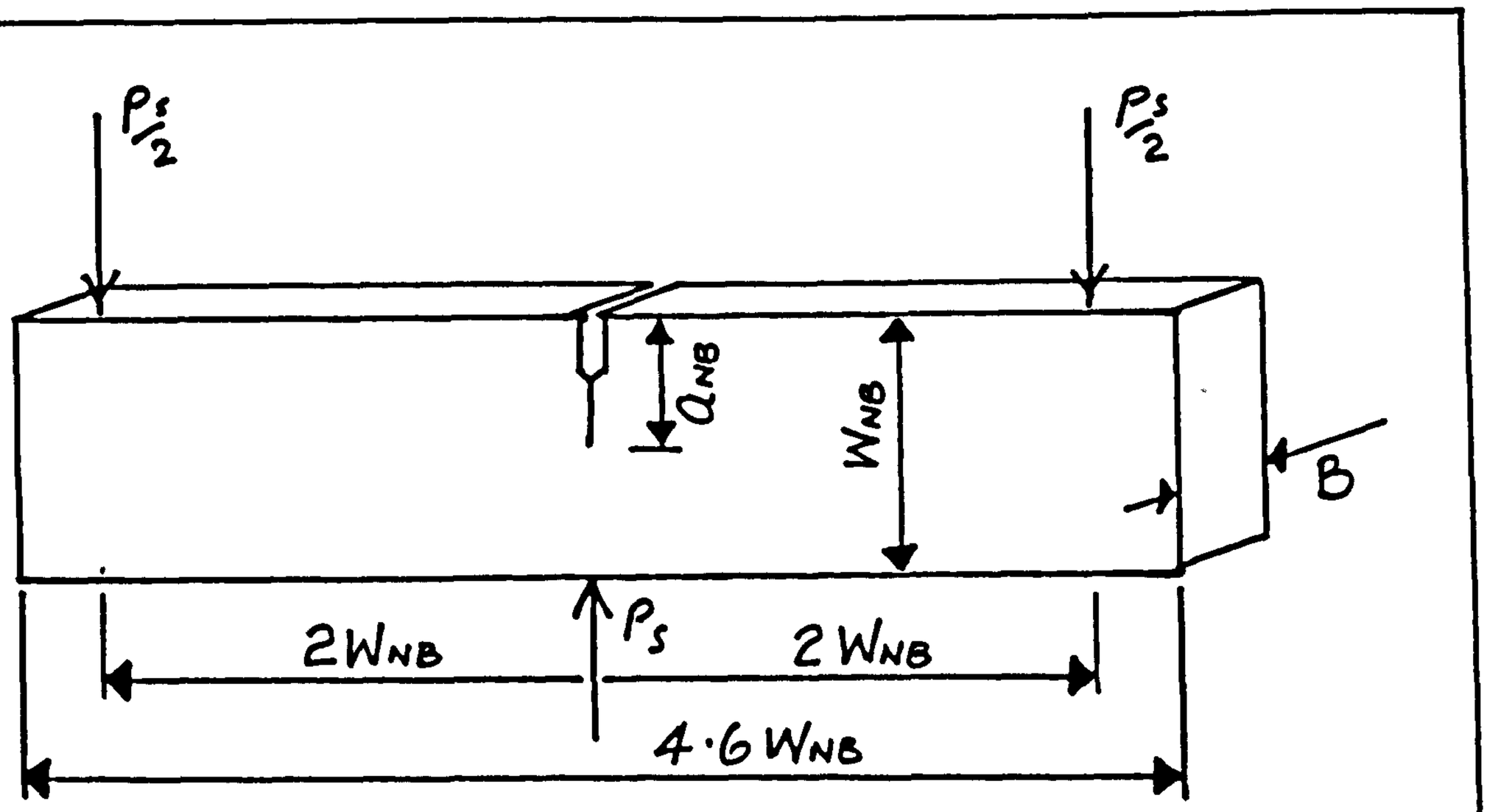

$B = 12$ m.m. $W_{NB} = 24$ m.m. $a_{NB} = 12{\cdot}2$ m.m. (a/W 0·51).

P_s = preload magnitude - static.

Fig. 47. NOTCH BEND CONFIGURATION OF IMPACT TEST SPECIMEN, PRELOAD SYSTEM.

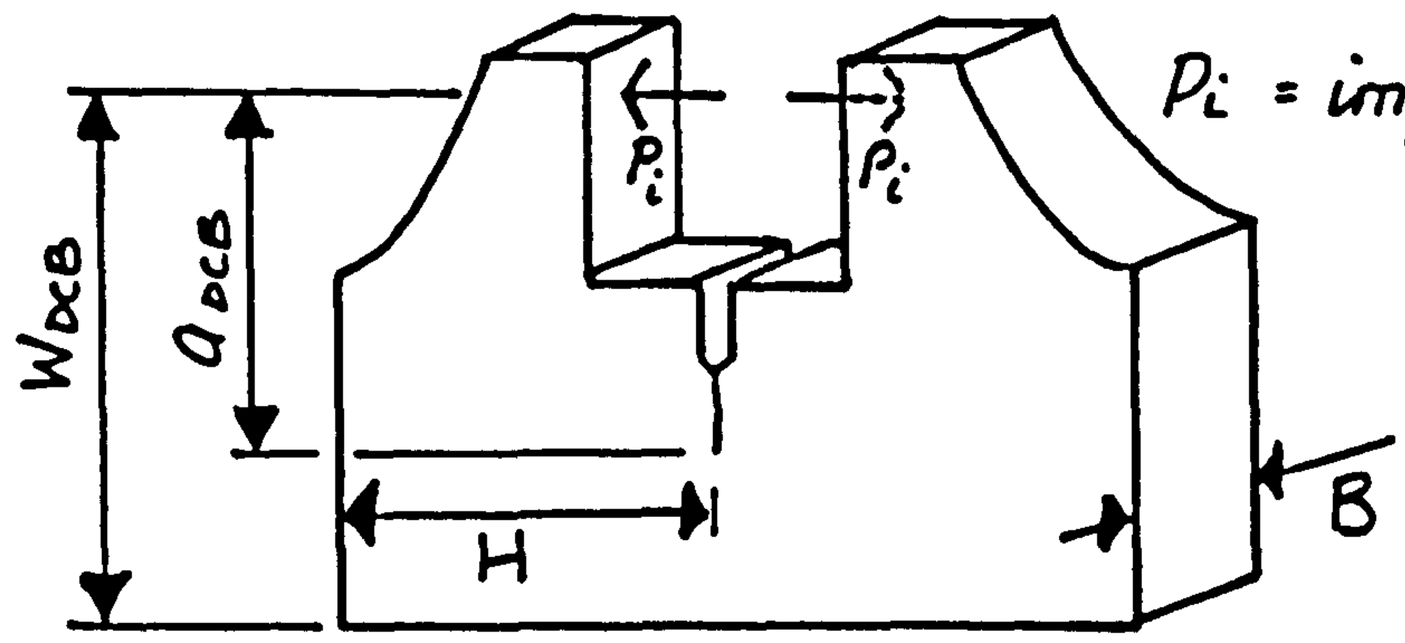

P_i = impact loading.

$B = 12$ m.m. $W_{DCB} = 36{\cdot}5$ m.m. (base to ram impact).

$a_{DCB} = 12{\cdot}2 + 12{\cdot}5 = 24{\cdot}7$ m.m.

$H = 26$ m.m. approximately.

Fig. 48. EQUIVALENT DCB CONFIGURATION OF IMPACT TEST SPECIMEN, IMPACT SYSTEM.

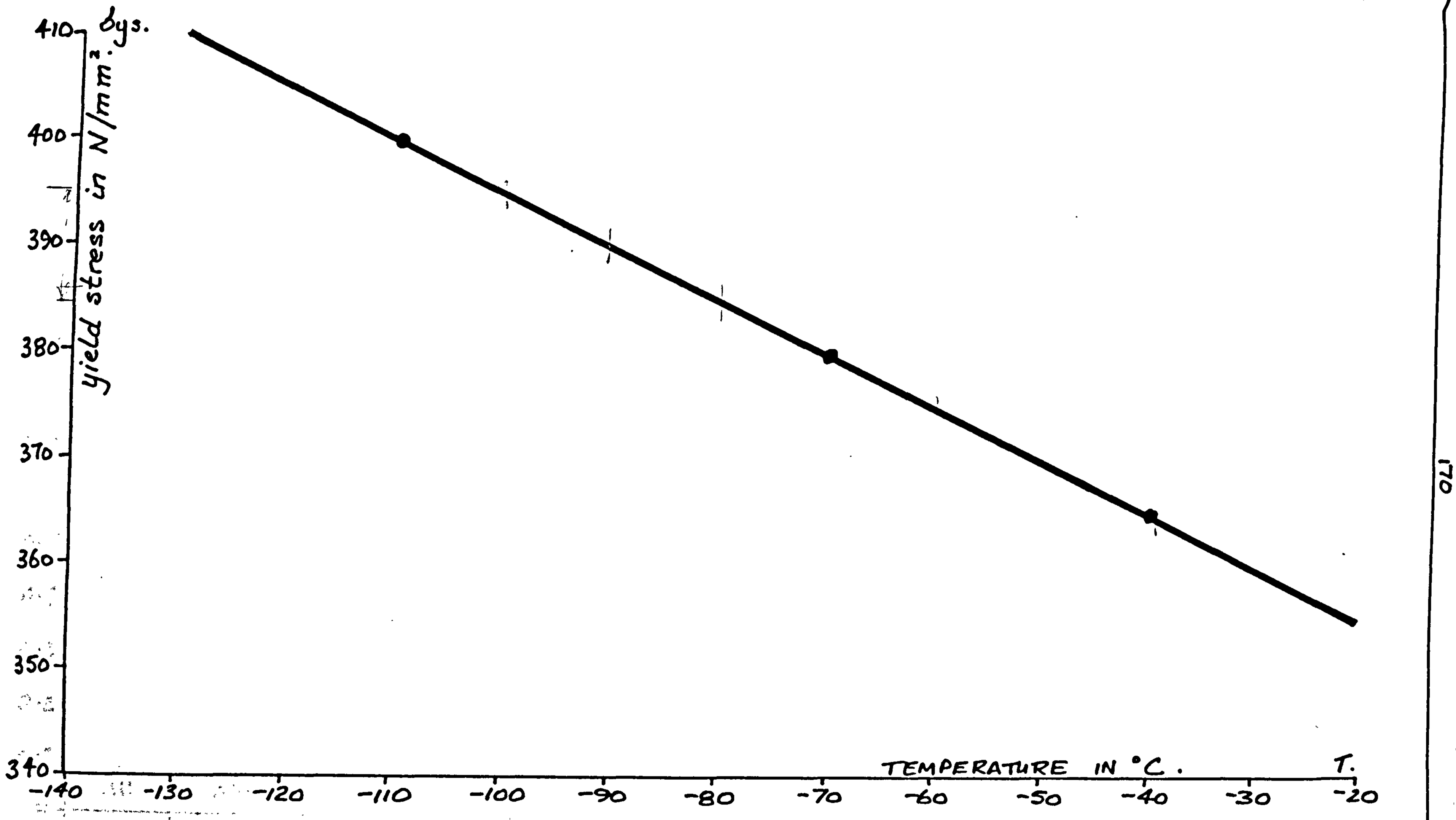

Fig.49. Relation between temperature and tensile yield stress for BS4360-50D.

Fig. 50. Maximum load COD data of Series A slow-static, stiff.

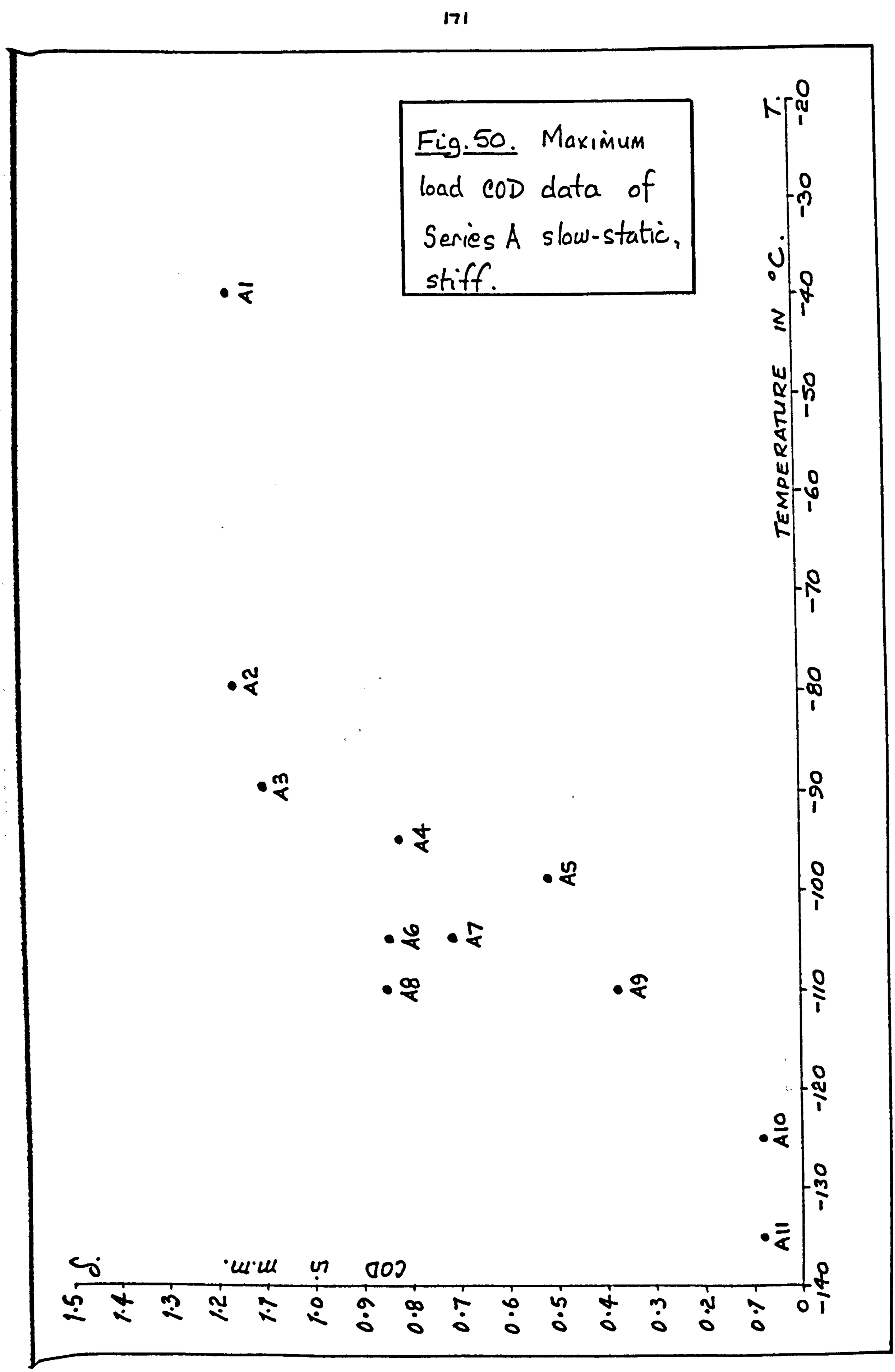

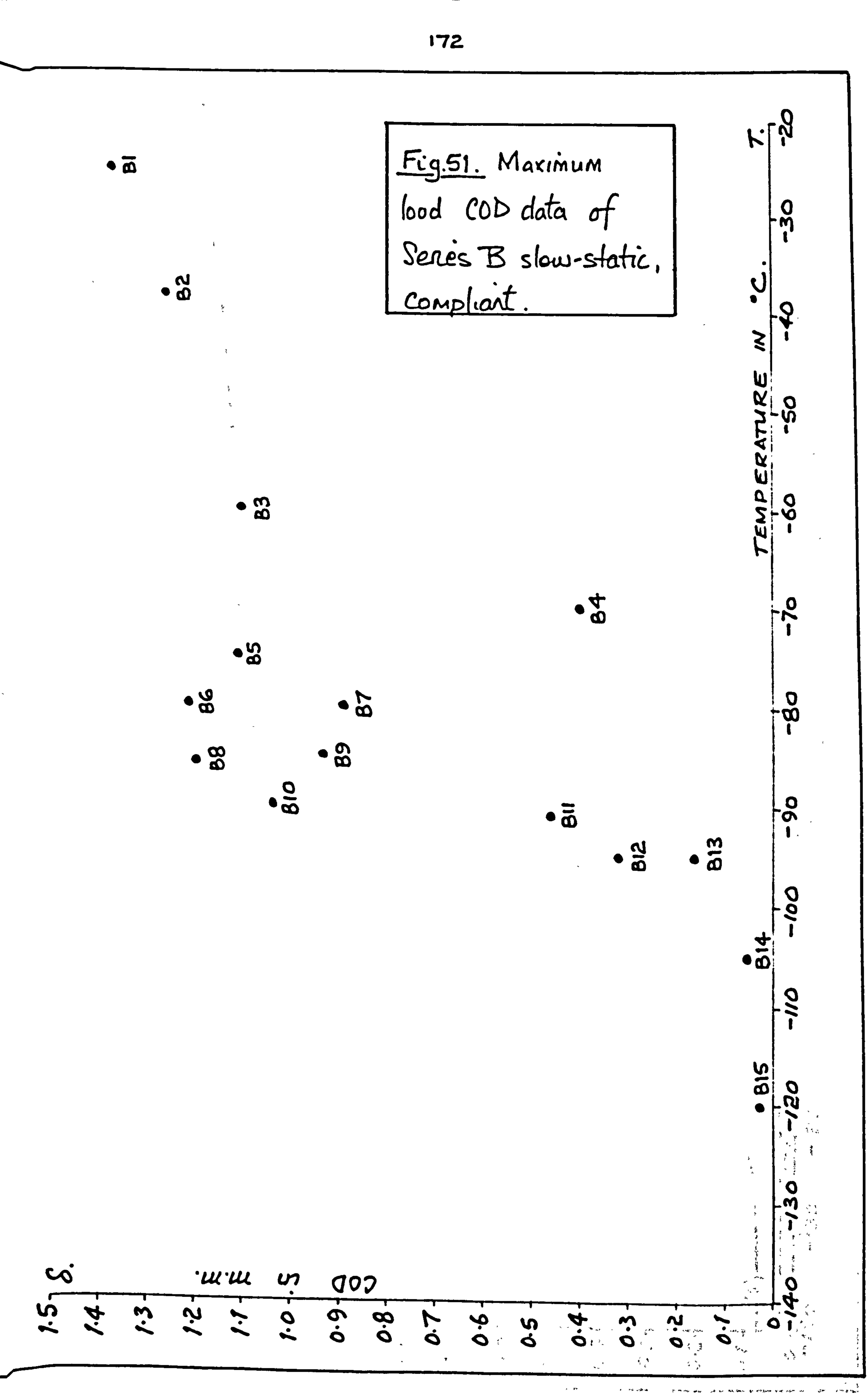

Fig.51. Maximum load COD data of Series B slow-static, compliant.

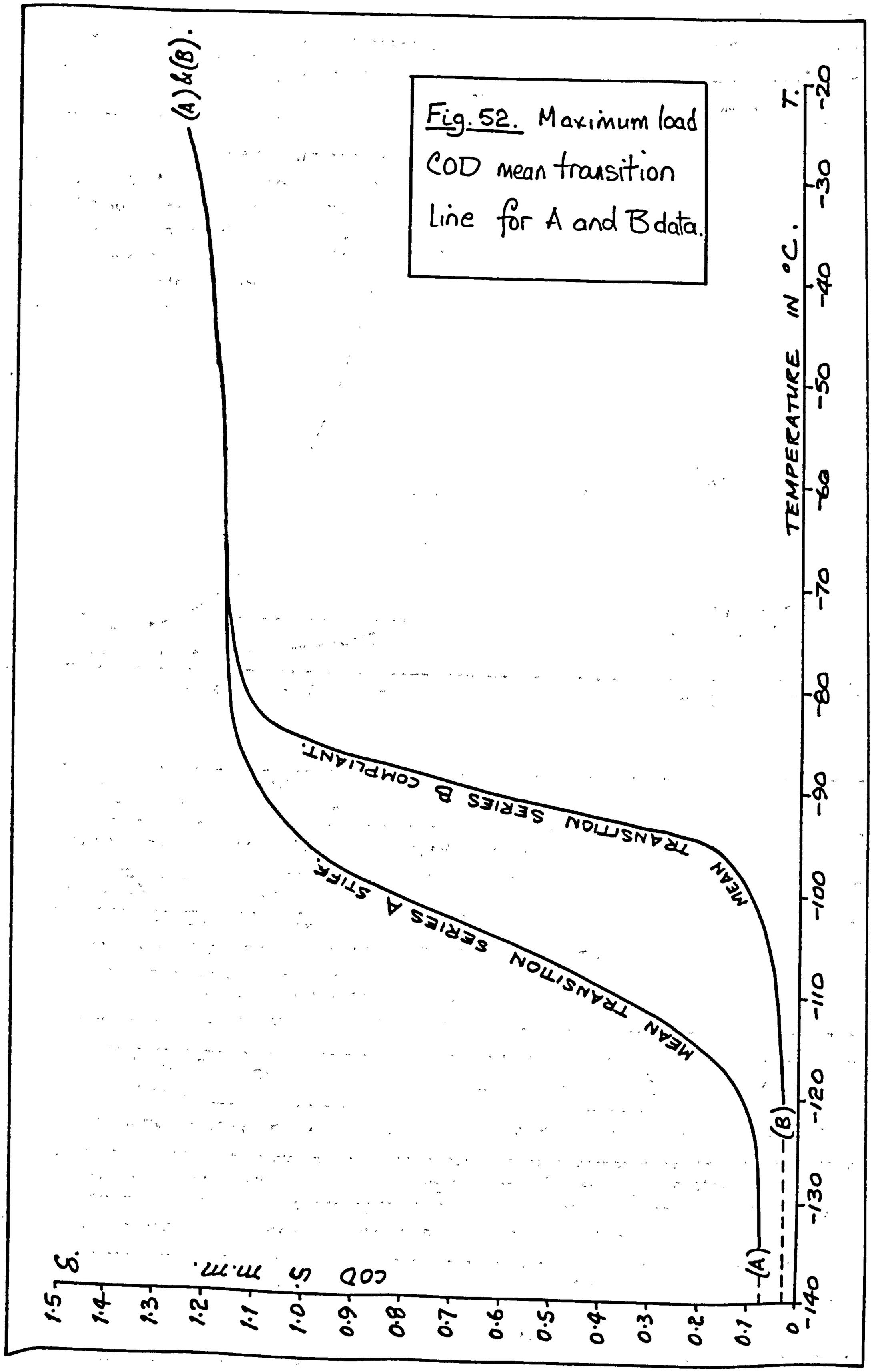

Fig. 52. Maximum load COD mean transition line for A and B data.

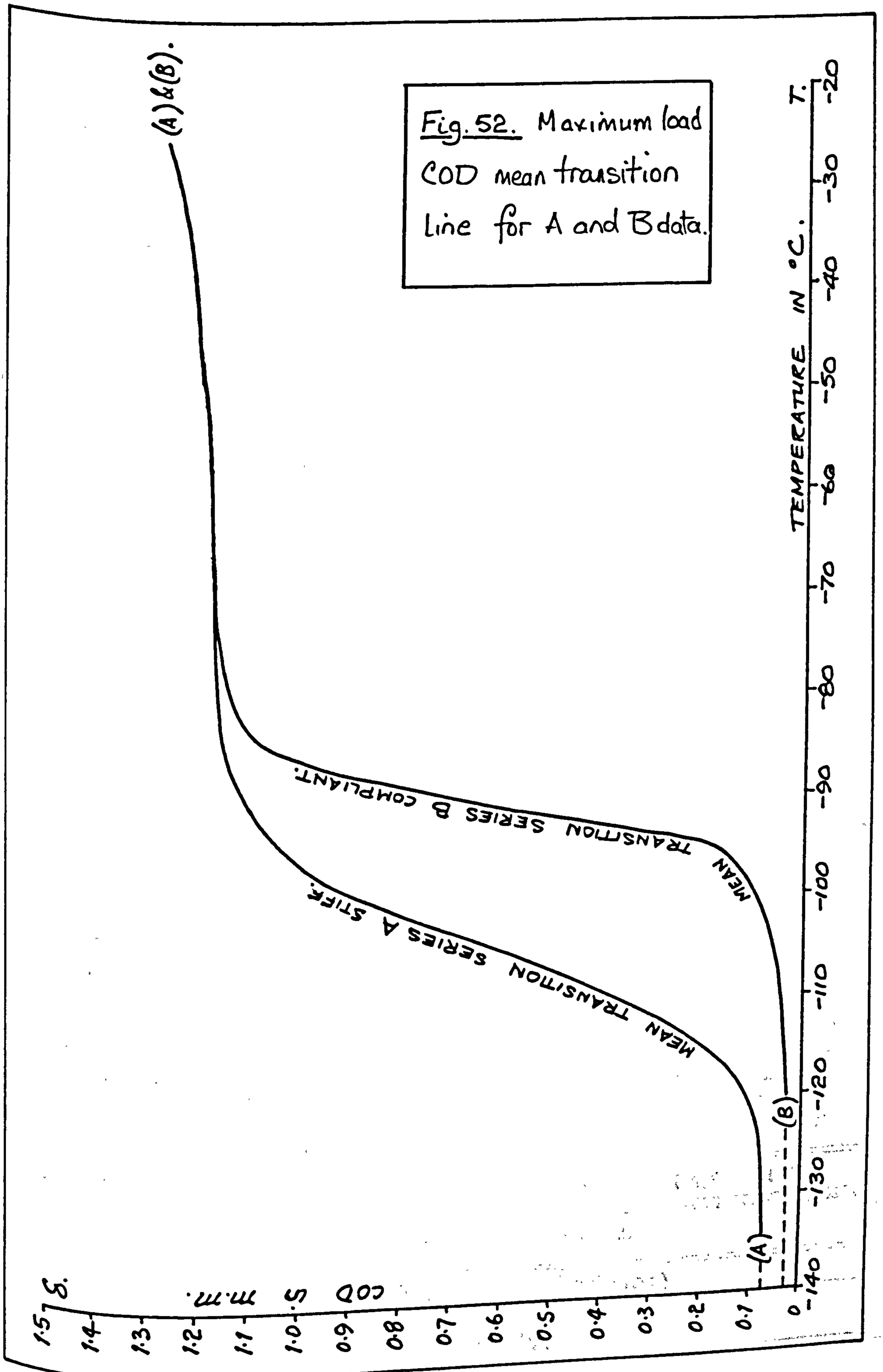

Fig. 52. Maximum load COD mean transition line for A and B data.

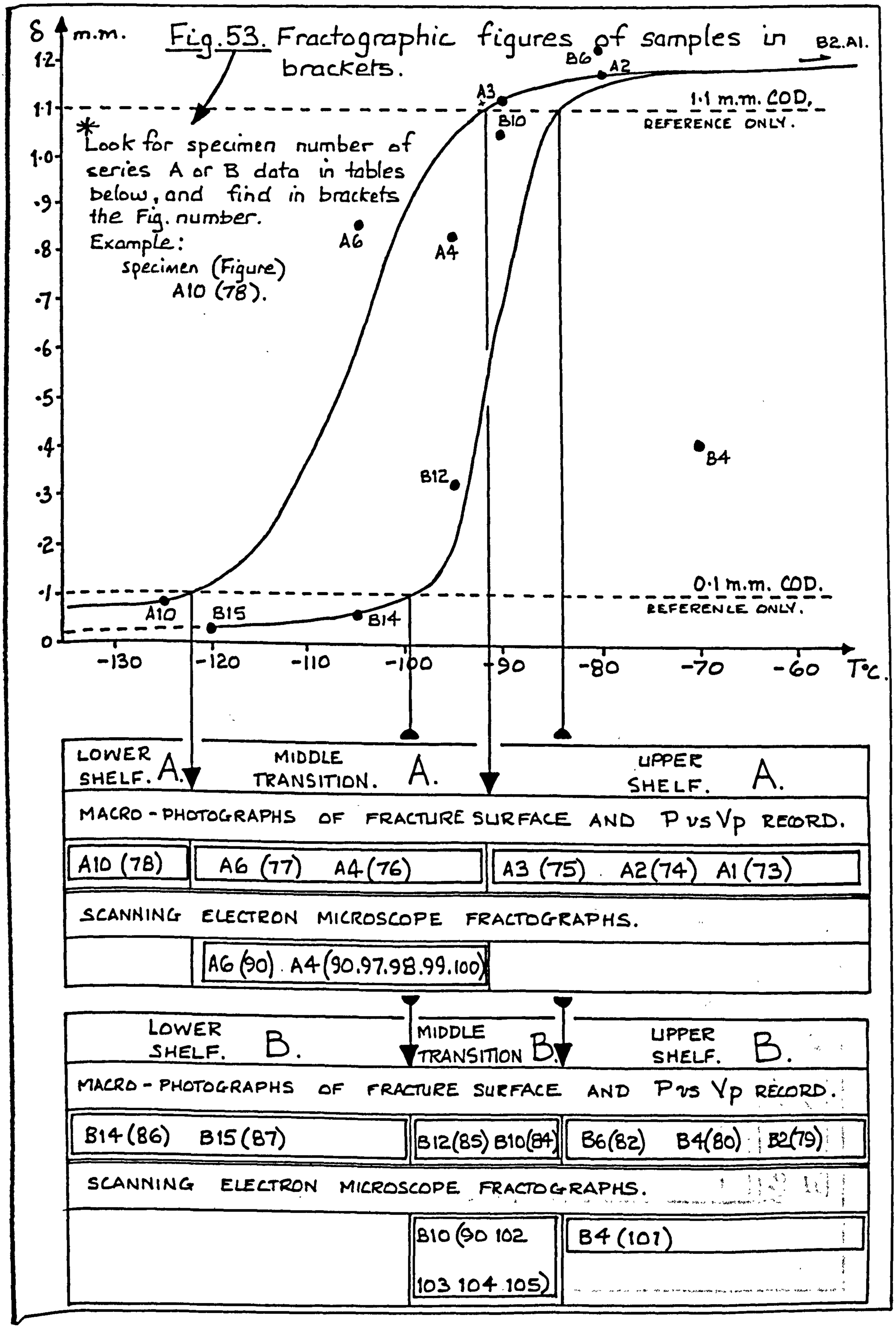
δ m.m.
Fig.53. Fractographic figures of samples in brackets.
B2.A1.
1·2
1·1
1·0
·9
·8
·7
·6
·5
·4
·3
·2
·1
0
* Look for specimen number of series A or B data in tables below, and find in brackets the Fig. number.
Example:
specimen (Figure)
A10 (78).
B6
A2
A3
1·1 m.m. COD, REFERENCE ONLY.
B10
A6
A4
B12
B4
0·1 m.m. COD. REFERENCE ONLY.
A10
B15
B14
-130
-120
-110
-100
-90
-80
-70
-60
T°C.
LOWER SHELF. A.
MIDDLE TRANSITION. A.
UPPER SHELF. A.
MACRO-PHOTOGRAPHS OF FRACTURE SURFACE AND P vs Vp RECORD.
A10 (78)
A6 (77) A4 (76)
A3 (75) A2 (74) A1 (73)
SCANNING ELECTRON MICROSCOPE FRACTOGRAPHS.
A6 (90) A4 (90.97.98.99.100)
LOWER SHELF. B.
MIDDLE TRANSITION B.
UPPER SHELF. B.
MACRO-PHOTOGRAPHS OF FRACTURE SURFACE AND P vs Vp RECORD.
B14 (86) B15 (87)
B12 (85) B10 (84)
B6 (82) B4 (80) B2 (79)
SCANNING ELECTRON MICROSCOPE FRACTOGRAPHS.
B10 (90 102 103 104 105)
B4 (101)

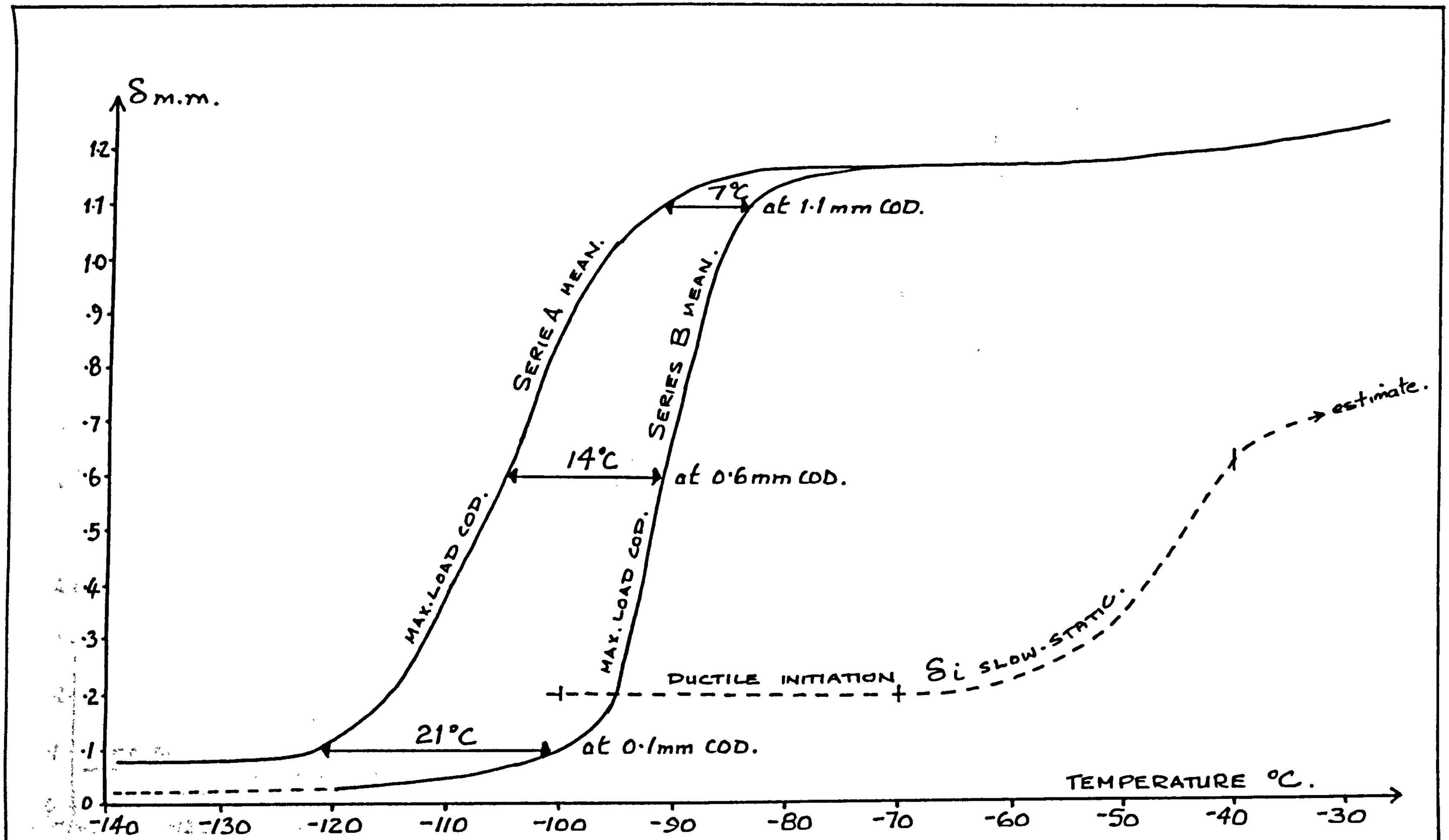

Fig. 54. Difference between series A and B mean transition lines.

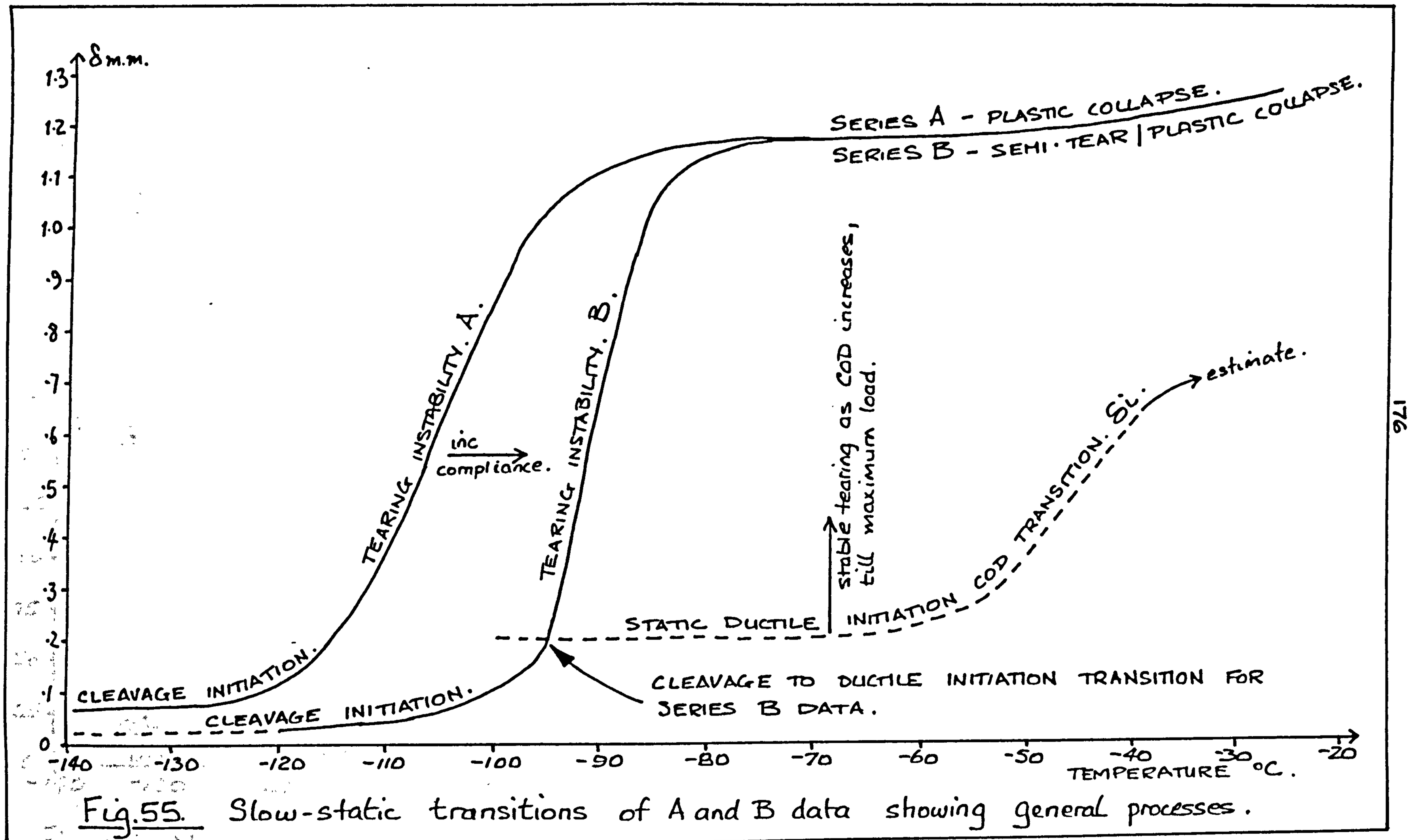

Fig.55. Slow-static transitions of A and B data showing general processes.

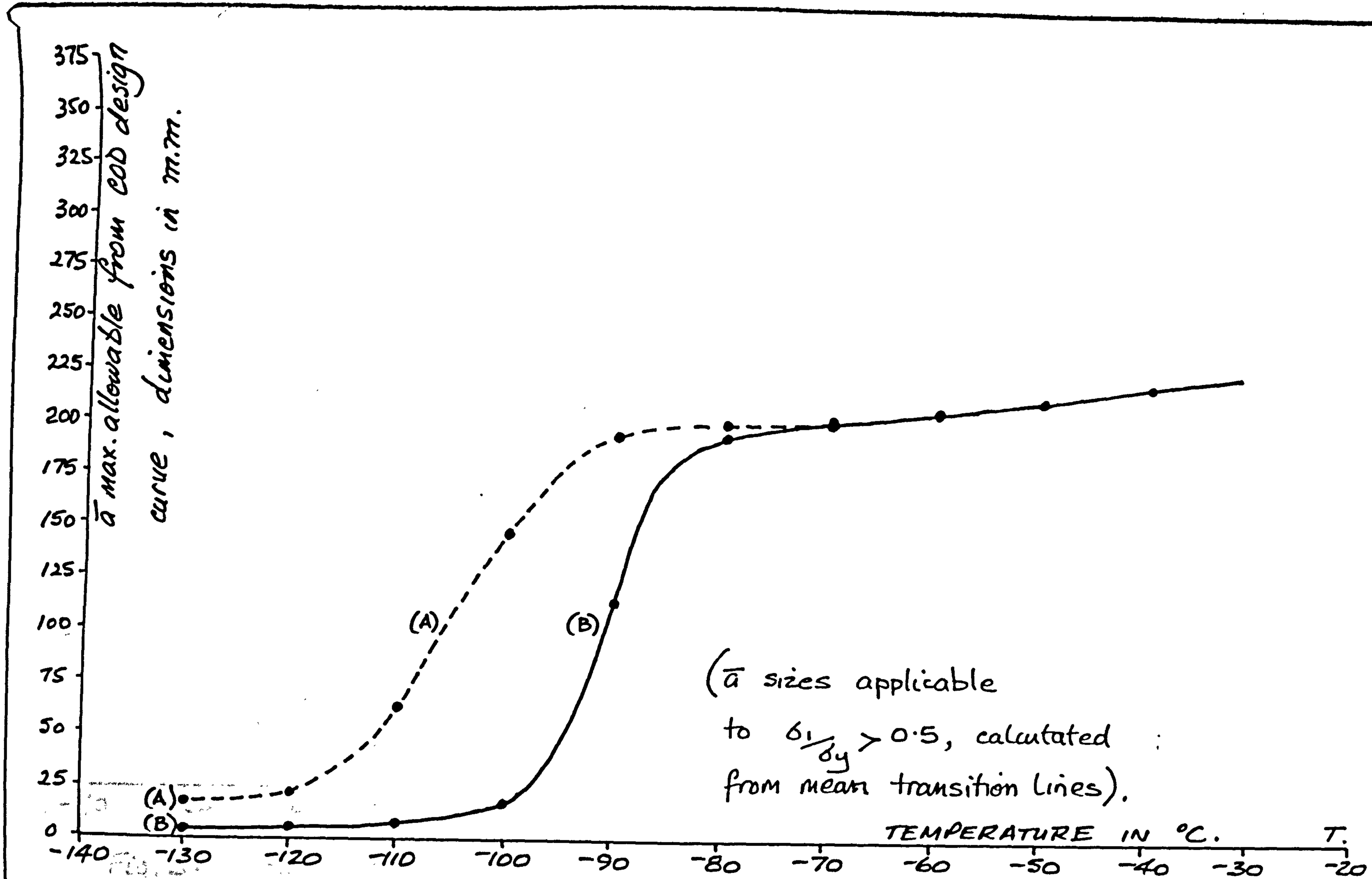

Fig. 56. Maximum allowable flawsizes evaluated from series A and B COD test data.

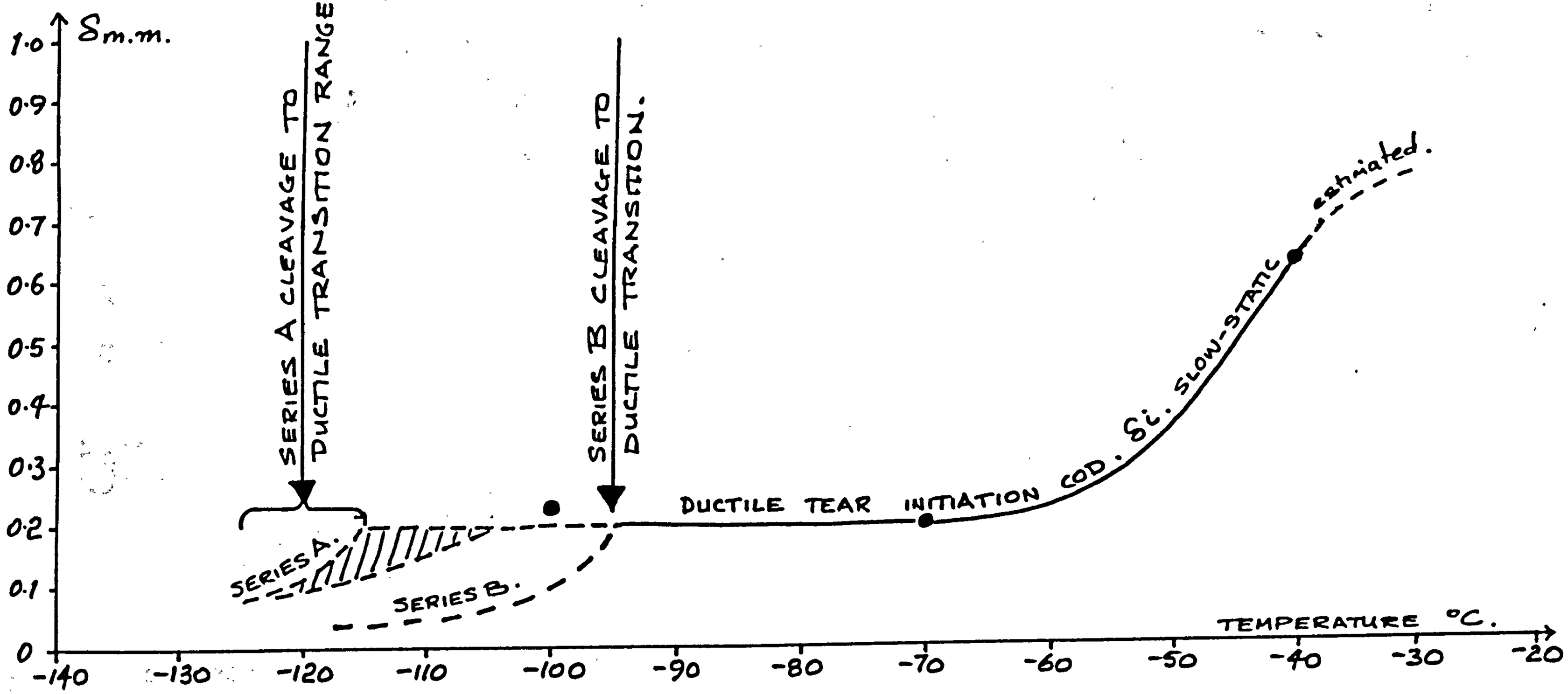

Fig. 57. Slow-static δi ductile initiation COD vs. temperature and cleavage to ductile initiation transitions for stiff (A) and compliant (B) loading systems.

STIFF LOADED TEARING

ZIG-ZAG CRACK

COMPLIANTLY LOADED TEARING

STRAIGHTER CRACK

PIT

PIT

PIT

LARGE PARTICLES. (MnS etc.).

INTERMEDIATE SIZE PARTICLES. (Si or AL compounds).

Fig 58a STIFFLY LOADED.

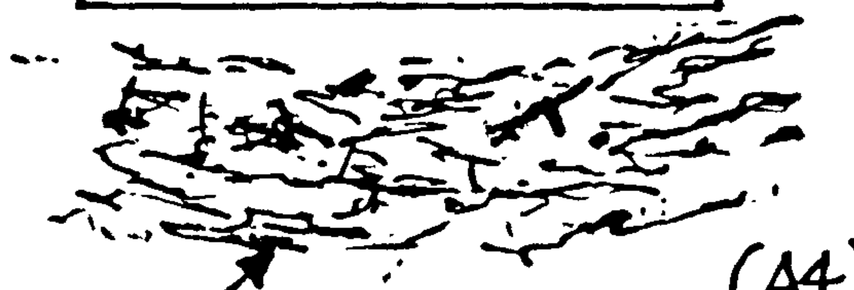

(A4)

See Fig 98.

STEPPED TEAR.

Fig 58b COMPLIANTLY LOADED.

(B10)

See Fig 103.

"PITTING".

"TRAMLINES".

Fig. 58. a&b. Ductile tearing morphology and process during stiff (a) and compliant (b) loading.

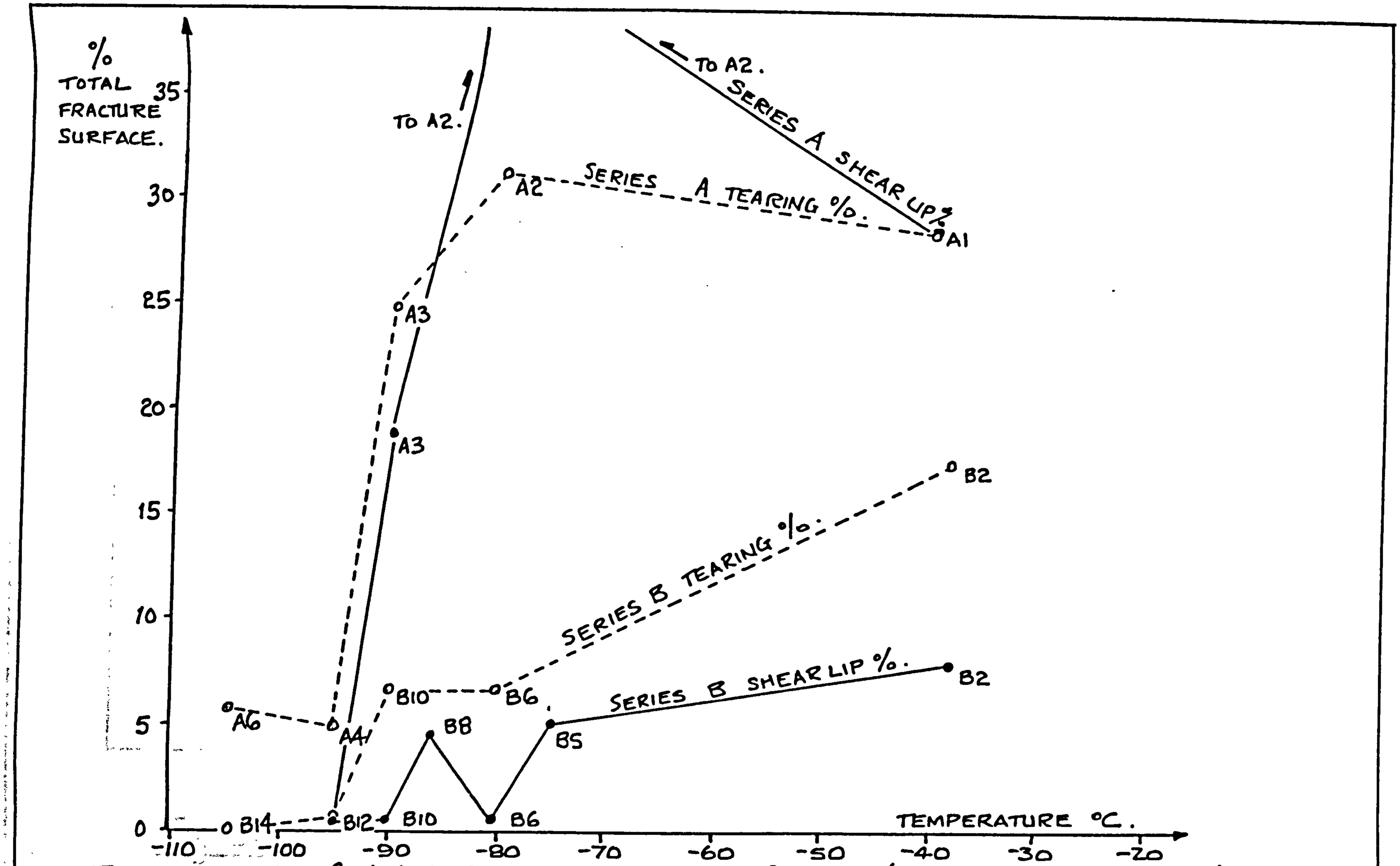

Fig. 59. % of total fracture surface of shearlips and tearing, series A and B.

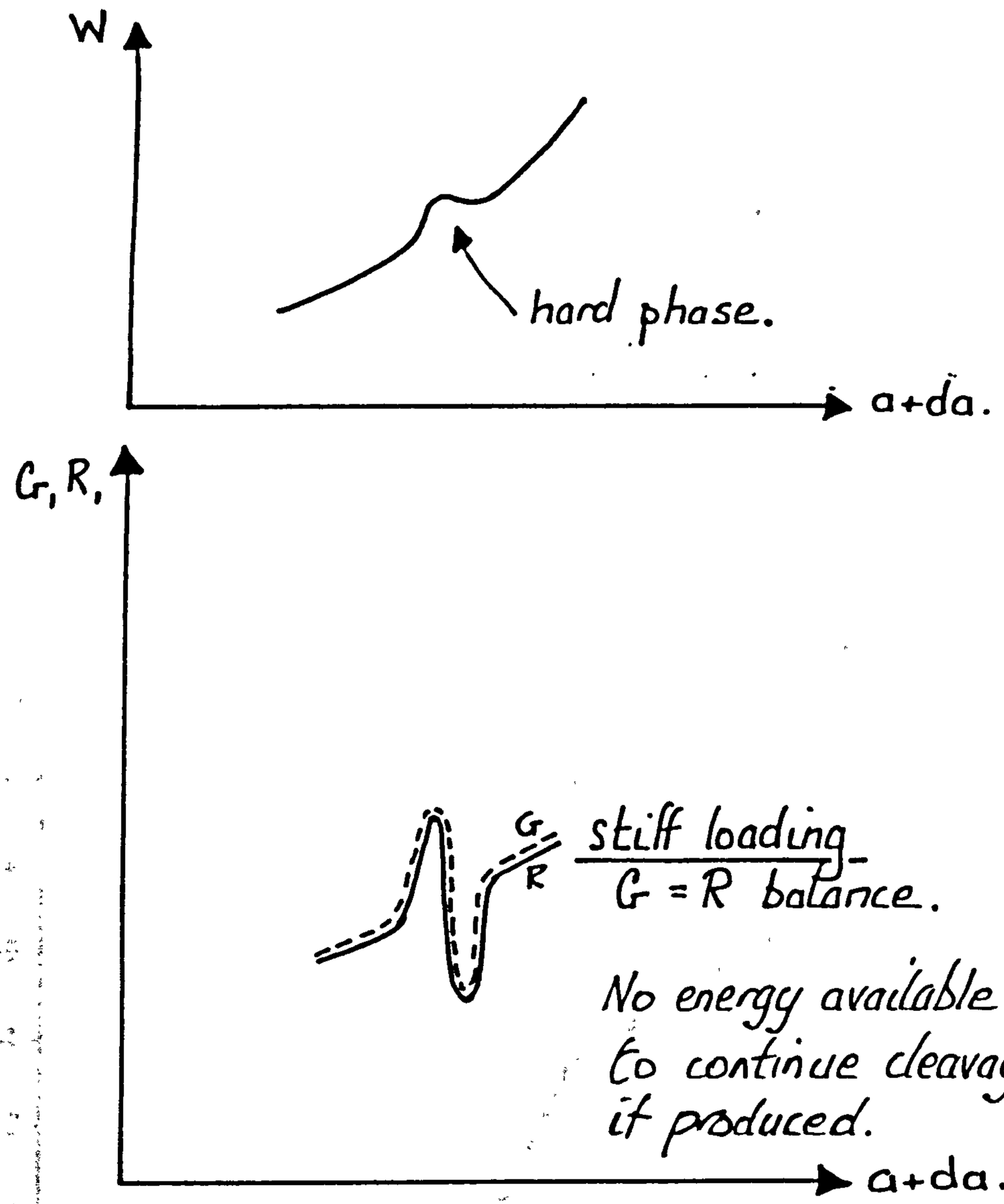

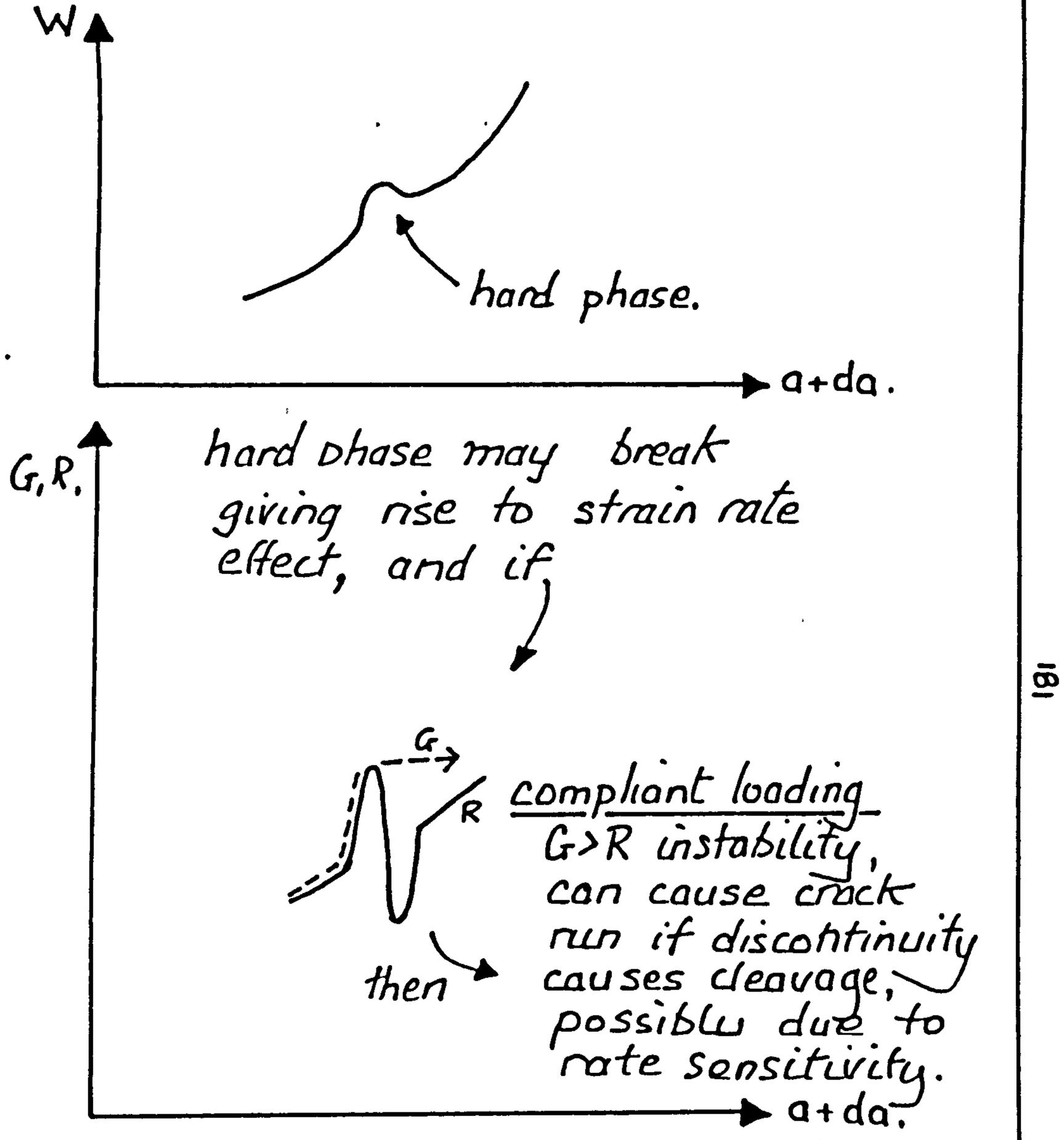

Fig:60. Stiff and compliant driving force in relation to crack restraining-resistance during a hard phase discontinuity.

Fig.61. Recommended industial samplina and conservative design criteria for determinate structures, see section 8.3.

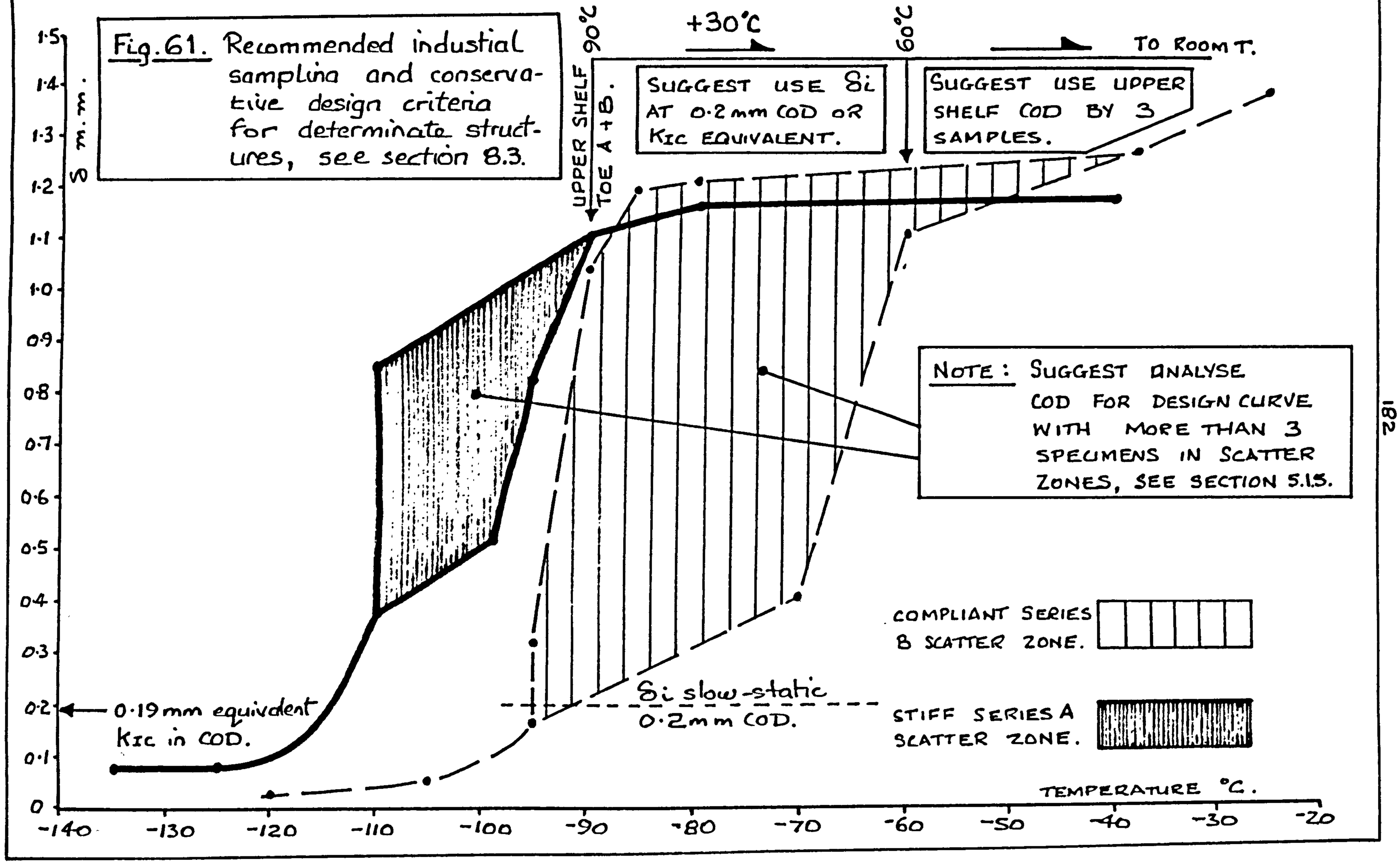

Please overlay transparency.

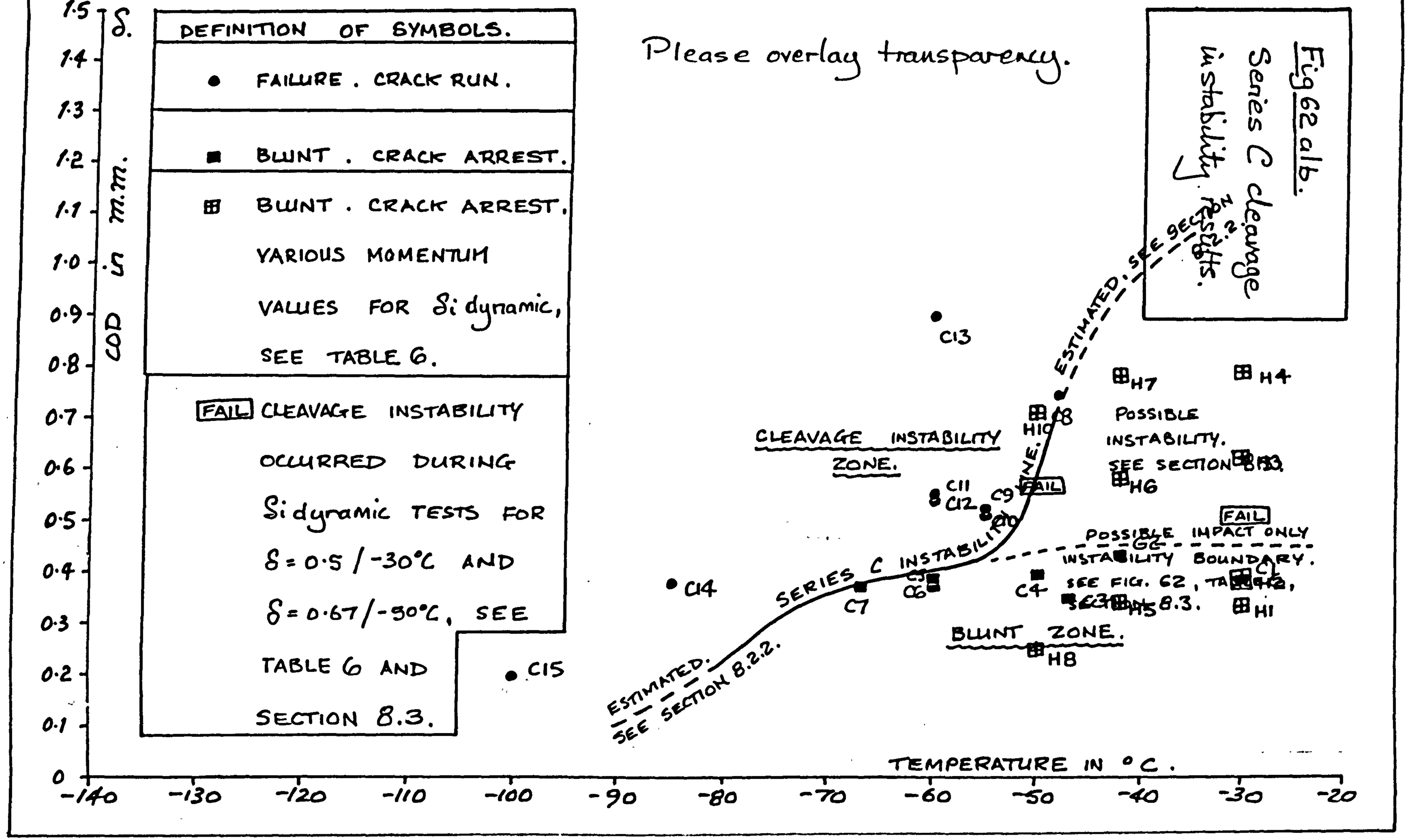

Fig.63a1b.

Series E cleavage instability

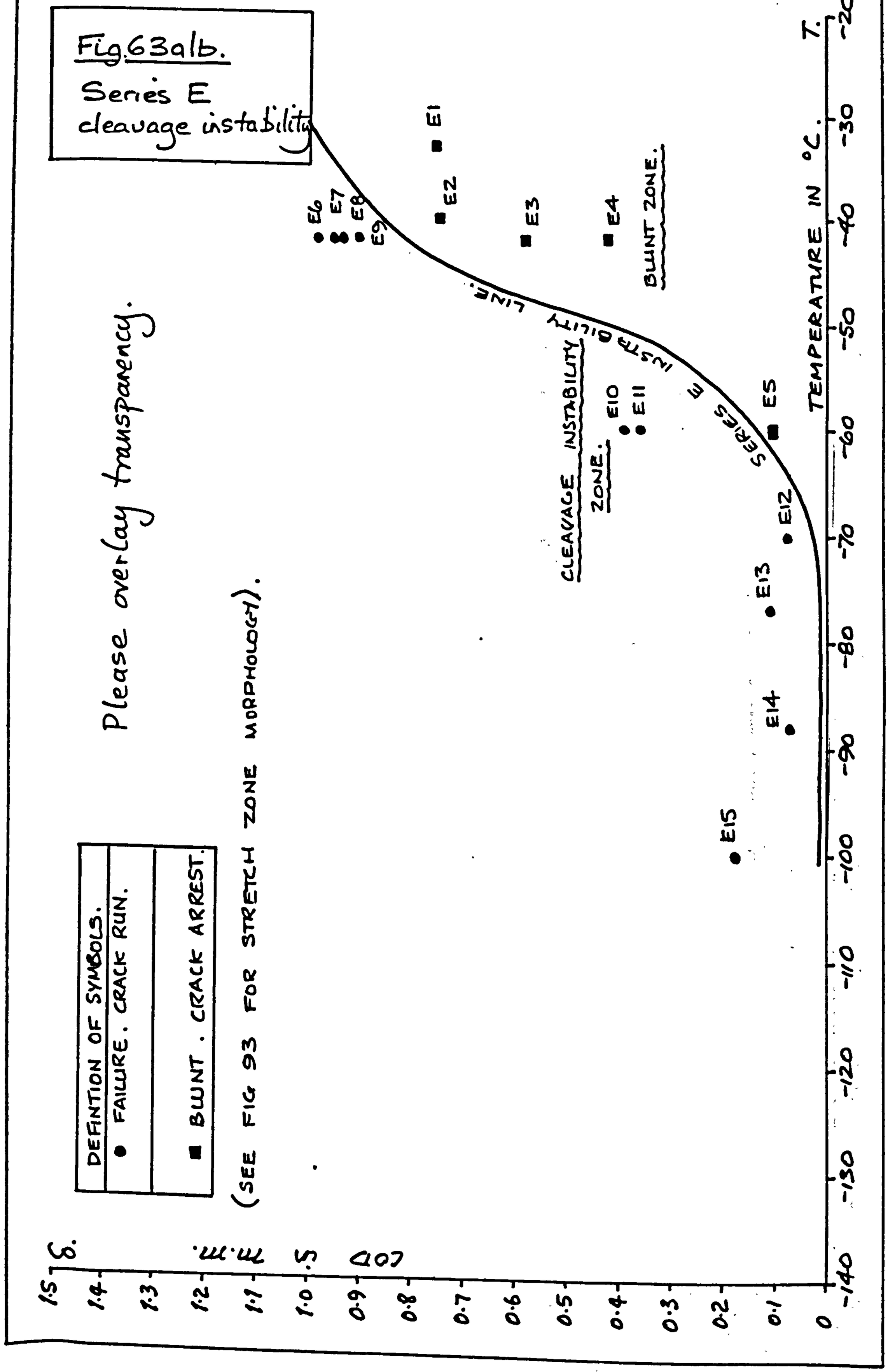

Please overlay transparency.

(SEE FIG 93 FOR STRETCH ZONE MORPHOLOGY).

DEFINTION OF SYMBOLS.
● FAILURE. CRACK RUN.
■ BLUNT. CRACK ARREST.

Please overlay transparency.

Fig. 63a1b.
Series E
cleavage instability

(SEE FIG 93 FOR STRETCH ZONE MORPHOLOGY).

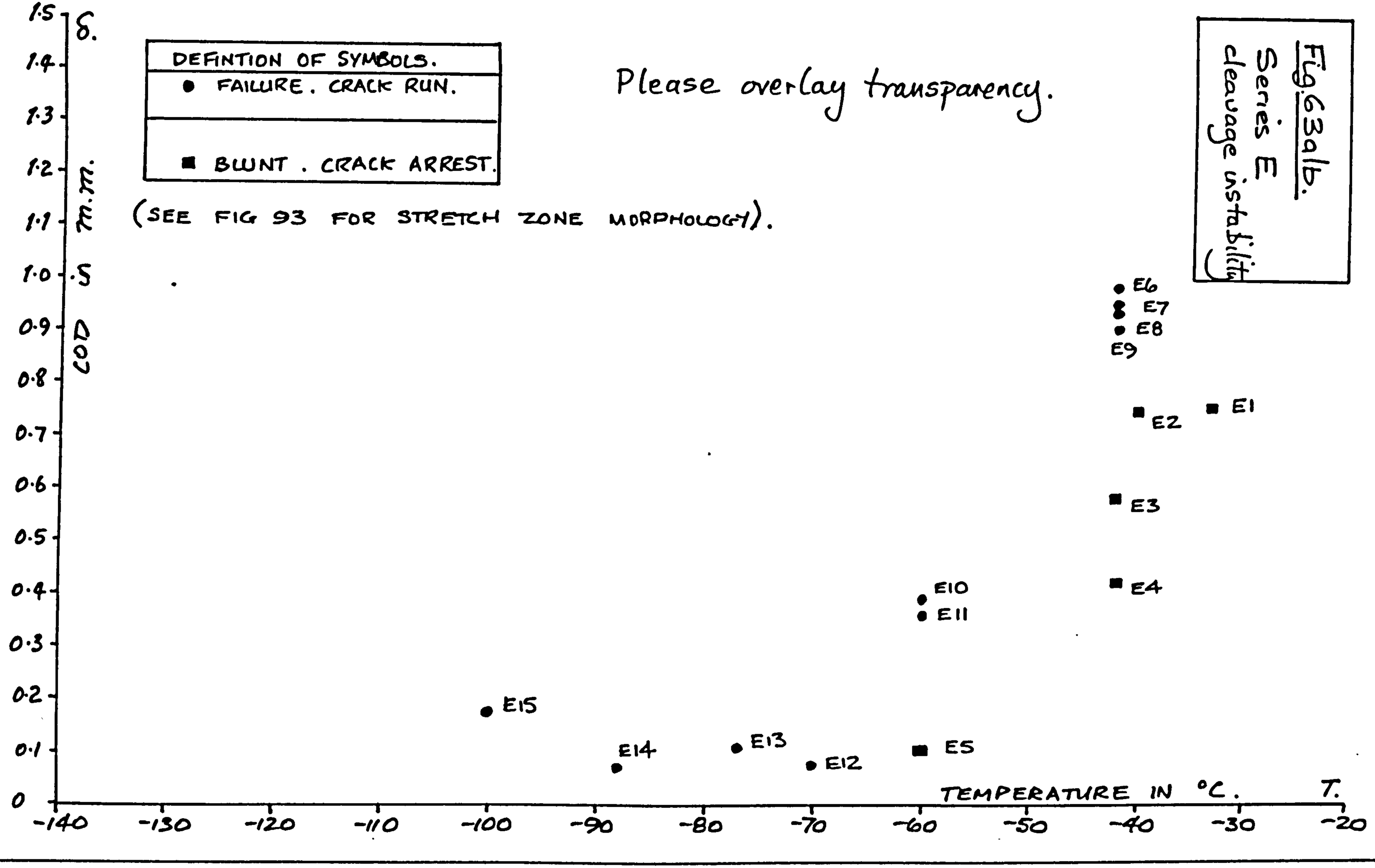

DEFINITION OF SYMBOLS.
● FAILURE. CRACK RUN.
■ BLUNT. CRACK ARREST.

(SEE FIG. 95. FOR STRETCH ZONE MORPHOLOGY).

Please overlay transparency.

Fig. 64a/b.
Series F
cleavage instab.

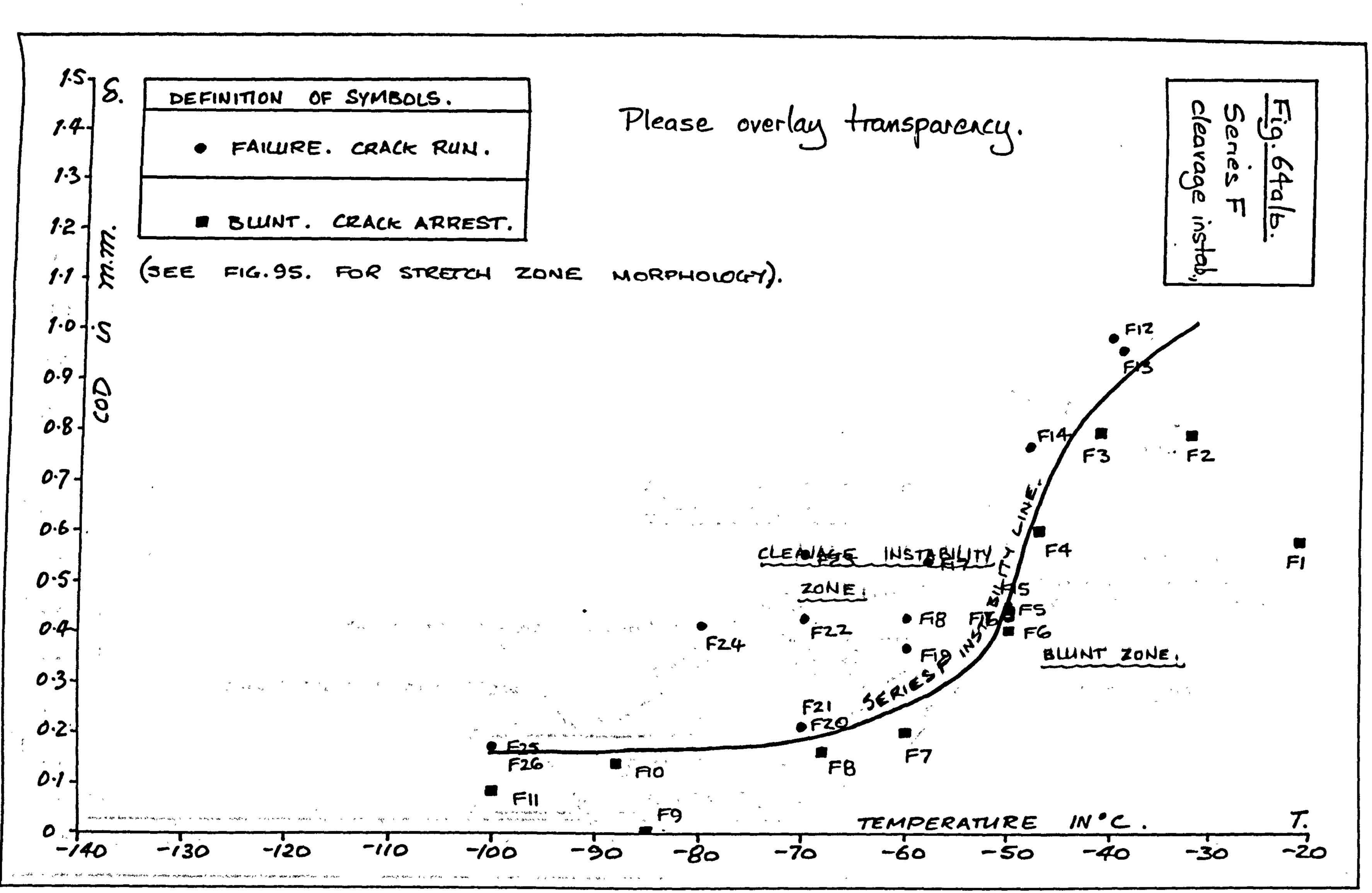

DEFINITION OF SYMBOLS.
● FAILURE. CRACK RUN.
■ BLUNT. CRACK ARREST.

Please overlay transparency.

Fig. 64a/b.
Series F
cleavage instab.

(SEE FIG. 95. FOR STRETCH ZONE MORPHOLOGY).

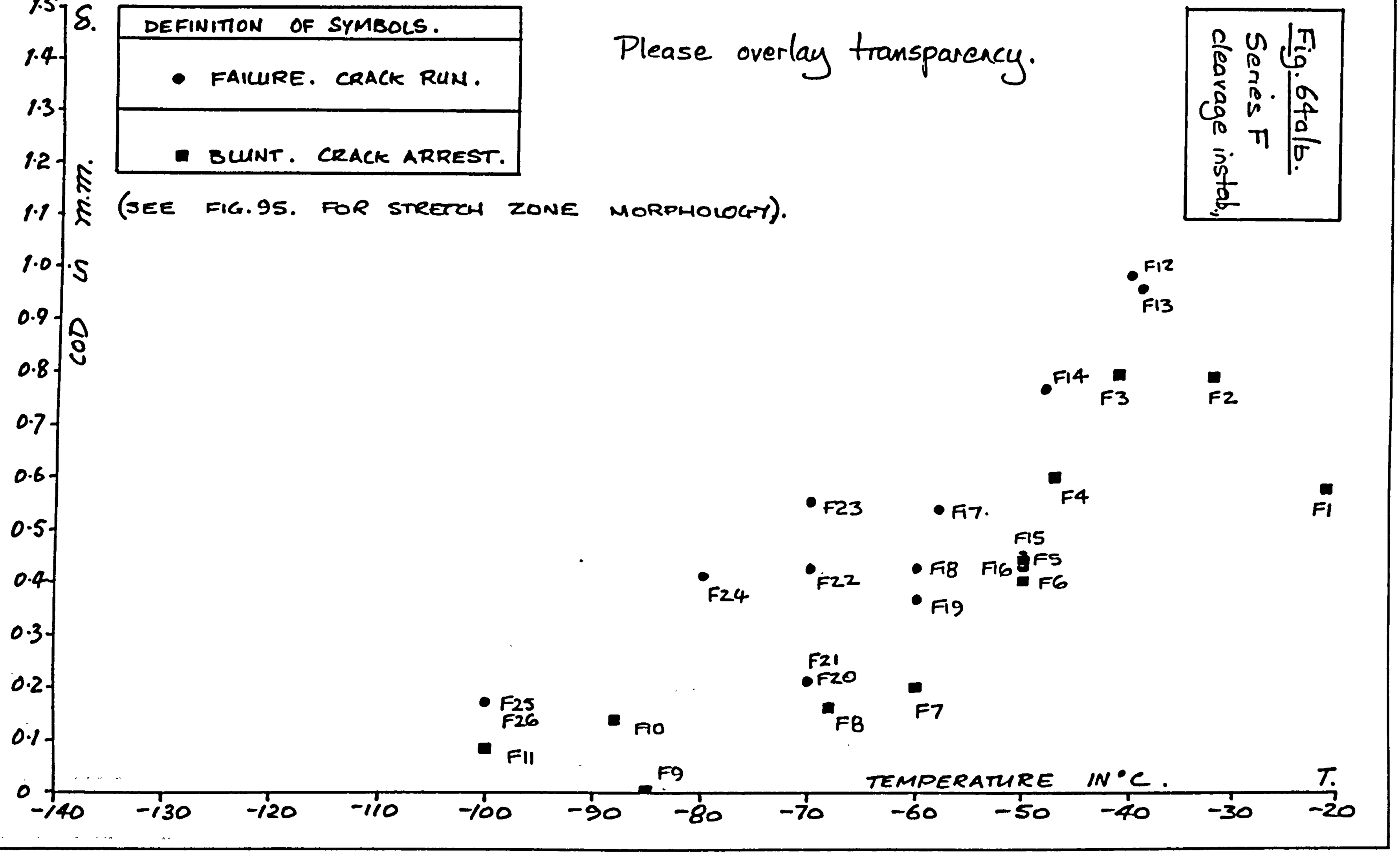

Fig.65. Dynamic impact cleavage instability transitions of series C, E and F results, also showing corresponding figures and tables relevant to resulting data.

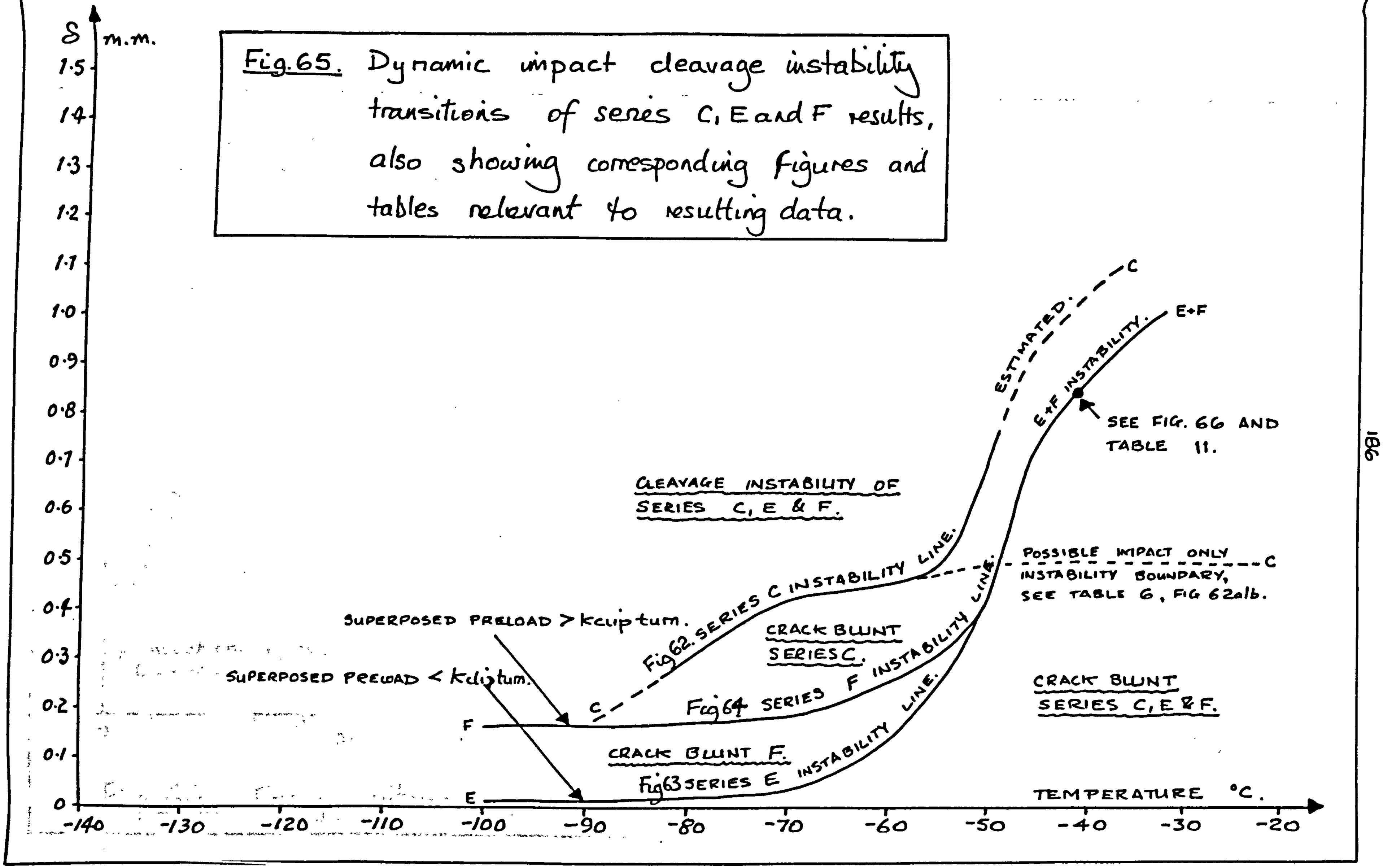

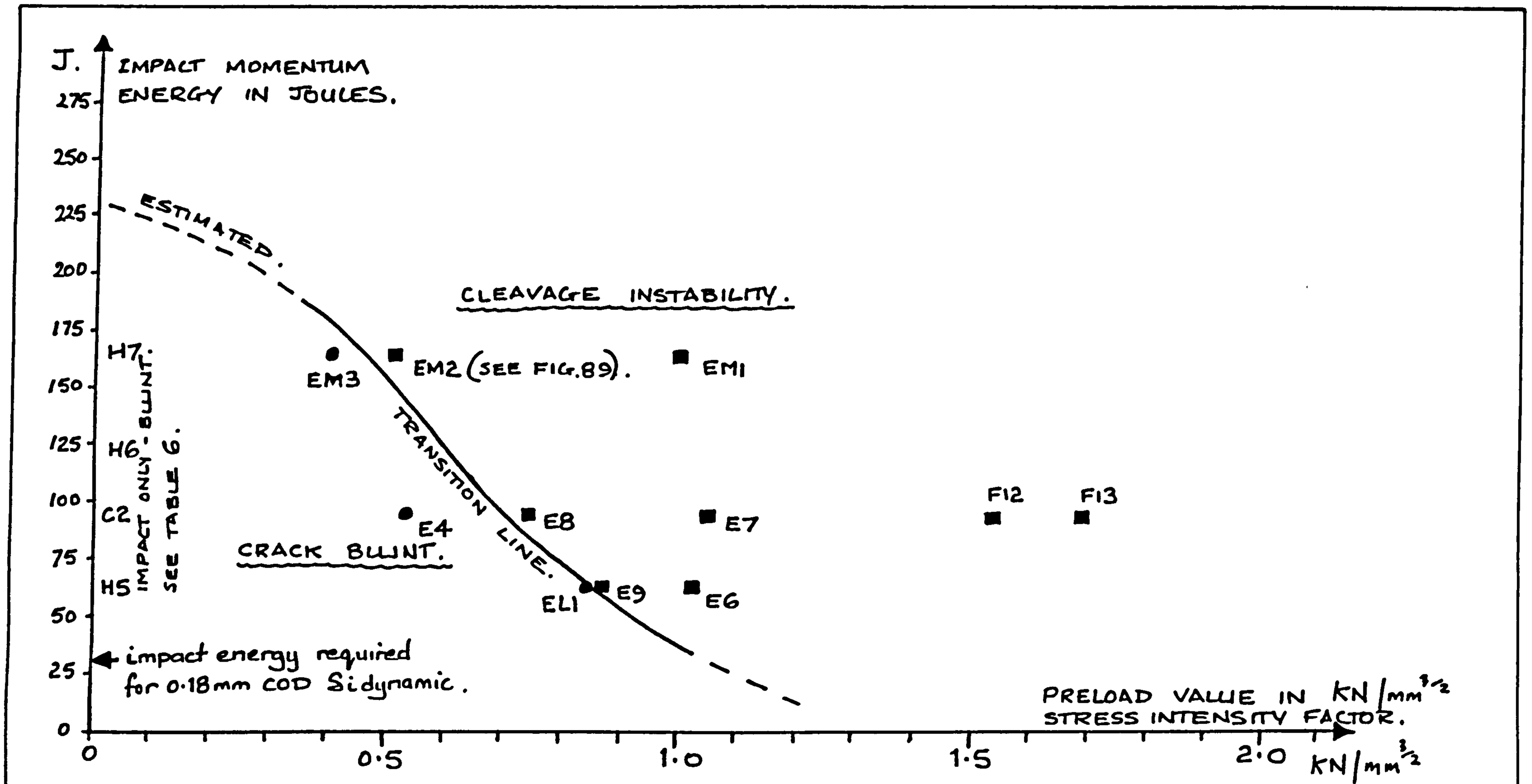

Fig.66. Energy criteria dynamic and superposed compliant loading - See table 11.

Please overlay top transparency for δ_i slow-static projection.

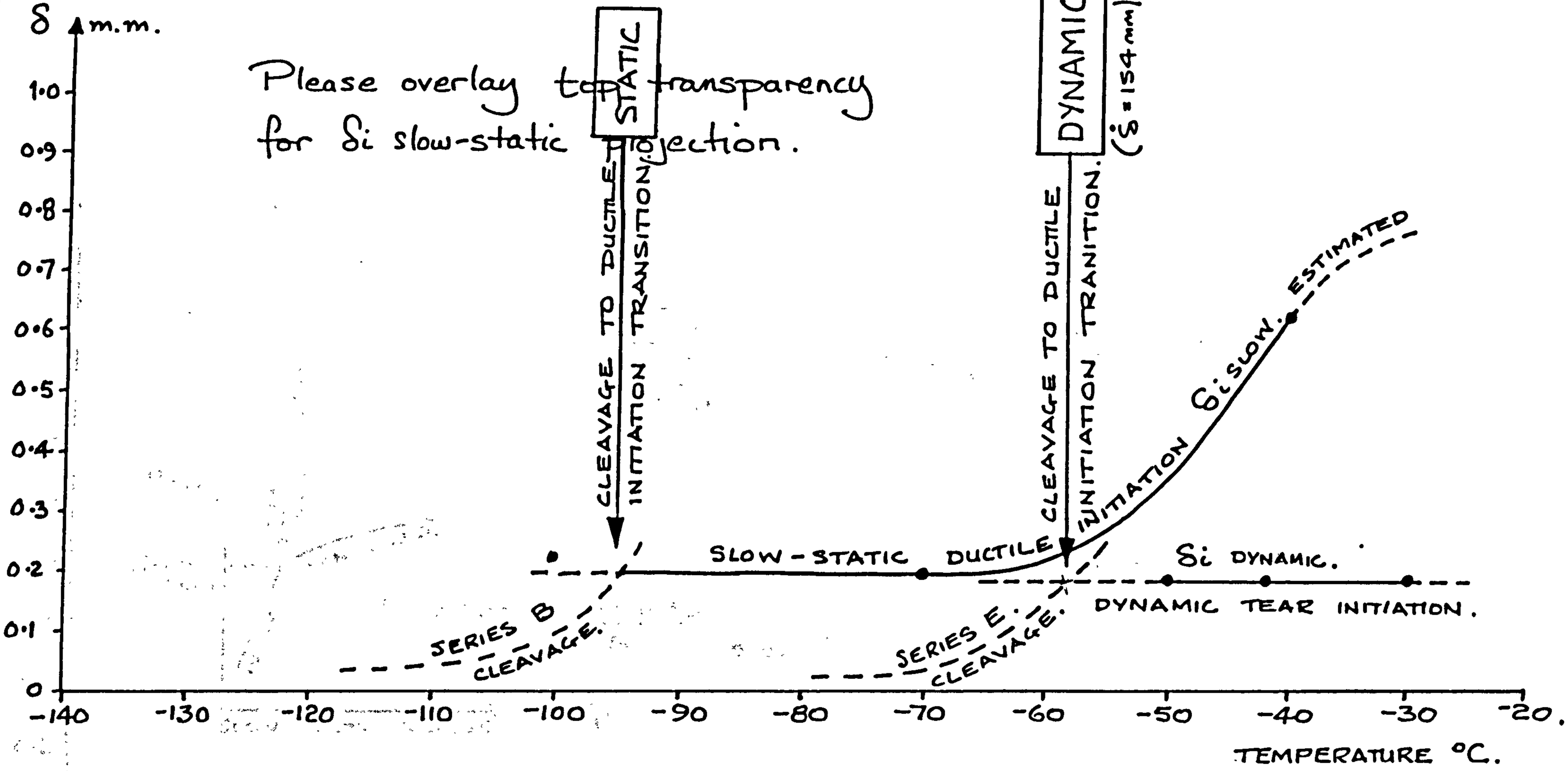

Fig. 67 a1b. Dynamic and static ductile initiation δ_i curves and dynamic and static cleavage to ductile initiation transitions.

Please overlay top transparency for δ_i slow-static projection.

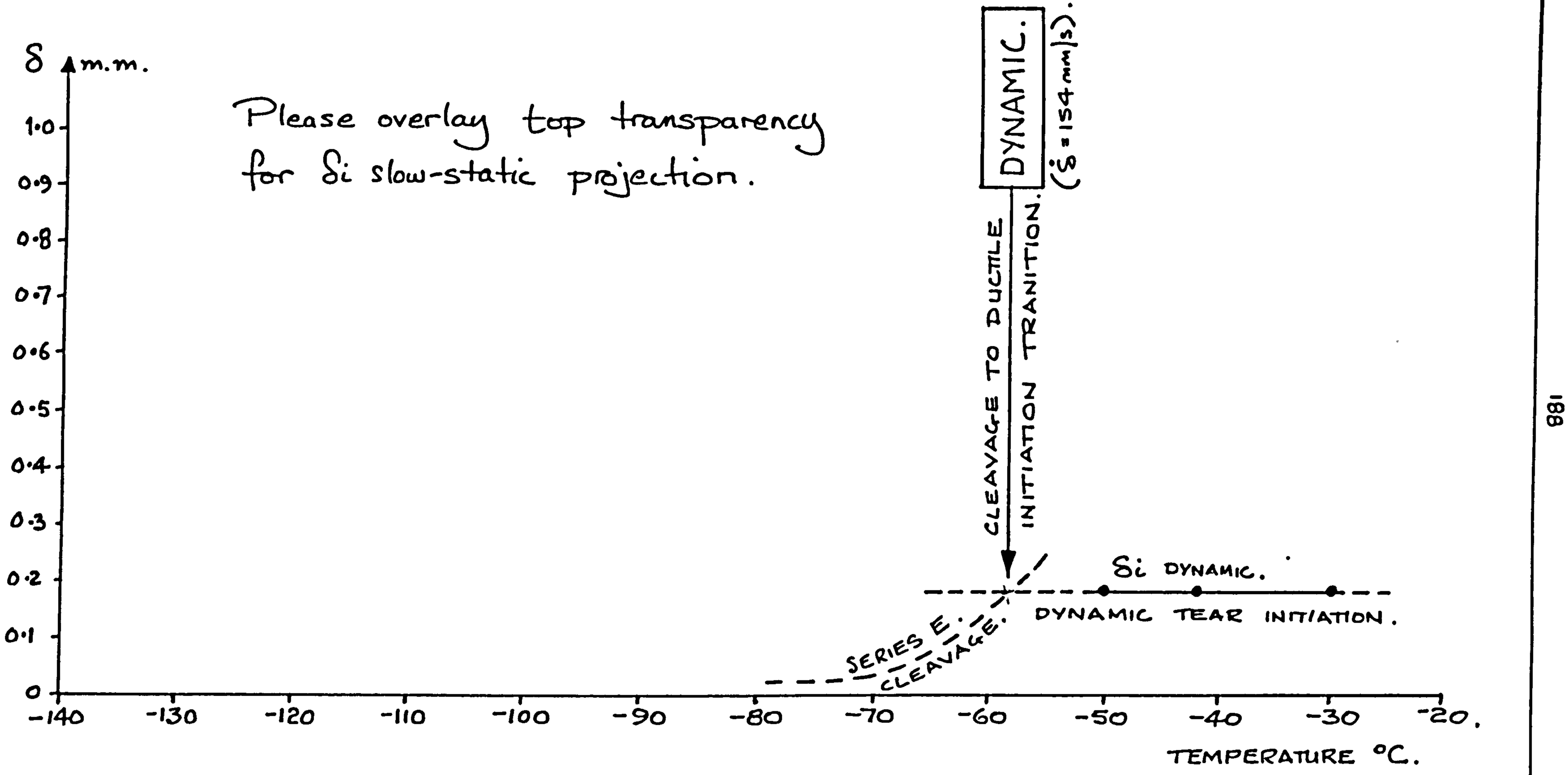

Fig. 67 a1b. Dynamic and static ductile initiation δ_i curves and dynamic and static cleavage to ductile initiation transitions.

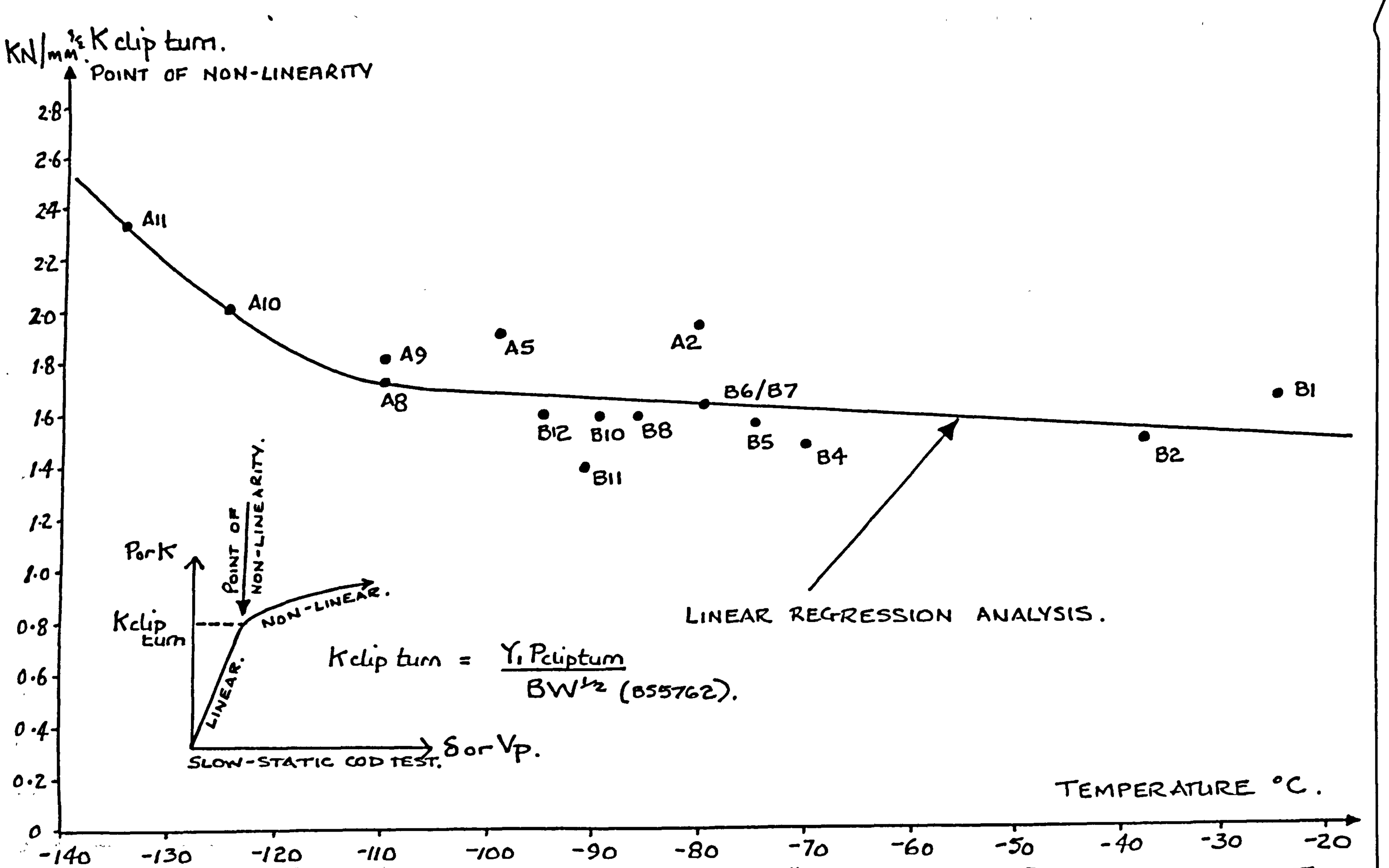

Fig.68. Point of non-linearity - "K clip tum" - in terms of average K vs T.

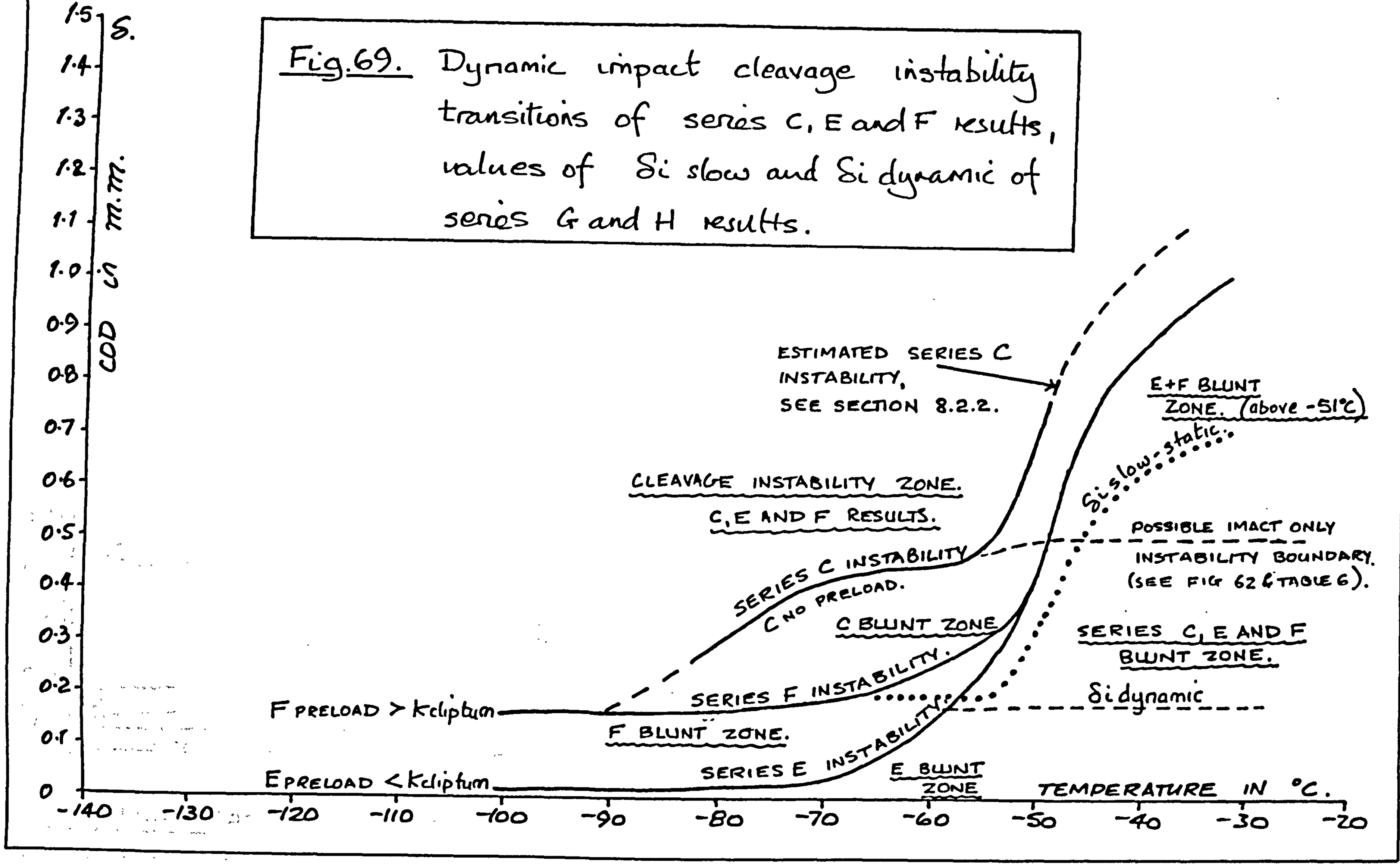

Fig.69. Dynamic impact cleavage instability transitions of series C, E and F results, values of δi slow and δi dynamic of series G and H results.

* Please overlay transparency.

δ m.m.

1.4
1.4
1.3
1.2
1.1
1.0
0.9
0.8
0.7
0.6
0.5
0.4
0.3
0.2
0.1
0

* K_{Ic} & K_{Id} ESTIMATED FROM ENGINEERING SLOW-STATIC STRAIN.

A SLOW-STATIC STIFF.

B SLOW-STATIC COMPLIANT.

C IMPACT ONLY.

E IMPACT + LOW COMPLIANT PRELOAD.

F IMPACT + HIGH COMPLIANT PRELOAD.

G δ_i SLOW-STATIC.

H δ_i DYNAMIC.

(SEE SECTION 7.3).

TOE

+30°C

A+B

UPPER SHELF COD δm.

A

-60°C

$\delta_{max\ load}$ -60°C

$\delta_{max\ load}$ -30°C

B

UPPER SHELF TURN + TOE REGION.

FROM UPPER SHELF

FOR SAFE DESIGN OF PRIVATE STRUCTURES, < (TOE TEMPERATURES

K_{Ic} VALUE OR COROLLARY

FOR TEMPERATURES > (TOE +30°C), USE δ_i OR COD.

COD IN TERMS OF δ_i USE UPPER SHELF

SEE SECTION 7.3. AND Fig. VALUE.

E+F

C

δ_i instability

δ_i +30°C

δ_i TOE, FOR DETERMINATION OF +30°C, USE

Fig. possible instability.

C

G

F

δ_i SLOW-STATIC δ 2mm COD.

δ_i DYNAMIC.

H

$\delta = 2E\delta_{ys}$.

K_{Ic} BS4360 50D (-25°C ≥175 $MN/m^{3/2}$)

δ_i instability

E

* ESTIMATED EQUIVALENT COD TO K_{Ic} FROM (-80°C ≥120 $MN/m^{3/2}$).

K_{Id}^2

* ESTIMATED EQUIVALENT COD TO K_{Id} FROM $\delta = \frac{1}{30}E\delta_{yd} - \frac{1}{20}K_{Id}^2$ (ASSUMING $\delta_{yd} \triangleq 2 \times \delta_{ys}$).

-140 -130 -120 -110 -100 -90 -80 -70 -60 -50 -40 -30 -20

-100°C

ESTIMATED STRUCT. STEEL (TURNER, REF. 115).

Fig. 70a1b. Combined impact and slow-static COD mean line transitions.

* Please overlay transparency.

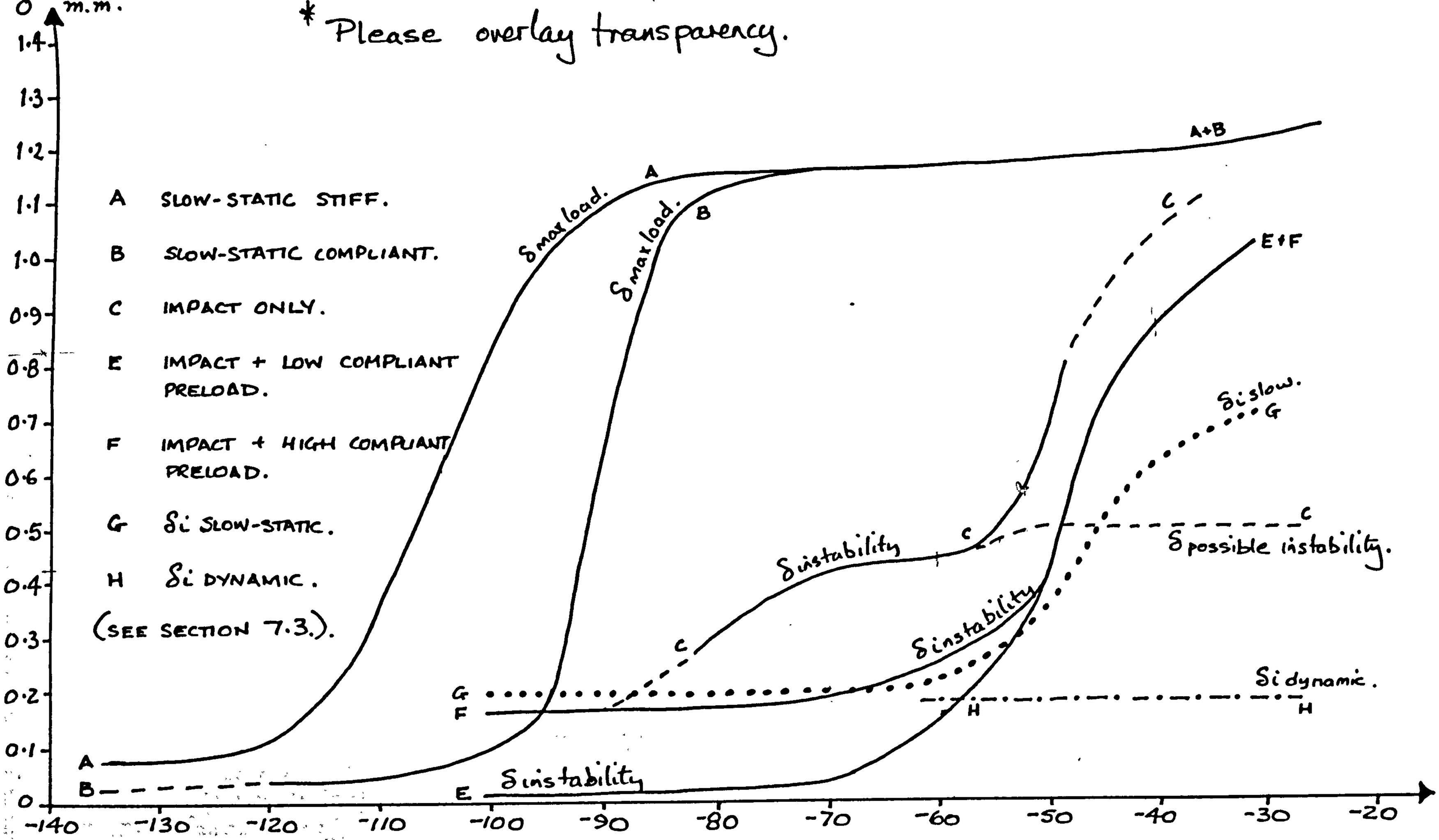

Fig. 70a1b. Combined impact and slow-static COD mean line transitions.

Fig. 71a1b. Combined impact and slow-static COD mean line transitions, with notes of behaviour during compliant, preload and dynamic straining rate changes. (Please overlay transparency).

δ m.m.

1.5 1.4 1.3 1.2 1.1 1.0 0.9 0.8 0.7 0.6 0.5 0.4 0.3 0.2 0.1 0

-140 -130 -120 -110 -100 -90 -80 -70 -60 -50 -40 -30 -20 -10 TEMPERATURE °C.

→ arrows indicate behavioural change due to attenuation of given operator - i.e. strain rate.

A+B plastic collapse.

plastic collapse becoming dominant. A+B

C

C

increased instantaneous stored strain energy.

E+F

E+F

A+B To C, E+F

increase in strain rate.

A

increasing compliance, and S.S.E.

SERIES: increasing stability

SERIES: increasing toughness

IMPACT ONLY DYNAMIC

increasing stored strain energy

d-b trans of initiation.

G

F

IMPACT PLUS HIGH STATIC PRELOAD

SERIES: SLOW STATIC

G

H

DYNAMIC δi

δi slow

δi dyn

Lower strain rate.

impact only - c.- possible crack tip microstructural c instability (?), preventing plastic zone.

cleavage at lower shelf of A&B.

increased comp/s.s.e.

A

B

blunting of crack tip

E

IMPACE PLUS LOW STATIC PRELOAD

d-b trans of initiation

Fig. 72. Evaluation of crack arrest temperature for size of specimen and available external energy. Evaluated as -24°C.

Preload values above and below Kdip turn, E and F resulting crack lengths are shown.

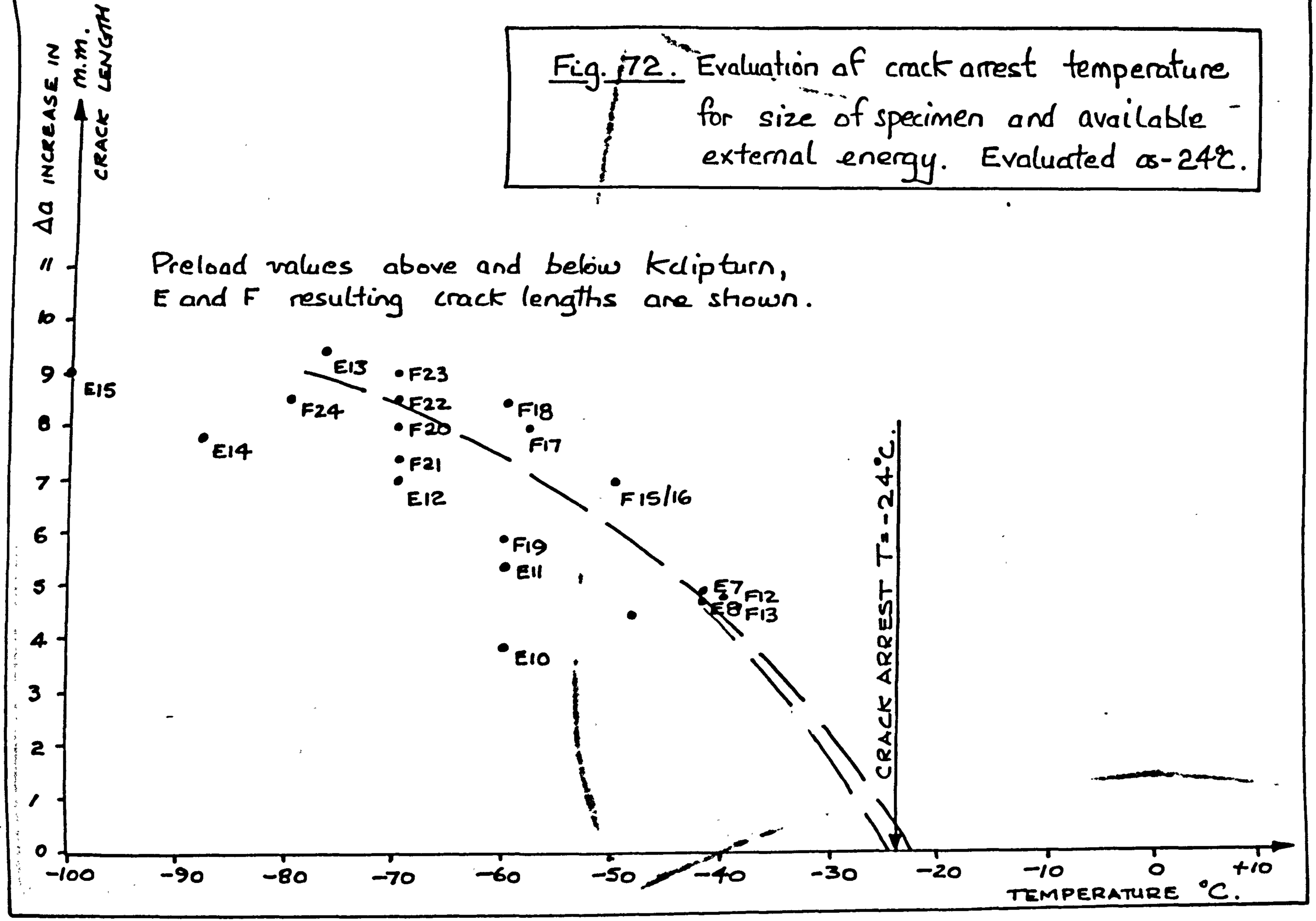

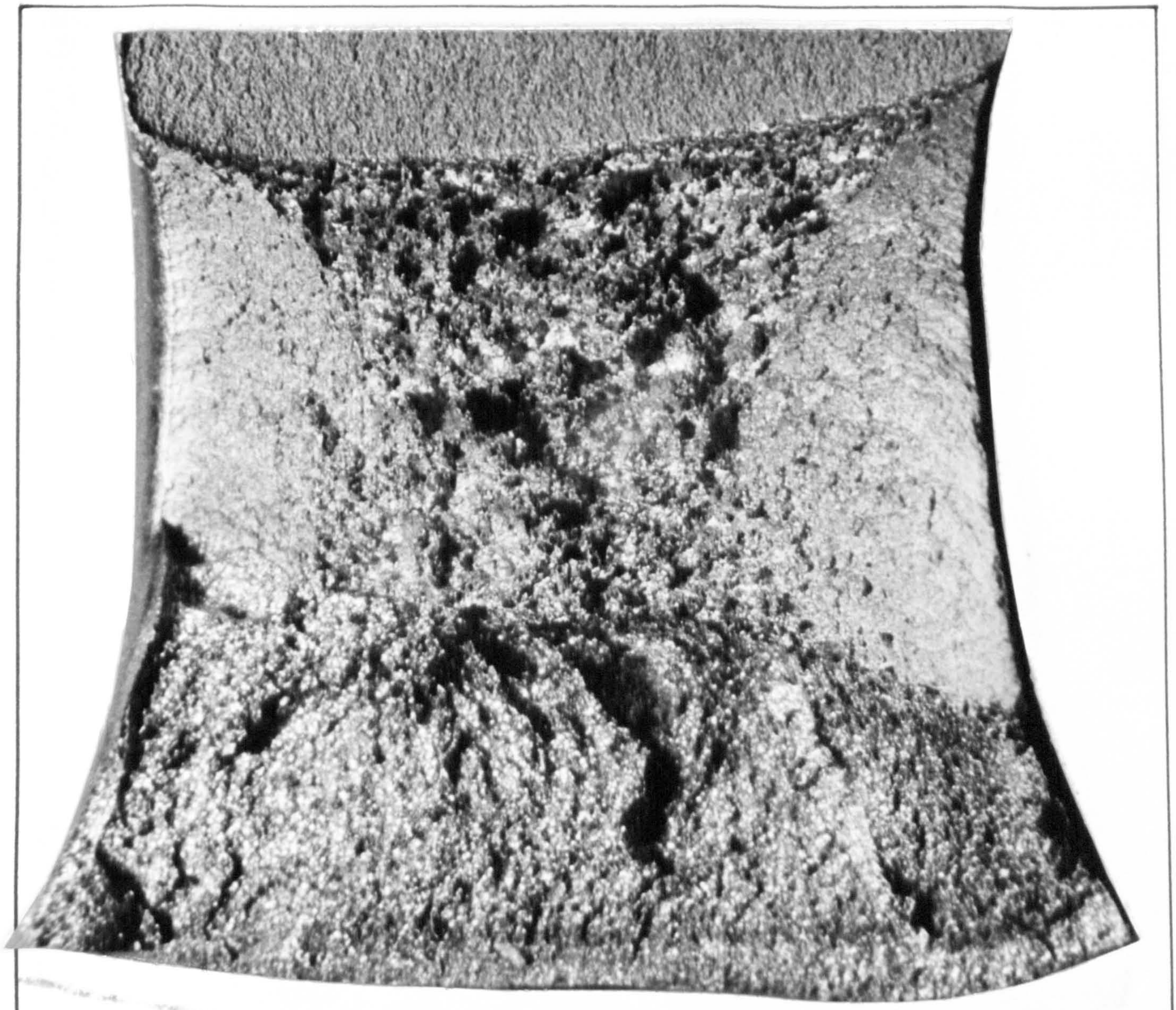

Fig. 73. Slow-static COD stiff test A1.
Photo x 11·25. $\delta_{max.}$ = 1·169 m.m. T = - 40°C.

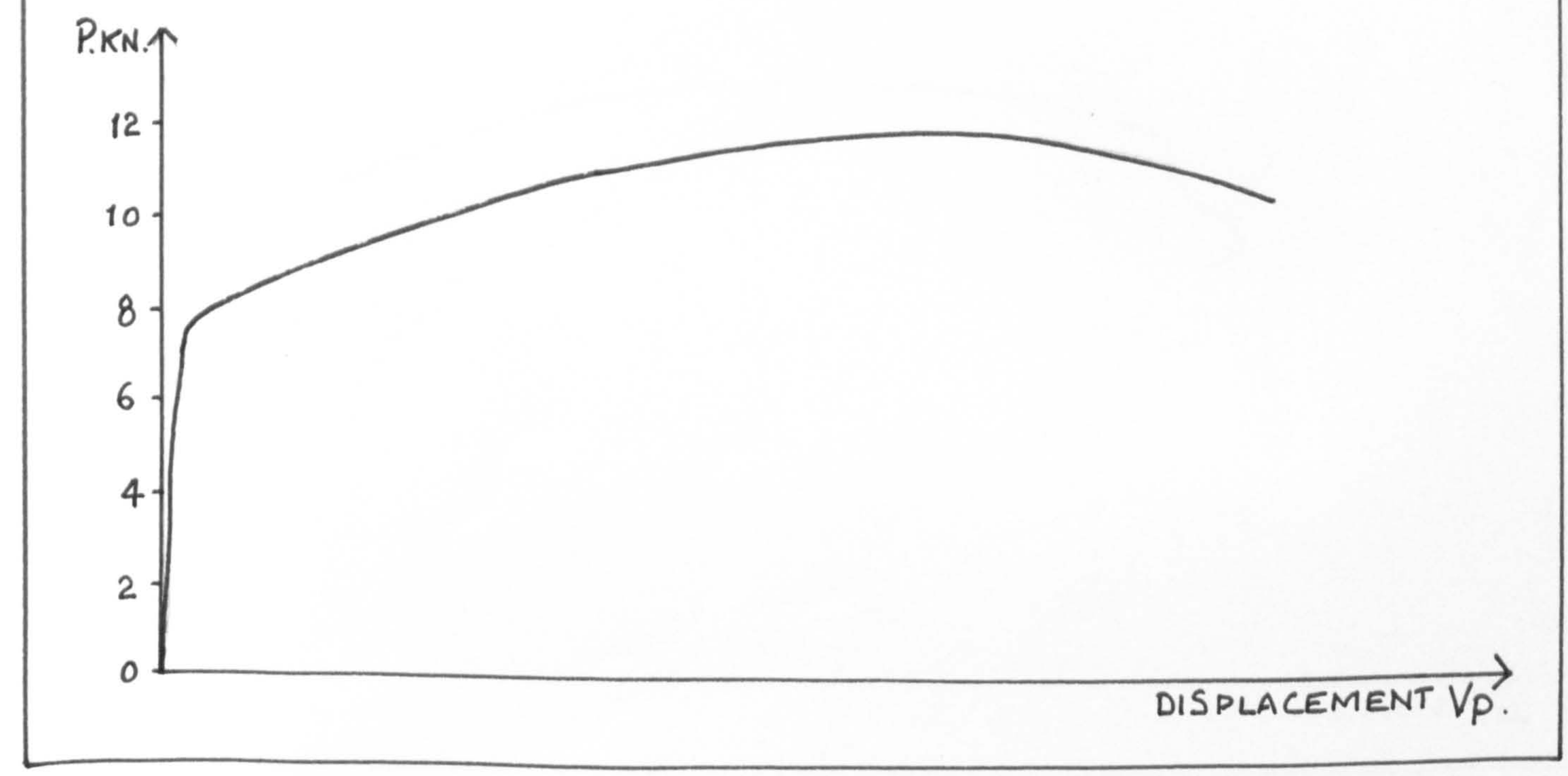

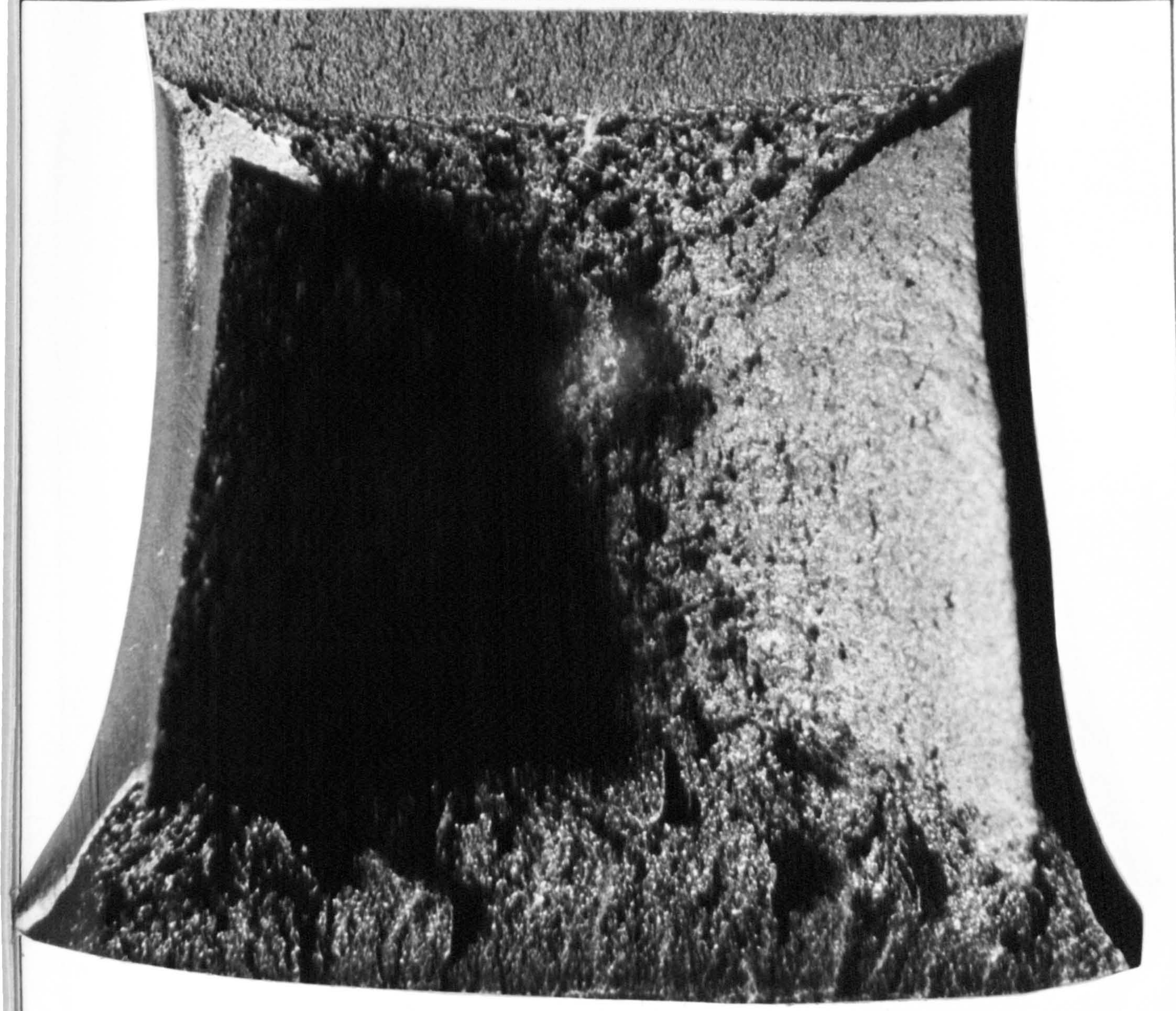

Fig. 74. Slow-static COD stiff test A2.
Photo x 11·25. $\delta_{max.}$ = 1·159 m.m. T = -80°C.

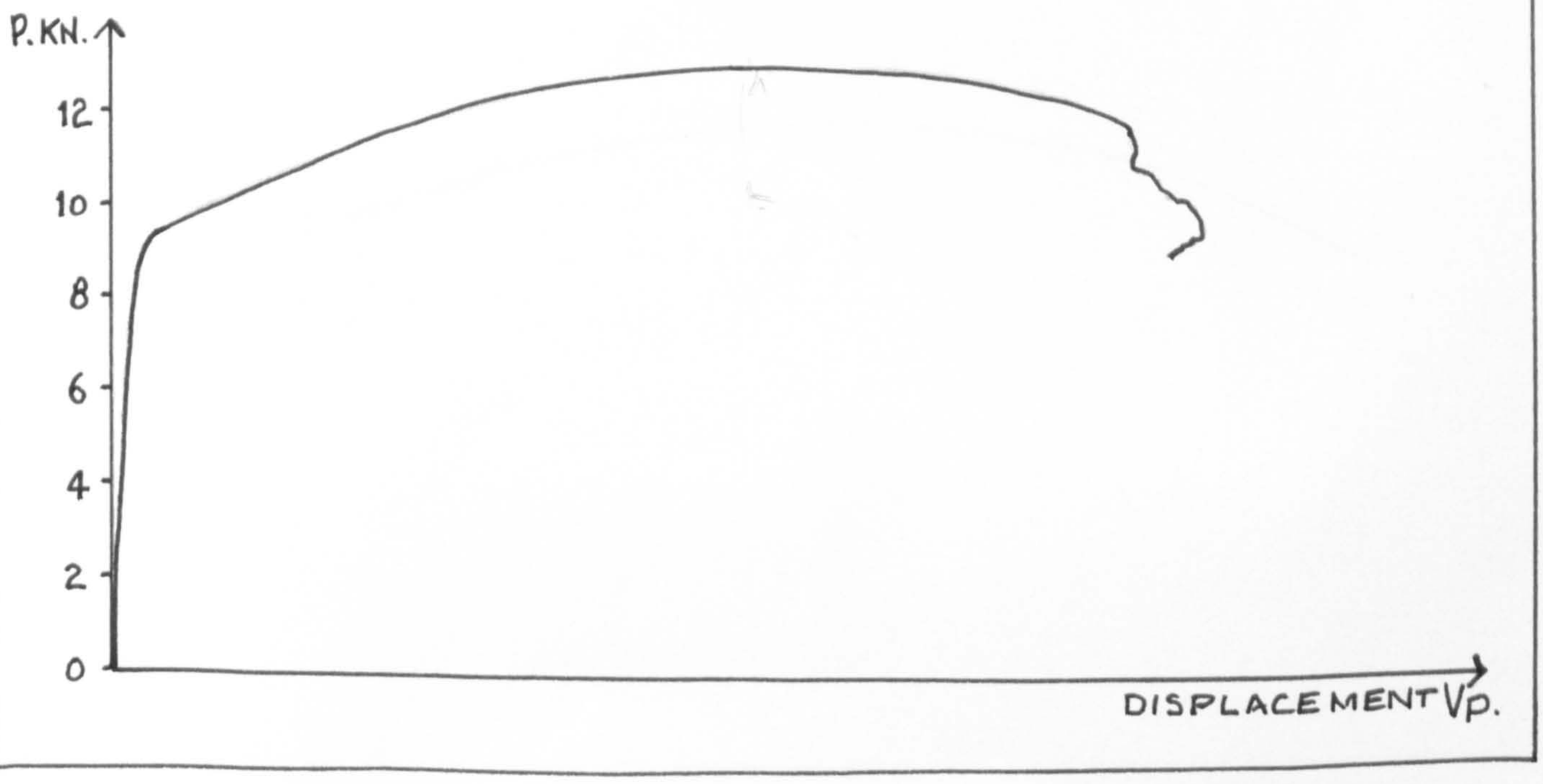

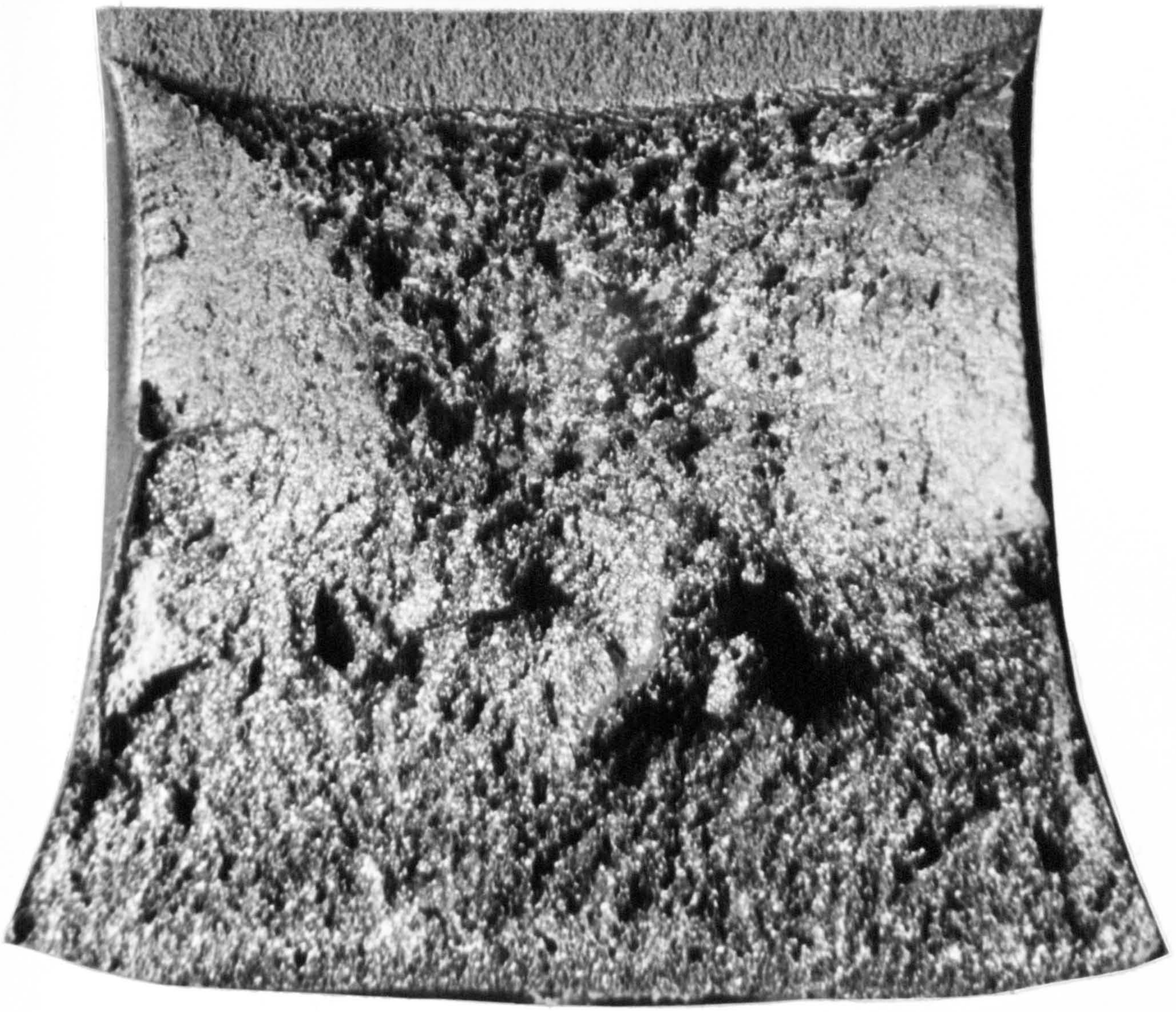

Fig. 75. Slow-static COD stiff test A3.
Photo x 11·25. $\delta_{max.}$ = 1·099 m.m. T = -90°C.

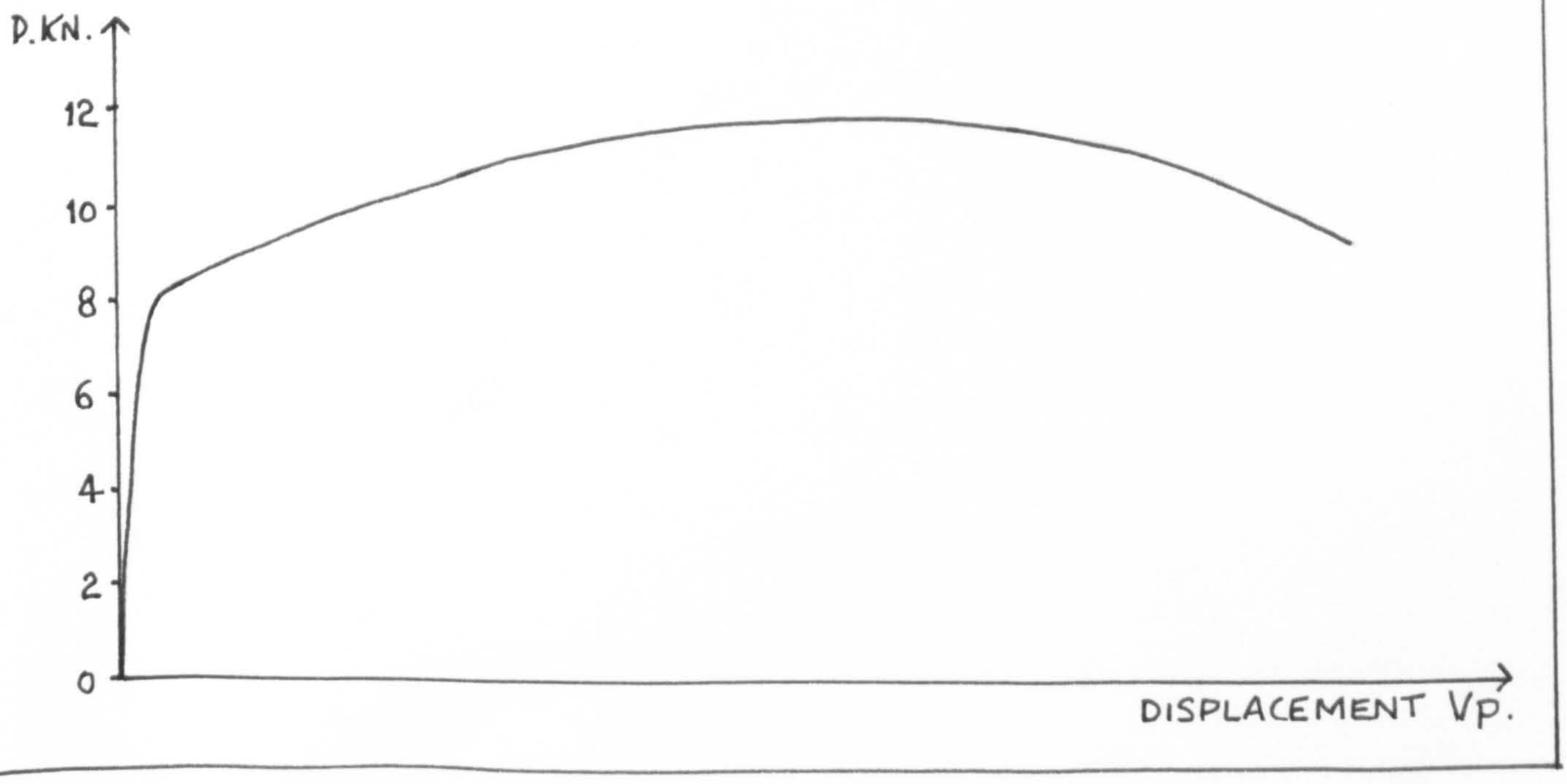

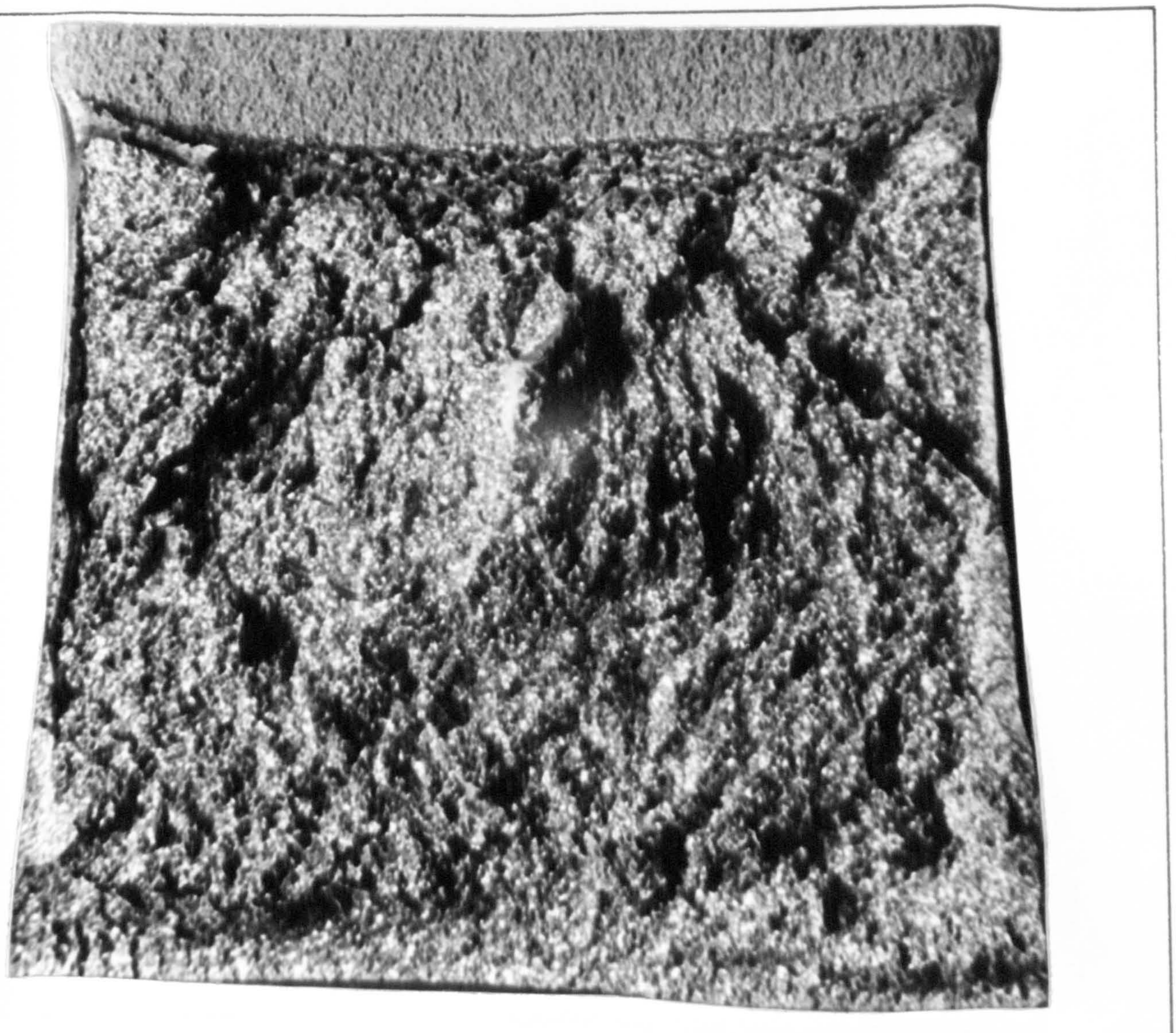

Fig.76. Slow-static COD stiff test A4.
Photo x 11·25. $\delta_{max.}$ = 0·819 m.m. T = -95°C.

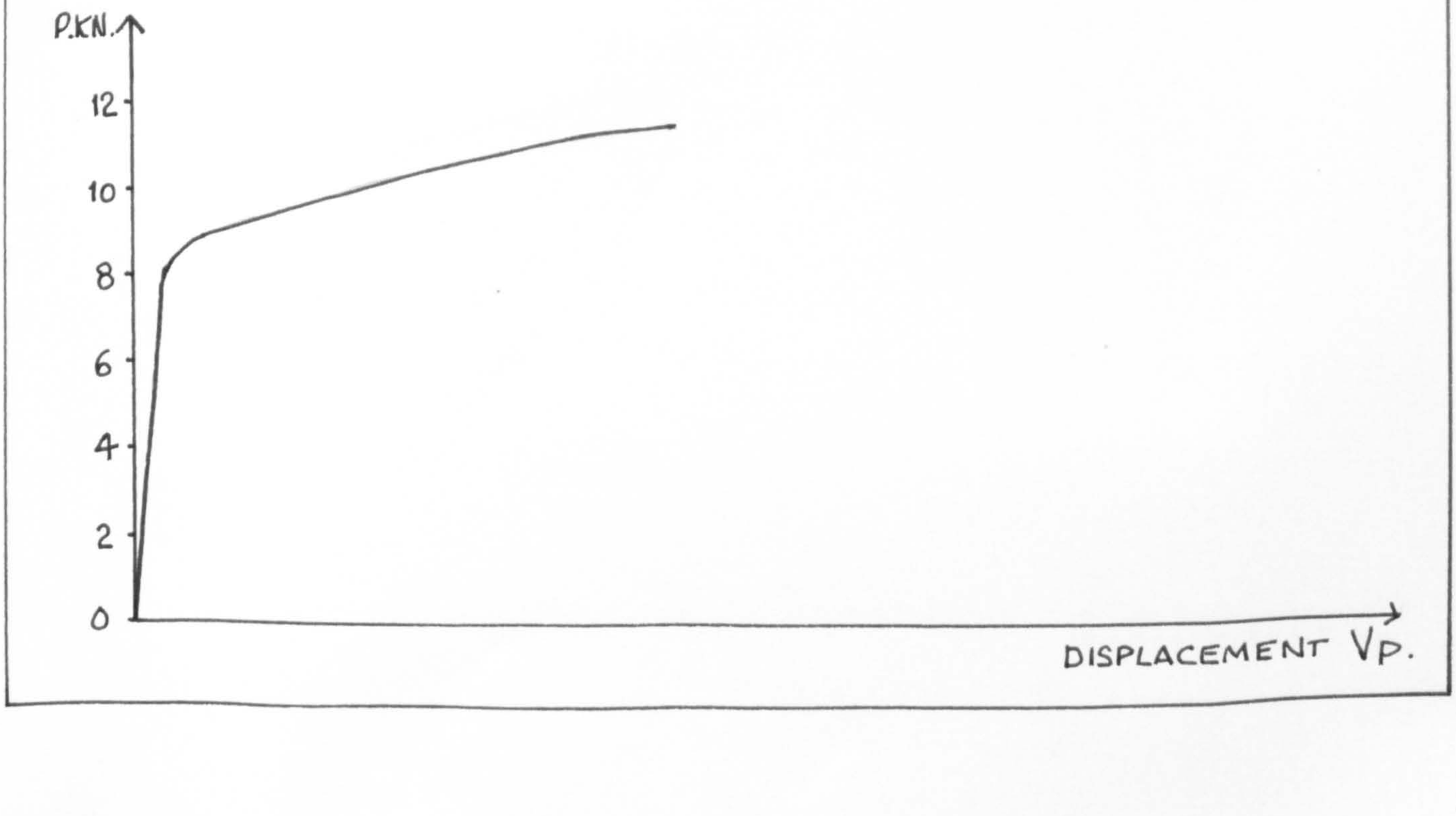

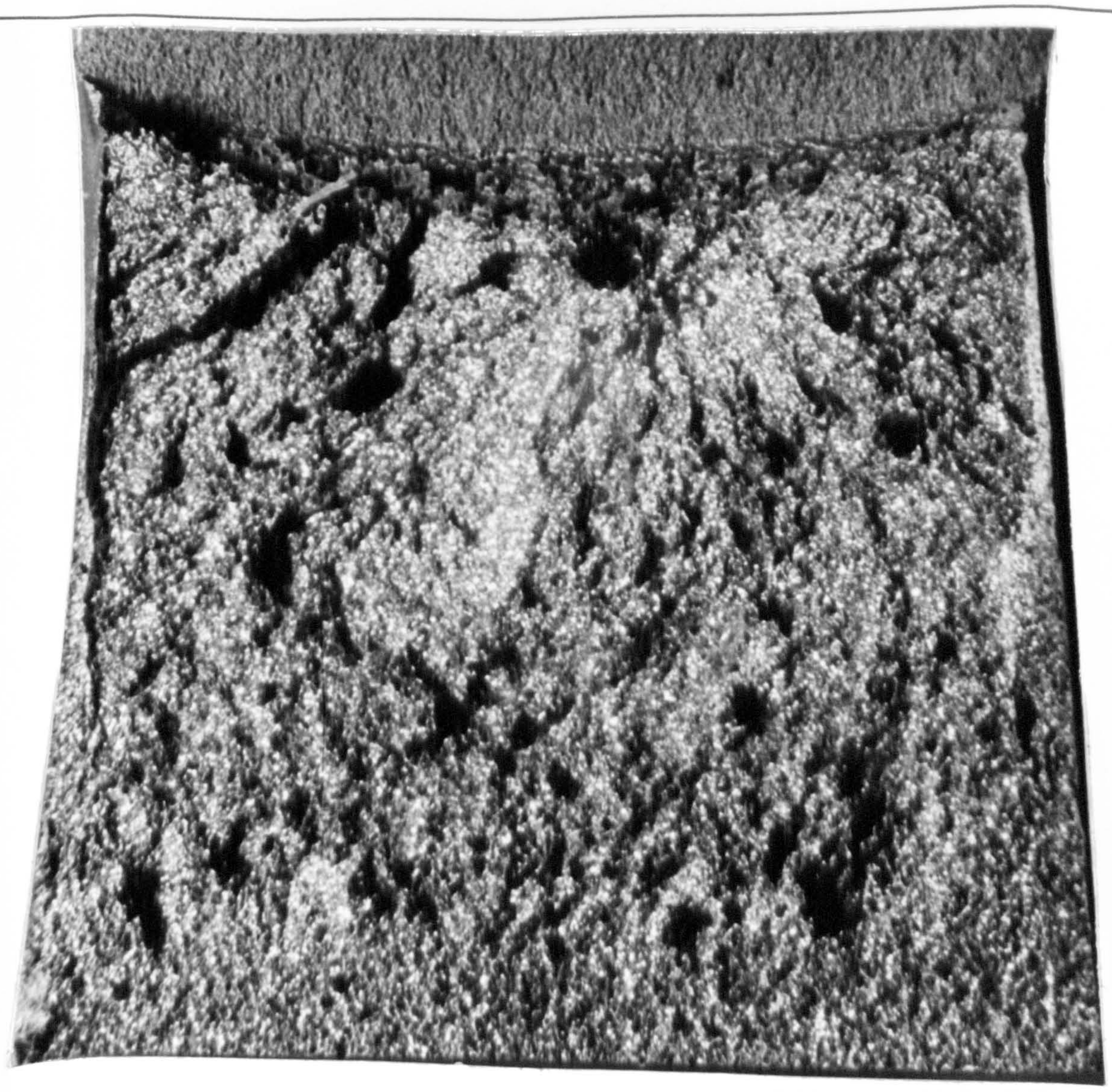

Fig.77. Slow-static COD stiff test A6.
Photo x 11·25. $\delta_{max.}$ = 0·806 m.m. T = -105°C.

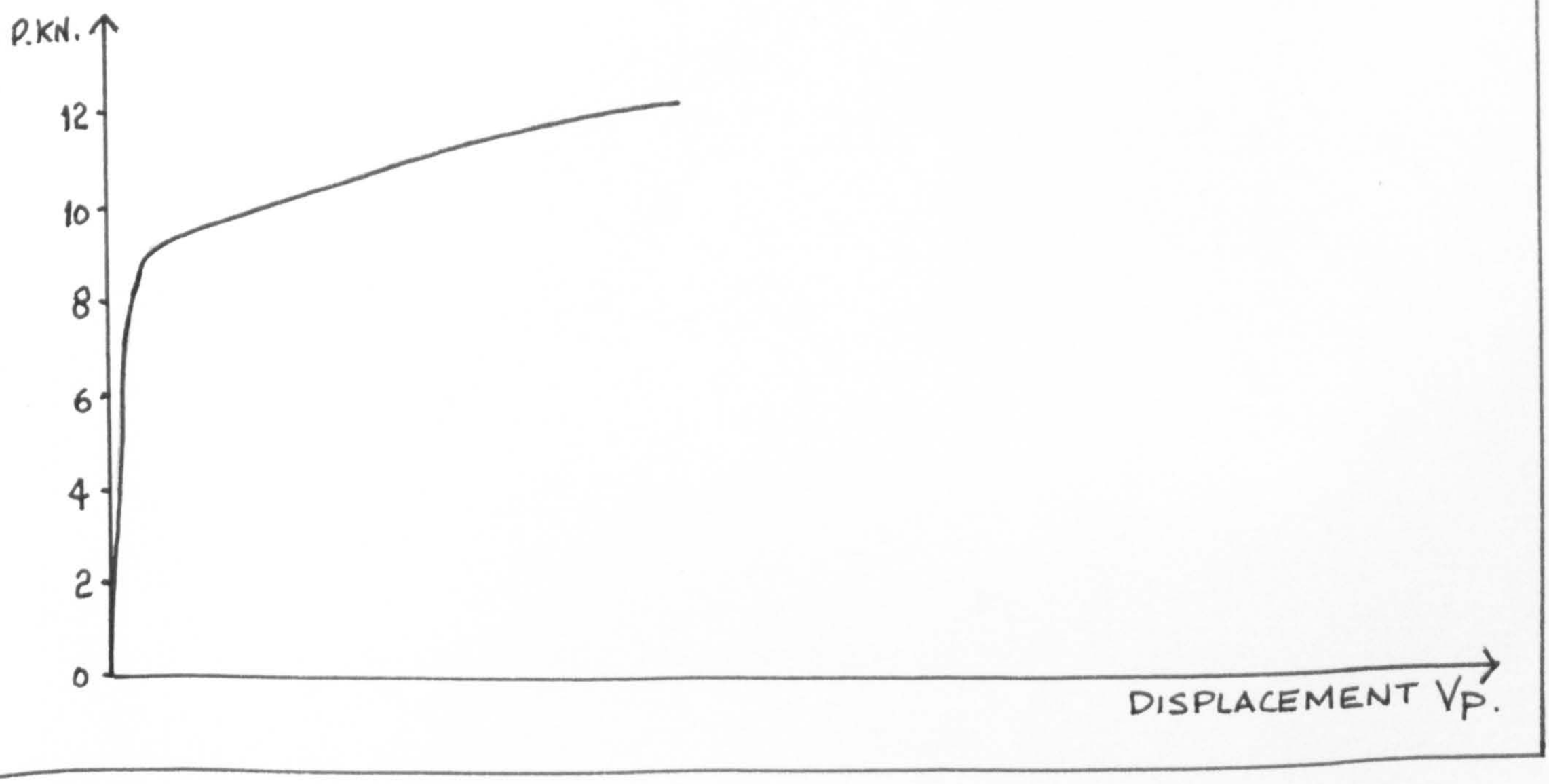

Fig.78. Slow-static COD stiff test A10.
Photo x 11·25. $\delta_{max.}$ = 0·081 m.m. T = -125 °C

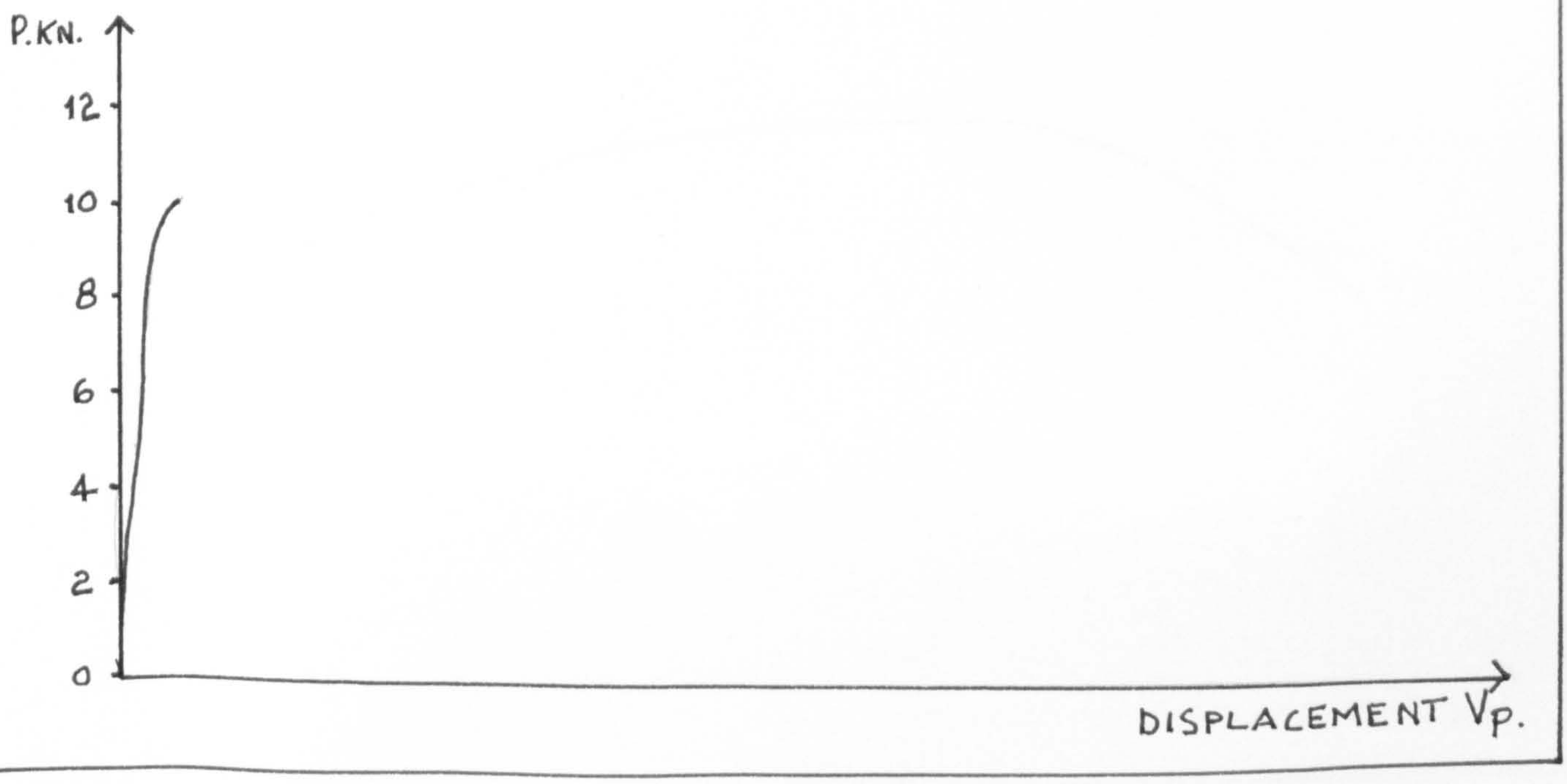

Fig.79. Slow-static COD compliant test B2.
Photo × 11·25. $\delta_{max.}$ = 1·266 m.m. T = −38°C.

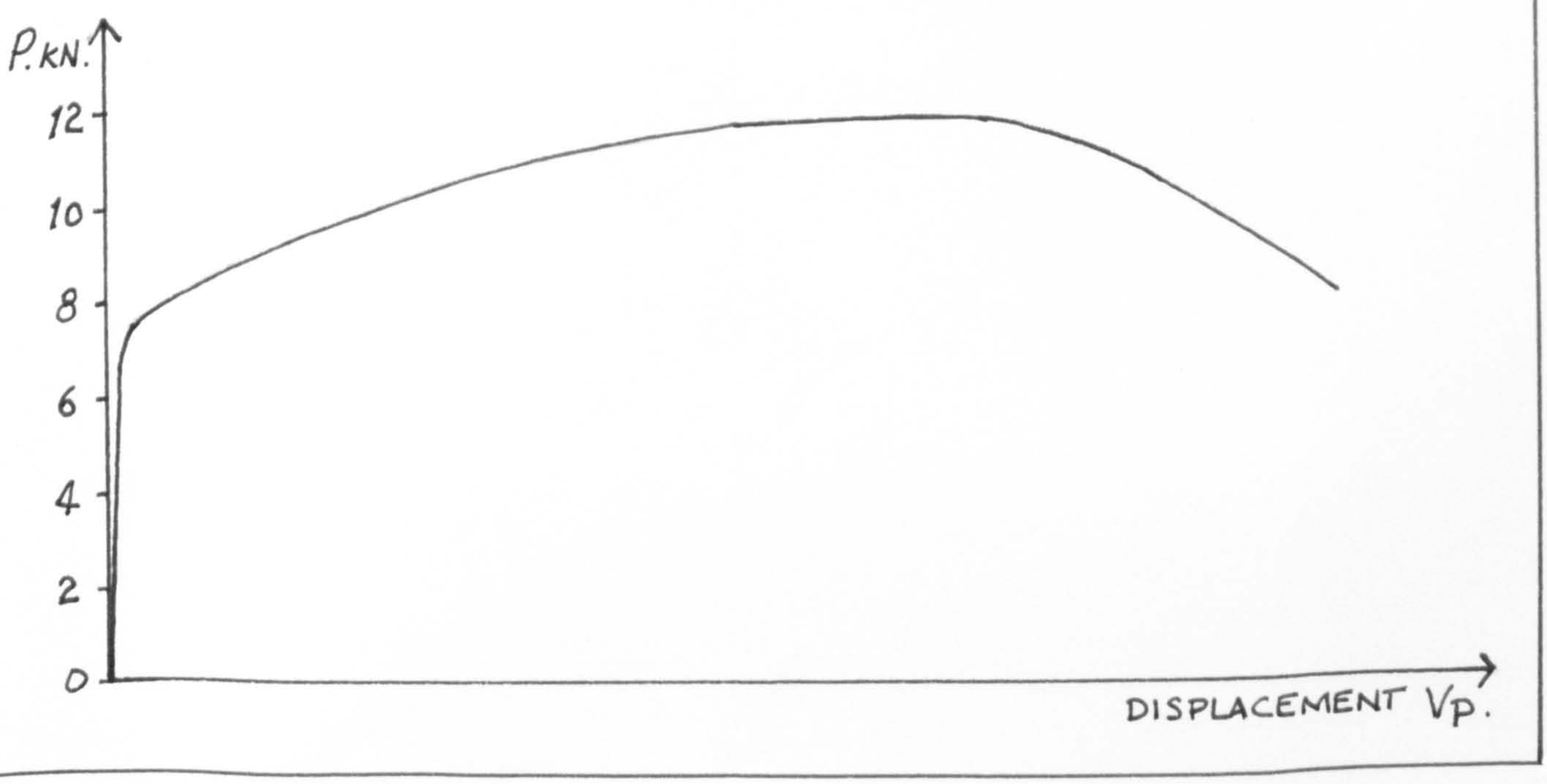

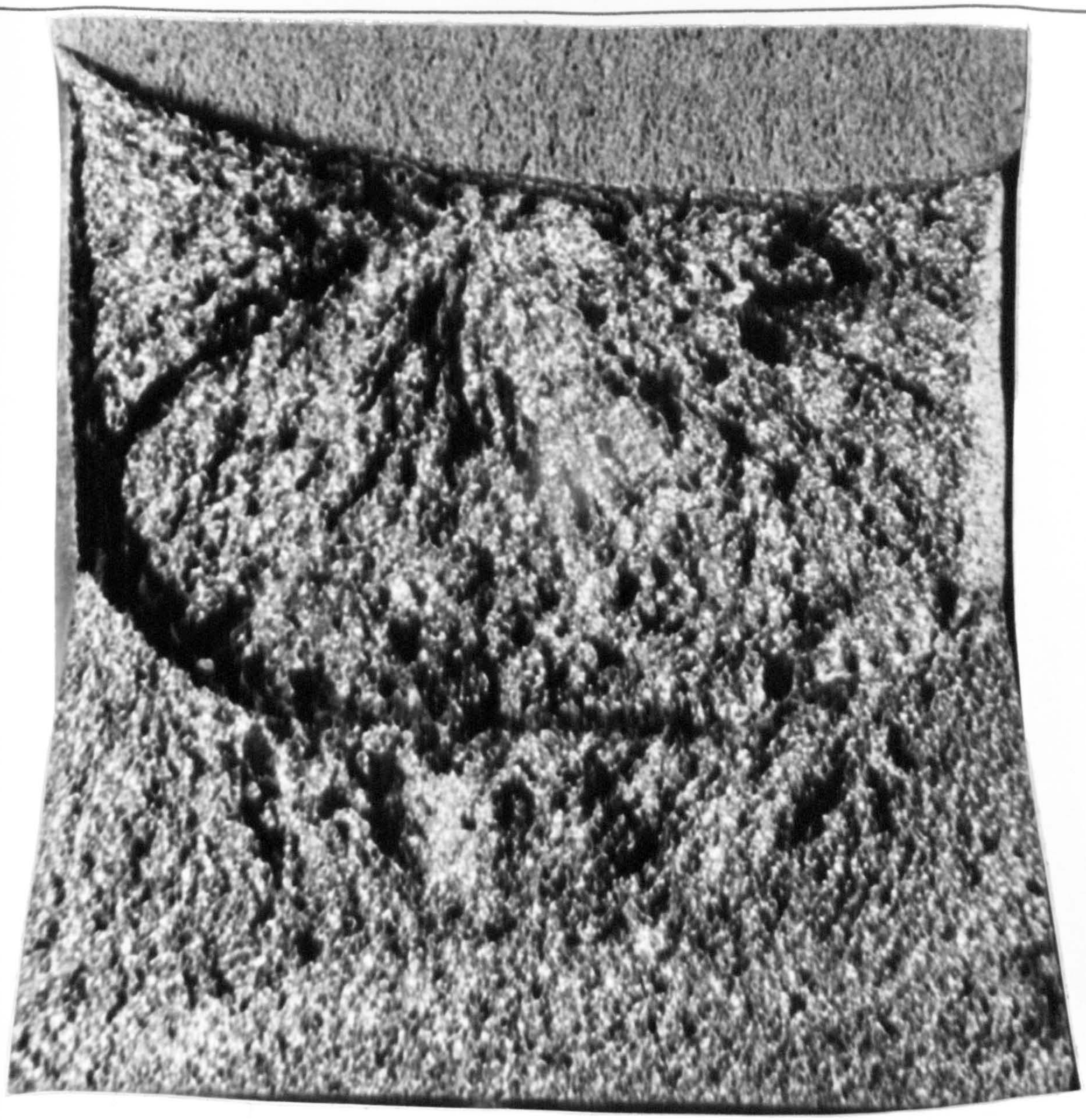

Fig. 80. Slow-static COD compliant test B4.
Photo x 11·25 . $\delta_{max.}$ = 0·397 m.m. T = -70°C.

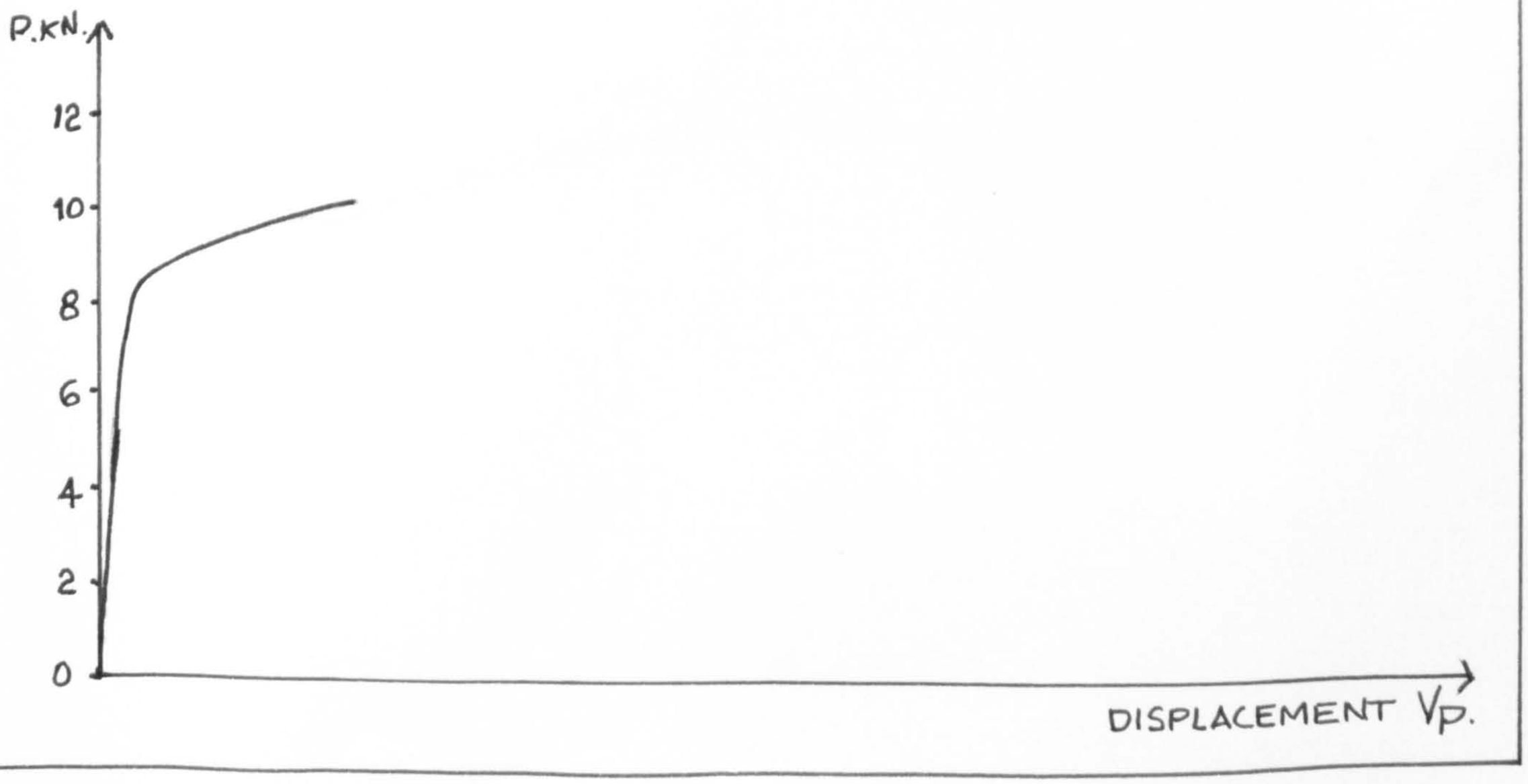

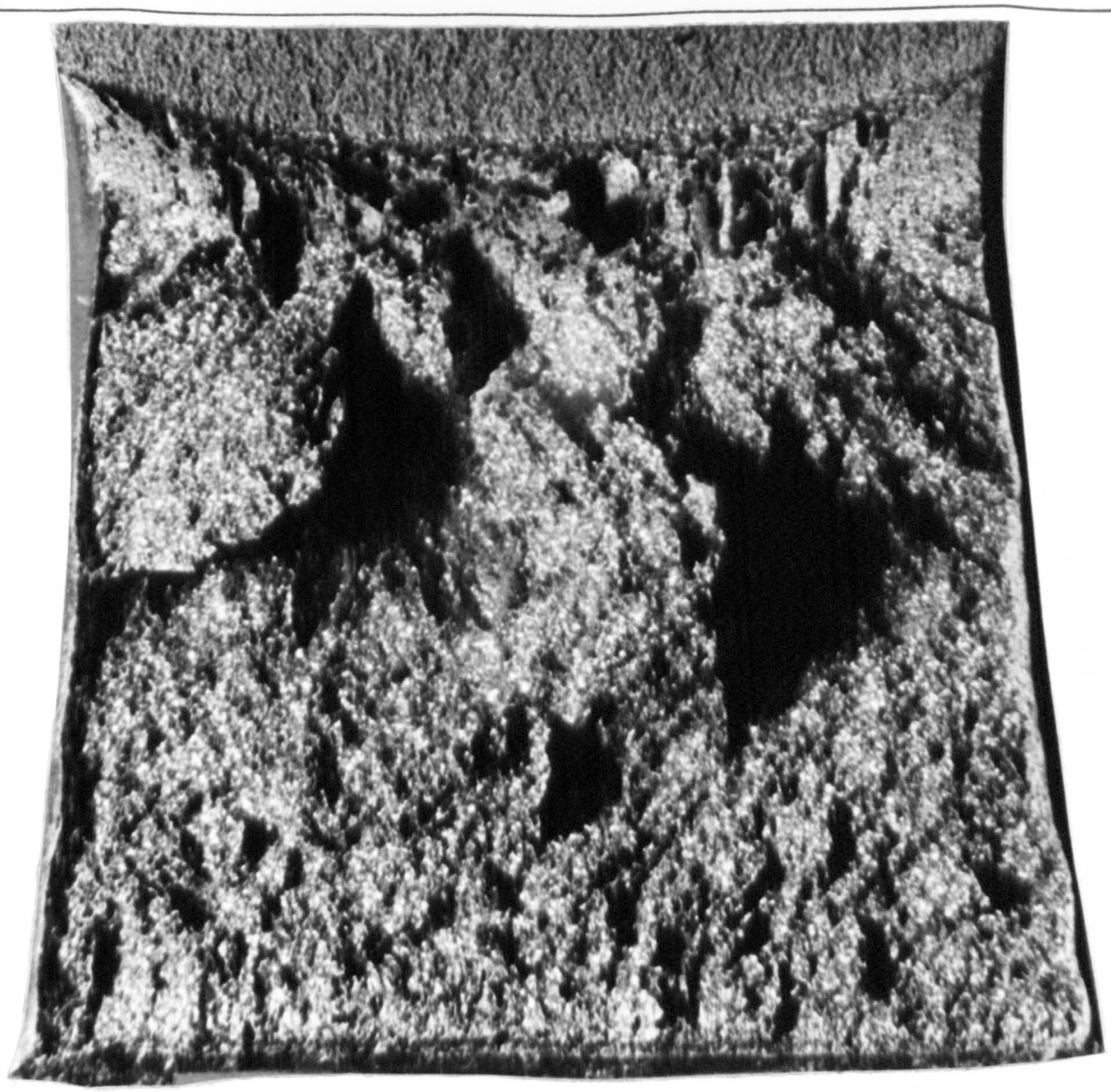

Fig. 81. Slow-static COD compliant test B5.
Photo x 11·25. $\delta_{max.}$ = 1·110 m.m. T = −75°C.

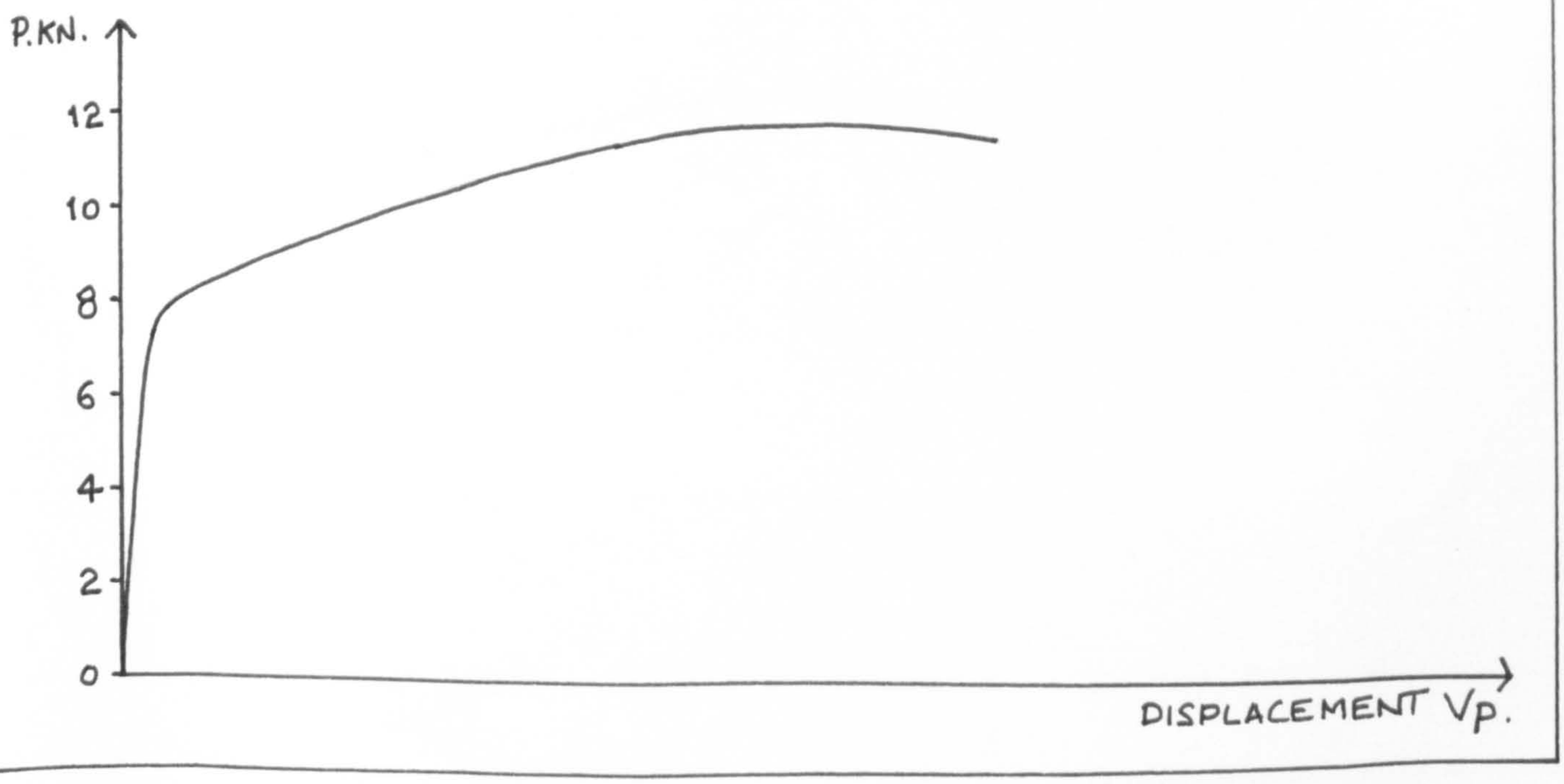

Fig.82. Slow-static COD compliant test B6.
Photo x 11·25. $\delta_{max.}$ = 1·213 m.m. T = -80°C.

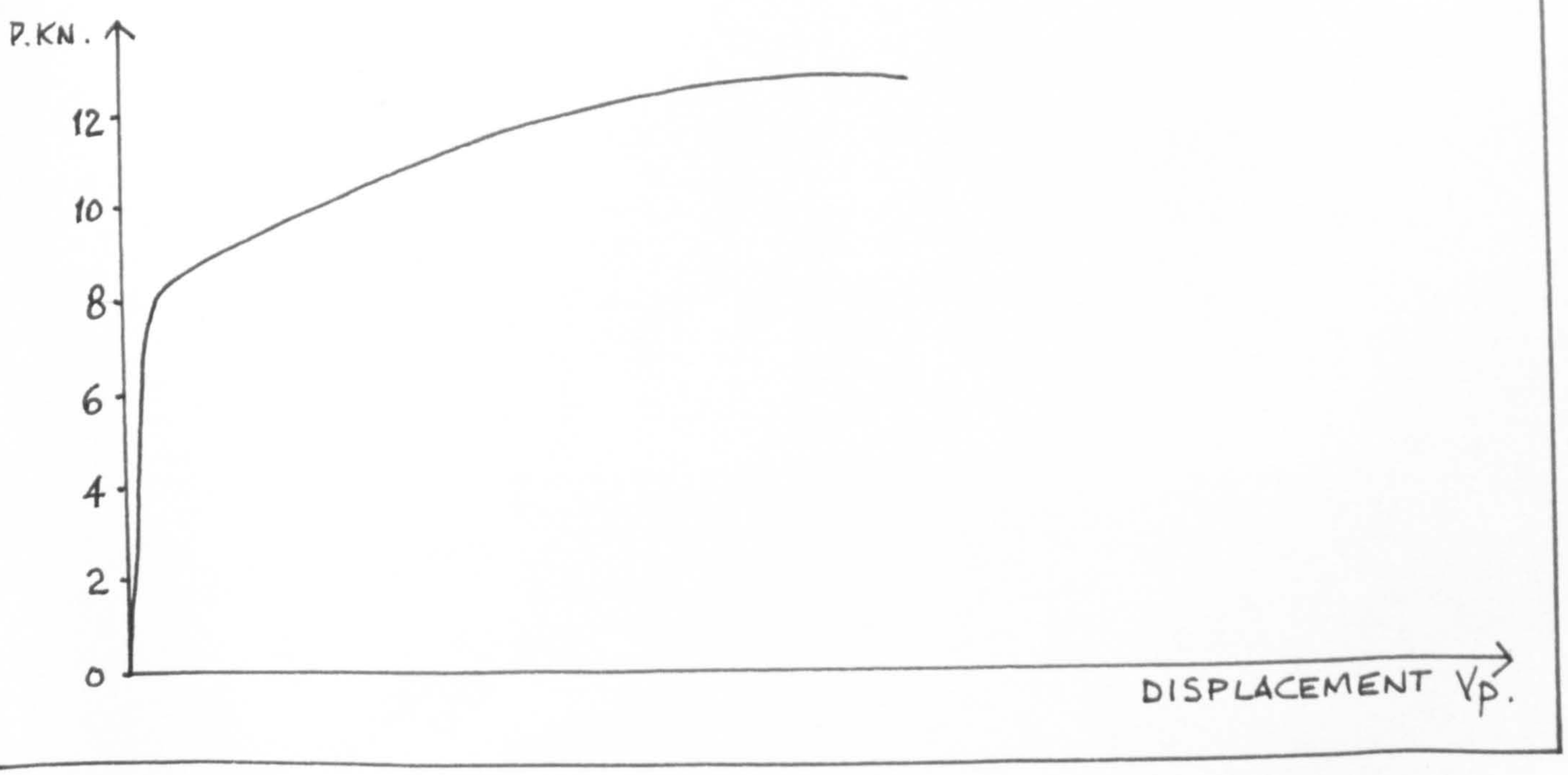

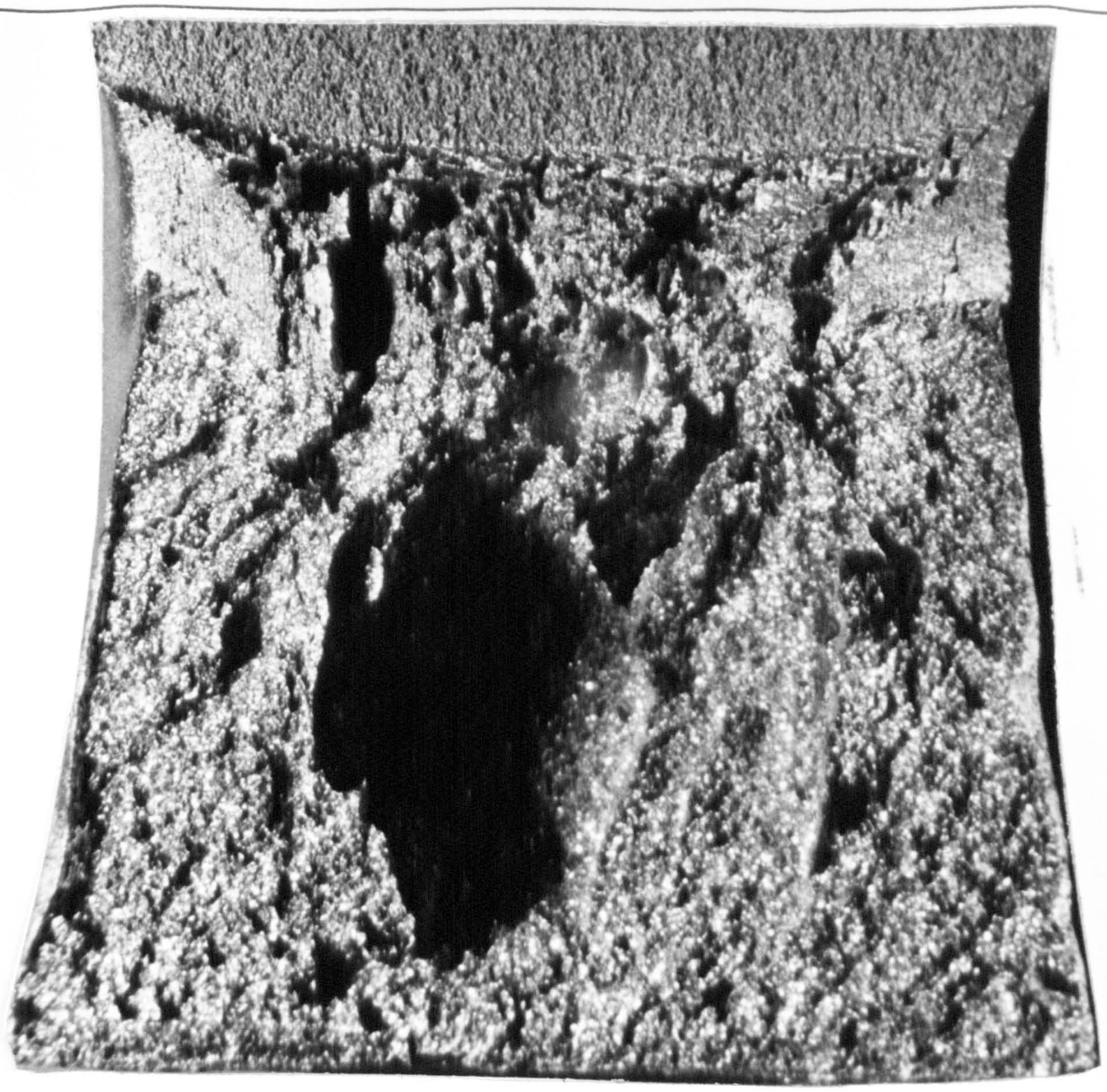

Fig 83. Slow-static COD compliant test B8.
Photo x 11·25. $\delta_{max.}$ = 1·194 m.m. T = -86°C.

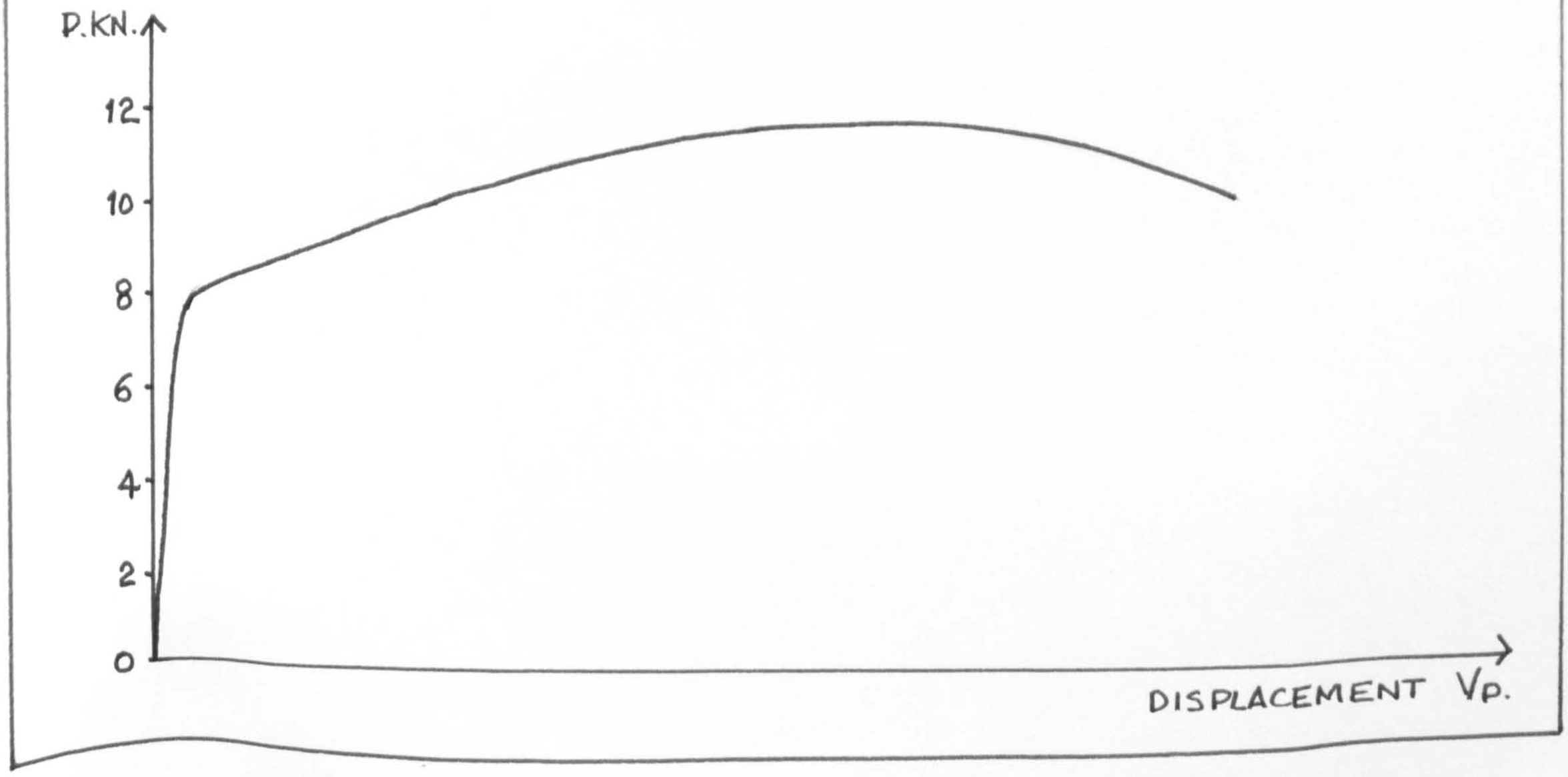

Fig.84. Slow-static COD compliant test B10.
Photo x 11·25. $\delta_{max.}$ = 1·033 m.m. T = -90°C.

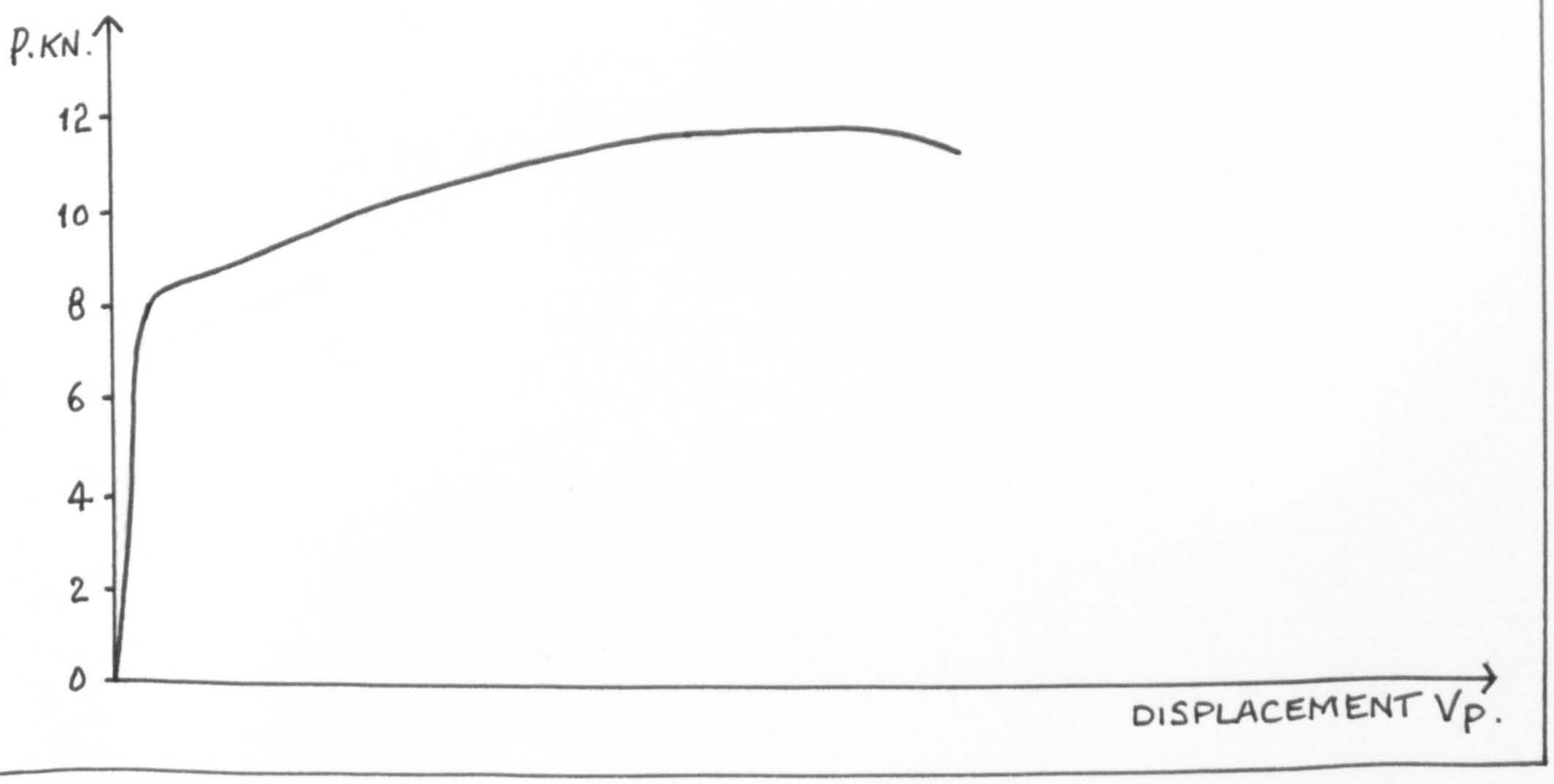

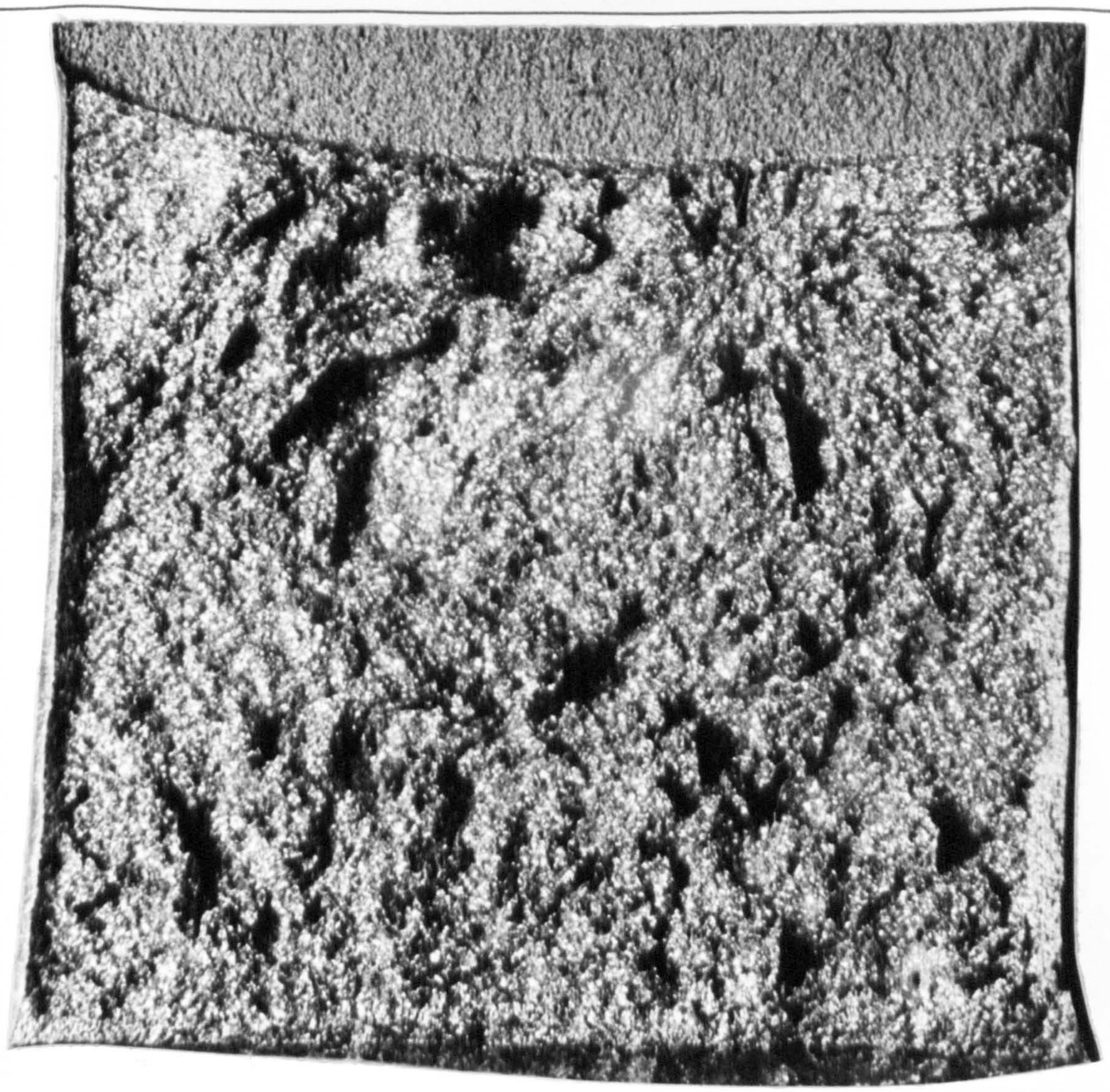

Fig. 85. Slow-static COD compliant test B12.
Photo x 11·25. $\delta_{max.}$ = 0·317 m.m. T = -95°C.

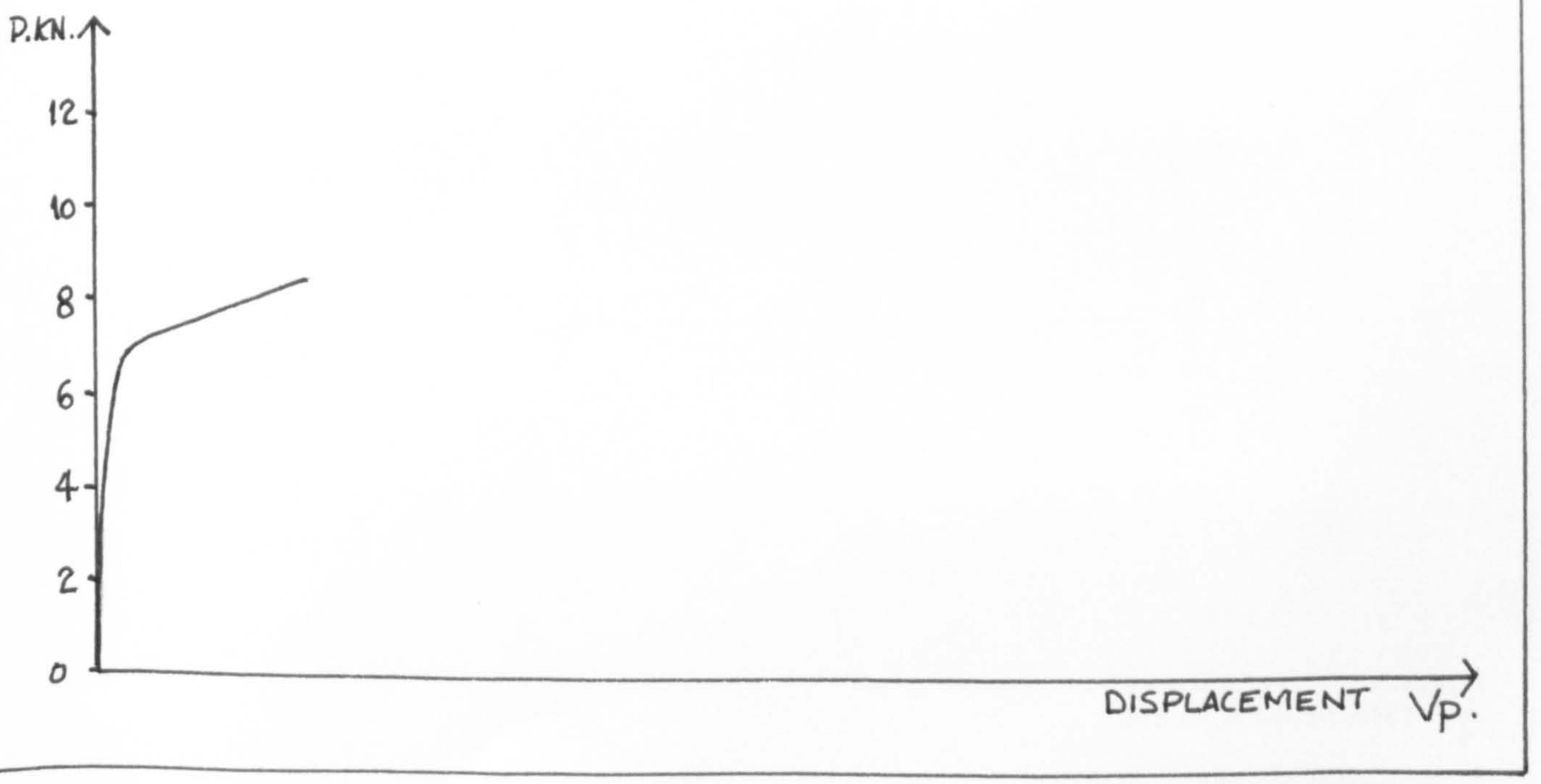

Fig. 86. Slow-static COD compliant test B14.
Photo x 11·25. $\delta_{max.}$ = 0·052 m.m. T = -105°C.

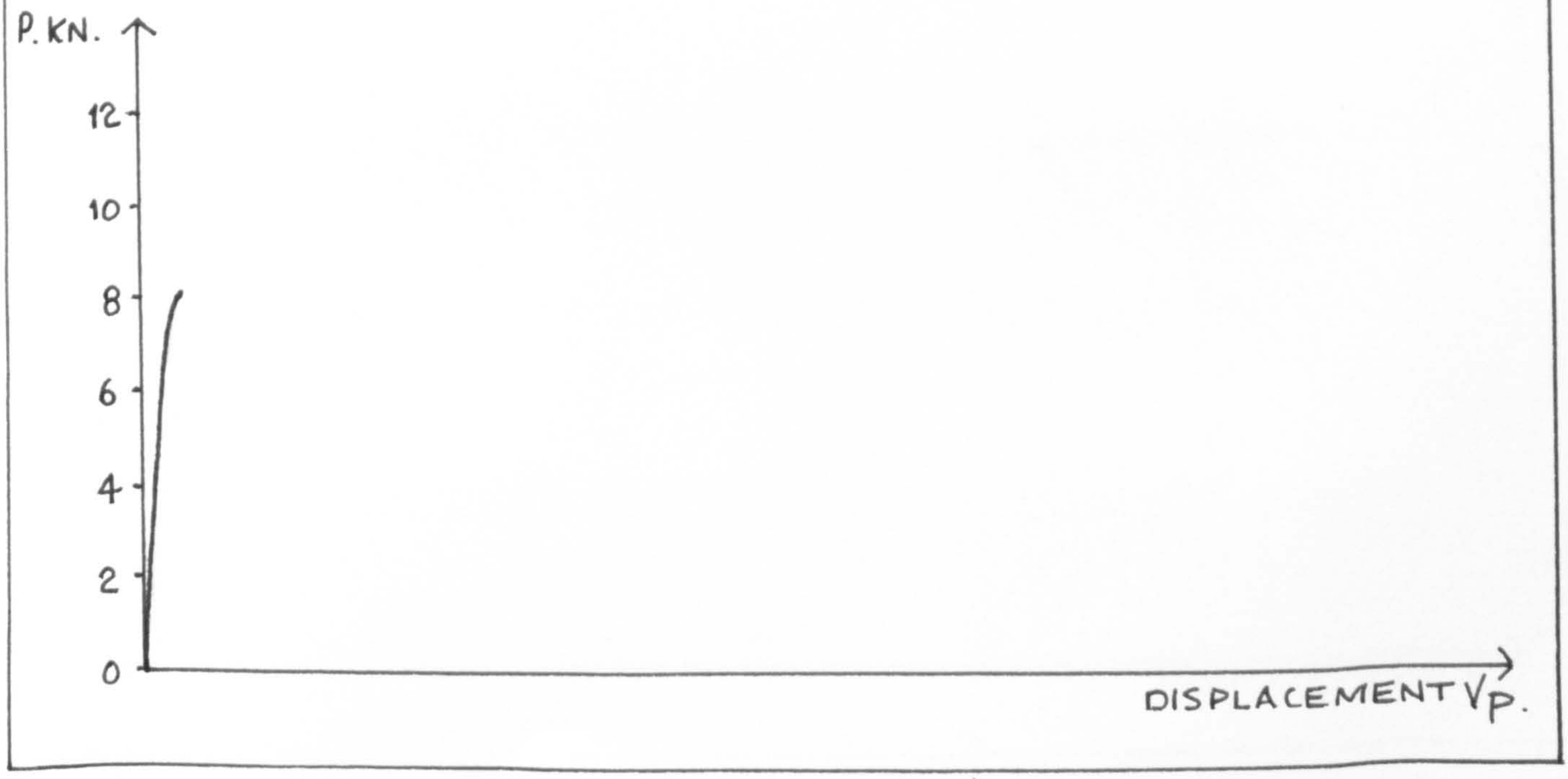

Fig. 87. Slow-static COD compliant test B15.
Photo x 11·25. $\delta_{max.}$ = 0·026 m.m. T = -120°C

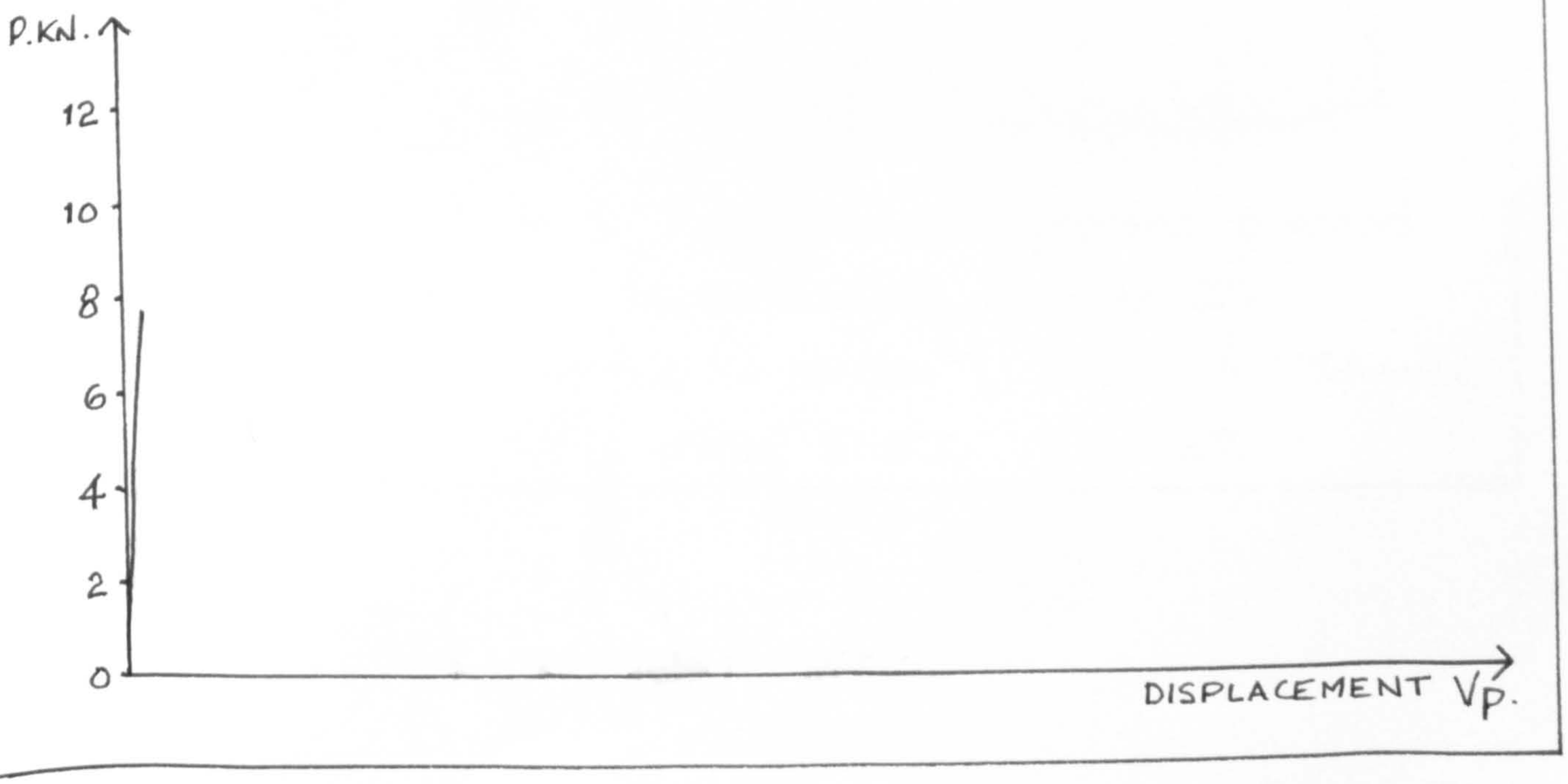

Fig.88. Dynamic Impact plus supeposed preladd test. Series E data, number E9. Preload = 0·86 KN/mm$^{3/2}$, Impact $\dot{\delta}$ = 154mm/s, dynamic energy 61·9J. T = -42°C.

Fig.89. Dynamic Impact plus superposed preload test. Series E data, number EM2.
Preload = 0·51 KN/mm$^{3/2}$ Impact $\dot{\delta}$ = 154 mm/s.
Dunamic enemu 163·3J, T = -42°C.

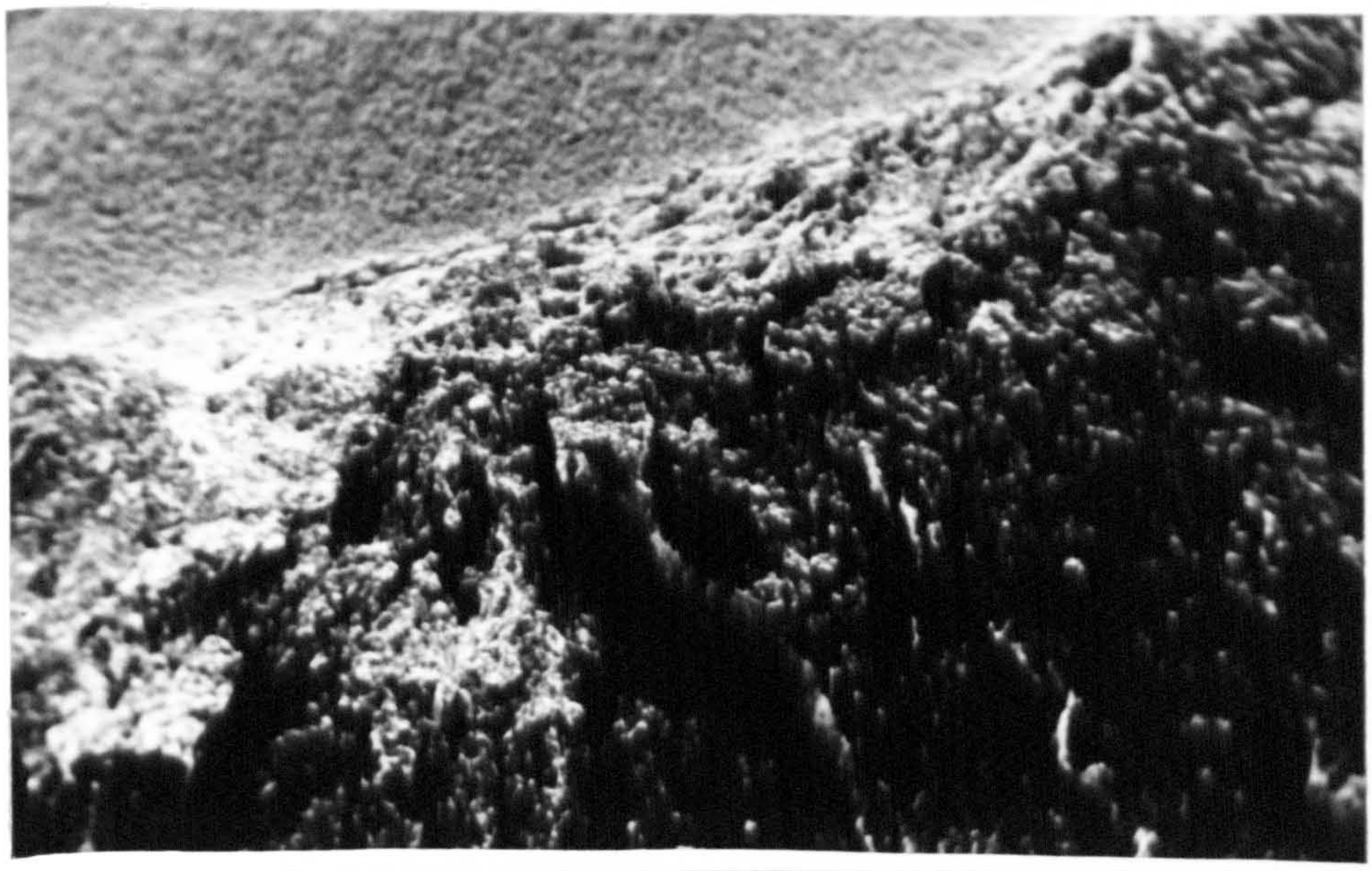

A4 -95°C.
x16 mag.

A6 -105°C.
x 16 mag.

B10 -90°C.
x 16 mag.

Fig.90. Comparison of tearing morphologies, static.

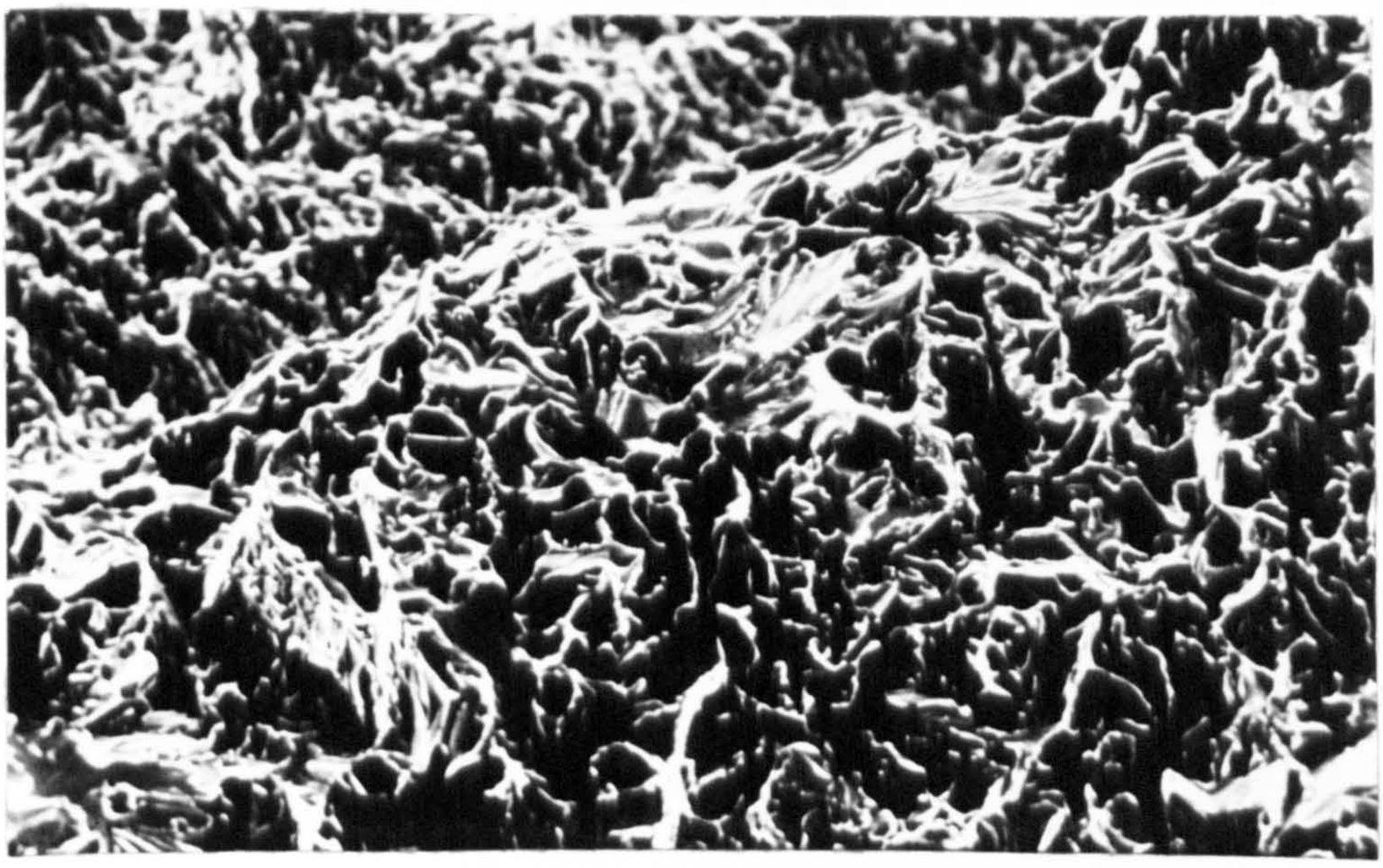

E9, -42°C, Preload < Kcliptum. x375 mag.

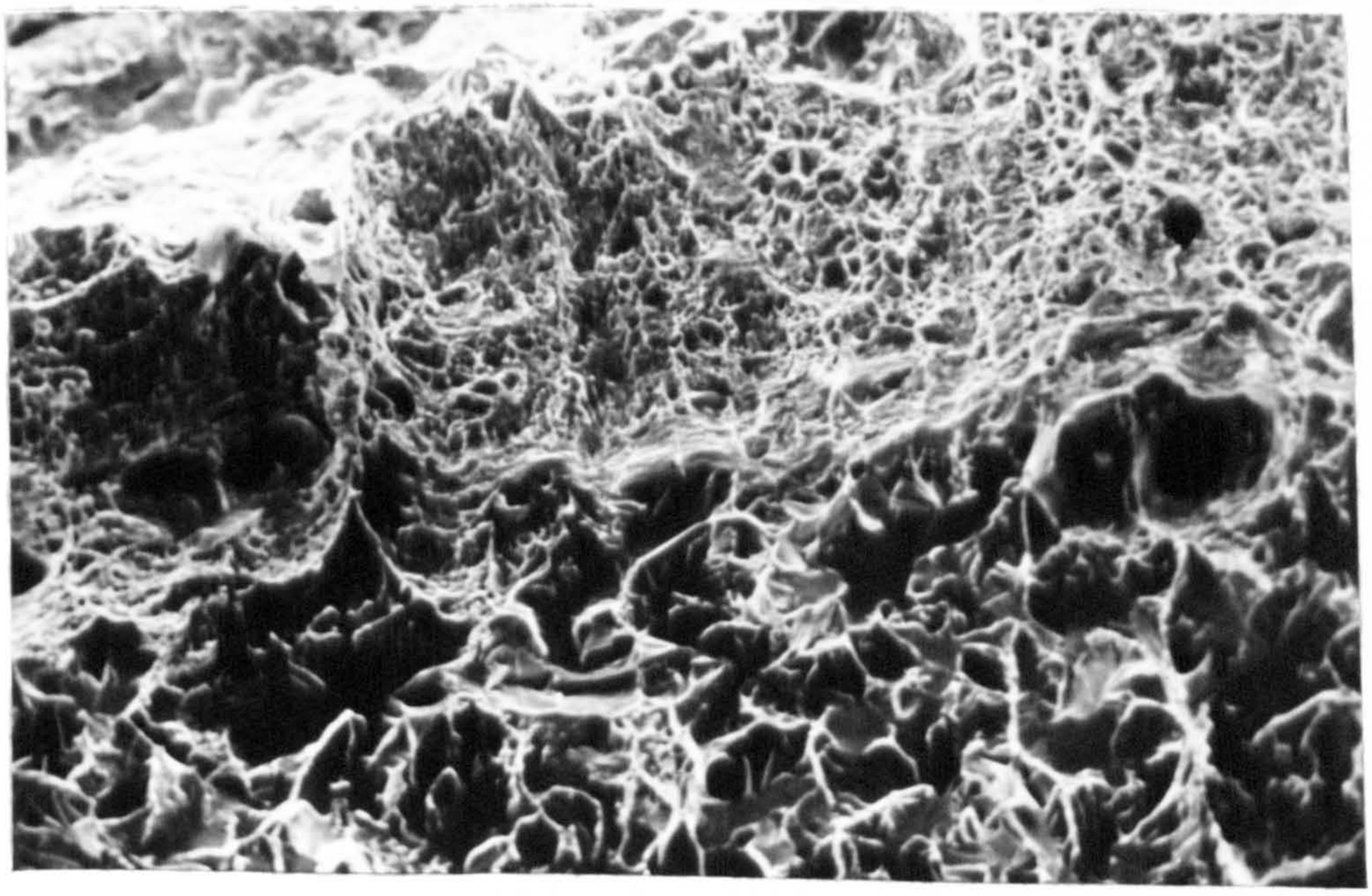

F12, -42°C, Preload > Kcliptum. x375 mag.

Fig. 91. Effect of preload at crack tip above and below Kcliptum, Fig 68.

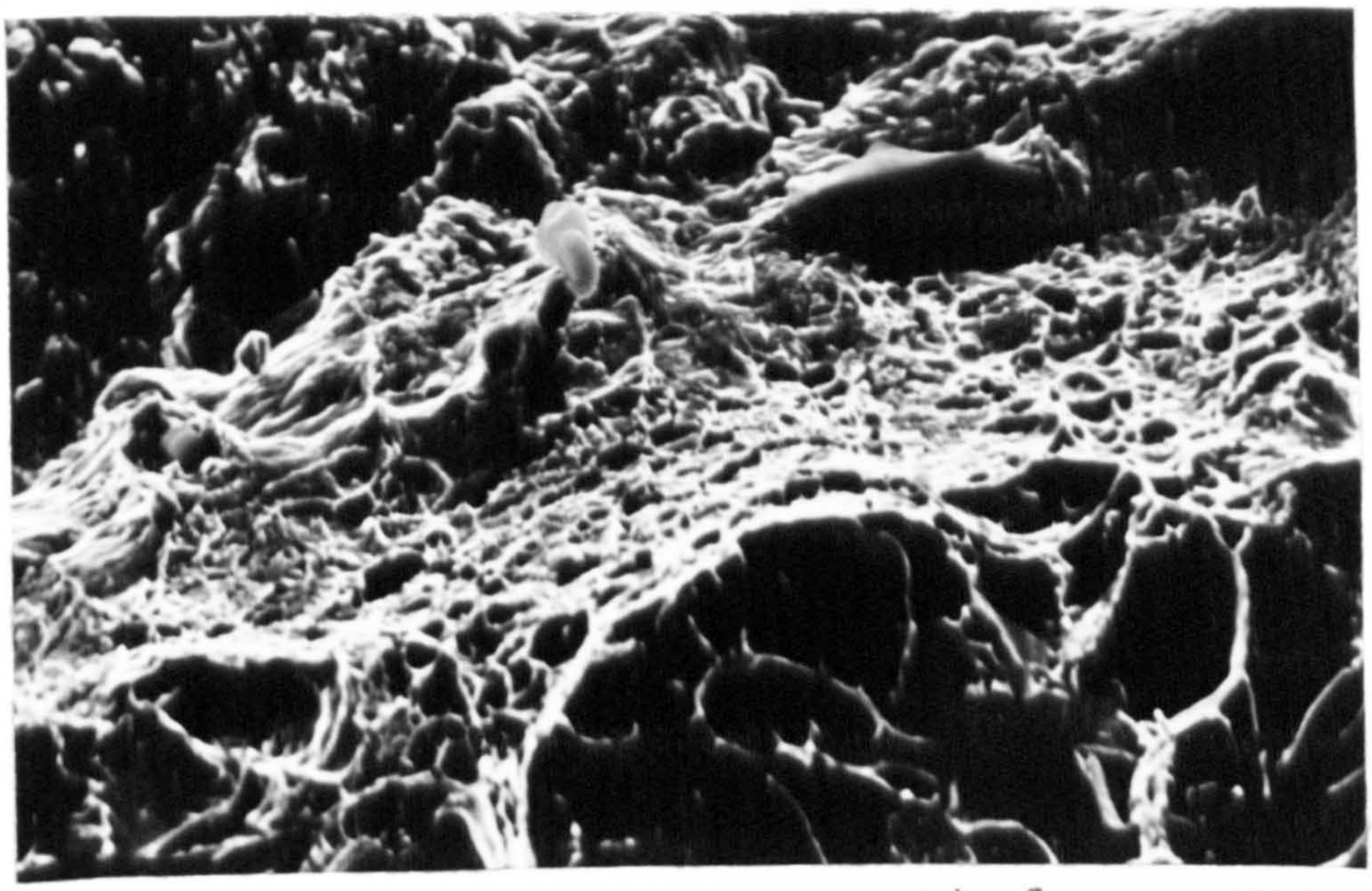

E8 -42°C Preload = 1·05KN/mm$^{3/2}$. x750 mag.
Momentum = 94·1J.
$\dot{\delta}$ = 154mm/s.

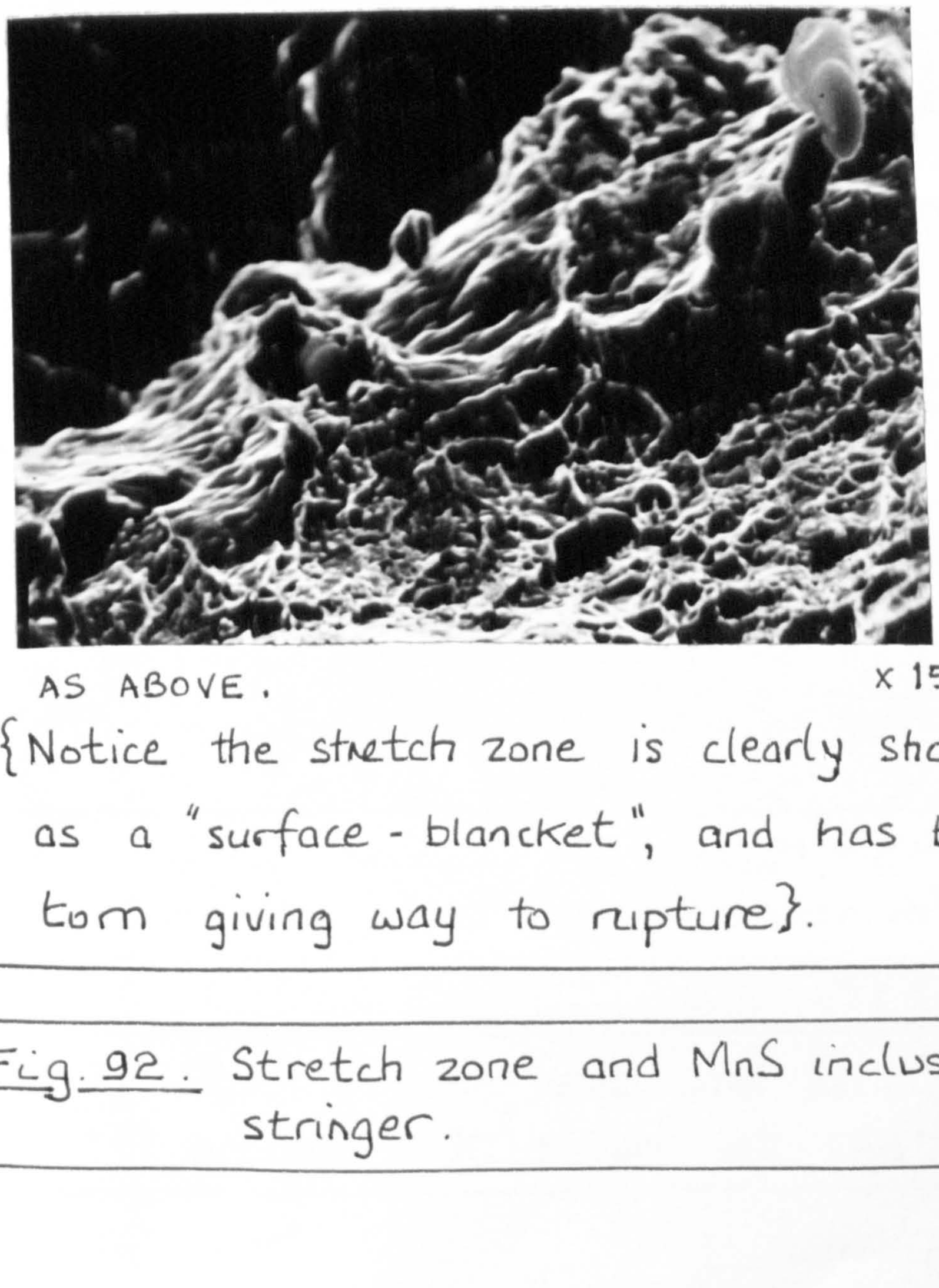

AS ABOVE. x1500mag.

{Notice the stretch zone is clearly shown as a "surface-blancket", and has been torn giving way to rupture}.

Fig. 92. Stretch zone and MnS inclusion-stringer.

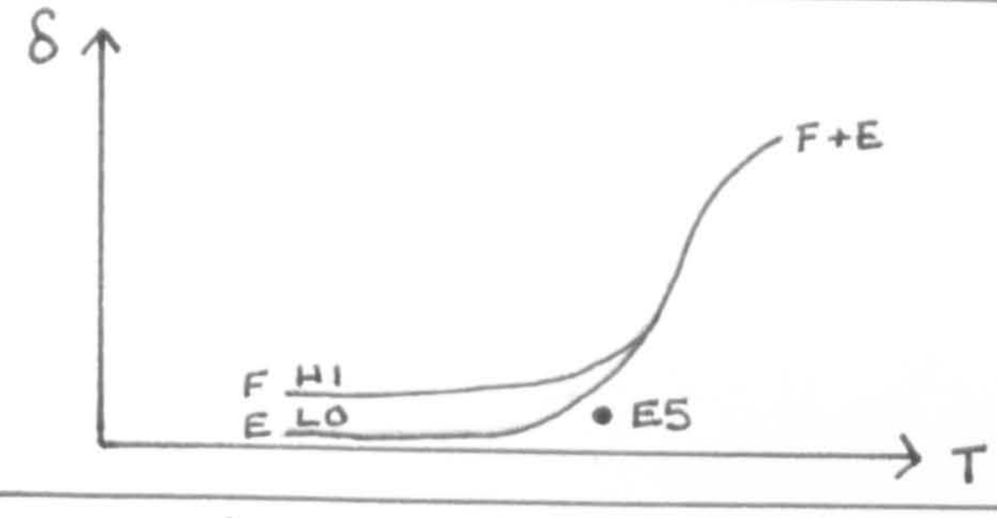

After dynamic impact, point of E5 test in relation to instability lines.

Schematic sectional diagram.

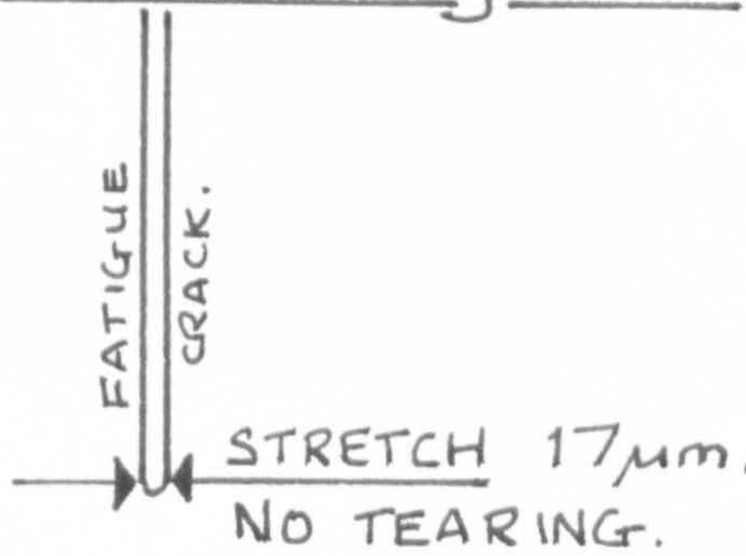

Low preload, < Kclip turn see Fig 68.
Crack still relatively sharp.

SEM fracture-photo, surface.

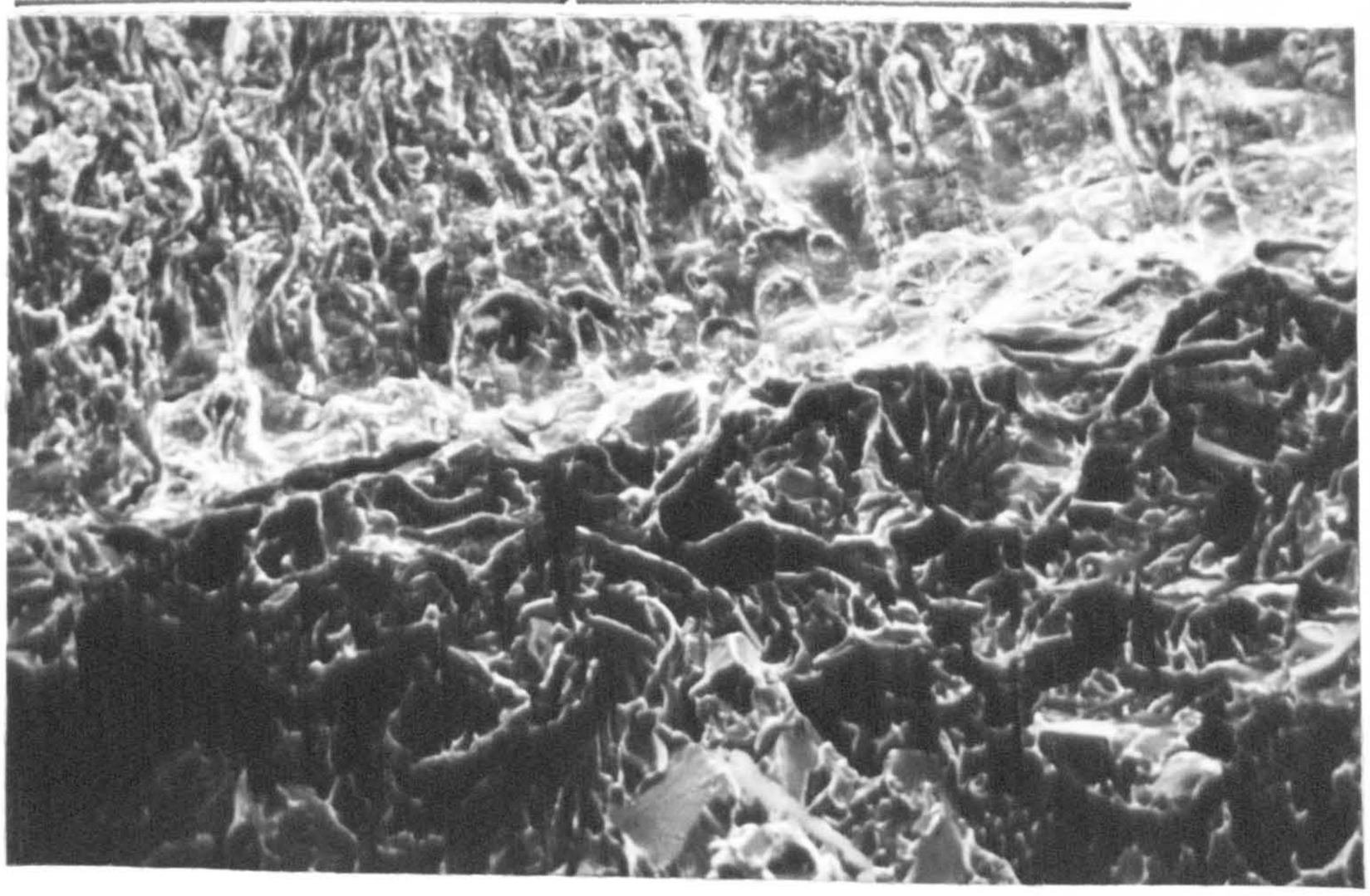

E5, -60°C, Preload = 0·863 KN/mm$^{3/2}$ x 375 mag.
Impact energy 94·1J. (ligament broken after test).

Fig. 93. Stretch zone size and blunting for preload < Kclip turn at -60°C.
SEE FIG 95.

SMALL STRETCH ZONE AT CRACK TIP WITH PRELOAD < 1·6KN/mm$^{3/2}$.

E12.
-70°C.

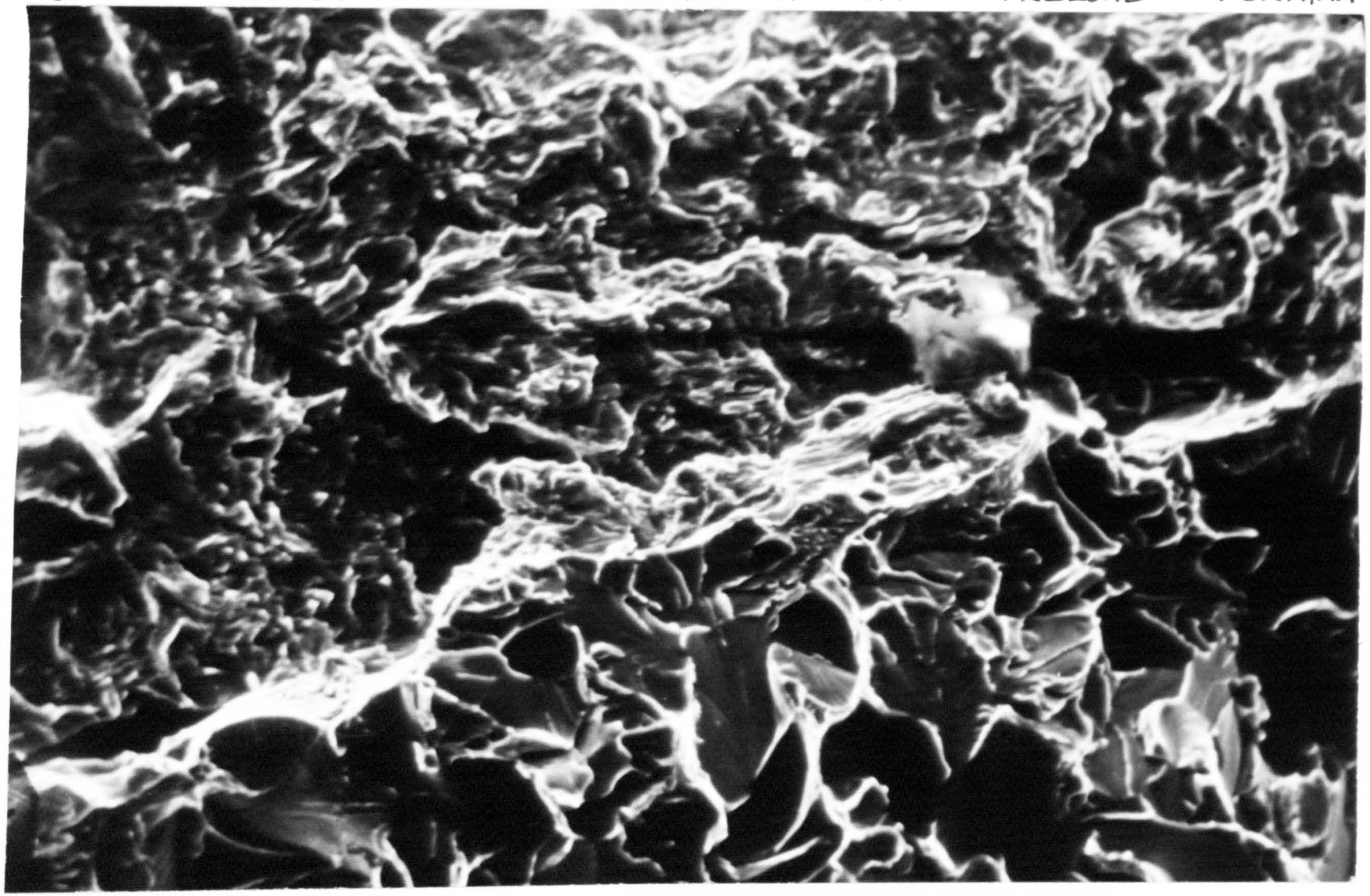

Fig. 94. Dynamic impact plus superposed compliant preload of x 1300mag. 1·0 KN/mm$^{3/2}$, $\dot{S}$ = 154 mm/s, momentum = 94·1 J, -70°C, spec, E12.

TABLE 7 FOR STRETCH SIZE.

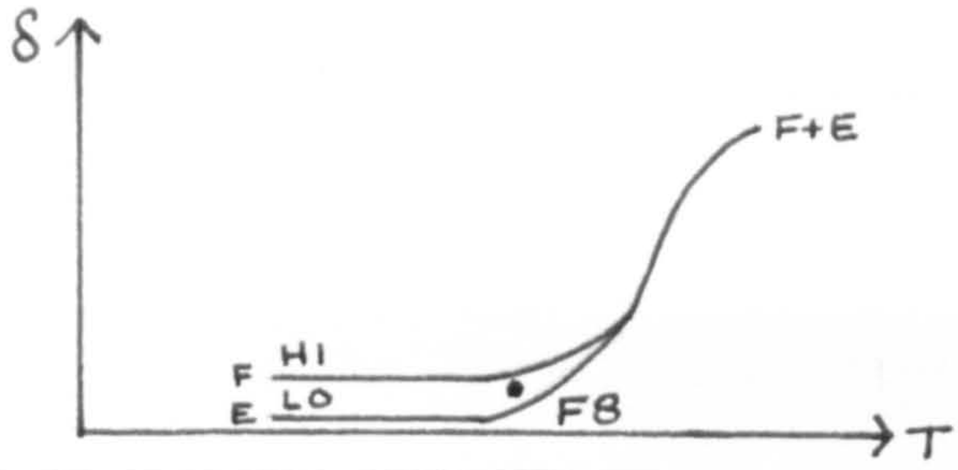

After dynamic impact, point of F8 test in relation to instability lines.

Schematic sectional diagram.

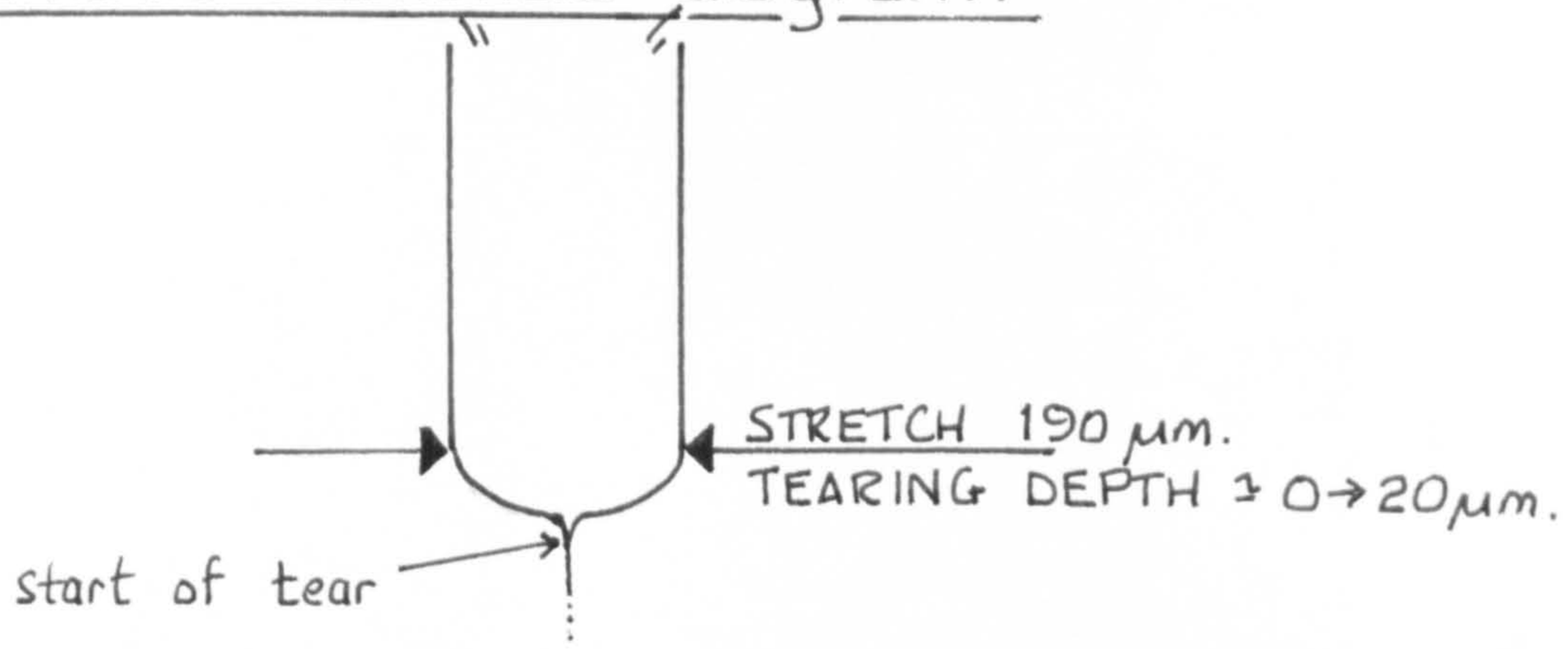

High preload, > K clip tum see Fig68.
Crack blunted with microvoid tearing beginning to form.

SEM fracture - photo, surface.

F8, -68°C, Preload = 1·56 kN/mm$^{3/2}$. x 375 mag.
Impact energy 94·1 J. (Ligament broken after test).

Fig. 95. SEE FIG 93. Blunting and beginning of rupture at stretched crack tip for a preload > K clip tum at -68°C.

LARGE STRETCH ZONE AT CRACK TIP WITH PRELOAD > 1·6 KN/mm$^{3/2}$. F20. -70°C.

Fig. 96. Dynamic impact plus superposed compliant preload of 1·81 KN/mm$^{3/2}$, $\dot{\delta}$ = 154 mm/s, momentum = 94·1 J, -70°C, spec. F20.
X 1300 mag.

TABLE 7 FOR STRETCH SIZE.

GENERAL VIEW OF CRACK TIP AND TEAR. A4. -95°C.

Fig.97. Slow-static COD, stiff A4, -95°C, SEM x29.

SLOW TEARING REGION AHEAD OF ORIGINAL CRACK TIP. A4, -95°C.

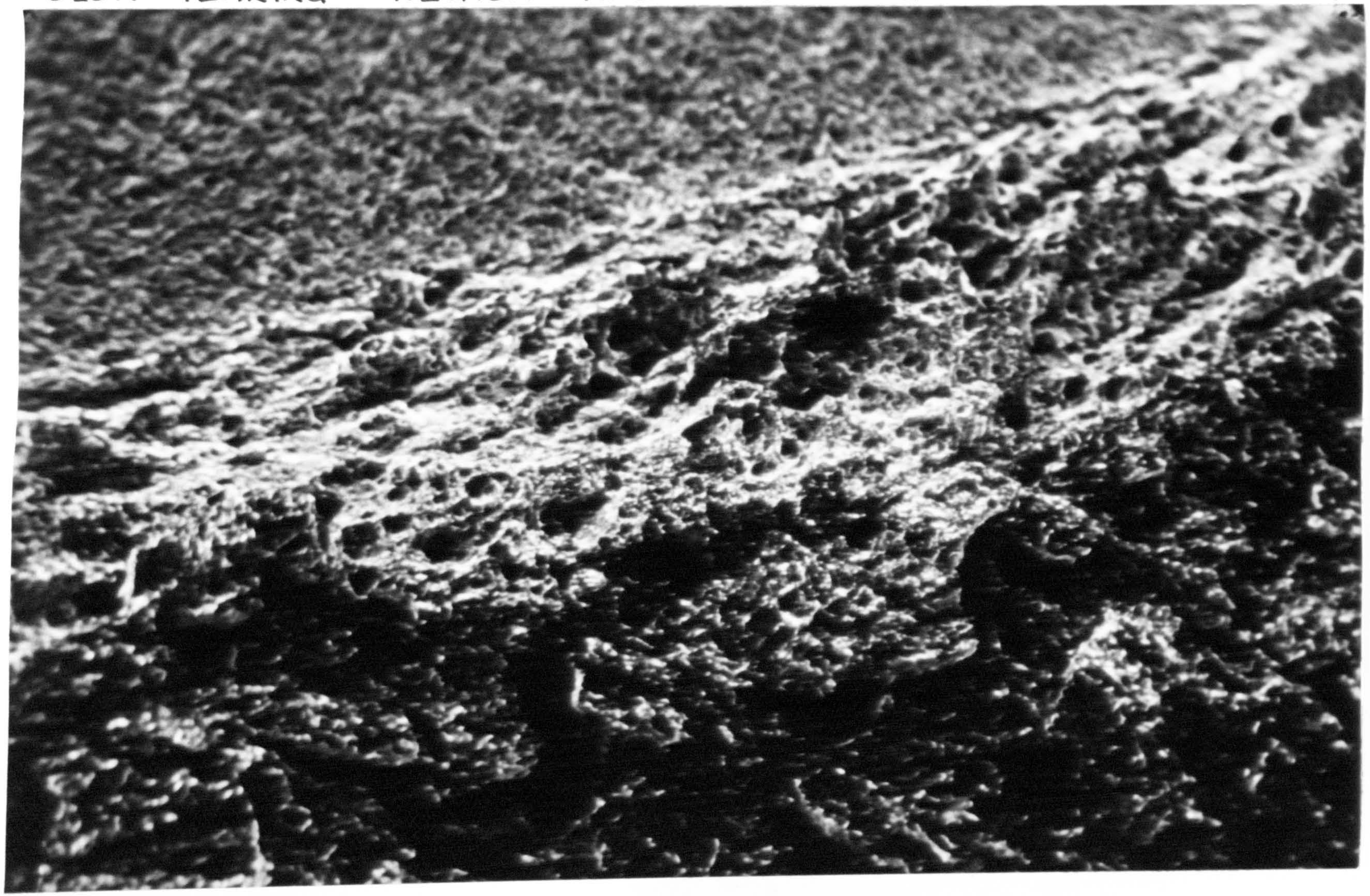

Fig. 98. Slow-static COD, stiff A4, -95°C, SEM x70.

TEARING RUPTURE MORPHOLOGY WITH DIMPLES AND MICROVOIDS.

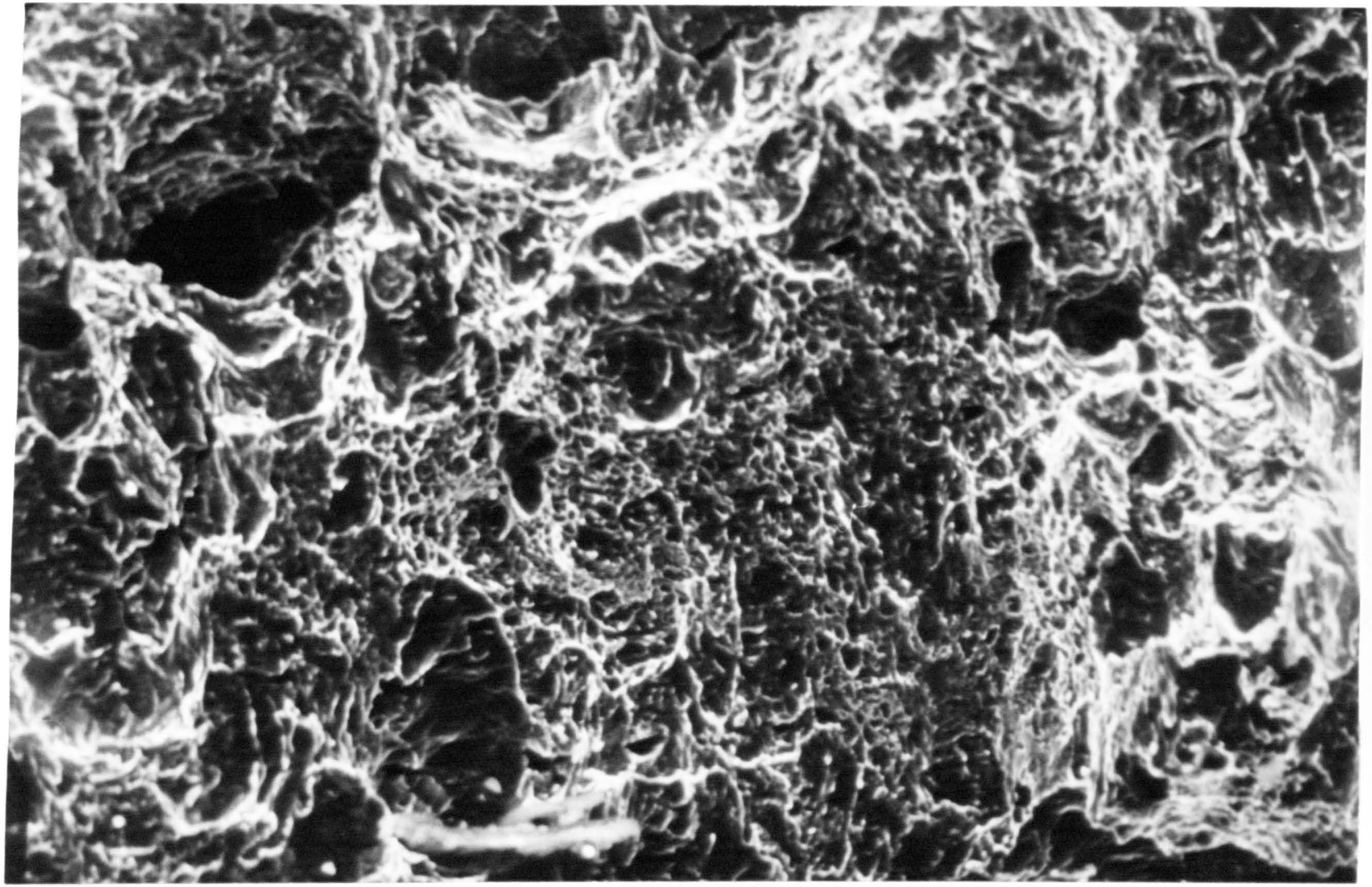

Fig. 99. Slow-static COD, stiff A4, -95°C, SEM x 725.

TRANSITION BOUNDARY BETWEEN SLOW TEARING AND CLEAVAGE INSTAB.,

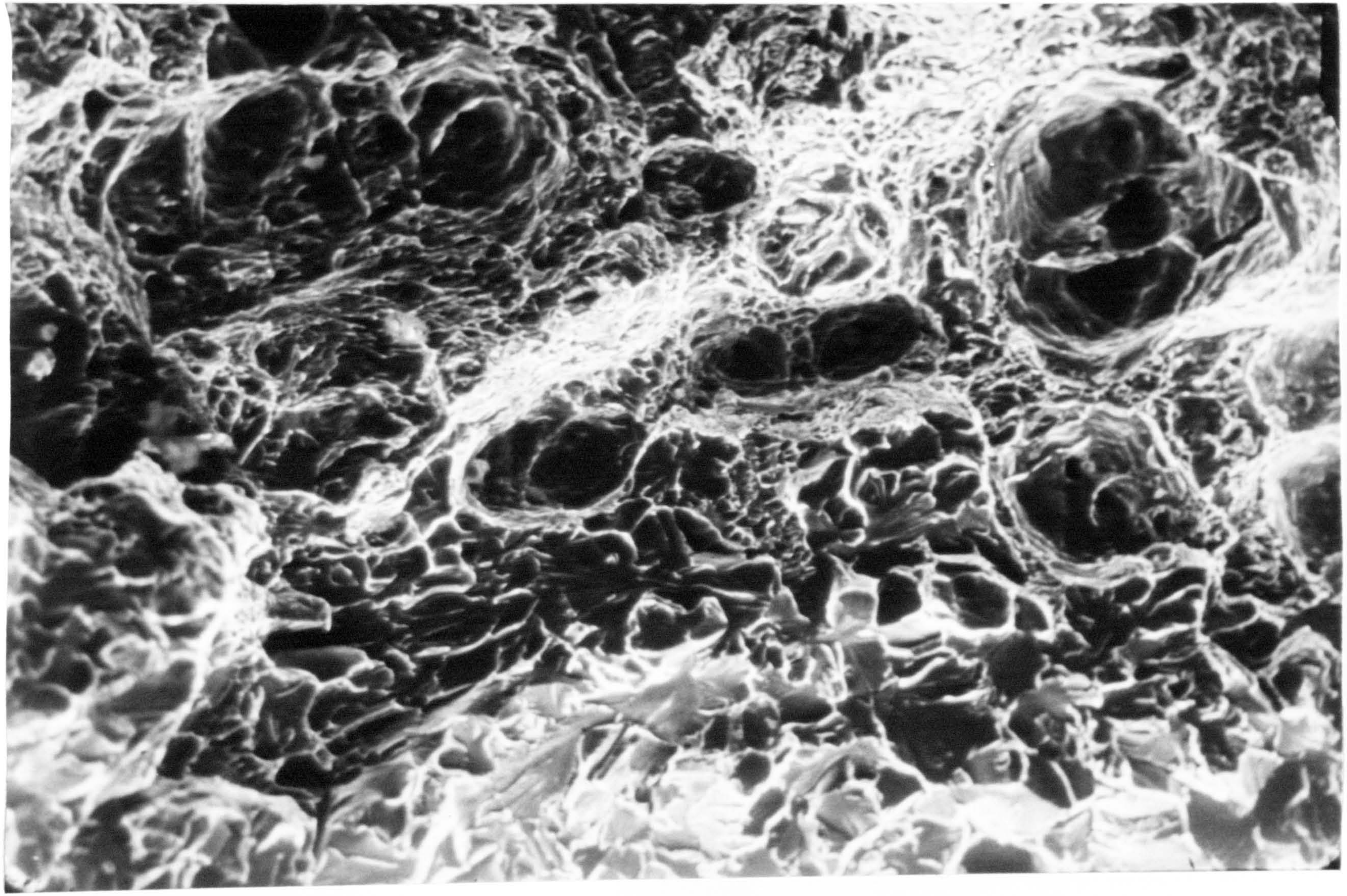

Fig. 100. Slow-static COD, stiff. A4, -95°C, SEM x 725.

INTERFACE BOUNDARY BETWEEN SLOW TEARING AND CLEAVAGE INSTABILITY.

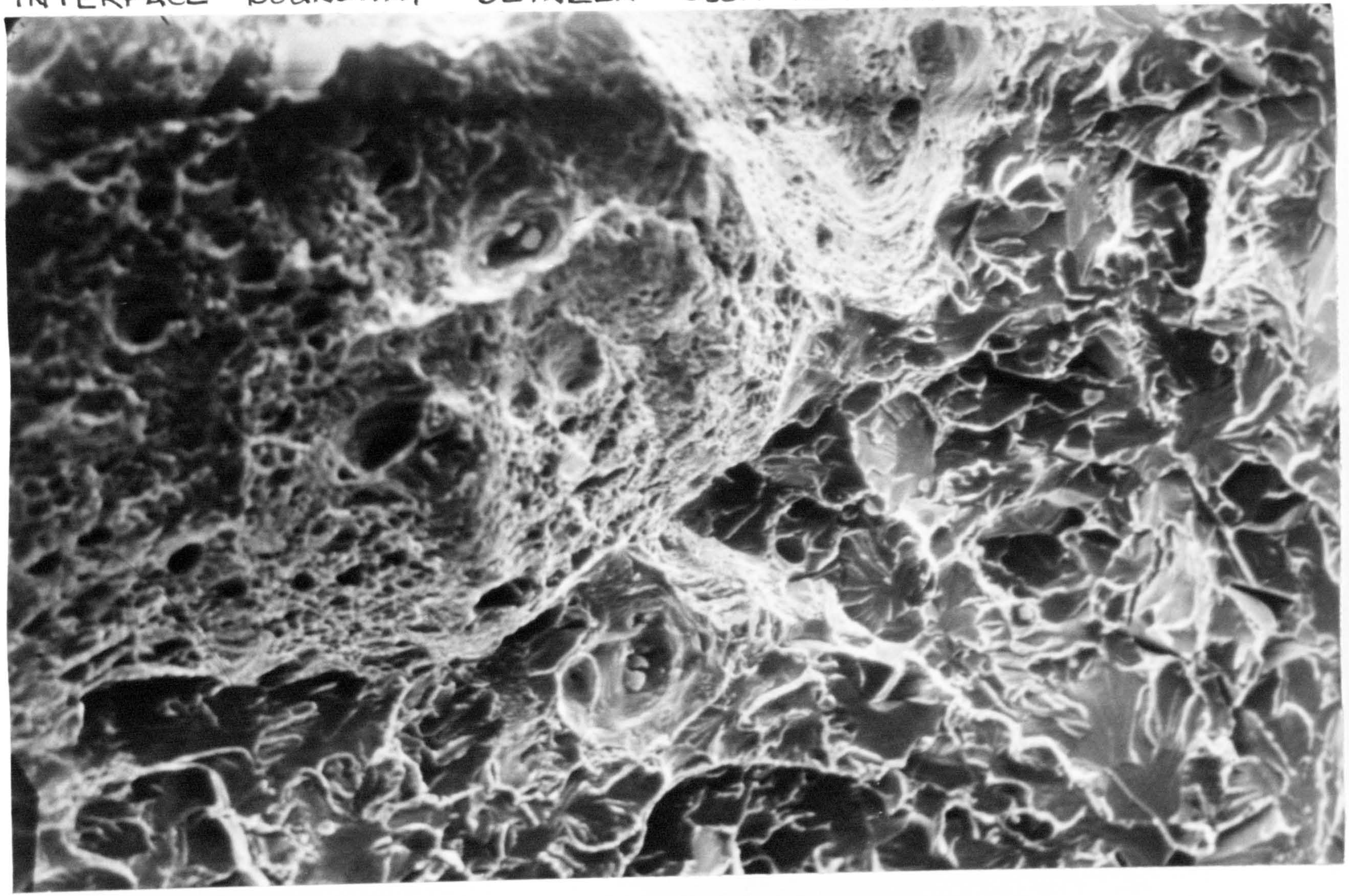

Fig. 101. SLow-static COD, comoliant B4, -70°C, SEM x 700 mag.

GENERAL VIEW OF CRACK TIP AND TEAR. B10. -90°C.

Fig. 102. Slow-static COD, compliant B10, -90°C, SEM x28mag.

TEARING REGION. B10. -90°C.

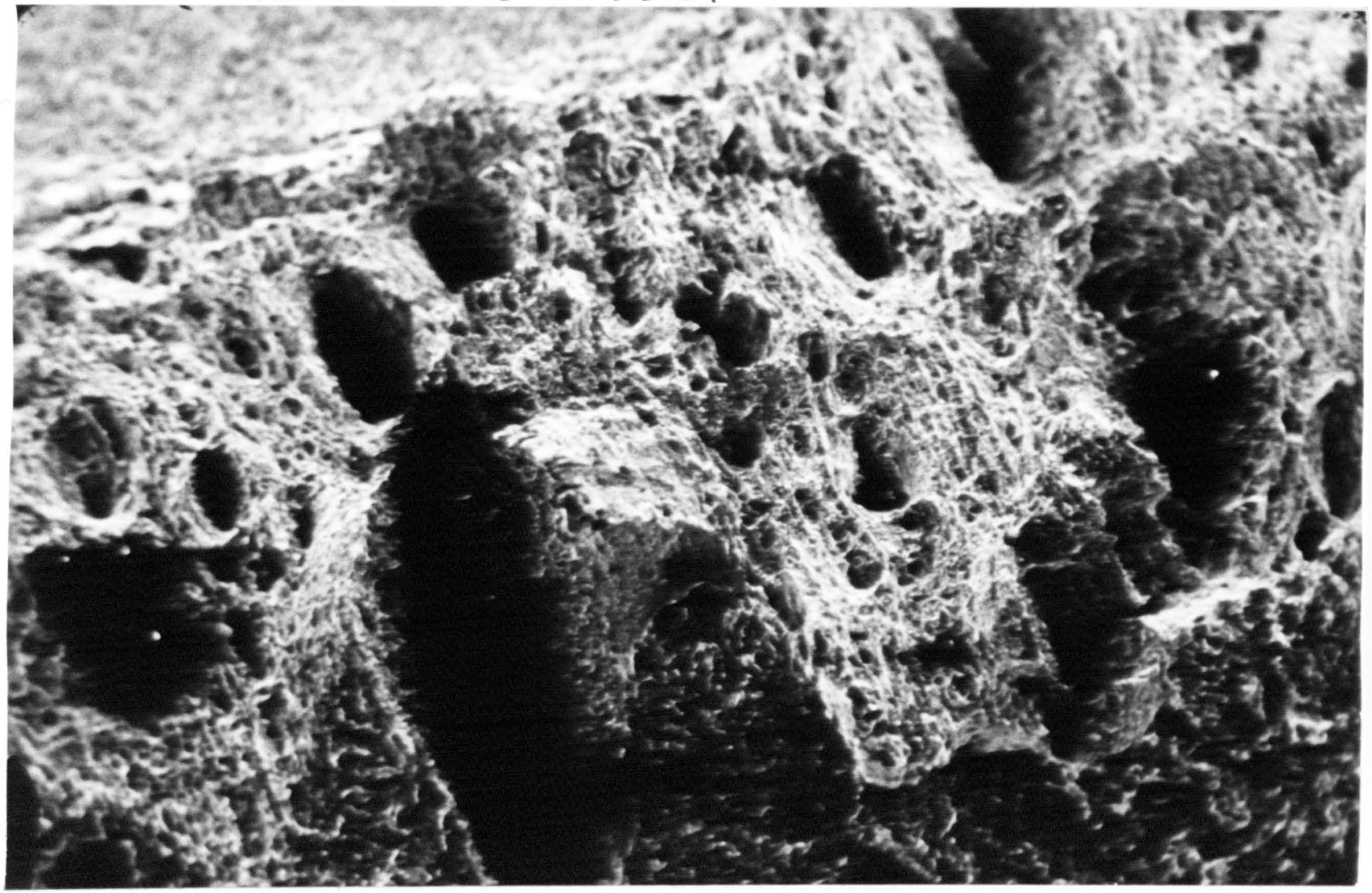

Fig. 103. Slow-static COD, compliant B10, -90°C, SEM x 70 mag.

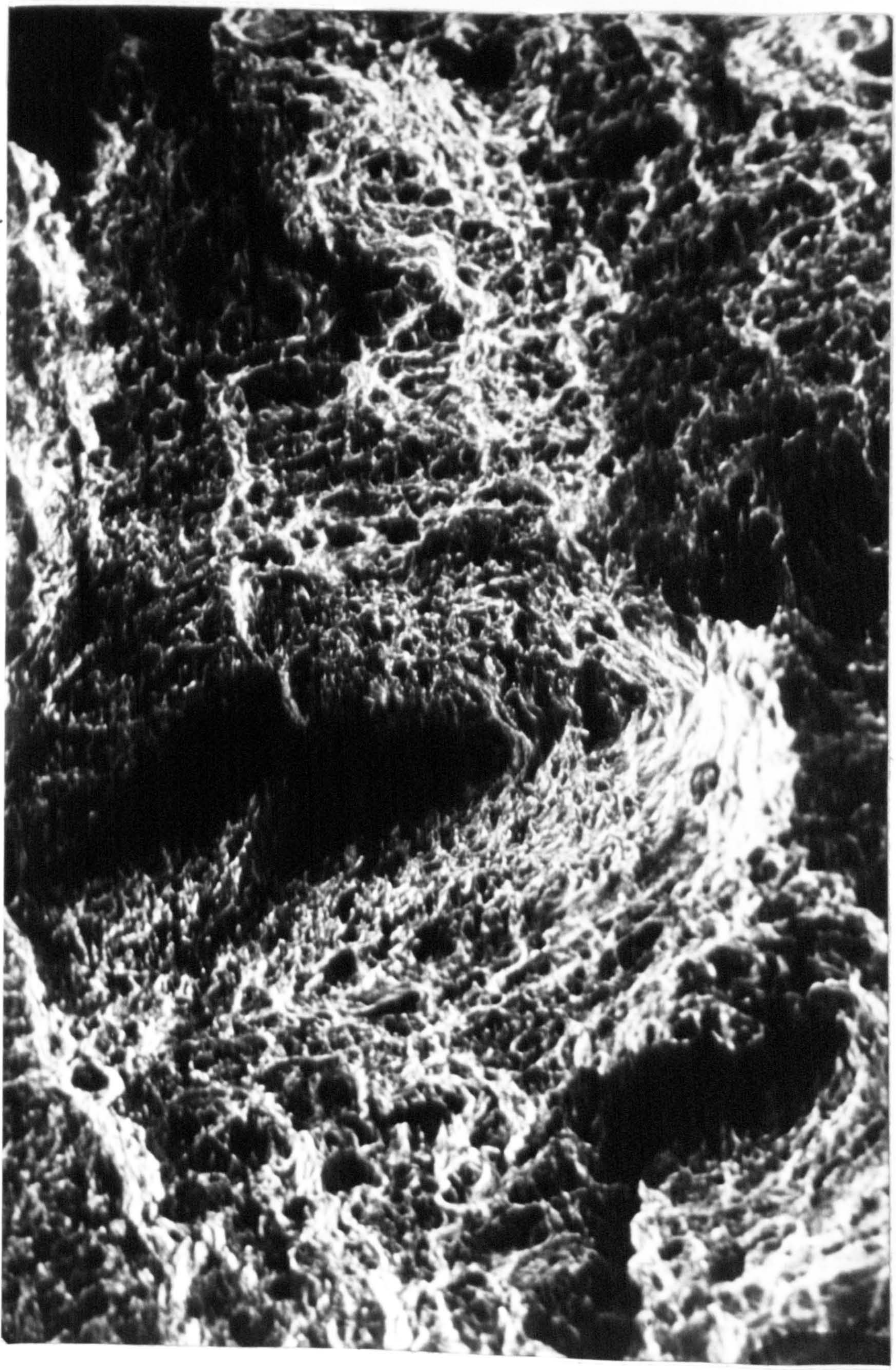

Fig 104. Slow-static COD, compliant B10, -90°C, SEM x 135 mag.

CLOSE VIEW OF "PITTED" REGION. B10. -90°C.

HIGH MAG. VIEW OF SIDE FROM PIT, MODE I - III BOUNDARY, B10.

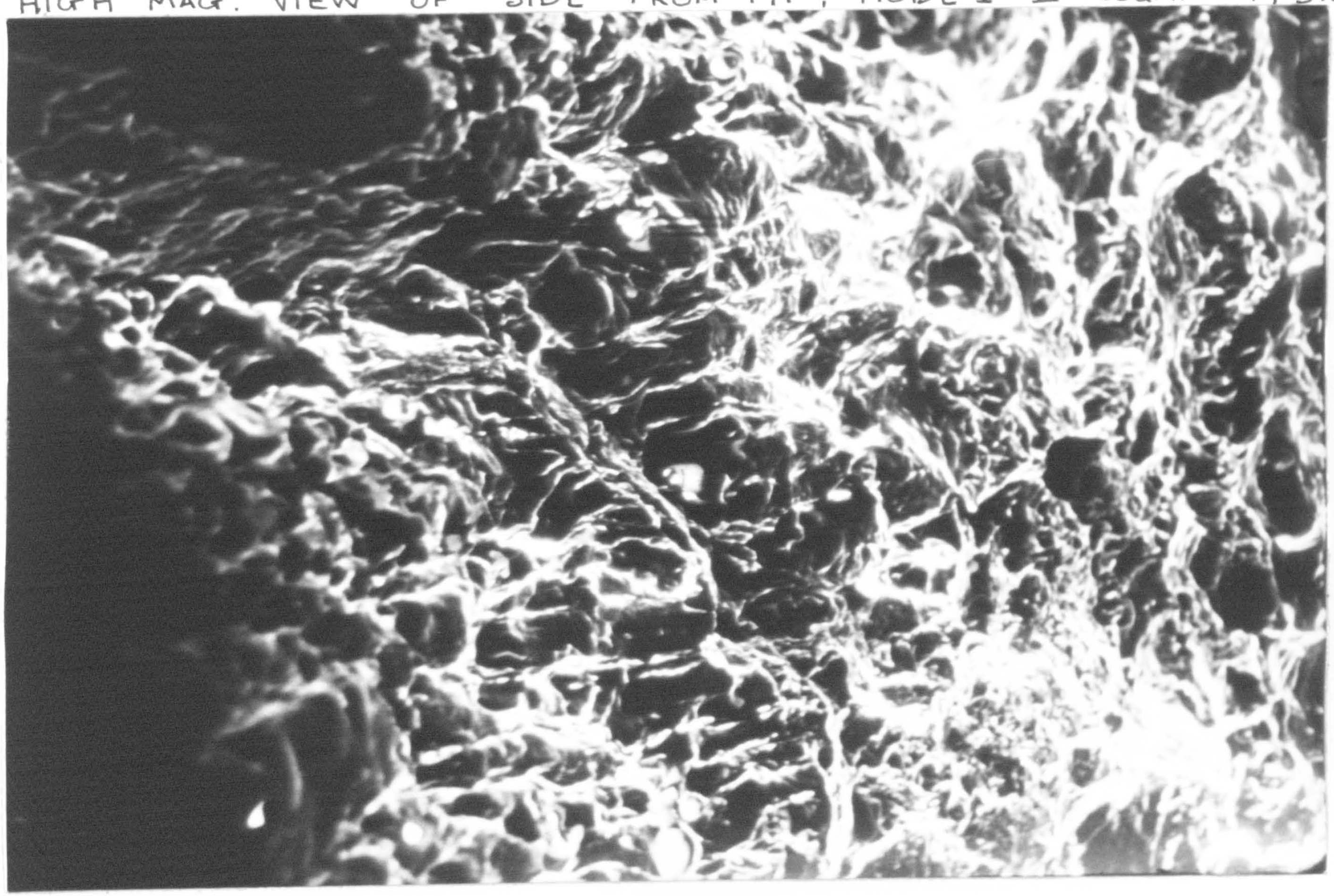

Fig 105. Slow-static COD, compliant B10, -90°C, SEM x 675 mag.

CRACK TIP STRETCH ZONE. H7. -42°C.

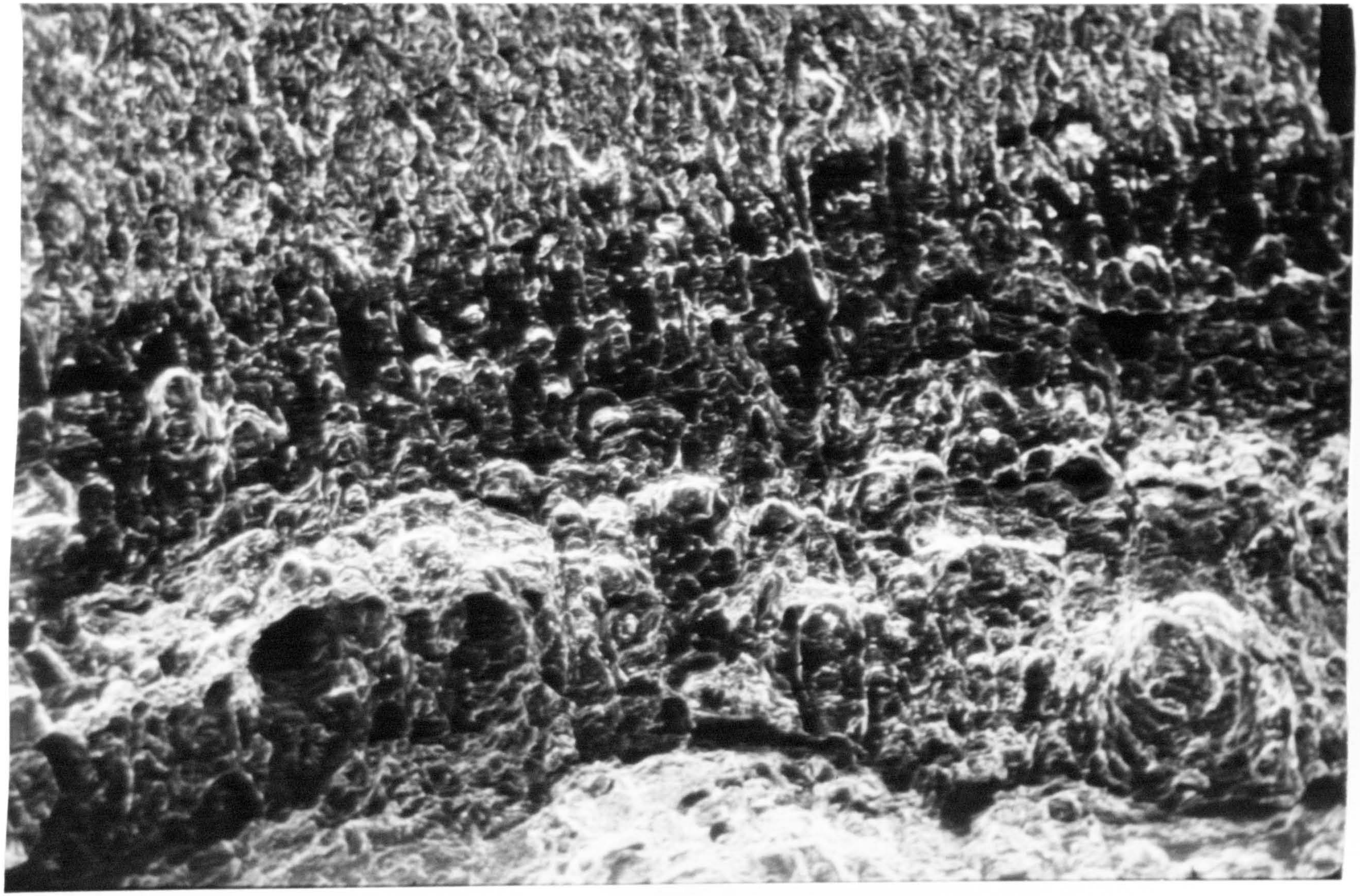

Fig. 106. Dynamic impact, no preload . $\dot{\delta}$ = 154mm/s, momentum = 163·35, x 250mag. -42°C, specimen number H7.

CLOSE VIEW OF DYNAMIC TEARING REGION. H7. -42°C.

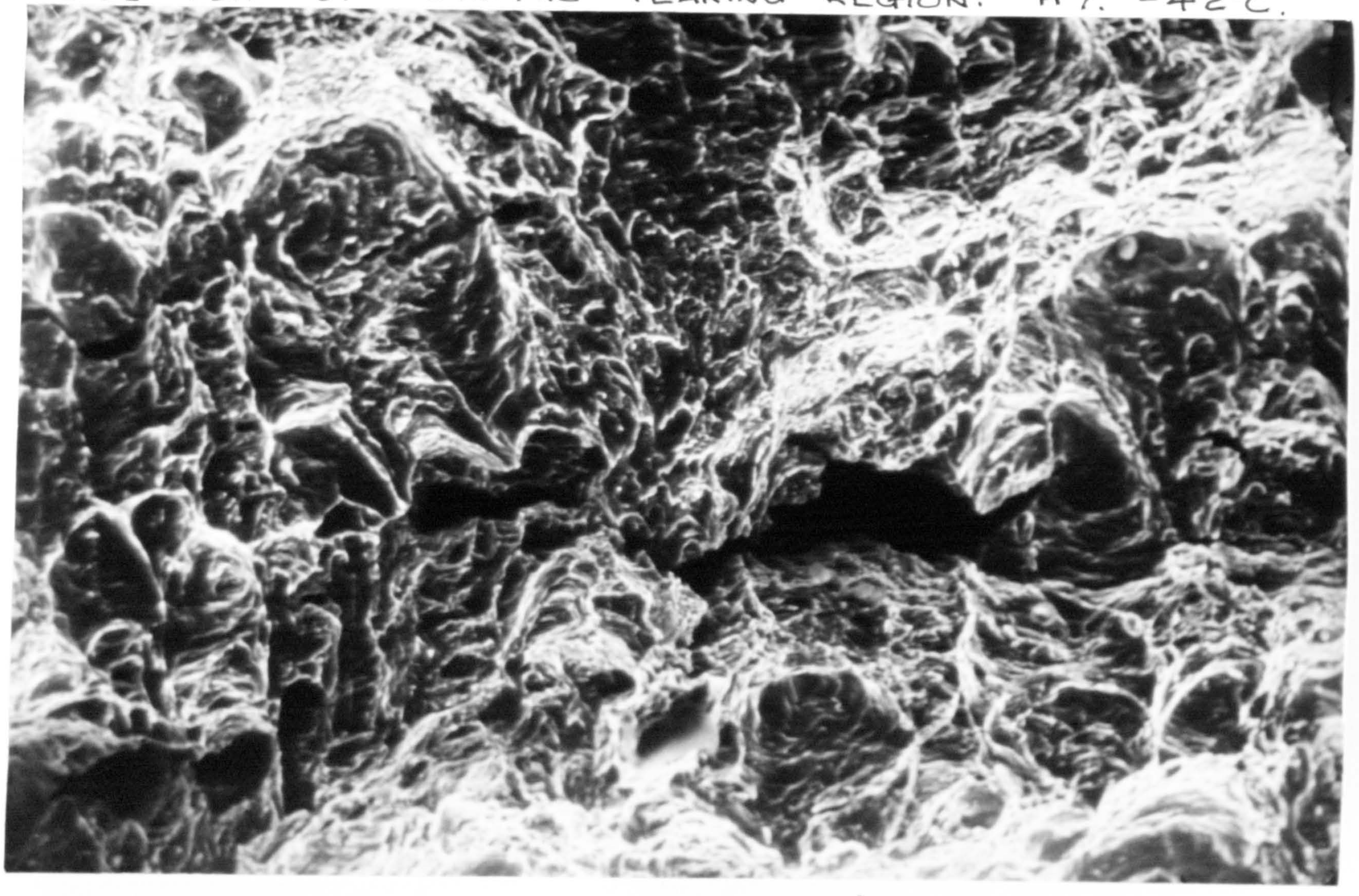

Fig. 107 Dynamic impact, no preload, $\dot{\delta}$ = 154 mm/s, Momentum = 163.3J, x650mag. -42°C, specimen number H7.

DYNAMIC TEAR REGION. H10. -50°C.

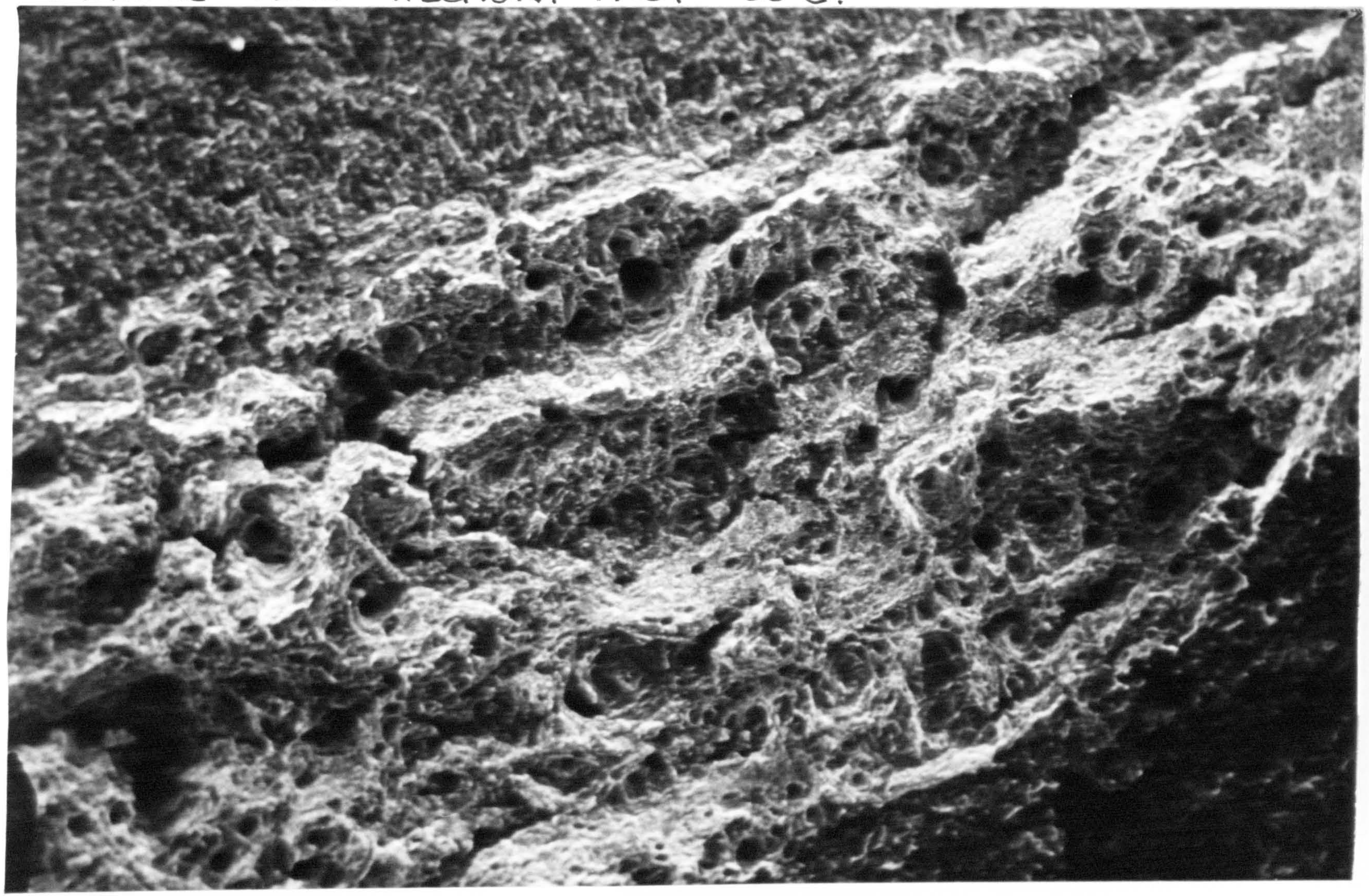

Fig. 108. Dynamic impact, no preload, $\dot{\delta}$ = 154 mm/s, momentum = 163·3J, x 130 mag. -50°C specimen number H10.

CRACK TIP STRETCH ZONE. H10. - 50°C.

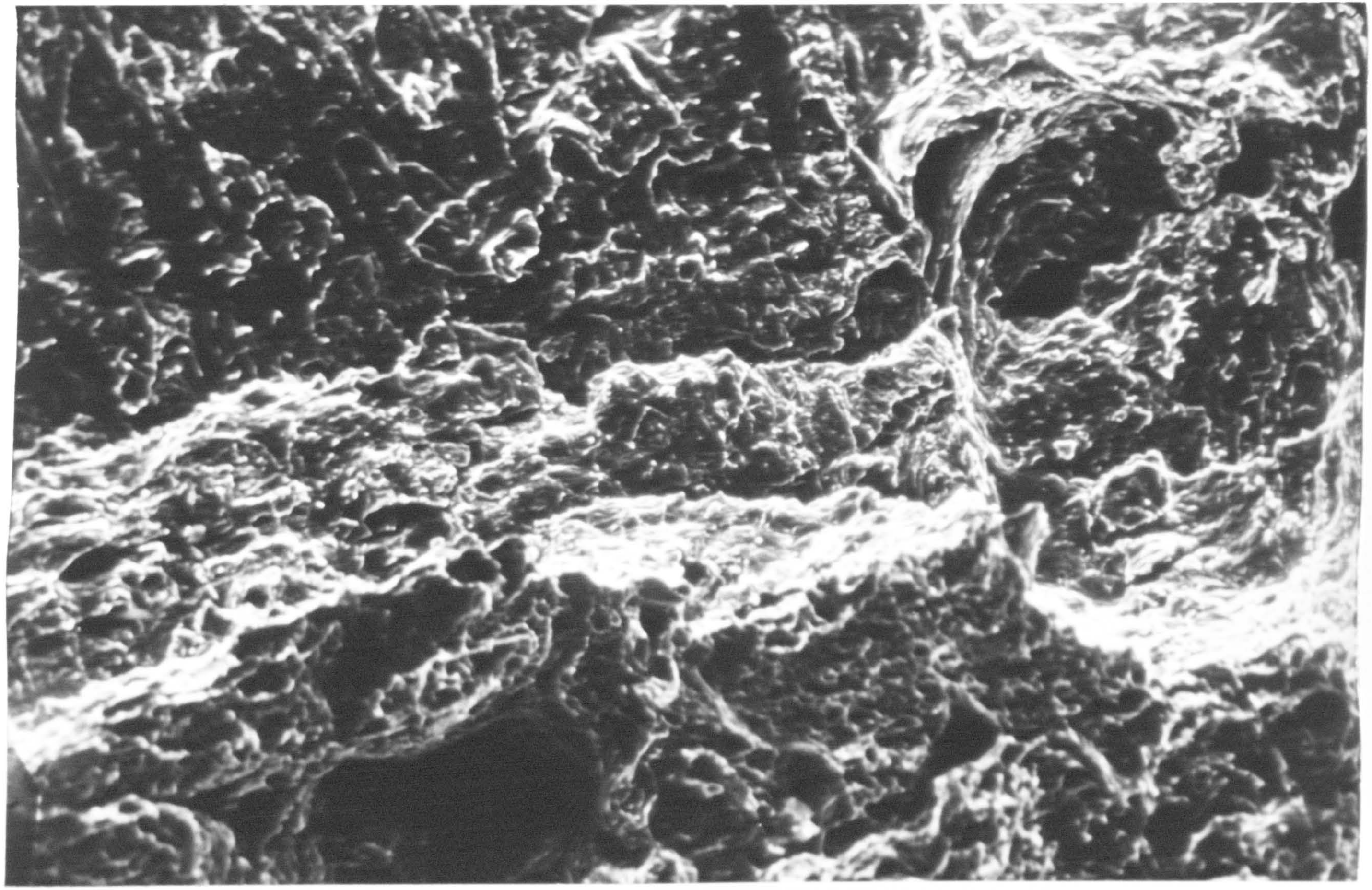

Fig. 109. Dynamic impact, no preload, $\dot{\delta}$ = 154 mm/s, momentum = 163·3 J,
x 650 mag. -50°C specimen number H10.

DYNAMIC CLEAVAGE INSTABILITY DIRECTLY AT CRACK TIP. C13. -60°C.

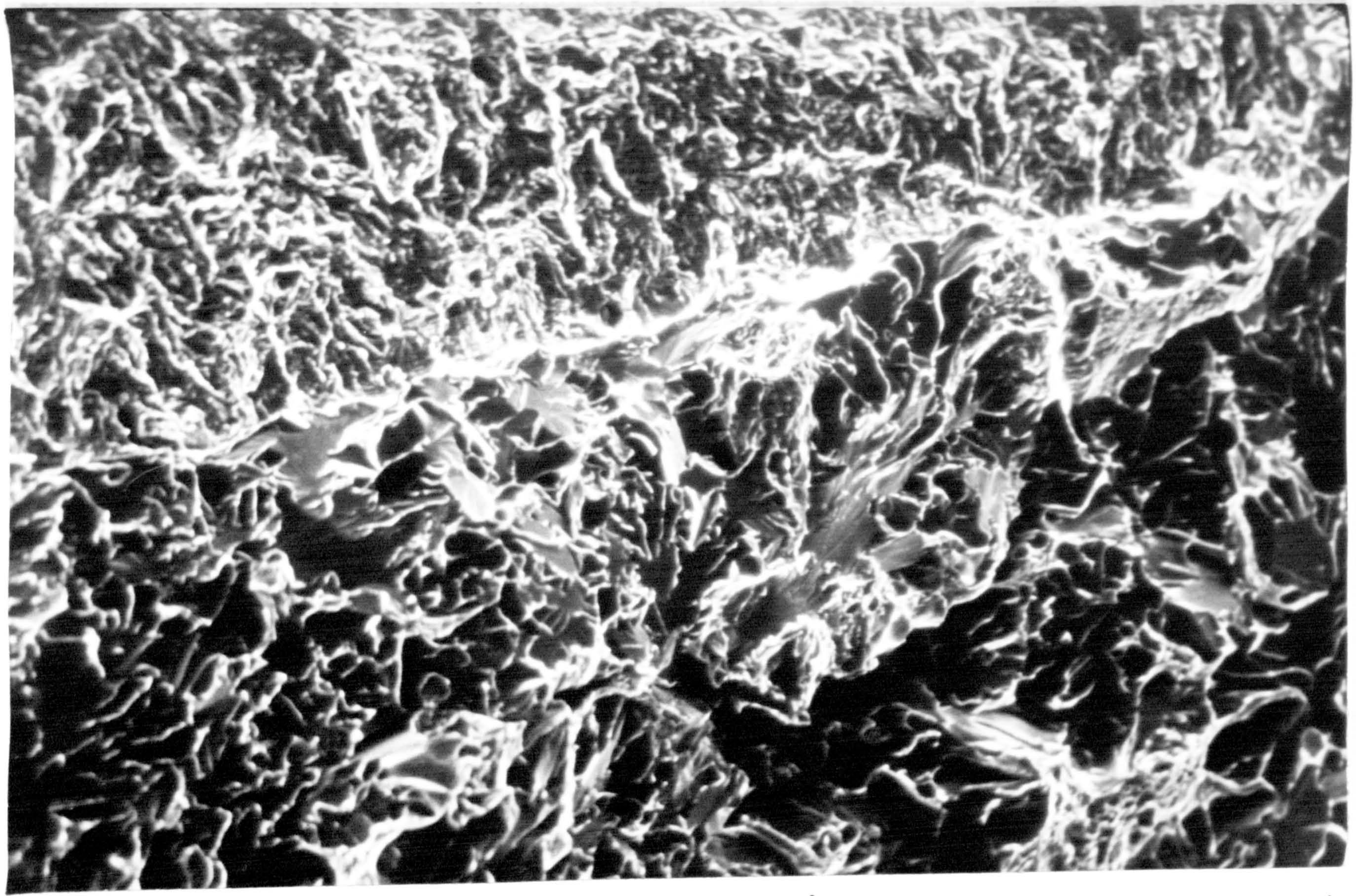

Fig. 110. Dynamic impact no preload, $\dot{\delta}$ = 154 mm/s, momentum = 94·1 J, x 650 mag. -60°C, specimen number C13.

CRACK TIP STRETCH ZONE WITH MICROVOID RUPTURE. F12. -42°C.

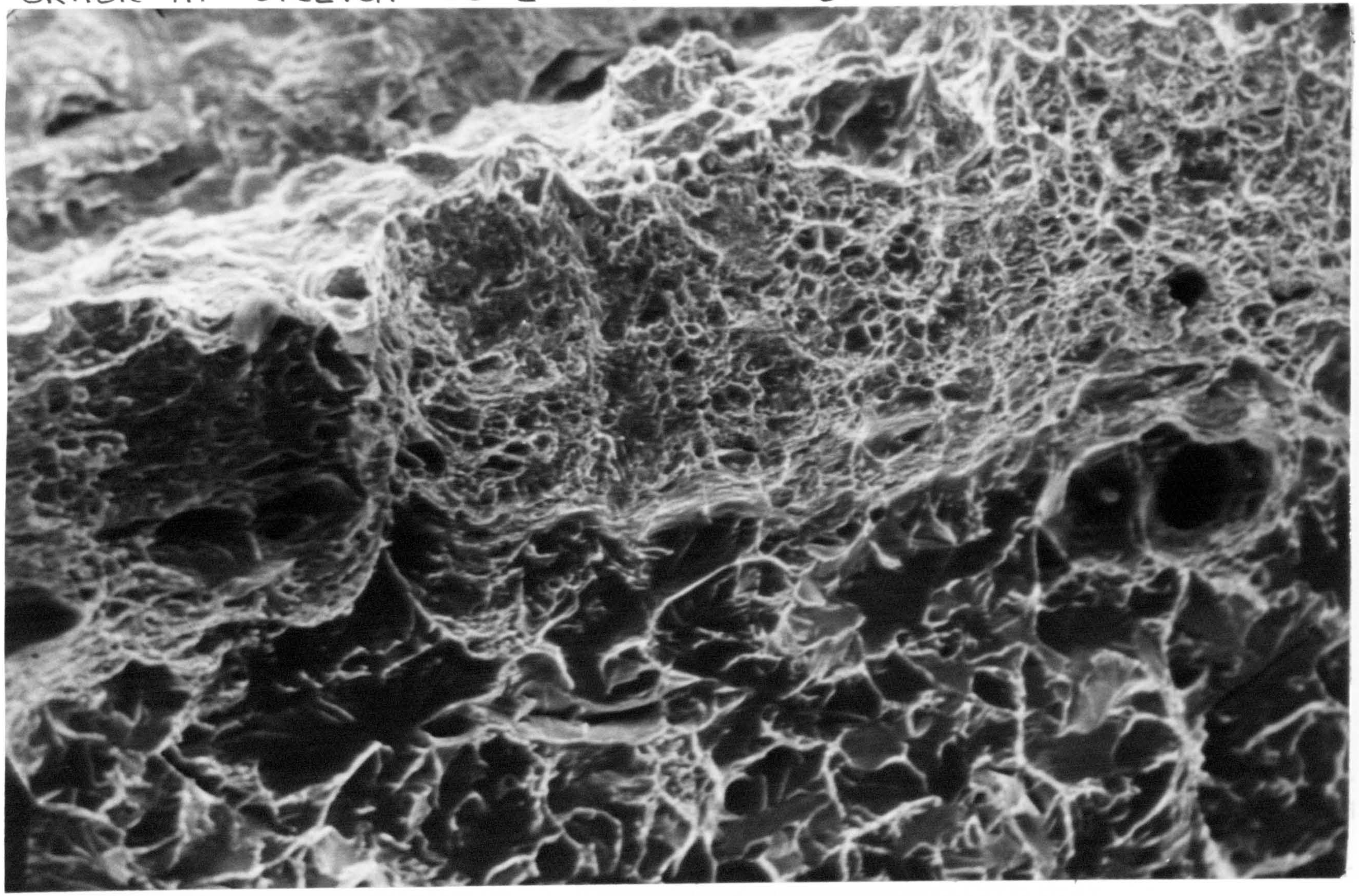

Fig. 111. Dynmaic impact plus superposed compliant preload of 1·53 KN/mm$^{3/2}$, $\dot{\delta}$ = 154 mm/s, momentum = 94.1 J, -42°C, spec. F12.
x650 mag.

STRETCH ZONE AND DYNAMIC MICROVOID RUPTURE WITH PRELOAD < 1·6 kN/mm$^{3/2}$
E7,
−42°C.

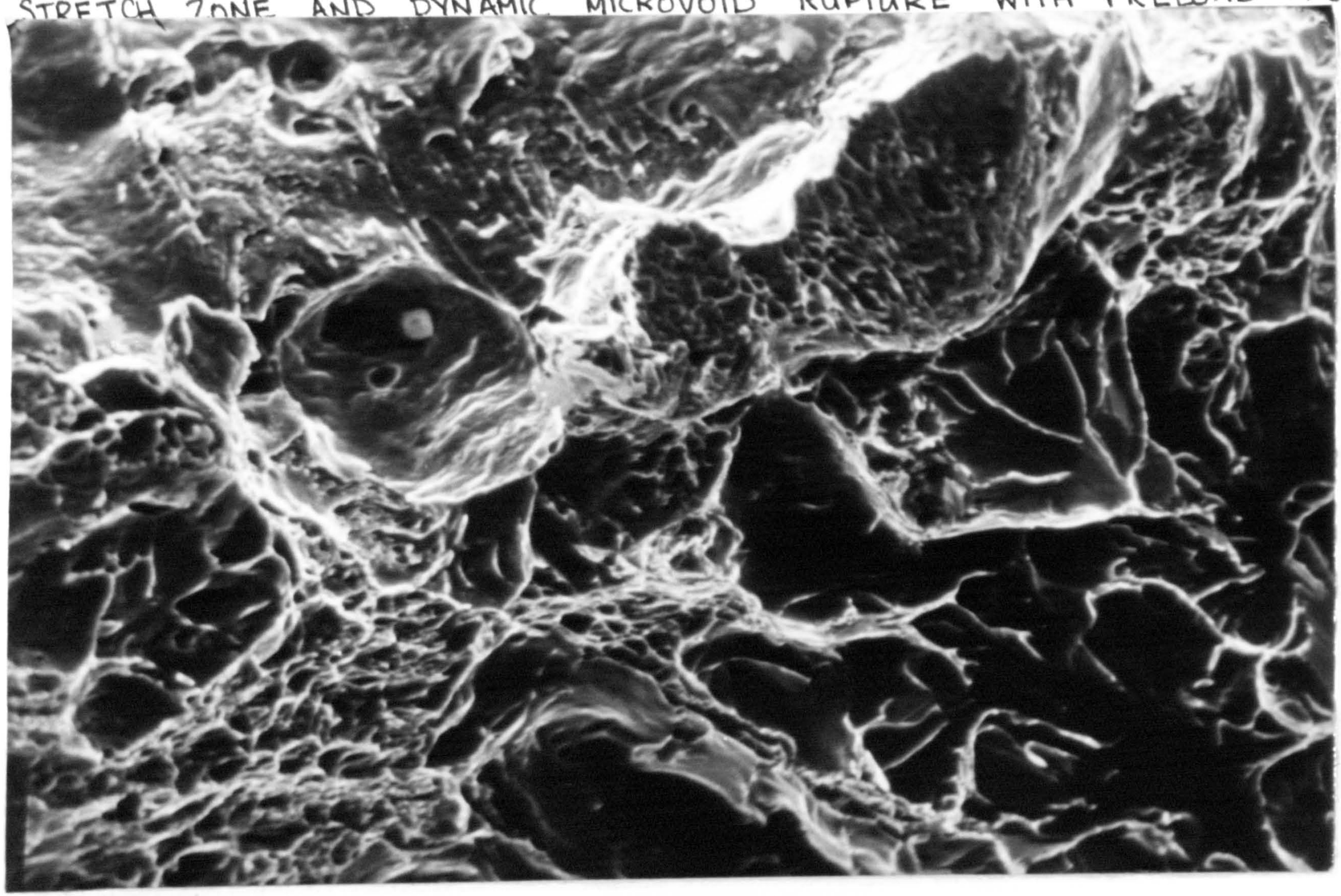

Fig 112. Dynamic impact plus superposed compliant preload of x 1250mag. 1KN/mm$^{3/2}$, $\dot{\delta}$ = 154 mm/s, momentum = 94·1 J, −42°C, spec. E7.

CRACK TIP INTERFACE BETWEEN FATIGUE AND CLEAVAGE. E9.-42°C.

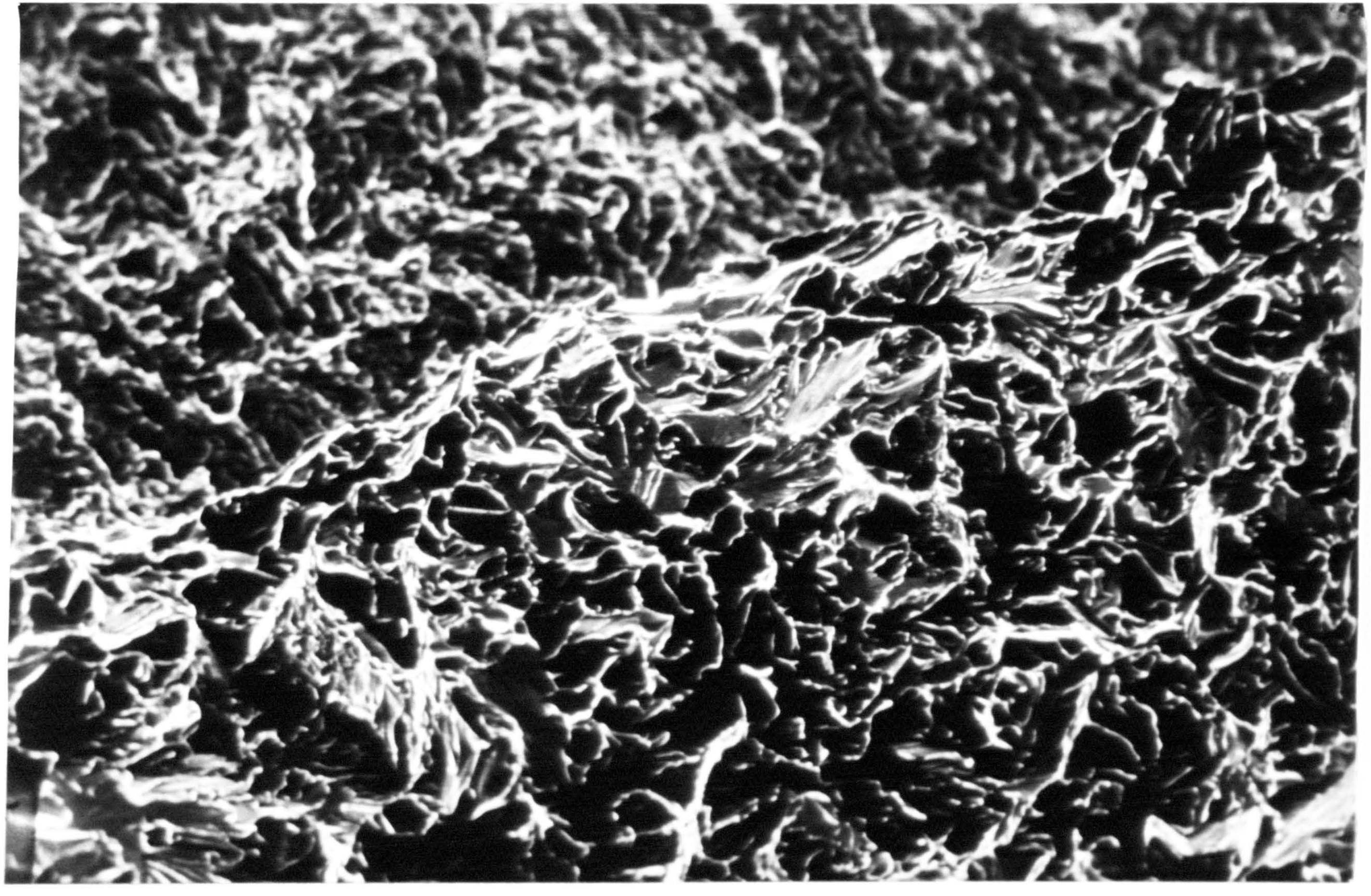

Fig. 113. Dynamic impact plus superposed compliant preload of 0.86 kN/mm$^{3/2}$, $\dot{\delta}$ = 154 mm/s, momentum = 61.9 J, -42°C, spec. E9.
x 650 mag.

CRACK TIP STRETCH ZONE WITH SMALL MICROVOIDS. EG. -42°C.

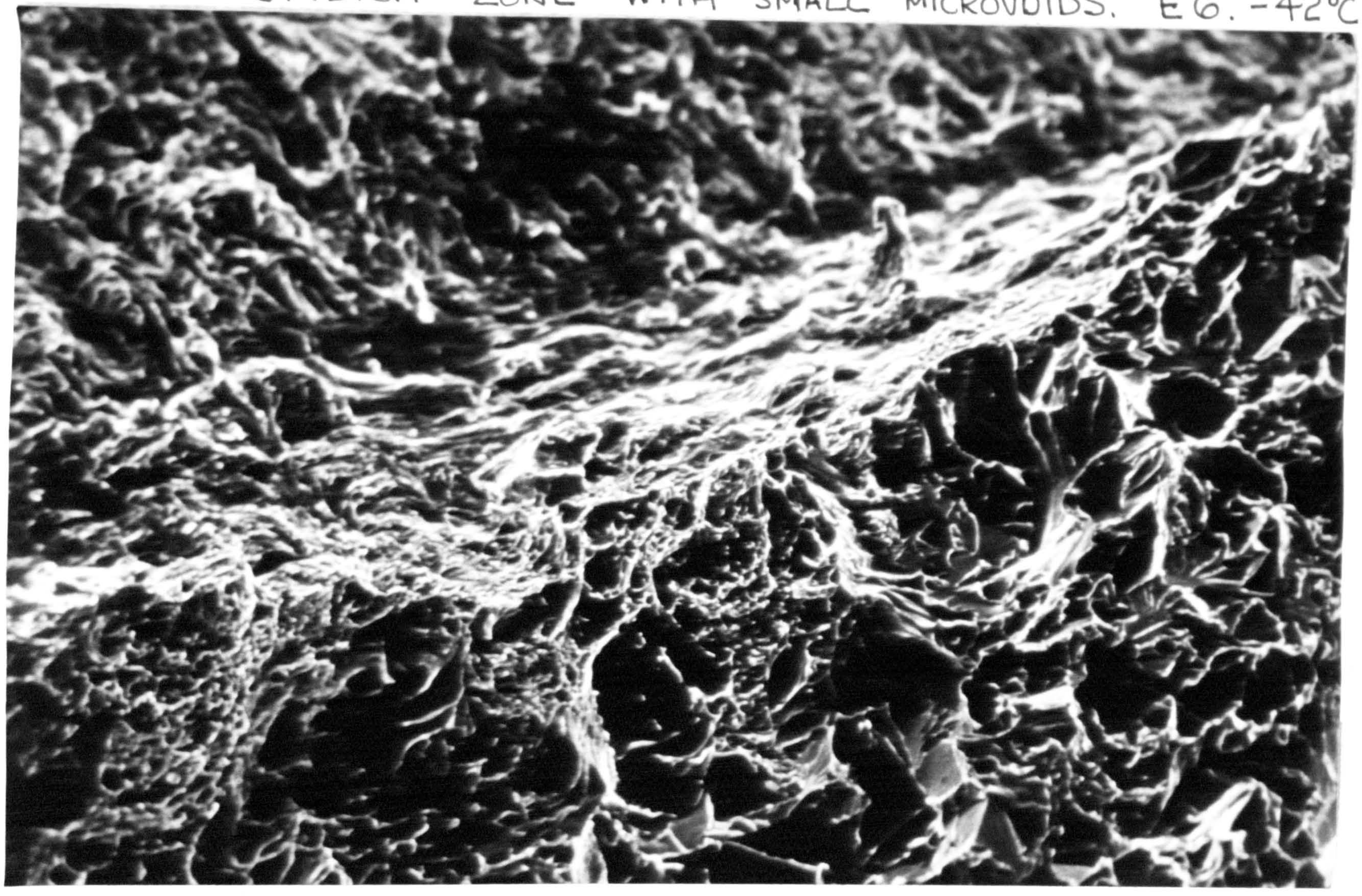

Fig. 114. Dynamic impact plus superposed compliant preload of 1·03 kN/mm$^{3/2}$, $\dot{\delta}$ = 154 mm/s, momentum = 61·9J, -42°C, spec EG. X 650 mag.

GENERAL VIEW OF INSTABILITY REGION. EM1. -42°C.

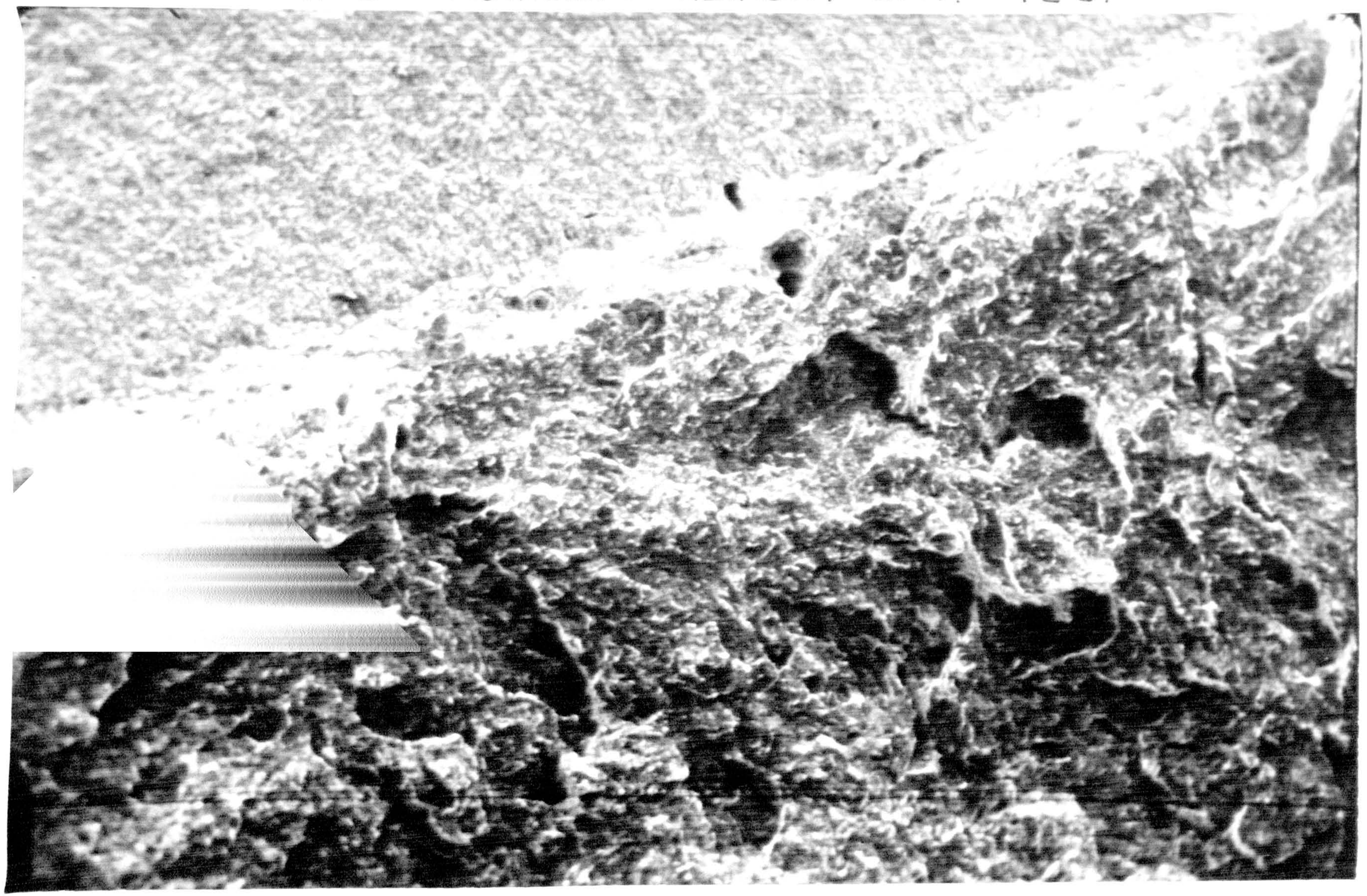

Fig. 115. Dynamic impact plus superposed compliant preload of 1 KN/mm$^{3/2}$, $\dot{\delta}$ = 154 mm/s, momentum = 94·1 J, -42°C, specimen EM1. x 65 mag.

CRACK TIP STRETCH ZONE. EM1. -42°C.

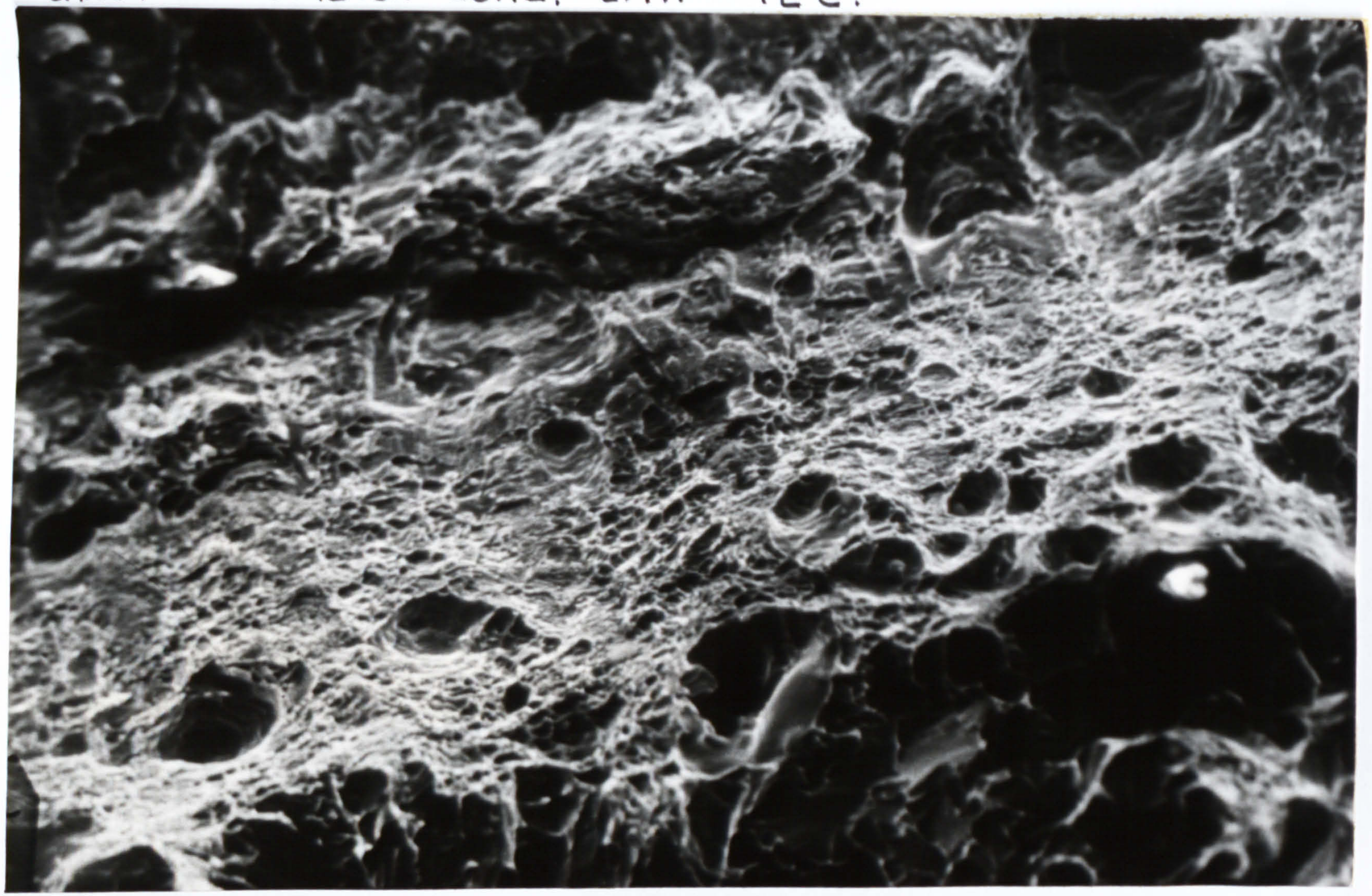

Fig. 116. Dynamic impact plus superposed compliant preload of 1KN/mm$^{3/2}$, $\dot{\delta}$ = 154 mm/s, momentum = 94·1 J, -42°C, specimen EM1.
x 650 mag.

CRACK TIP STRETCH ZONE WITH DYNAMIC MICROVOIDS. E8. -42°C.

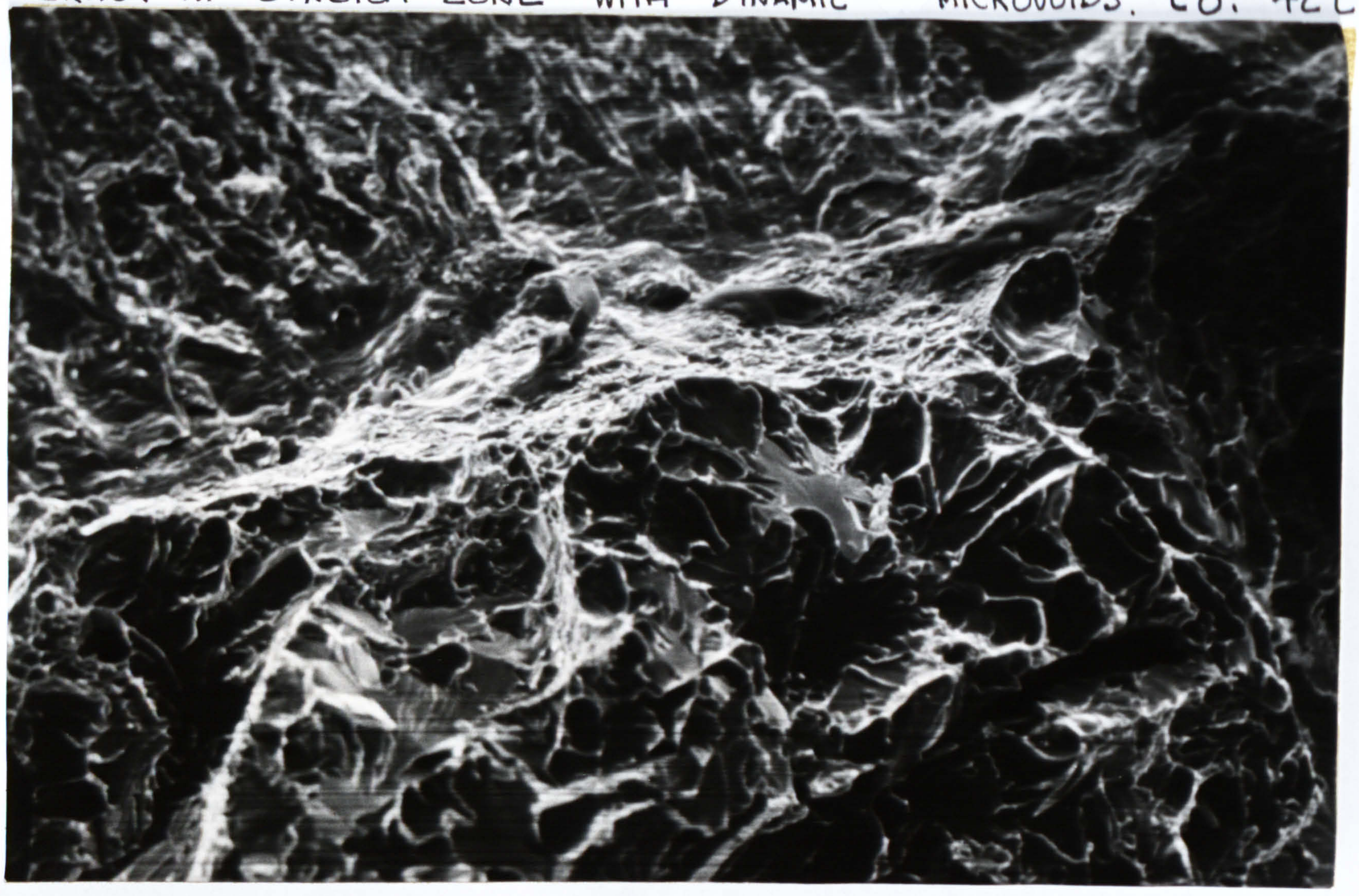

Fig. 117. Dynamic impact plus superposed compliant preload of x650 mag. 0·74 KN/mm$^{3/2}$, $\dot{\delta}$ = 154 mm/s, momentum = 94.1 J, -42°C, spec. E8.

CRACK TIP STRETCH ZONE WITH DYNAMIC MICROVOIDS. EM2. -42°C.

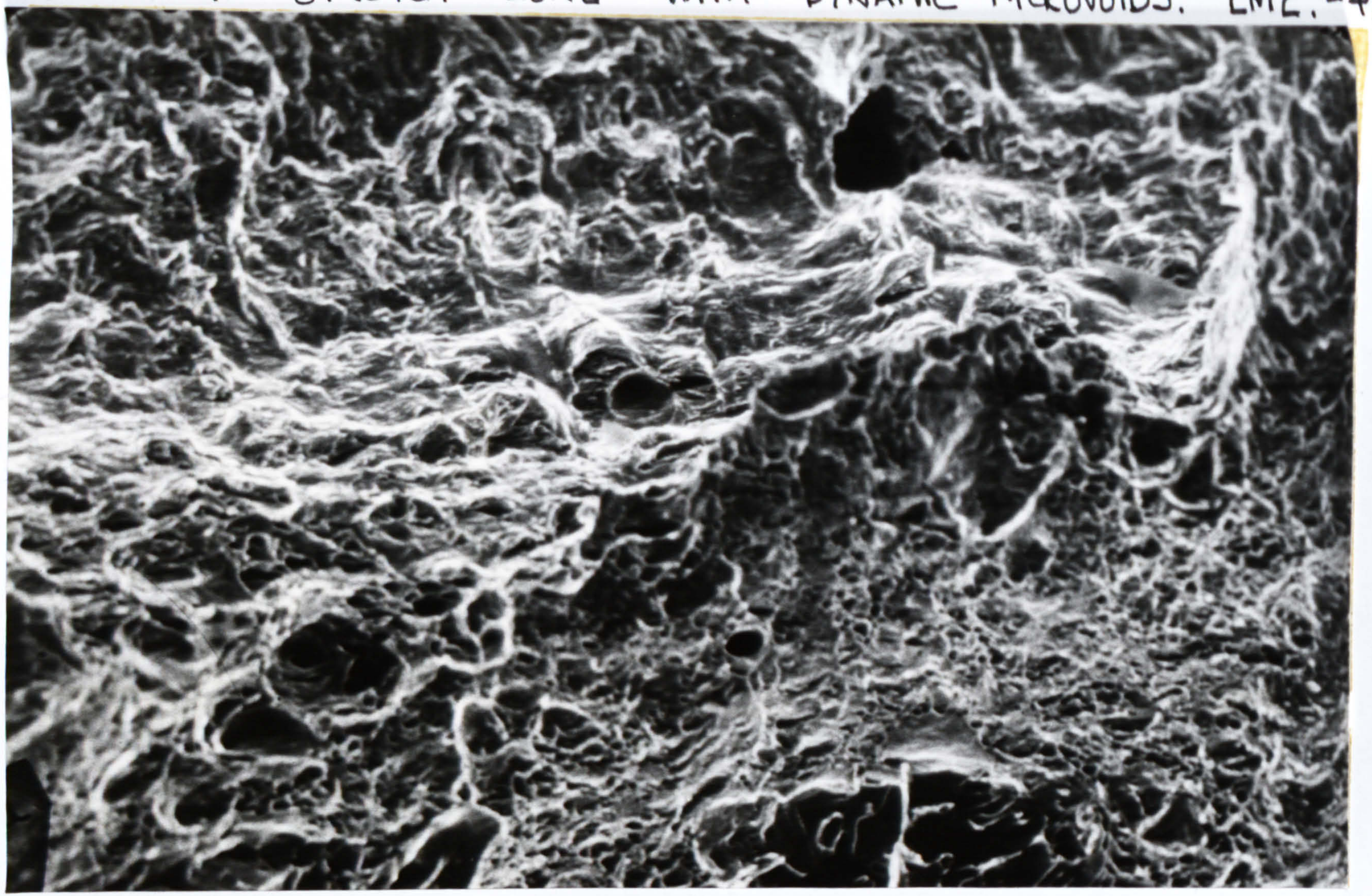

Fig. 118. Dynamic impact plus superposed compliant preload of x650mag. 0·51 kN/mm$^{3/2}$, $\dot{\delta}$ = 154 mm/s, momentum = 163·3J, -42°C, spec. EM2.

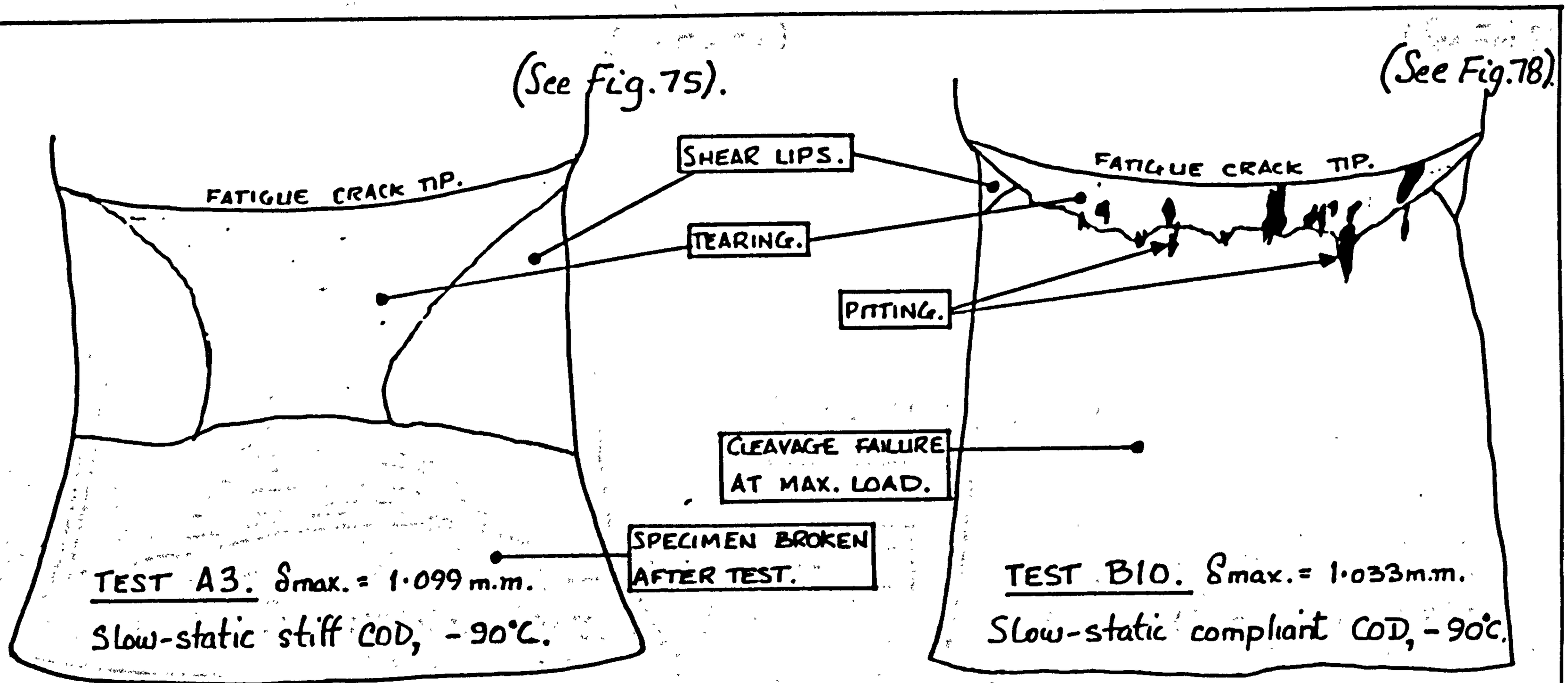

Fig.119. Comparison of stiff and compliant COD tests, fracture surfaces at -90°C.
Magnification x 7.

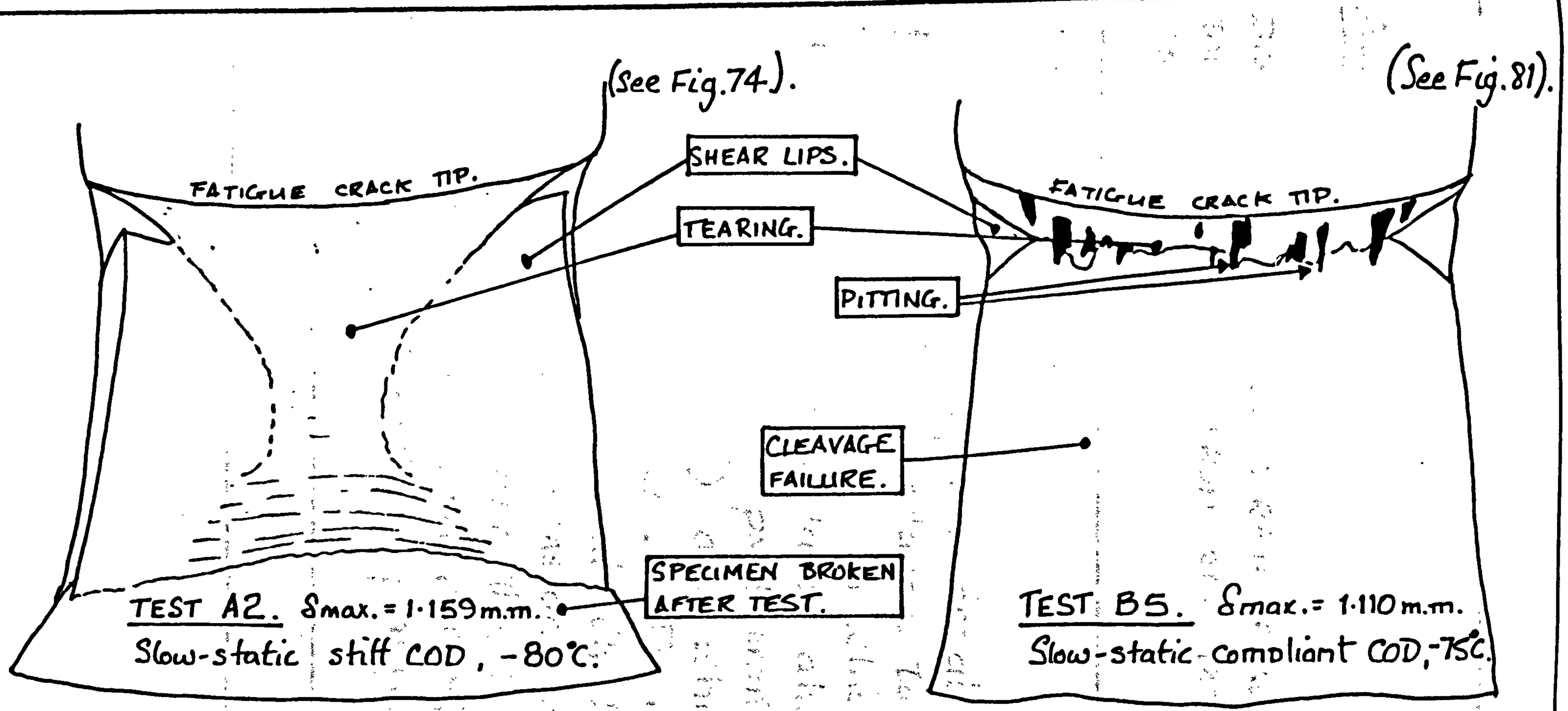

Fig.120. Comparison of stiff and compliant COD tests, fracture surfaces at -80°C and -75°C respectively.
Magnification x 7.

APPENDIX A.

DEFINITION OF PLANE STRAIN FRACTURE TOUGHNESS K_{IC}, FROM REF 127, BS 5447 (BSI).

SECTION 3.2., K_{IC},

"A property of a material indicative of the materials resistance to crack growth under conditions in which the stress at a short distance ahead of the crack front is predominantly triaxial (plane strain) and which plastic deformation is limited. It is the critical value of K_I at which the first significant extension of the crack occurs under the influence of a rising force under conditions of high constraint to plastic deformation."

APPENDIX B. Please see REF.S. 28 and 132.

Authors' derivation of Tearing Modulus after Paris, REF 28, using the COD technique.

In a bend specimen, as tearing begins, ligament b, decreases in size (W-a-da), and so the equivalent limit load will decrease by dP_L, where P_L is the limit load, da is the crack extension, After Green and Hundy, REF 132, Limit bending mom.

$$\frac{dP_L}{da} = -\frac{d}{da}\left\{\frac{0.7\,\sigma_0\,B(W-a)^2}{L}\right\}$$

$M_L = P_L.L.$

$M_L = 0.7\sigma_0 Bb^2$

where L = span,

$b = (W-a)$.

$$dP_L = \frac{-0.7\sigma_0 B}{L}(-2W + 2a)\,da.$$

$$dP_L = \frac{-1.4\sigma_0 B(a-W)}{L}\,da.$$

Now from geometry of notch-bend COD specimen,

$$d\theta = \frac{4d\Delta}{L} \quad \text{or} \quad d\theta = \frac{dV_p}{(a + r(W-a))}$$

then

$$\frac{\delta}{V_p} = \frac{r(W-a)}{a + r(W-a)}$$

$$\text{COD } \delta = \left\{\frac{V_p\,(r(W-a))}{(a + r(W-a))}\right\}$$

PTO. →

APPENDIX B. (CONTINUED).

And from Engineers' bending theory.

$$\text{deflection } d\Delta = \frac{dP_L L^3}{48EI} \qquad \therefore\ d\theta = \frac{4\,dP_L L^{3/2}}{48_{12} EI\sqrt{L}}$$

and

$$d\theta = \frac{dP_L L^2}{12EI} = \frac{dV_p.}{(a+r(W-a))}$$

now $$d\theta = \frac{d\delta}{r(W-a)}$$

$$\therefore \quad d\delta = \frac{dP_L L^2}{12EI}\left\{r[W-a)\right\}$$

And,

$$d\delta = \frac{-1.4\sigma_o B(a-W)\,da\,L^2\left\{r(W-a)\right\}}{12EIL}$$

$$\frac{d\delta}{da} = \frac{-1.4\sigma_o L}{EW^3}\left\{r(2aW-a^2-W^2)\right\}$$

Then instability occurs if,

$$\boxed{\frac{d\delta}{da}\cdot\frac{E}{\sigma_o} \leqslant -\frac{1.4L}{W^3}\cdot r(2aW-a^2-W^2)}$$

OR IN GENERAL TERMS :

$$\frac{d\delta}{da}\cdot\frac{E}{\sigma_o} \leqslant -\beta\,\frac{L\text{equivalent}}{W^3}\cdot f(r, a^2, W^2).$$

with $$L\text{equivalent} = L\left(1+\frac{\delta_{SB}}{\delta_{TB}}\right)$$

δ_{SB} = spring deflection, δ_{TB} = test bar def.,

APPENDIX C.

Plastic zone correction to series E and F instability line above -50°C, see section 8.3.

For 0·52 Y/W,

$$\delta = 0.157\ Vp.$$

At -50°C, $\sigma_{ys} = 370 N/mm^2$, and $K = 1.6 kN/mm^{3/2}$,

using $r_y = \frac{1}{2\pi}\left(\frac{K_1^2}{\sigma_{ys}^2}\right)$

$$r_{y50} = 2.98 mm.$$

now $a_{effective} = (a_{fatigue} + r_y)$

$a_f + r_{y-50} = 15.376$ mm, use this effective crack length to determine critical COD for the same Vp opening at instability, simply then, correcting COD for longer crack length a_{eff},

$$V_{p\,critical\ -50°C} = \frac{0.46}{0.157} = 2.93 mm,$$ (0·46 mm COD from mean transition).

$$\therefore \delta_{eff} = 2.93 \left\{ \frac{0.4\ (24 - 15.376)}{0.4\ (24) + 0.6\ (15.376) + 12.5} \right\}$$

$\therefore \delta_{eff} =$ 0·32 mm COD, for -50°C.

PTO →

Similarly, for $-42°C$, $\sigma_{ys} = 367 N/mm^2$,
$K = 1.6 KN/mm^{3/2}$,

$r_y = 3.025 mm$, $a_{eff} = 15.425 mm$,

then

$$\delta_{eff} = \frac{0.85}{0.157} \cdot 0.1093 = 0.59 mm \text{ COD},$$

and at $-30°C$, $\sigma_{ys} = 360 N/mm^2$, $K = 1.6 KN/mm^{3/2}$,

$r_y = 3.14 mm$, $a_{eff} = 15.54 mm$,

then

$$\delta_{eff} = \frac{1.05}{0.157} \cdot 0.108 = 0.72 mm \text{ COD}.$$

∴ Using plastic zone correction for crack length, critical instability COD occurs ahead of the crack tip, at the outer boundary of the plastic zone,

T°C	$\delta_{effective}$ (mm)	$a_{effective}$ (mm)
-50	0.32	15.38
-42	0.59	15.43
-30	0.72	15.54 (for $a/W = 0.52$).